

1. Report No. 4145-1	2. Government Accession No.	3. Recipient's Catalog No.	
4. Title and Subtitle LATERAL BRACING OF BRIDGE GIRDERS BY PERMANENT METAL DECK FORMS		5. Report Date January 10, 2005	
7. Author(s) Todd A. Helwig, Ozgur Egilmez, and Charles Jetann		6. Performing Organization Code	
		8. Performing Organization Report No. Research Report 4145-1	
9. Performing Organization Name and Address University of Houston 4800 Calhoun, Eng. Bldg. I Rm. N107 Houston, Texas 77204-4003		10. Work Unit No. (TRAIS)	
		11. Contract or Grant No. Research Study 0-4145	
12. Sponsoring Agency Name and Address Texas Department of Transportation Research and Technology Transfer Section/Construction Division P.O. Box 5080 Austin, TX 78763-5080		13. Type of Report and Period Covered Final	
		14. Sponsoring Agency Code	
15. Supplementary Notes Project conducted in cooperation with the Federal Highway Administration. Research Study Title: Lateral Bracing of Bridge Girders by Permanent Metal Deck Forms			
16. Abstract Lateral torsional buckling is a failure mode that often controls the design of steel bridge girders during construction. Bracing in the form of cross-frames and diaphragms are often provided at locations along the bridge length to reduce the unbraced length and increase the buckling capacity. Although they are not currently relied upon for bracing, permanent metal deck forms (PMDF) are frequently used to support the wet concrete for the bridge deck during construction. Similar forms used in the building industry are commonly relied upon for beam bracing. The forms typically behave as a shear diaphragm that restrains the warping deformation in the top flange. The main difference between the forms used in the building and bridge industries are the method of connection. In the building industry, the forms are typically fastened directly to the top girder flange by the shear studs, puddle welds or other mechanical connections. In the bridge industry, the forms are supported on a cold-formed angle that allows the contractor to adjust the form elevation to account for variations in the flange thickness or differential camber between adjacent girders. The support angles lead to eccentric connections that substantially reduce the stiffness of the PMDF systems. The objective of the research outlined in this report is to improve the understanding of the bracing behavior of PMDF systems used in the bridge industry as well as developing improved connection details between the support angles and the girder flanges. The research included laboratory tests and finite element analytical (FEA) modeling. The laboratory studies included shear tests, full scale testing of a twin girder system with a 50 ft. span. Both lateral load tests and buckling tests were conducted on the twin girder system with PMDF for bracing. In addition to demonstrating the behavior of the bracing systems, the laboratory studies were also used to validate the computer models of the bracing systems so that parametric FEA studies could be conducted. Modified details for the connection angles consisted of stiffening angles that span between adjacent girders at intermediate locations along the girder length. The stiffening angles substantially increased the stiffness of the PMDF system. The modified details make PMDF systems a viable bracing alternative in steel bridges that can significantly reduce the number of cross-frames and diaphragms required for stability bracing.			
17. Key Words permanent metal deck forms, shear diaphragm, bracing, steel bridge, buckling		18. Distribution Statement No restrictions. This document is available to the public through the National Technical Information Service, Springfield, Virginia 22161.	
19. Security Classif. (of report) Unclassified	20. Security Classif. (of this page) Unclassified	21. No. of pages 150	22. Price

**LATERAL BRACING OF BRIDGE GIRDERS BY PERMANENT METAL DECK
FORMS**

by

Todd Helwig, Ozgur Egilmez, and Charles Jetann

Research Report Number 4145-1

Research Project 0-4145

Lateral Bracing of Bridge Girders by Permanent Metal Deck Forms

Conducted for the

TEXAS DEPARTMENT OF TRANSPORTATION

in cooperation with the

U.S. DEPARTMENT OF TRANSPORTATION

Federal Highway Administration

by the

UNIVERSITY OF HOUSTON

JANUARY 2005

DISCLAIMERS

The contents of this report reflect the views of the authors, who are responsible for the facts and the accuracy of the data presented herein. The contents do not necessarily reflect the official views or policies of the Federal Highway Administration or the Texas Department of Transportation. This report does not constitute a standard, specification, or regulation.

There was no invention or discovery conceived or first actually reduced to practice in the course of or under this contract, including any art, method, process, machine, manufacture, design or composition of matter, or any new and useful improvement thereof, or any variety of plant, which is or may be patentable under the patent laws of the United States of America or any foreign country.

**NOT INTENDED FOR CONSTRUCTION,
BIDDING, OR PERMIT PURPOSES**

Todd A. Helwig
Research Supervisor

ACKNOWLEDGMENTS

The authors would like to thank the project coordinator, J.C. Liu, and the project director, John Vogel for their cooperation and recommendations during this research study. In addition the authors would like to thank several TxDOT engineers that provided feedback during this project, including Tim Chase, John Holt, and Kenny Ozuna.

Research performed in cooperation with the Texas Department of Transportation and the U.S. Department of Transportation, Federal Highway Administration.

SUMMARY

Lateral torsional buckling is a failure mode that often controls the design of steel bridge girders during construction. Bracing in the form of cross-frames and diaphragms are often provided at locations along the bridge length to reduce the unbraced length and increase the buckling capacity. Although they are not currently relied upon for bracing, permanent metal deck forms (PMDF) are frequently used to support the wet concrete for the bridge deck during construction. Similar forms used in the building industry are commonly relied upon for beam bracing. The forms typically behave as a shear diaphragm that restrains the warping deformation in the top flange. The main difference between the forms used in the building and bridge industries are the method of connection. In the building industry, the forms are typically fastened directly to the top girder flange by the shear studs, puddle welds or other mechanical connections. In the bridge industry, the forms are supported on a cold-formed angle that allows the contractor to adjust the form elevation to account for variations in the flange thickness or differential camber between adjacent girders. The support angles lead to eccentric connections that substantially reduce the stiffness of the PMDF systems.

The objective of the research outlined in this report is to improve the understanding of the bracing behavior of PMDF systems used in the bridge industry as well as developing improved connection details between the support angles and the girder flanges. The research included laboratory tests and finite element analytical (FEA) modeling. The laboratory studies included shear tests, full scale testing of a twin girder system with a 50 ft. span. Both lateral load tests and buckling tests were conducted on the twin girder system with PMDF for bracing. In addition to demonstrating the behavior of the bracing systems, the laboratory studies were also used to validate the computer models of the bracing systems so that parametric FEA studies could be conducted.

Modified details for the connection angles consisted of stiffening angles that span between adjacent girders at intermediate locations along the girder length. The stiffening angles substantially increased the stiffness of the PMDF system. The modified details make PMDF systems a viable bracing alternative in steel bridges that can significantly reduce the number of cross-frames and diaphragms required for stability bracing.

Note to Designers

Although the entire report contains important information regarding the behavior of PMDF bracing in steel bridges, bridge designers should pay particular emphasis to Chapters 1, 2, 8, 9, and 10. Two design examples are presented in Chapter 9 that illustrate the recommended procedure for checking the bracing performance of the PMDF.

This page replaces an intentionally blank page in the original.

-- CTR Library Digitization Team

Table of Contents

Chapter 1	Introduction.....	1
1.1	Research Overview and Objectives	1
1.2	Industry Applications for PMDF	3
1.2.1	Building Applications	4
1.2.2	Bridge Applications	4
1.3	Overview.....	5
Chapter 2	Background.....	7
2.1	Introduction.....	7
2.2	Lateral Torsional Buckling	7
2.3	Beam Bracing.....	11
2.4	Shear Stiffness of PMDF Systems	13
2.5	Shear Strength of PMDF Systems	16
2.6	Diaphragm Braced Beams	17
Chapter 3	Finite Element Model.....	23
3.1	Overview.....	23
3.2	Finite Element Model	23
3.3	Computational Study	26
3.4	Imperfections Considered in the Study.....	29
Chapter 4	Laboratory Test Set-ups.....	33
4.1	Overview.....	33
4.2	Shear Tests	34
4.2.1	Shear Frame Test Set-Up	34
4.2.2	Shear Frame Friction Tests	36
4.2.3	Shear Test Instrumentation	37
4.2.4	PMDF Specimens and Connection Details (Shear Tests).....	37
4.3	Lateral Displacement Tests.....	43
4.3.1	Twin Girder Set-Up	43
4.3.2	Lateral Loading Frames	48
4.3.3	Lateral Displacement Test Instrumentation.....	50
4.3.4	PMDF Specimens and Connection Details (Lateral Displacement Tests)	50

4.4 Buckling Tests	52
4.4.1 Test Set-Up	52
4.4.2 Buckling Test Instrumentation.....	54
4.4.3 PMDF Specimens and Connection Details (Buckling Tests).....	56
Chapter 5 Shear Tests.....	59
5.1 Overview.....	59
5.2 Shear Test Phases 1 & 2: Elastic, Cyclic Loading and Initial Stiffness	59
5.3 Shear Test Phase 3: Ultimate Capacity and Secant Stiffness	61
5.4 Results.....	62
Chapter 6 Twin Girder Lateral Displacement Tests.....	71
6.1 Overview.....	71
6.2 Partially Decked Tests	71
6.3 Fully Decked Tests	73
6.4 Results.....	74
Chapter 7 Twin Girder Buckling Tests.....	85
7.1 Overview.....	85
7.2 Test Phases.....	85
7.3 Initial Imperfections.....	86
7.4 Test Results.....	88
7.4.1 20ga01 Tests	88
7.4.2 20ga02 Tests	102
7.4.3 20ga03 Tests	116
Chapter 8 Parametric Studies.....	121
8.1 Overview.....	121
8.2 Eigenvalue Buckling Analyses	122
8.3 Large Displacement Analyses.....	130
8.4 Design Recommendations	133
8.4.1 Recommendations for Stiffness	133
8.4.2 Recommendations for Strength.....	134

Chapter 9	Bracing Design Example.....	137
9.1	Introduction.....	137
9.2	Design Examples	137
9.2.1	Steel Bridge with 100 ft. span.....	137
9.2.2	Steel Bridge with 50 ft. span.....	141
Chapter 10	Conclusions.....	145
10.1	Conclusions.....	145
10.1.1	Shear Tests	145
10.1.2	Twin Girder, Lateral Displacement Tests.....	146
10.1.3	Twin Girder, Buckling Tests.....	147
10.1.4	Design Recommendations for Stiffened Deck Braced Girders	147
10.2	Future Research	148

This page replaces an intentionally blank page in the original.

-- CTR Library Digitization Team

List of Figures

Figure 1.1	Metal Deck Forms viewed from the underside of a Bridge.....	1
Figure 1.2	PMDF as Beam Bracing	3
Figure 1.3	Deck Form Arrangement for Building Applications	4
Figure 1.4	Deck Form Arrangement for Bridge Applications	5
Figure 2.1	Buckling Deformations on Girder Cross Section	7
Figure 2.2	Plastic Stress Distribution.....	8
Figure 2.3	Singly-Symmetric Cross Section.....	9
Figure 2.4	Load Height Effects.....	10
Figure 2.5	Lateral Torsional Beam Bracing Systems.....	11
Figure 2.6	Effect of Brace Stiffness on Deformations using Winter’s Model.....	13
Figure 2.7	Shear Test Frame with PMDF Specimen.....	14
Figure 2.8	Internal Forces on a PMDF Specimen.....	15
Figure 2.9	PMDF Stress vs. Strain Behavior	16
Figure 2.10	Fastener Force Distribution Assumption	17
Figure 2.11	Comparison of Eq. (2.11) and Eq. (2.12).....	18
Figure 3.1	Finite Element Model of the Girder Cross Section.....	24
Figure 3.2	Truss Elements used to Simulate the Shear Diaphragm	25
Figure 3.3	Finite Element Stiffening Angle Model.....	26
Figure 3.4	Girder Cross Sections Considered in Computational Study	27
Figure 3.5	Assumed Initial Imperfection	30
Figure 3.6	Shape and Magnitude of the Initial Imperfections in FEA Studies	31
Figure 4.1	Shear Test Frame	35
Figure 4.2	PMDF Profile.....	37
Figure 4.3	Support Angle-PMDF Connection	38
Figure 4.4	Diagonal Tension and Compression Fields on Sheared PMDF Specimen..	39
Figure 4.5	Failure Mode of Unstiffened Eccentric Connection	40
Figure 4.6	Transverse Stiffening Angle to Control Support Angle Deformation.....	40
Figure 4.7	Eccentric T-Stub – Stiffening Angle Connection.....	41
Figure 4.8	Connection Detail Symbol Illustration	42
Figure 4.9	Regions of Shear and Flexural Contribution to Lateral Stiffness.....	44
Figure 4.10	Twin Girder Test Set-Up	45
Figure 4.11	Twin Girder Lateral Displacement Test Set-Up	46
Figure 4.12	Twin Girder Supports	47
Figure 4.13	Lateral Loading Frame and Linking Member.....	49
Figure 4.14	Lateral Loading Frame with Turnbuckle to Load Cell Attachment	50
Figure 4.15	Gravity Load Simulator	52
Figure 4.16	Gravity Load Simulator Beam.....	53
Figure 4.17	Knife Edges.....	54
Figure 4.18	Linear Spring Potentiometers	55
Figure 4.19	Rotary String Linear Potentiometers	56
Figure 5.1	Shear Test Frame and Specimen with Simulated Concrete Load	60
Figure 5.2	Elastic, Reversed Cyclic Loading (Initial Stiffness).....	61
Figure 5.3	Phase 3 Loading Stress vs. Strain Behavior.....	62

Figure 5.4	Effect of Stiffened Connections on PMDF Stress vs. Strain Behavior.....	63
Figure 5.5	Support Angle Eccentricity Reduces the Stiffness of Unstiffened Deck Panels	64
Figure 5.6	Failure of PMDF Systems with Stiffening Angles do not Result in Large Deformations at the Support Angle	64
Figure 5.7	Ductility of 18ga and 16ga PMDF Systems with Stiffened Connection Details (8 ft Panel Width and Stiffener Spacing).....	69
Figure 5.8	Ductility of 18ga and 16ga PMDF Systems with Stiffened Connection Details (12 ft Panel Width and Stiffener Spacing).....	69
Figure 5.9	Ductility of 18ga and 16ga PMDF Systems with Stiffened Connection Details (16 ft Panel Width – 8 ft Stiffener Spacing).....	70
Figure 5.10	Ductility of 18ga and 16ga PMDF Systems with Stiffened Connection Details (16 ft Panel Width and Stiffener Spacing).....	70
Figure 6.1	Left- Partially Decked (12ft) PMDF Specimen with Concrete Dead Load; Right- Calibration of FEA from Unstiffened Partially Decked System	72
Figure 6.2	FEA Stiffening Angle Truss	73
Figure 6.3	Left- Fully Decked (24ft) PMDF Specimen with Concrete Dead Load; Right- Calibration of Beam Element from Unstiffened Fully Decked System	74
Figure 7.1	Initial Imperfections of 20ga01 Tests	87
Figure 7.2	Initial Imperfections of 20ga02 Tests	87
Figure 7.3	Initial Imperfections of 20ga03 Tests	87
Figure 7.4	Midspan Moment vs. Twist Data (20ga01.no Test - North Girder)	89
Figure 7.5	Midspan Moment vs. Twist Data for 20ga01.no Tests (South Girder)	89
Figure 7.6	Comparison of Midspan Moment vs. Twist for 20ga01.st8ft.no (North Girder).....	90
Figure 7.7	Comparison of Midspan Moment vs. Twist for 20ga01.st8ft.no (South Girder).....	91
Figure 7.8	Comparison of Midspan Moment vs. Twist for 20ga01.st16ft.no (North Girder).....	92
Figure 7.9	Comparison of Midspan Moment vs. Twist for 20ga01.st16ft.no (South Girder).....	92
Figure 7.10	Comparison of Midspan Moment vs. Twist for 20ga01.st24ft.no (North Girder).....	93
Figure 7.11	Comparison of Midspan Moment vs. Twist for 20ga01.st24ft.no (South Girder).....	93
Figure 7.12	Comparison of Midspan Moment vs. Twist for 20ga01.unst.no (North Girder).....	94
Figure 7.13	Comparison of Midspan Moment vs. Twist for 20ga01.unst.no (South Girder).....	94
Figure 7.14	Midspan Moment vs. Twist Data for 20ga01.hio Tests (North Girder)	96
Figure 7.15	Midspan Moment vs. Twist Data for 20ga01.hio Tests (South Girder)	96
Figure 7.16	Comparison of Midspan Moment vs. Twist for 20ga01.st8ft.no & 20ga01.st8ft.hio (North Girder)	97
Figure 7.17	Comparison of Midspan Moment vs. Twist for 20ga01.st8ft.hio (North Girder).....	97

Figure 7.18	Comparison of Midspan Moment vs. Twist for 20ga01.st8ft.hio (South Girder).....	98
Figure 7.19	Comparison of Midspan Moment vs. Twist for 20ga01.st16ft.hio (North Girder).....	98
Figure 7.20	Comparison of Midspan Moment vs. Twist for 20ga01.st16ft.hio (South Girder).....	99
Figure 7.21	Comparison of Midspan Moment vs. Twist for 20ga01.st24ft.hio (North Girder).....	99
Figure 7.22	Comparison of Midspan Moment vs. Twist for 20ga01.st24ft.hio (South Girder).....	100
Figure 7.23	Comparison of Midspan Moment vs. Twist for 20ga01.unst.hio (North Girder).....	101
Figure 7.24	Comparison of Midspan Moment vs. Twist for 20ga01.unst.hio (South Girder).....	101
Figure 7.25	Midspan Moment vs. Twist Data for 20ga02.no Tests (North Girder)	103
Figure 7.26	Midspan Moment vs. Twist Data for 20ga02.no Tests (South Girder)	103
Figure 7.27	Comparison of Midspan Moment vs. Twist for 20ga02.st8ft.no (North Girder).....	104
Figure 7.28	Comparison of Midspan Moment vs. Twist for 20ga02.st8ft.no (South Girder).....	104
Figure 7.29	Comparison of Midspan Moment vs. Twist for 20ga02.st16ft.no (North Girder).....	105
Figure 7.30	Comparison of Midspan Moment vs. Twist for 20ga02.st16ft.no (South Girder).....	105
Figure 7.31	Comparison of Midspan Moment vs. Twist for 20ga02.st24ft.no (North Girder).....	107
Figure 7.32	Comparison of Midspan Moment vs. Twist for 20ga02.st24ft.no (South Girder).....	107
Figure 7.33	Comparison of Midspan Moment vs. Twist for 20ga02.st16ft.no, 20ga02.st16ft.hio and 20ga01.st16ft.hio Tests (North Girder).....	108
Figure 7.34	Comparison of Midspan Moment vs. Twist for 20ga02.st16ft.no, 20ga02.st16ft.hio and 20ga01.st16ft.hio Tests (North Girder).....	108
Figure 7.35	Comparison of Midspan Moment vs. Twist for 20ga02.st16ft.hio (North Girder).....	109
Figure 7.36	Comparison of Midspan Moment vs. Twist for 20ga02.st16ft.hio (South Girder).....	109
Figure 7.37	Comparison of Midspan Moment vs. Twist for 20ga02.st16ft.hio to Determine the Offset of the Applied Load (North Girder).....	110
Figure 7.38	Comparison of Midspan Moment vs. Twist for 20ga02.st16ft.hio to Determine the Offset of the Applied Load (South Girder).....	110
Figure 7.39	Photo of Failure of the Deck to Support Angle Connection.....	111
Figure 7.40	Midspan Moment vs. Total Twist / Initial Twist Test Data for 20ga02.st16ft Failure Test (North Girder).....	113
Figure 7.41	Midspan Moment vs. Total Twist / Initial Twist Test Data for 20ga02.st16ft Failure Test (South Girder).....	113
Figure 7.42	Photo of Deformed Support Angle after 20ga02.st16ft Failure Test.....	114

Figure 7.43	Comparison of Midspan Moment vs. Total Twist / Initial Twist Test Data for 20ga02.st16f Failure Test (North Girder)	115
Figure 7.44	Comparison of Midspan Moment vs. Total Twist / Initial Twist Test Data for 20ga02.st16f Failure Test (South Girder)	115
Figure 7.45	Distribution of Brace Moments along Girder Length.....	116
Figure 7.46	Comparison of Midspan Moment vs. Twist Test Data for 20ga02.st16f Failure Test (North Girder).....	117
Figure 7.47	Comparison of Midspan Moment vs. Total Twist Test Data for 20ga02.st16f Failure Test (South Girder).....	117
Figure 7.48	Comparison of Midspan Moment vs. Total Twist / Initial Twist Test Data for 20ga02.st16f and 20ga03.unst Failure Tests (North Girder).....	118
Figure 7.49	Comparison of Midspan Moment vs. Total Twist / Initial Twist Test Data for 20ga02.st16f and 20ga03.unst Failure Tests (South Girder).....	119
Figure 8.1	Comparison of FEA Results and Deck Component from Eq. (8.2) (Section #3, Third Point Loading).....	124
Figure 8.2	Comparison of FEA Results and Deck Component from Eq. (8.2) (Section #3, Uniformly Distributed Load)	125
Figure 8.3	Distribution of 20ft Spaced Stiffening Angles (Plan View)	126
Figure 8.4	Comparison of FEA Results and Deck Component from Eq. (8.2) (W18x119).....	126
Figure 8.5	Comparison of FEA Results and Deck Component from Eq. (8.2) (W18x71)	127
Figure 8.6	Comparison of FEM Results and Deck Component from Eq. (8.2) (Section #4, Unbraced).....	128
Figure 8.7	Comparison of FEM Results and Deck Component from Eq. (8.2) (Section #4, Midspan Torsional Brace).....	128
Figure 8.8	Comparison of FEA Results and Deck Component from Eq. (8.2) (Section #5, Midspan Torsional Brace).....	129
Figure 8.9	Comparison of FEA Results and Deck Component from Eq. (8.2) (Section #5, Third Point Torsional Braces).....	130
Figure 8.10	Moment vs. Twist Behavior for W18x119	131
Figure 8.11	Distribution of Brace Moments along Girder Length (W18x119)	132
Figure 8.12	Moment vs. Twist Behavior for W18x71	132
Figure 8.13	Distribution of Brace Moments along Girder Length (W18x71)	133
Figure 9.1	Plan view of bridge for Design Example A.....	137
Figure 9.2	Plan view of bridge for Design Example B	141

List of Tables

Table 2.1	Design m Values for Eq. (2.14)	19
Table 3.1	Parameters for Cross Sections Studied	28
Table 3.2	Doubly-Symmetric Sections	29
Table 3.3	Singly-Symmetric Section	29
Table 5.1	Shear Test Results for 18 ga. PMDF Specimens	65
Table 5.2	Shear Test Results for 16ga PMDF Specimens	67
Table 5.3	Shear Test Results for 20ga PMDF Specimens	67
Table 5.4	Shear Test Results for 20ga 18ga and 16ga PMDF Specimens.....	68
Table 6.1	18ga Tests Unstiffened, Comparison of Laboratory and FEA Results.....	76
Table 6.2	16ga Unstiffened Tests, Comparison of Laboratory and FEA Results.....	76
Table 6.3	20ga(01) Unstiffened Tests, Comparison of Laboratory and FEA Results....	76
Table 6.4	20ga(02) Unstiffened Tests, Comparison of Laboratory and FEA Results....	77
Table 6.5	20ga(03) Unstiffened Tests, Comparison of Laboratory and FEA Results....	77
Table 6.6	18ga Stiffened 8ft Tests, Comparison of Laboratory and FEA Results	78
Table 6.7	16ga Stiffened 8ft Tests, Comparison of Laboratory and FEA Results	78
Table 6.8	20ga(01) Stiffened 8ft Tests, Comparison of Laboratory and FEA Results...	78
Table 6.9	20ga(02) Stiffened 8ft Tests, Comparison of Laboratory and FEA Results...	79
Table 6.10	18ga Stiffened 16ft Tests, Comparison of Laboratory and FEA Results	80
Table 6.11	16ga Stiffened 16ft Tests, Comparison of Laboratory and FEA Results	80
Table 6.12	20ga(01) Stiffened 16ft Tests, Comparison of Laboratory and FEA Results.	80
Table 6.13	20ga(02) Stiffened 16ft Tests, Comparison of Laboratory and FEA Results.	81
Table 6.14	18ga Stiffened 24ft Tests, Comparison of Laboratory and FEA Results	81
Table 6.15	16ga Stiffened 24ft Tests, Comparison of Laboratory and FEA Results	82
Table 6.16	20ga(01) Stiffened 24ft Tests, Comparison of Laboratory and FEA Results.	82
Table 6.17	20ga(02) Stiffened 24ft Tests, Comparison of Laboratory and FEA Results.	82
Table 6.18	Properties of the FEA Elements.....	83
Table 8.1	Design m Values for Eq. (8.1)	134
Table 8.2	Design k Values for Eq. (8.4)	135

Chapter 1

Introduction

1.1 Research Overview and Objectives

Permanent metal deck forms (PMDF) are commonly used to support the wet concrete during construction in both the building and bridge industries. Figure 1.1 shows the forms that are commonly used in the bridge industry. Before the concrete cures and composite behavior between the concrete slab and steel girder is achieved, the girders must carry the entire construction load.



Figure 1.1 Metal Deck Forms viewed from the underside of a Bridge

The construction load usually consists of the weights of the steel girders and wet concrete, the formwork, and the construction live loads such as the personnel and equipment necessary to cast the concrete slab. During this critical stage, lateral-torsional buckling is often the limit state that controls the capacity of bridge girders. Reducing the

girder's laterally unbraced length can increase the buckling capacity. This is accomplished by providing bracing at either discrete locations or continuously along the girder span. Traditional discrete bracing systems for steel bridge girders often consist of cross-frames or diaphragms spaced along the length of the bridge. In past AASHTO (American Association of State Highway and Transportation Officials) specifications, the maximum spacing between cross-frames and diaphragms was limited to 25 feet. The spacing limit was removed in the AASHTO LRFD (Load and Resistance Factor Design) Specification, primarily due to fatigue problems that were frequently found around the brace locations. These fatigue problems have been documented in previous studies such as TxDOT (Texas Department of Transportation) research report TX 92/1313 1-F. Cross-frames and diaphragms can also complicate girder fabrication and erection leading to increased construction costs. For these reasons, alternative bracing systems are of interest.

Although the building industry has long relied on the in-plane strength and stiffness of light gage metal sheeting to prevent lateral-torsional buckling, AASHTO does not currently permit PMDF to be considered for bracing in steel bridge girders. The primary difference between the formwork utilized in the building and bridge industries are the connection details that are employed between the formwork and the steel girders. PMDF in the bridge industry are typically connected to the girders using an eccentric connection, while the forms in the building industry are often connected directly to the top flange. The eccentric connection in the bridge industry can substantially reduce the in-plane stiffness of the forms. The connection details will be discussed in more detail later in this chapter.

In the building industry, forms are usually modeled as shear diaphragms that provide continuous warping restraint to the girder top flanges. However, previous studies have shown that modeling PMDF as a shear diaphragm can underestimate the actual capacity of PMDF systems and lead to relatively large brace forces (Helwig 1994 "Lateral bracing of Bridge Girders by Metal Deck Forms" PhD. Dissertation, University of Texas at Austin; Helwig and Yura 2003 "Strength requirements for diaphragm bracing of beams" draft manuscript to be submitted; and Soderberg 1994 "Strength and Stiffness of Stay-in-Place Metal Deck Form Systems" MS thesis, Univ. of Texas at Austin). In reality, the bracing provided from metal sheeting comes from a combination of in-plane, shear and flexural contributions. One of the goals of this investigation was to improve the understanding of the actual bracing behavior of PMDF systems and potentially isolate the shear and flexural contributions of deck forms.

The primary difference between forms in the building and bridge industries is the method of connection between the forms and girders. Connection details for PMDF in the bridge industry often involve eccentricities that reduce the system stiffness and strength. Another goal of this research was to develop a practical and economical method to improve the stiffness and strength of existing PMDF connection details.

The purpose of this study was to enhance the understanding of the bracing behavior of PMDF while improving connection details that are utilized on the forms in bridge applications. The investigation included both laboratory and computational studies. Experimental tests in a shear frame and full-scale lateral displacement tests using a twin girder set-up with a 48 ft. span were performed on PMDF systems with and without modified connection details. Results from these laboratory experiments were then compared to a finite element analysis (FEA) to insure proper modeling of the deck system. The FEA models were then used to develop a more accurate model of PMDF bracing behavior.

1.2 Industry Applications for PMDF

Permanent metal deck forms (PMDF) have a substantial amount of stiffness and strength in the plane of the sheeting that can provide bracing to the beams or girders to which they are attached. Metal deck form systems are commonly relied upon for beam bracing in the building industry. For these bracing applications the forms have traditionally been modeled as a shear diaphragm that restrains the warping deformation of the top flange of the beams to which they are attached (Figure 1.2). Although the building industry has long relied on the in-plane capacity of light gage metal sheeting, AASHTO does not currently permit PMDF to be considered for bracing in steel bridge girders. The reluctance by the bridge industry to consider PMDF as a reliable bracing element stems from the flexible connection details between the girders and the deck forms. The following two sections will highlight the primary differences between the forms utilized in the building and bridge industries.

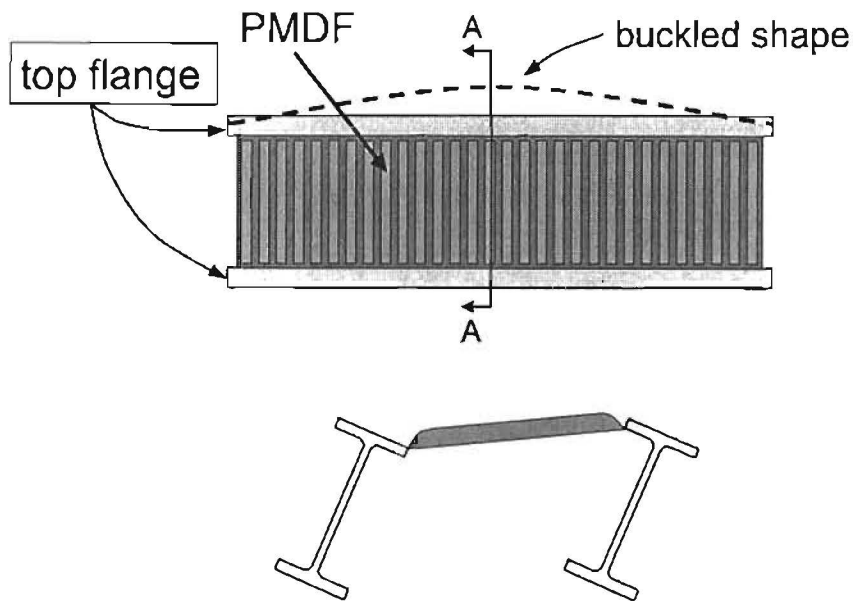


Figure 1.2 PMDF as Beam Bracing

1.2.1 Building Applications

In the building industry, shear diaphragms in the roof or flooring system are often treated similar to short, deep beams that help resist lateral deformations from wind loads. The forms are also routinely relied upon for providing stability bracing to the beams or columns to which they are attached. Figure 1.3 shows a typical PMDF panel arrangement for building applications in which the forms are often continuous over the tops of the beams.

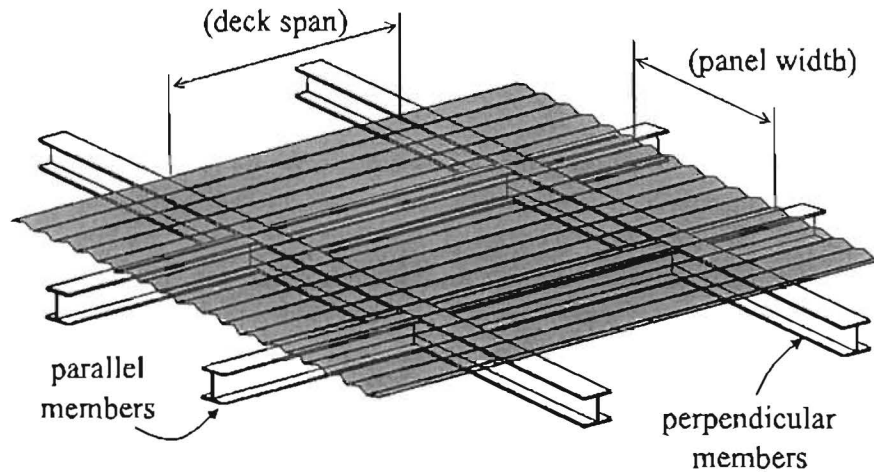


Figure 1.3 Deck Form Arrangement for Building Applications

In these applications, the forms are typically attached directly to the top flange by welding shear studs directly through the forms or by using puddle welds or mechanical fasteners. The connections directly between the main members and the PMDF efficiently harness the large stiffness of the deck forms.

1.2.2 Bridge Applications

The formwork that is utilized in the bridge industry differs substantially from the formwork that is utilized in the building industry. Figure 1.4 illustrates a PMDF panel arrangement for a typical bridge application. Instead of being continuous over the tops of the beams or girders, the deck forms span between adjacent girders. The ends of the corrugations of each sheet are closed to provide a seal for the concrete. The closed ends of the corrugations tend to stiffen the forms. The individual sheets tend to be stiffer than comparable building forms, in which the stiffness is reduced due to warping deformations of the corrugations.

In addition, whereas some applications in the building industry may have a deck panel supported on all four sides, conventional bridge decking provides support from the girder flanges on only two sides. Rather than passing over the top flanges, bridge deck form sheets are fastened to cold-formed angles (support angles) that are attached to the girders as shown in Figure 1.4. The support angles allow the contractor to adjust the

form elevation to account for changes in flange thickness, super-elevation and differential camber between adjacent girders. Although the adjustable support angle connection provides some convenience with constructability issues, the eccentricities that are often encountered can substantially reduce the stiffness and strength of deck form system. As will be discussed in Chapter 2, stability bracing systems must possess adequate stiffness and adequate strength to provide suitable bracing. Failures in the bracing system can result if the system has either inadequate stiffness or strength. The bracing behavior of PMDF in the bridge industry can be substantially enhanced by providing better connection details that improve the connection details

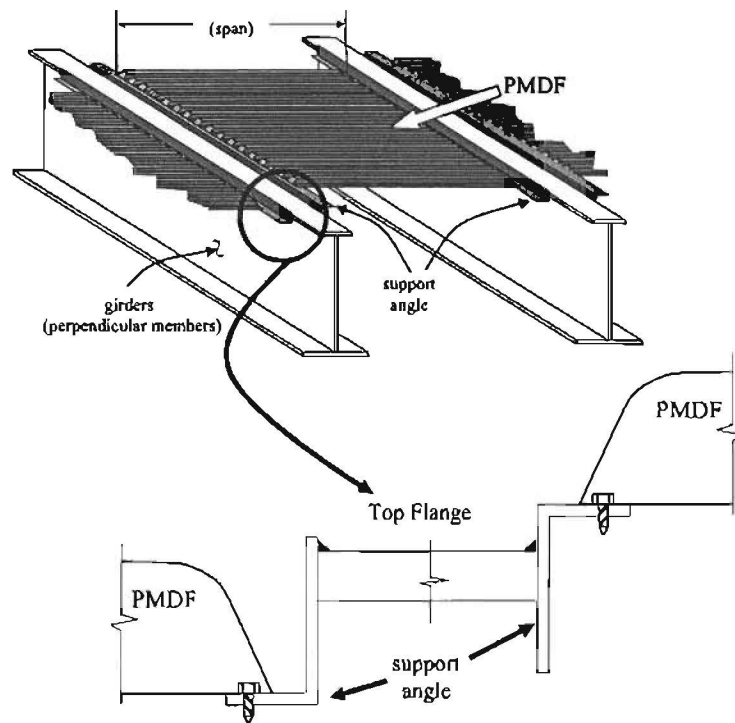


Figure 1.4 Deck Form Arrangement for Bridge Applications

1.3 Overview

This report documents the findings from a research investigation on the bracing behavior of PMDF systems utilized in the bridge industry. The study included both laboratory testing and finite element analytical (FEA) models. Metal deck forms from two different manufactures were tested. The metal gages that were considered include 22 gage, 20 gage, 18 gage, and 16 gage. The testing program included both shear tests as well as full size lateral load and buckling tests on a twin girder system with PMDF for bracing. A variety of details were tested. Results from the laboratory tests were compared with FEA solutions as a precursor to parametric studies.

The report is divided into ten chapters. Following this introduction, Chapter 2 presents background information that is necessary to understand the bracing behavior of PMDF systems. Chapter 3 presents an overview of the finite element model that was used for the PMDF systems. The models that were developed were used for PMDF systems with both conventional connections as well as newly proposed connection details. Chapter 4 provides an overview of the two test setups that were designed and fabricated for the laboratory investigations. Results from the shear tests are presented in Chapter 5, while Chapter 6 presents the results from the lateral load tests using the twin girder setup. Results from the twin girder buckling tests with PMDF for bracing are presented in Chapter 7. Chapters 6 and 7 also include comparisons between the FEA models and the laboratory test results. After getting good correlation between the FEA results and the laboratory tests, parametric studies were conducted on girder systems with PMDF for bracing. These results are presented in Chapter 8. A design example is presented in Chapter 9. Finally, a summary of the study and findings is presented in Chapter 10.

Chapter 2

Background

2.1 Introduction

This chapter provides background information on lateral torsional buckling of beams and bracing systems. Following this introductory section, some of the basic factors affecting the lateral torsional buckling behavior will be discussed for doubly-symmetric and singly-symmetric sections. Effects of moment gradient load height will also be discussed. Some of the general factors affecting stability bracing will then be discussed followed by a summary of the background information on bracing by metal deck forms.

2.2 Lateral Torsional Buckling

Lateral-torsional buckling of beams is a failure mode that generally involves a lateral displacement of the compression flange accompanied by a twist of the girder cross-section as illustrated in (Figure 2.1). The buckled shape of the cross-section that is often shown is similar to the cross-section in Figure 2.1, in which the center of twist lies below the cross-section.

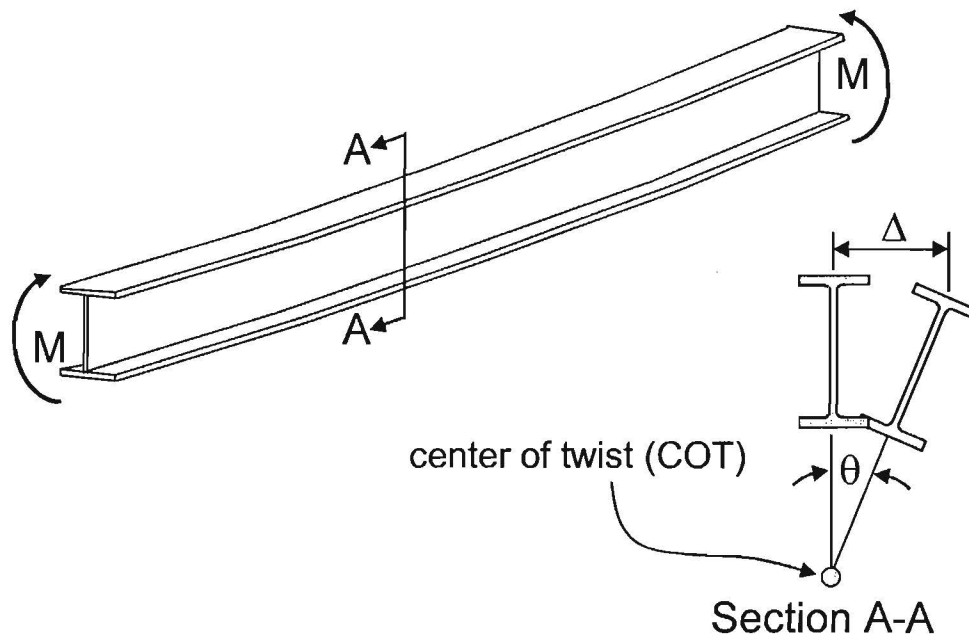


Figure 2.1 Buckling Deformations on Girder Cross Section

The center of twist is the point that the weak axis of unbuckled girder and the buckled girder intersect. Although the center of twist for the case of uniform moment often lies below the cross-section, for other load cases the COT may lie within the depth

of the beam. The location of the COT has a significant affect on the effectiveness of bracing.

The elastic solution for the lateral torsional buckling capacity of doubly-symmetric cross sections subjected to uniform moment can be evaluated using the expression that was derived by Timoshenko and is given in the following expression:

$$M_g = \frac{\pi}{L_b} \sqrt{EI_y GJ + \left(\frac{\pi E}{L_b}\right)^2 I_y C_w} \quad (2.1)$$

In this equation; L_b = distance between points of zero twist, E = Young's modulus, I_y = weak axis moment of inertia, J = torsional constant, G = bulk modulus and C_w = section warping constant.

For bridge girders, composite action between the steel section and the concrete deck is usually employed in the finished bridge. The plastic neutral axis (PNA) of the composite section is typically located near the top flange of the section as shown in Figure 2.2.

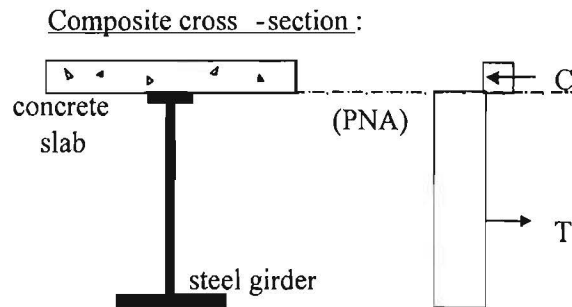


Figure 2.2 Plastic Stress Distribution

Therefore the contribution of the top flange of the steel girder to the composite girder strength is relatively insignificant in the finished bridge. Because the top flange plays little role in the ultimate capacity of the system, a smaller top flange is often utilized resulting in a section with a single plane of symmetry. Figure 2.3 shows the typical shape of the steel cross-section utilized in steel bridge girders.

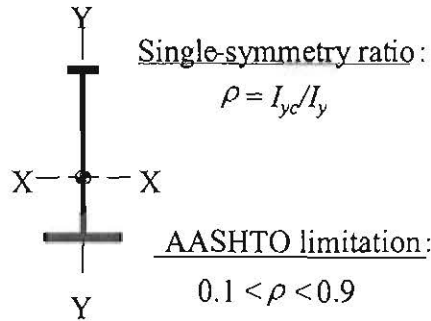


Figure 2.3 Singly-Symmetric Cross Section

The degree of mono-symmetry can often be determined from the single symmetry ratio, $\rho = I_{yc} / I_y$, where; I_{yc} and I_y are the compression flange and the cross-section moments of inertia about the Y-Y axis respectively. For a doubly-symmetric section the value of ρ is 0.5. For sections with a smaller compression flange the ρ -value will be less than 0.5. For sections with a larger compression flange the ρ -value will be larger than 0.5. A T-section with the flange in tension has a ρ of 0, and a value of 1.0 if the flange is in compression. The AASHTO specification limits bridge girders to $0.1 < \rho < 0.9$.

Although the reduced top flange improves the efficiency of the steel girder in the finished bridge, during construction, the smaller top flange makes the girders susceptible to lateral torsional buckling. The approximate elastic solution for the uniform moment capacity on singly-symmetric cross-sections as given by AASHTO is:

$$M_g = \pi E \left(\frac{I_{yc}}{L_b} \right) \sqrt{0.772 \left(\frac{J}{I_y} \right) + 9.87 \left(\frac{d}{L_b} \right)^2} \quad (2.2)$$

For the AASHTO solution; L_b = distance between points of zero twist, I_{yc} = compression flange moment of inertia, J = torsional constant, E = Young's modulus, and d = depth of the girder. Equations (2.1) and (2.2) produce identical solutions for doubly-symmetric sections.

Equations (2.1) and (2.2) were derived for uniform moment loading. In most problems encountered in practice, the distribution of moment varies along the length of the span. Variable moment is typically advantageous and usually results in larger capacities than predicted by the uniform moment solution. To account for the moment gradient C_b factors are usually applied to the solutions for uniform moment loading. The following C_b expression is applicable to both doubly-symmetric and singly-symmetric sections. (Helwig et. al 1997)

$$C_b = R \left[\frac{12.5 M_{\max}}{(2.5 M_{\max} + 3 M_A + 4 M_B + 3 M_C)} \right] \leq 3 \quad (2.3)$$

Where; M_{max} = maximum moment; M_A and M_C are moments at outer quarter points between bracing; M_B = midspan moment; $R = 1.0$ for single curvature and $(0.5 + 2\rho^2)$ for double curvature. For doubly-symmetric sections the value of R is 1.0 and Eq. (2.3) reduces to the C_b expression that is in the AISC and AASHTO LRFD Specifications.

In most practical applications, the variation in bending moments along the unbraced length are caused by transverse loads applied to the cross-section. If these transverse loads are applied at midheight of the section, the C_b factor presented in Eq. (2.3) will provide good estimates of the buckling capacity. However in many applications, the transverse loads are not applied at midheight, which can have a significant affect on the lateral torsional buckling capacity of the member. Load height effects can be either beneficial or detrimental to the buckling capacity of the girder depending on the location of the transverse load relative to midheight. When loads are applied above midheight, such as at the top flange, the buckling capacity is decreased because the load produces an overturning torque on the cross-section (Figure 2.4a). On the other hand, when loads are applied below midheight such as at the bottom flange, a restoring torque develops that increases the buckling capacity (Figure 2.4b).

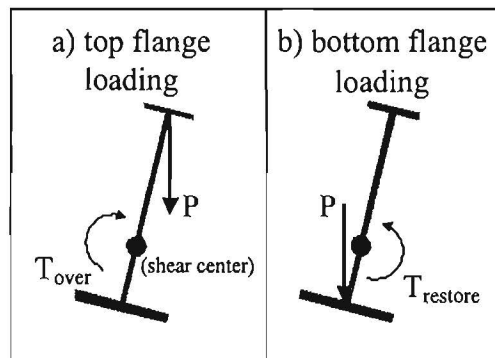


Figure 2.4 Load Height Effects

To approximate the effects of moment gradient and load height, the following modified moment gradient factor can be utilized (Helwig, Todd A.; Frank, Karl H.; and Yura, Joseph A., "Lateral-Torsional Buckling of Singly-Symmetric I-Beams," *ASCE Journal of Structural Engineering*, V. 123, No. 9, Sept. 1997, pp. 1172-1179) :

$$C_b^* = C_b (1.4)^{(2y/d)} \quad (2.4)$$

where; C_b = usual moment gradient factor (Eqn(2.3)), d = depth of girder and y = location of load measured from mid height positively toward the bottom flange. If the load is applied at the bottom flange, the exponent on the constant 1.4 in Eq. (2.4) is +1 so that

the value of C_b^* will simply be 40 % higher than the C_b from Eq. (2.3). If instead the load is applied at the top flange, the C_b^* will be the C_b from Eq. (2.3) divided by 1.4.

2.3 Beam Bracing

There are a number of methods that provide stability bracing to beams, however the majority of beam bracing systems can be categorized as either lateral bracing or torsional bracing. Figure 2.5 shows some of the typical bracing systems that might be employed in bridge systems. The figure shows that most of the conventional bracing systems fit into the category of torsional bracing.

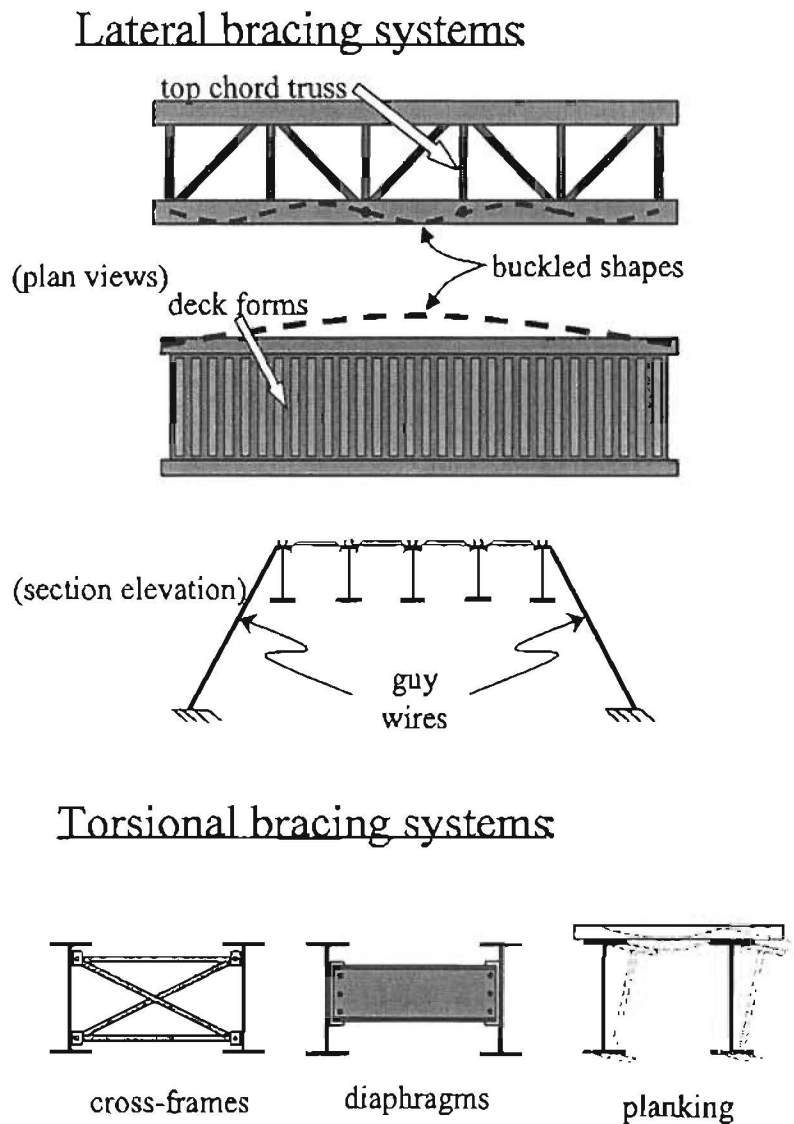


Figure 2.5 Lateral Torsional Beam Bracing Systems

The effectiveness of a bracing system lies in its ability to prevent twist of the cross-section. The location of the center of twist (COT), as shown previously in Figure 2.1 has a significant impact on the effectiveness of lateral bracing systems. Although the COT location is often shown below the girder cross-section, effects such as top flange loading frequently result in buckled shapes with the COT positioned above the bottom flange. Therefore, a lateral brace is most effective when it is located at or near the top flange. Although torsional braces like cross-frames and diaphragms permit lateral displacement, they are effective because they directly prevent twist.

There have been a number of previous investigations on the bracing requirements for stability. Winter (1960), was the first to recognize the dual criteria of both stiffness and strength. He was able to demonstrate the stiffness requirements using a relatively simple model that consisted of rigid links with hinges at the brace locations. Winter's simple model could be used to determine the "ideal stiffness" requirements, which is defined as the stiffness necessary so that a perfectly straight member buckles between the brace points.

If the ideal stiffness is provided in an imperfect structure, the member to be braced will generally not reach a load level corresponding to buckling between the brace points. This is demonstrated in Figure 2.6 using Winter's simple model for a column with a single lateral brace at midheight. The applied load is graphed versus the lateral displacement at the brace location. The applied load has been normalized by P_E , which is the load corresponding to buckling between the brace points. The graphs show that if the ideal stiffness, β_i , is used on the imperfect system, the deformations become very large and the buckling load is not reached. Since brace forces are a direct function of the deformation at the brace point, the brace forces also become very large if the ideal stiffness is used. Figure 2.6 also shows that providing a stiffness larger than the ideal value results in much better behavior. For example, providing a stiffness equal to $2\beta_i$ results in a deformation at the brace point that is equal to the initial imperfection and likewise does a much better job of controlling brace forces. To control deformations and brace forces, the bracing provisions in the AISC LRFD Specification (2001) recommend providing at least $2\beta_i$.

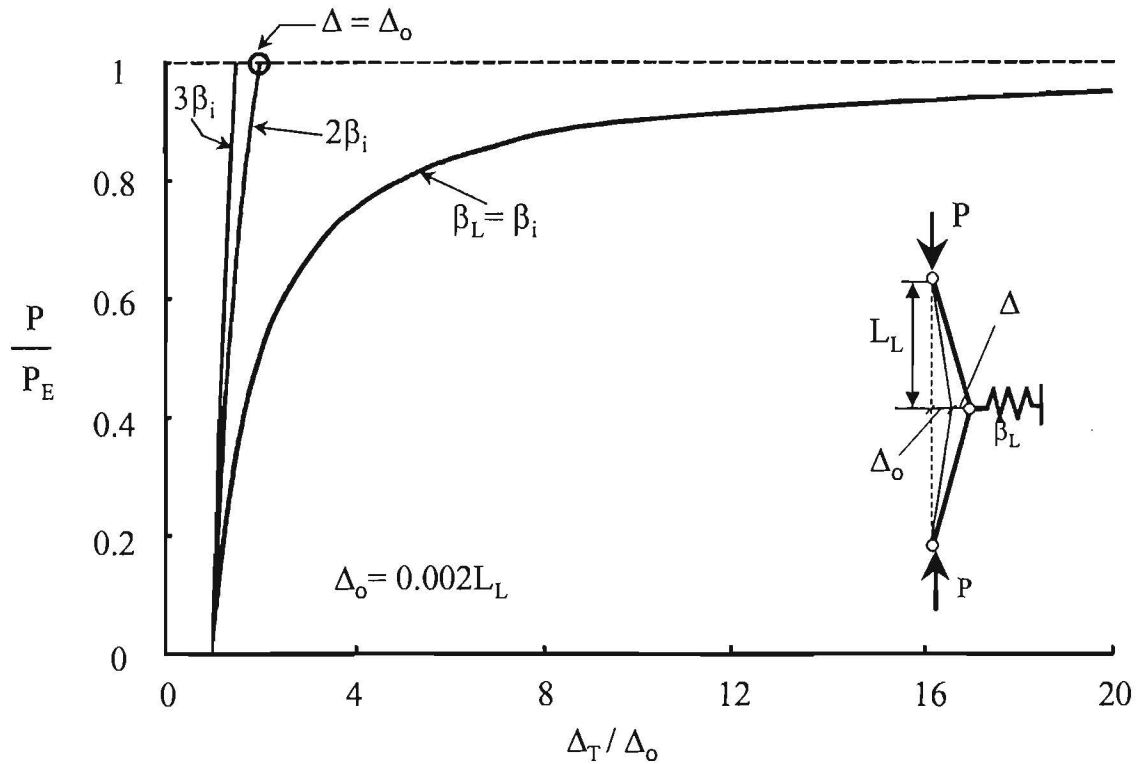


Figure 2.6 *Effect of Brace Stiffness on Deformations using Winter's Model*

Although the results shown in Figure 2.6 focus on column bracing behavior, beam bracing has the same basic behavior. However, beam bracing often appears more complicated than column bracing due to the larger number of factors that affect a beam's buckling behavior such as the effects of moment gradient and load height effects that were discussed earlier in this chapter. A comprehensive summary of the factors that affect discrete beam bracing systems has been presented by Yura (2001).

2.4 Shear Stiffness of PMDF Systems

From a stiffness perspective, the material property of interest in PMDF for bracing purposes is the shear rigidity, Q , which has units of force per unit radian (kN/rad or kip/rad). The following expression relates the shear rigidity to the effective shear stiffness of the PMDF system:

$$Q = G's_d \quad (\text{kN/rad or kip/rad}) \quad (2.5)$$

where; G' (kip/in-rad or kN/m-rad) = effective modulus of shear rigidity and s_d = tributary width of diaphragm bracing a single girder:

$$s_d = \frac{(s_g - b_{lf})(n-1)}{n} \quad (2.6)$$

In the above expression for the tributary width: n = number of girders in the system; s_g = spacing between girders and b_{lf} = width of the girder top flange. In the building industry, the effective shear modulus, G' , can be determined either using design tables or through laboratory testing. The Steel Deck Institute (SDI – 1995) provides equations and design tables that can be utilized to evaluate the stiffness of various building PMDF systems. Currah (1993) found that the SDI expressions had reasonable agreement with laboratory test results on bridge decking provided the terms for warping deformation in the corrugations were neglected (Currah, R. M., "Shear Strength and Shear Stiffness of Permanent Steel Bridge Deck Forms," M. S. Thesis, The University of Texas at Austin, August 1993). To conduct experiments on the PMDF systems and connections used in the bridge industry, a testing frame similar to that depicted in Figure 2.7 was designed and fabricated.

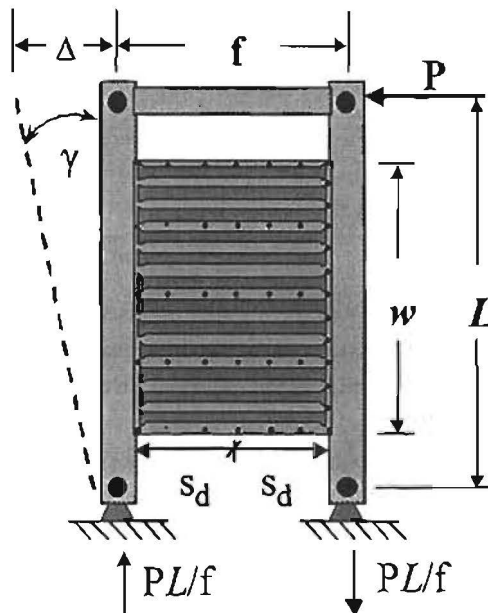


Figure 2.7 Shear Test Frame with PMDF Specimen

Parameters that are shown in Figure 2.7 include: γ = shear strain; Δ = lateral deflection at the end of the testing frame; P = lateral load; L = length of the testing frame; f = spacing between test frame support beams and w = PMDF specimen panel width. The usual definition for the shear modulus, G , is the shear stress divided by the shear strain. However, since the shear stress versus shear strain relationship of corrugated metal sheeting is generally not a linear function of the material thickness, (SDI-1995), an "effective" shear stress is utilized that is not dependent on the thickness of the form (Luttrell, L. D., *Steel Deck Institute Diaphragm Design Manual*, 2nd Ed., Canton, Ohio,

1995). To distinguish the effective modulus a “prime” is usually incorporated into the variable, G' .

By employing the ‘method of sections’ on a portion of the test frame shown in Figure 2.8, it can be seen that in order to satisfy equilibrium of forces there must be a total internal shear, $V=PL/f$. The effective shear stress in Figure 2.8(a) can then be calculated as, $\tau' = V/w$, which has units of force per unit length (kN/m or k/in). The corresponding shear strain is, $\gamma = \Delta/L$.

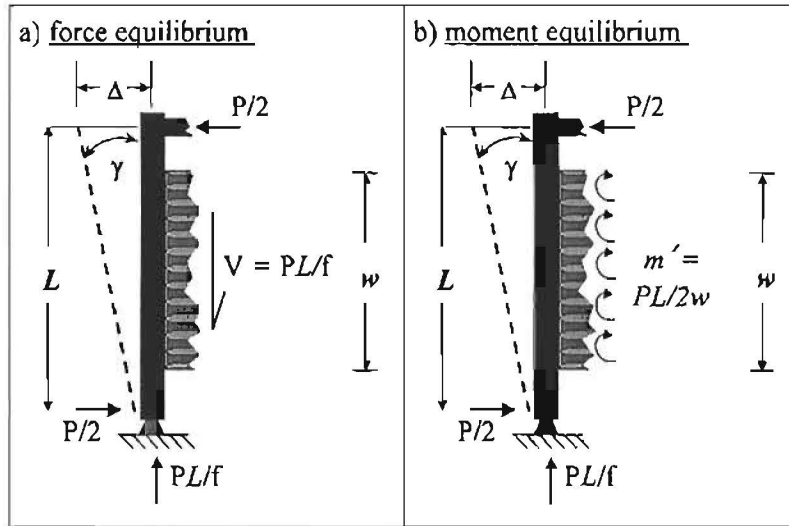


Figure 2.8 Internal Forces on a PMDF Specimen

The effective shear modulus can then be determined in the following manner:

$$G' = \frac{\tau'}{\gamma} \text{ (kN/(mm-rad) or kip/(in-rad))} \quad (2.7)$$

The above definition of the diaphragm shear stiffness is based solely on the equilibrium of forces. If equilibrium is to be completely satisfied, then moments about the same section in Figure 2.8(b) must also be considered. By summing moments about the support, it is evident that there must exist an equivalent distributed moment over the width of the panel, $m' = PL/2w$, which has units of moment per unit length; i.e., (kN-mm)/mm or (kip-in)/in. Then an effective rotational stiffness of this system can be calculated as:

$$M' = \frac{m'}{\gamma} \text{ (kN-mm)/(mm-rad) or (kip-in)/(in-rad)} \quad (2.8)$$

This effective rotational stiffness of shear diaphragms is not a traditional property that is recognized by specifications on steel deck design. It has been introduced in this study to help identify all possible forces acting on PMDF systems.

2.5 Shear Strength of PMDF Systems

Figure 2.9 depicts a typical stress versus strain curve for a PMDF shear test conducted in a shear test frame like the one in Figure 2.7.

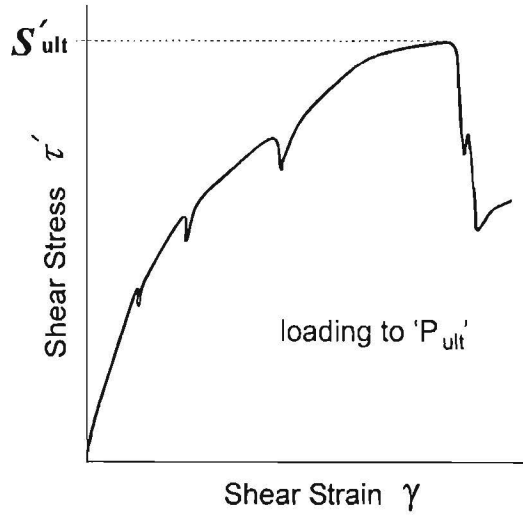


Figure 2.9 PMDF Stress vs. Strain Behavior

In the previous section, it was shown that the average effective stress along the panel width at any stage of loading is, $\tau' = PL/fw$. When the system reaches its ultimate capacity, the applied load becomes its maximum sustained value, P_{ult} . For this study, the ultimate effective shear capacity of the diaphragm is computed as:

$$S'_{ult} = \frac{(P_{ult}L)}{(fw)} \quad (kN/m \text{ or } k/in) \quad (2.9)$$

Similarly, the ultimate effective rotational strength of the system can be defined as the equivalent distributed moment along the PMDF panel width at the maximum applied load. In the interest of quantifying fastener forces in bracing applications, this ultimate effective rotational capacity will be calculated as:

$$M'_{br} = \frac{(P_{ult}L)}{(2w)} \quad (kN-mm)/mm \text{ or } (kip-in)/in \quad (2.10)$$

The failure mode of PMDF panel systems is often characterized by the fracture of fasteners or bearing deformations on the deck at a fastener location. It can be assumed for simplicity that when bearing deformations occur along a side-lap seam and adjacent panels begin to separate, there is a linear distribution of forces at the end fasteners along the support angle as shown in Figure 2.10.

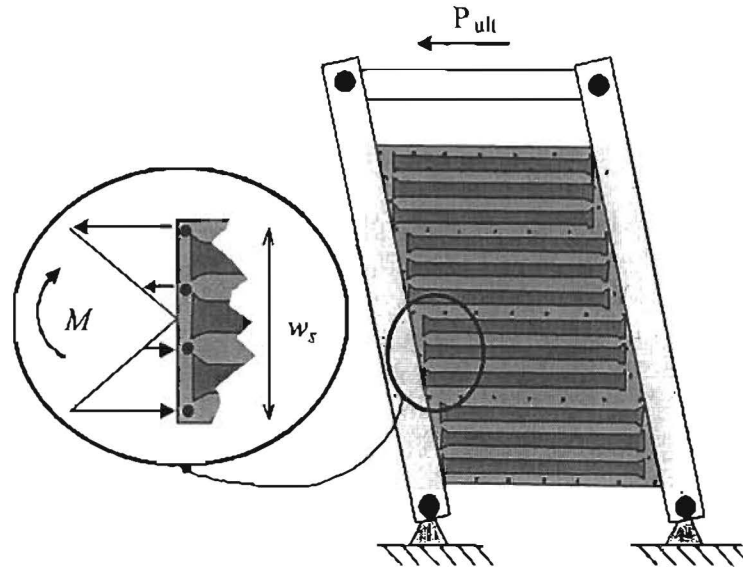


Figure 2.10 Fastener Force Distribution Assumption

This distribution of forces may be resolved into an equivalent moment, $M = M'_{br}(w_s)$, where w_s = width of an individual PMDF sheet.

2.6 Diaphragm Braced Beams

There have been a number of previous research investigations on the bracing behavior of shear diaphragms. The most significant work on diaphragm bracing was performed at Cornell during the 1960's and early 1970's. A closed-form solution for beams with uniform moment loading and bracing by a shear diaphragm resulted from these studies and was presented by Errera and Apparao (1976, "Design Of I-shaped beams with diaphragm bracing" J. Struct. Div., ASCE, 102(4), 769-781). The following energy-based solution was derived by assuming a sinusoidal lateral displacement and twist of the cross-section along the girder length:

$$M_{cr} = \sqrt{\left(\frac{\pi^2 EI_y}{L^2}\right) \left(\frac{\pi^2 EC_w}{L^2} + GJ + Qe^2\right)} + Qe \quad (2.11)$$

where: M_{cr} = buckling moment of shear diaphragm braced girder; E = modulus of elasticity; I_y = weak-axis moment of inertia; L = spacing between points of zero twist on the beam; C_w = warping coefficient of beam; Q = shear rigidity of the diaphragm and e = distance from center of gravity of the girder to plane of the shear diaphragm.

Errera and Apparao (1976, "Design Of I-shaped beams with diaphragm bracing" J. Struct. Div., ASCE, 102(4), 769-781) as well as Nethercot and Trabair (1975, "Design of diaphragm-braced I-beams" Struct. Div., ASCE, 101(10), 2045-2061) suggested that a simple approximation for the buckling capacity for a girder braced by a shear diaphragm

on the top flange and uniform moment loading can be obtained with the following expression.

$$M_{cr} = M_g + 2Qe \quad (2.12)$$

M_g is the buckling capacity of the girder with no deck for bracing, while Q and e have been defined in Eq. (2.11). Figure 2.11 shows a comparison of Eq. (2.11) and Eq. (2.12) for a W30x90 with a span to depth ratio, $(L/d) = 20$, and uniform moment loading with a shear diaphragm for bracing (Helwig, T. A. and Frank, K. H. (1999), "Stiffness Requirements for diaphragm bracing of beams," J. of Structural Engineering, ASCE, Vol. 125, No. 11, pp. 1249-1256). The graph shows that the simple expression in Eq. (2.12) has excellent agreement with the energy-based solution. The curves from the two expressions are nearly coincident.

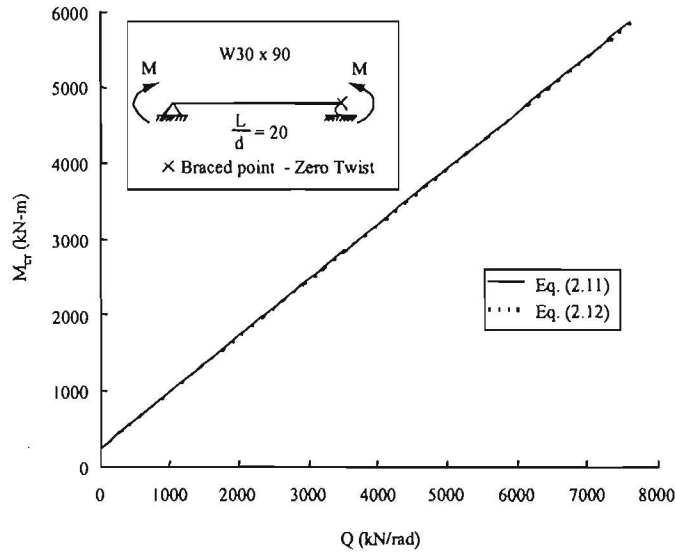


Figure 2.11 Comparison of Eq. (2.11) and Eq. (2.12)

The expressions given in Eq. (2.11) and Eq. (2.12) are valid for girders subject to uniform moment. Lawson and Nethercot (1985 "Lateral Stability of I-beams Restrained by Profiled Sheeting" The Struct. Engr., London, 63B(1), 3-13) presented the following expression for beams with transverse loading.

$$M_{cr} = C_b d \left[\frac{-P_e g + Q(1-g)}{2} + \sqrt{\left(\frac{-P_e g + Q(1-g)}{2} \right)^2 - \frac{Q^2}{4} + \left(\frac{P_e}{2} + \frac{Q}{2} \right) \left(\frac{P_e}{2} + 2P_T + \frac{Q}{2} \right)} \right] \quad (2.13)$$

where: d = depth of the girders; P_e = weak axis Euler load = $(\pi^2 EI_y / L^2)$; C_b = moment gradient factor and g = load height factor. The term P_T is given by, GJ/d^2 , where G = shear modulus of the beam material and J = torsional constant of the beam. The C_b factor

outside the square brackets accounts for moment gradients, while the factor g accounts for load height effects. Helwig (1994 “Lateral bracing of Bridge Girders by Metal Deck Forms”, PhD. Dissertation, University of Texas at Austin) compared Eq. (2.13) with results from a parametrical finite element study and found the equation tended to overestimate the bracing behavior of shear diaphragm bracing. In addition, a solution of the form shown in Eq. (2.13) is relatively complicated for design applications, particularly since a solution of the form shown in Eq. (2.12) had such good agreement with the energy based solution. Therefore, pursuing a solution of the form in Eq. (2.12) is much more desirable for design applications due to its simplicity. Another attractive feature of Eq. (2.12) is that it allows the designer to select a suitable solution for the girder buckling capacity, M_g . This is particularly attractive for singly-symmetric sections in which there are a variety of approximate solutions available.

Helwig and Frank (1999 “Stiffness Requirements for diaphragm bracing of beams,” J. of Structural Engineering, ASCE, Vol. 125, No. 11, pp. 1249-1256) presented finite element results that demonstrate the effects of moment gradient and load height on the bracing behavior of shear diaphragms. They modified Eq. (2.12) to be applicable to general loading conditions and produced the following expression to approximate the ideal stiffness requirements:

$$M_{cr} = C_b^* M_g + mQd \quad (2.14)$$

where: C_b^* = moment gradient factor that considers load height effects; m = constant that depends on loading and d = depth of the section. M_{cr} , M_g and Q are as defined previously.

Helwig and Frank demonstrated that, $e = (d/2)$, for both singly and doubly-symmetric girders is a good approximation. For uniform moment the value of, $m =$ unity, and Eq. (2.14) reduces to the same expression given in Eq. (2.12). In most practical applications, the transverse loading on beams is applied at the top flange. For cases with uniformly distributed loads applied at the top flange, m can be obtained from Table 2.1.

Table 2.1: Design m Values for Eq. (2.14)

Web Slenderness	Top Flange Loading w/o Midspan Torsional Brace (Helwig and Frank 1999)	Top Flange Loading with Midspan Torsional Brace (Helwig and Yura manuscript – 2003)
$h / t_w < 60$	0.5	0.85
$h / t_w > 60$	0.375	0.64

The references to torsional bracing in Table 2.1 apply to the presence of intermediate cross-frames or diaphragms. The values for m are also applicable for concentrated loads applied at the top flange; however, if the load point is also a braced point (no twist), $m = 1.0$ may be used. Web buckling due to bending or shear stresses needs to be considered when bracing girders with slender webs. The buckling capacity for diaphragm-braced beams should be limited to the lowest value based on the limit states of web bend buckling, shear buckling or lateral-torsional buckling given by Eq. (2.14).

The expression of Eq. (2.14) can be rearranged to solve for the ideal effective shear modulus in terms of the maximum moment, M_u , and the buckling capacity of the girder without diaphragm bracing, $C_b^* M_g$, between points of zero twist:

$$G'_{ideal} = \frac{(M_u - C_b^* M_g)}{s_d m d} \quad (2.15)$$

The expressions presented so far represent the capacity for perfectly straight beams braced by a shear diaphragm. For a particular maximum moment, the diaphragm stiffness derived from these expressions would represent the “ideal stiffness”. Helwig and Yura (2003 “Strength requirements for diaphragm bracing of beams” draft manuscript to be submitted) conducted large displacement finite element analysis (FEA) on girders with initial imperfections. They found that providing four times the ideal stiffness could effectively control deformations and brace forces. For design considerations, Eq. (2.15) becomes:

$$G'_{req'd} = \frac{4(M_u - C_b^* M_g)}{s_d m d} \quad (2.16)$$

The stiffness requirement for the shear diaphragm given in Eq. (2.16) is based on an analysis of beams with an initial twist, $\theta_0 = L/(500d)$, where d = section depth and L is the spacing between cross-frames. Helwig and Yura also found that the strength requirement for shear diaphragm bracing is a function of the span and depth of the beam. If a diaphragm with a stiffness given by Eq. (2.16) is provided, $M'_{req'd}$, the required bracing moment per unit length of the beam can be approximated as follows:

$$M'_{req'd} = 0.0011 \frac{(M_u L)}{d^2} \quad (2.17)$$

where: L = total beam span and d = beam depth. The brace moment given in Eq. (2.17) represents the warping restraint provided to the top flange of the girder per unit length of the span. Eq. (2.17) has the same units as Eq. (2.10), (kN-mm)/mm or (kip-in)/in. The

expression in Eq. (2.17) can be used to determine the forces in the fasteners used to connect the shear diaphragm to the beams. However, in many instances the stresses that would result from the fastener forces predicted by Eq. (2.17) can be large, particularly since the fasteners are relatively small. Although a shear diaphragm model predicts relatively large fastener forces, the magnitude of fastener forces in actual PMDF braced systems are most probably not this high because deck contributions to bracing comes from both shear and flexural behavior.

The purpose of this chapter was to provide a general overview of beam buckling and beam bracing. In addition, this chapter also summarized the historical development of the treatment of diaphragm-braced beams. The expressions presented in this chapter for diaphragm bracing will be utilized as a starting point for the development of design expressions that consider existing PMDF systems as well as systems with proposed connection details.

This page replaces an intentionally blank page in the original.

-- CTR Library Digitization Team

Chapter 3

Finite Element Model

3.1 Overview

The three-dimensional finite element program ANSYS (2002) was used to perform parametric studies on the behavior of steel I-girders braced with permanent metal deck forms (PMDF). Both eigenvalue buckling and large displacement analyses were conducted. An eigenvalue buckling analysis provides a linear-elastic solution that gives the critical buckling load of a system. For bracing problems, the solution establishes the ideal stiffness requirements for the bracing. Because the solution is relatively insensitive to imperfections, the analysis is generally performed on perfect systems. Since there is always an initial imperfection acquainted with the structural members of a system, a non-linear analysis that reflects the effects of geometrical imperfections is required to investigate the effects on the buckling behavior. A large displacement analysis is a non-linear geometrical analysis of an imperfect system that can be used to determine the strength requirements for bracing. The load is applied in increments up to the buckling load. The size of the load steps are typically reduced as the buckling load is approached to account for the nonlinear deformational behavior. The Newton-Raphson approach to solve non-linear problems was employed using ANSYS (2002). At each load step the program performs a number of equilibrium iterations to obtain a converged solution based upon force and deformation tolerance limits. Although nonlinear geometry was considered, all of the analysis was conducted using linear elastic analysis. The assumption of linear elastic materials is generally consistent with the bracing conditions during construction when the PMDF would be relied upon.

The finite element model was developed using the experimental test results outlined in Chapter 6. The model's accuracy was verified in Chapter 7 by comparing large displacement analyses results with the laboratory buckling tests. In Chapter 8 results from parametric investigations including both eigenvalue buckling and large displacement analyses for girders intermediately (between the supports) braced only with PMDF and also with PMDF and intermediate cross frames is presented.

3.2 Finite Element Model

A combination of shell, beam and truss elements was used to model the structural components of the twin-girder system. The cross section of the girders and the transverse stiffeners were modeled using 8-node quadrilateral shell elements that can model both out-of-plane bending and in-plane membrane deformations. The shell elements have six degrees of freedom (DOF) at each node: translations in the x, y and z directions and rotations about the nodal x, y, and z-axes. The input data of the shell elements consists of the thickness and the material properties. Figure 3.1 shows the model of the girder cross section. Two shell elements were used to model both the flanges and the web. Based upon past experiences, these elements generally provide good solutions for aspect ratios

less than approximately 3. Therefore, the aspect ratio was kept below 3 for these elements.

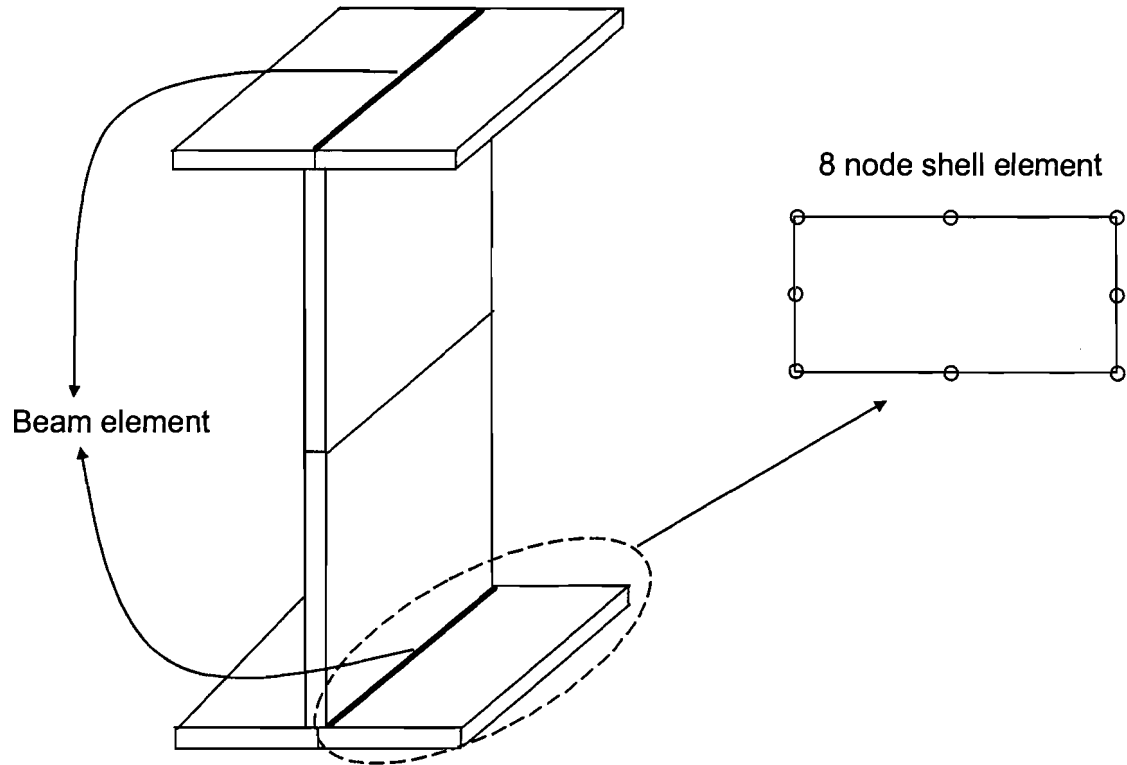


Figure 3.1 Finite Element Model of the Girder Cross Section

Three-dimensional beam elements were used to model the fillets of the rolled section (Figure 3.1), the in-plane flexural contribution of the deck panels, as well as the stiffening angles and the cross frames. These beam elements were 2-node uniaxial elements with tension, compression and bending capabilities. The element has six DOF at each node: translation in the nodal x , y and z directions and rotation about the nodal x , y and z -axes. The input for the beam element consists of the cross sectional area and the moment of inertia about the x - x and y - y axes. The beam elements used to model the fillets were rigidly coupled to the top and bottom of the web, to more accurately model the torsional stiffness of the sections. The beam elements that were used to model the flexural contribution of the deck panels were rigidly coupled to the tip of the top flange.

A shear diaphragm truss panel model similar to that developed by Helwig and Yura (2003) was adopted for this study to model the deck panels spanning between adjacent girders. Figure 3.2 shows an illustration of the truss panel model. These truss panels were built up from three-dimensional truss elements connected to the centerline of the girder top flanges. The truss element is a uniaxial tension-compression element with three DOF at each node: translations in the x , y and z directions. Truss elements cannot model bending or torsional deformations. The input for the truss elements consists of the cross sectional area.

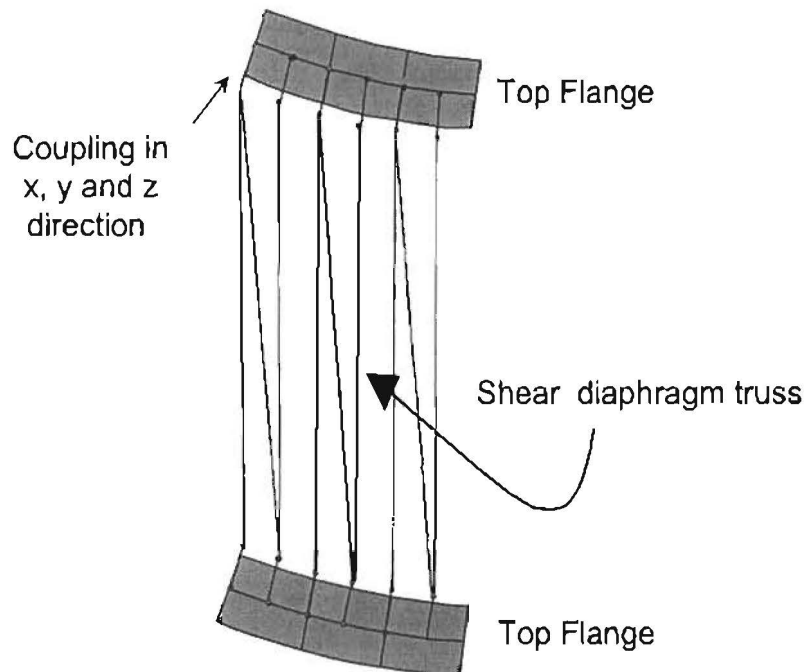


Figure 3.2 Truss Elements used to Simulate the Shear Diaphragm

Another important aspect of this study was to improve the connections between the girder flanges and the PMDF. As will be shown in the following chapters, the recommended detail incorporates stiffening angles that span between the top flanges of adjacent girders. The spacing of the stiffening angles along the girder length is typically in the range of 8 to 20 ft. These stiffening angles are located at the intersection of two adjacent sheets (referred to as a sidelap). The deck is therefore fastened directly to the stiffening angle. A challenging aspect of the FEA studies was to develop a finite element model that reflects the behavior of stiffened PMDF systems. This model was achieved by attaching a stiffening truss system as depicted in Figure 3.3. Two rigid beam elements with pinned ends were used to simulate the stiffening angles to which the stiffening trusses were connected. Results from the laboratory tests were used to size the shear diaphragm truss elements and the stiffening truss elements. The shear diaphragm truss elements were sized using results on the PMDF system with the unstiffened connections. To model the system with the stiffened connections, the area of the shear diaphragm truss elements were the same as determined from the unstiffened tests and the area of the stiffening truss members were determined from the test results.

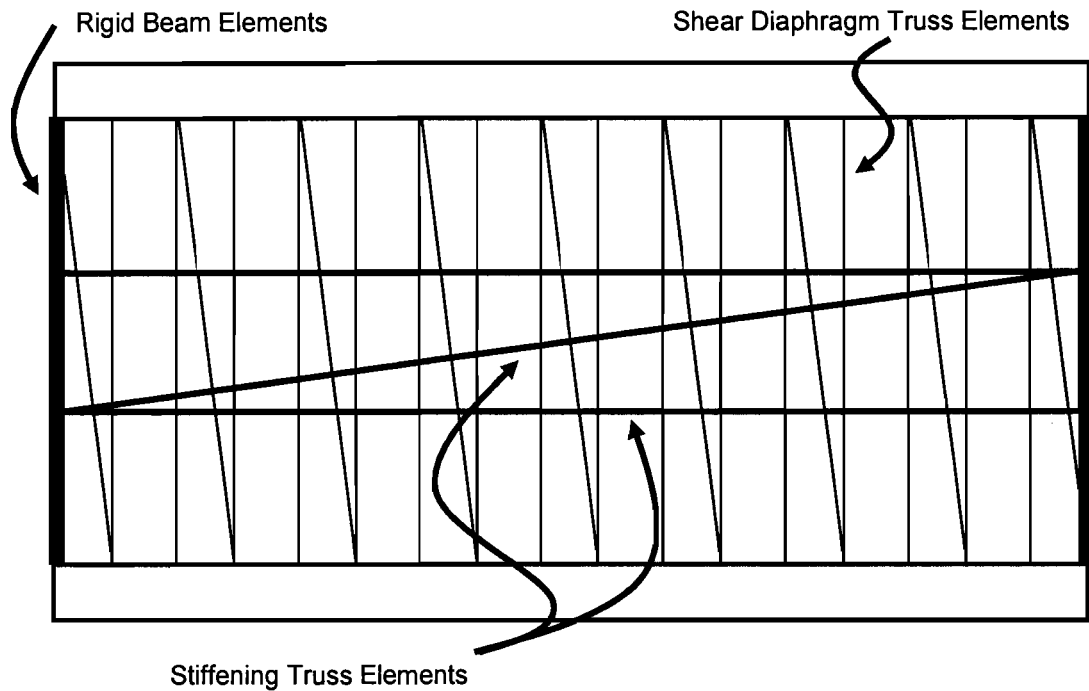


Figure 3.3 Finite Element Stiffening Angle Model

The twin-girder FEA model used in Chapters 6 and 7 consisted of two 48 ft. long girders with the same layout as the laboratory tests that will be discussed in Chapter 4. Simple supports were used at the ends of the girders. Although the section was free to warp at the supports, the out-of-plane translation was restrained at the top and bottom of the web at both ends to prevent girder twist.

Many of the twin-girder models used in the parametric studies in Chapter 8 had transverse stiffeners at both ends in order to prevent web crippling. These stiffeners were modeled using 8-node shell elements and extended from the top of the web to the bottom of the web.

3.3 Computational Study

The systems that were considered in the computational studies include the following parameters:

- 1) Girder span (50 ft. to 150 ft.)
- 2) Girder cross section (Singly and doubly symmetric)
- 3) Number of intermediate braces (cross-frames)
- 4) Shear rigidity of the deck system (Q)

Figure 3.4 shows the cross sections considered in the computational study. The sections consisted of two doubly-symmetric rolled sections (W18x119 and W18x71), one singly-symmetric built-up section labeled Section #3, and two doubly symmetric built-up

sections labeled Sections #4 and #5. The singly symmetric section was the section used in the laboratory twin girder tests. The value of ρ for this section was equal to 0.18, where $\rho = I_{yc}/I_y$, I_{yc} is the weak axis moment of inertia of the compression flange, and I_y the weak axis moment of inertia of the entire cross section. The AASHTO Specification requires this ratio to be within the following limits: $0.1 \leq I_{yc}/I_y \leq 0.9$.

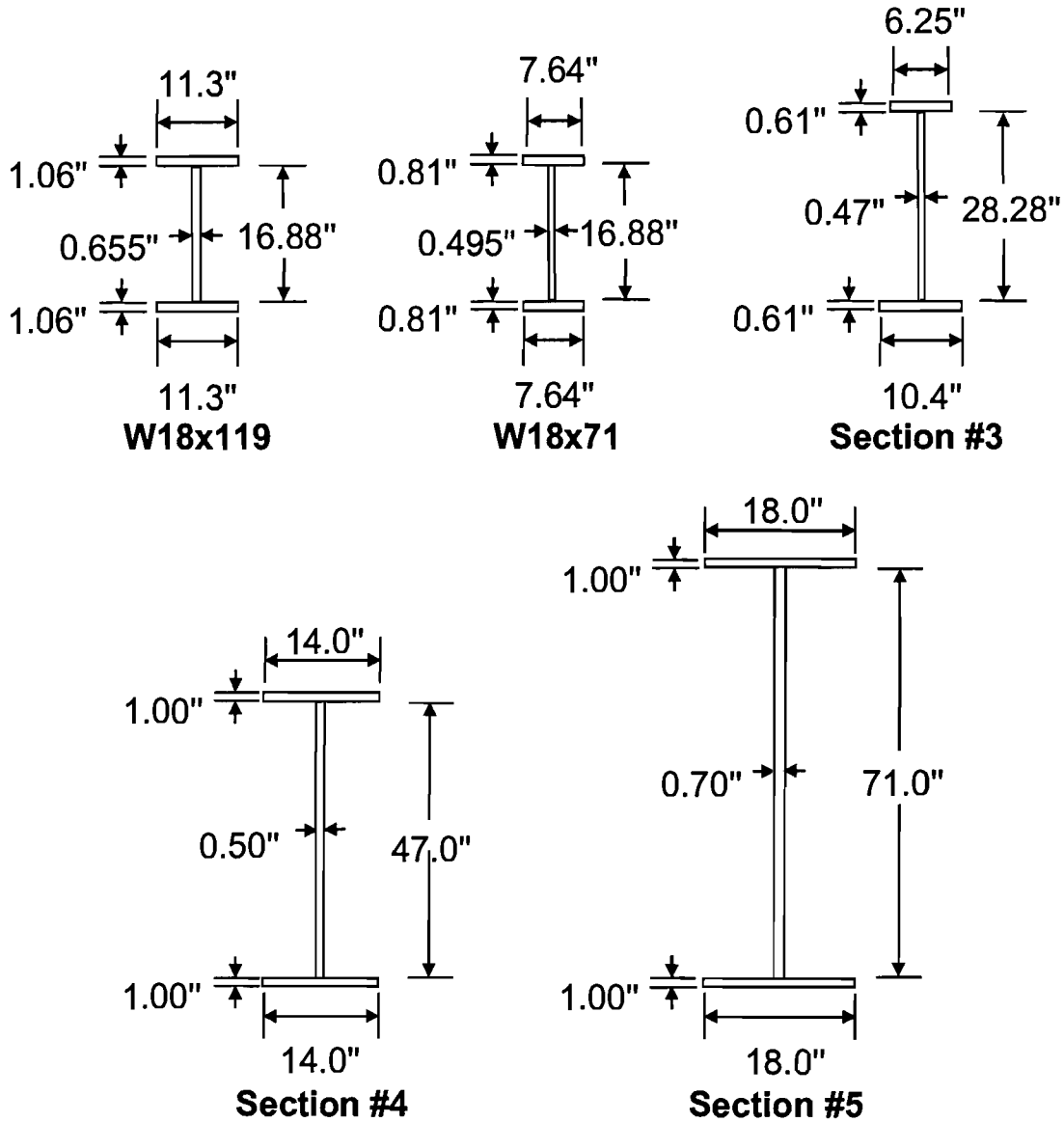


Figure 3.4 *Girder Cross Sections Considered in Computational Study*

All the sections analyzed were simply supported. The W18x119 has a flange width of 11.3 in. that provides a substantial amount of warping restraint. Relative to the W18x119, the W18x71 section (Flange width = 7.64in) requires more bracing from the PMDF since the warping restraint provided by the top flange is significantly different.

Table 3.1 presents the key parameters such as span, span to depth ratio, and the number and spacing between intermediate cross-frames for the sections studied.

Table 3.1 Parameters for Cross Sections Studied

Sections	Span (ft)	L/d Ratio	No. of Braces	Unbraced Length (ft)
W18x119	50	31.6	-	50
W18x71	50	32.4	-	50
Section #3	50	20.3	-	50
Section #4	100	24.5	1	50
Section #5	150	24.7	1	75
Section #5	150	24.7	2	50

Table 3.2 and Table 3.3 show comparisons between the FEA results for single girders and predictions from equations outlined in Chapter 2. The results presented are for uniform moment loading and simply supported girders. For the doubly-symmetric sections shown in Table 3.2, Timoshenko's solution given in equation (2.1) was used in the comparison. The last column in Table 3.2 shows the percent difference. A positive value of the percent difference indicates that the equation was conservative with respect to the FEA result. For singly-symmetric section shown in Table 3.3 Eqs.(2.2) was used as recommended by the AASHTO specifications. The numbers in parenthesis indicate the percent difference between the equations and FEA solution.

Table 3.2 Doubly-Symmetric Sections

Sections	Unbraced Length (ft)	Eq. (2.1) (k.ft)	FEA Results (k.ft)	% Difference
W18x119	50	426.2	413.3	-3.13
W18x71	50	118.0	112.5	-4.85
Section #4	100	336.3	320.8	-4.83
Section #5	150	448.5	440.8	-1.74

Table 3.3 Singly-Symmetric Section

Section	Unbraced Length (ft)	AASHTO Eq. (2.2) (k.ft)	FEA Results (k.ft)
Section #3	50	63.4 (+15.55)	75.1

3.4 Imperfections Considered in the Study

Two of the primary factors that affect the magnitude of brace forces are the brace stiffness and the magnitude and distribution of the initial imperfections. For shear diaphragm bracing, the brace stiffness that results from the eigenvalue analysis is analogous to the ideal stiffness since it reflects the behavior of a perfect system. The philosophy behind stability bracing is to limit the deformations to twice the initial imperfection at a desired design load. This can be achieved by providing a brace stiffness greater than the ideal stiffness. Past studies have shown that brace forces are directly proportional to the initial imperfection of the structure (Yura 2001 “Fundamentals of Beam Bracing”, AISC Engineering Journal, 1st Quarter, pp. 11-26., Wang and Helwig 2003 “Cross frame and diaphragm behavior for steel bridges with skewed supports” TxDOT Research Report # 1772-1). It is therefore imperative to select an initial twist magnitude to be used in the finite element analysis that is reasonably expected to be encountered in practice. Figure 3.5 shows the initial imperfection that the provisions in the AISC LRFD Specifications are based upon. The top flange lateral sweep is $L_b/500$ and the bottom flange is straight. Wang and Helwig (2003 “Cross frame and diaphragm behavior for steel bridges with skewed supports” TxDOT Research Report # 1772-1) concluded that although the maximum brace forces probably occur when both of the flanges have an initial sweep of $L_b/500$ in opposite directions, the probability of such a case is relatively low. Hence the magnitude and shape of the initial imperfection of the girders were assumed to be the same as that shown in Figure 3.5.

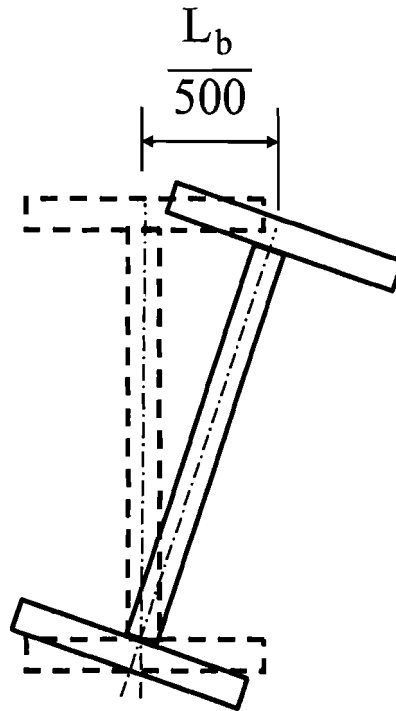


Figure 3.5 Assumed Initial Imperfection

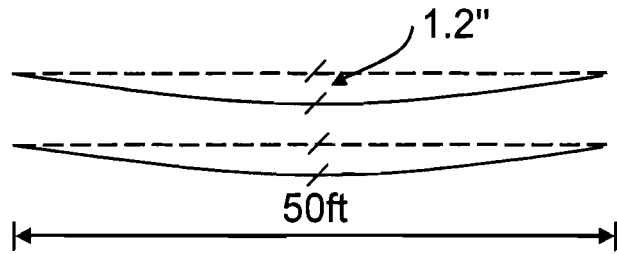
In addition to the magnitude of the initial imperfection, the distribution of the initial imperfection along the girder also has a significant affect on brace moments. This affect is particularly true for systems with multiple intermediate braces. In the finite element analyses presented in Chapter 8 the maximum twist was applied at midspan for systems with no intermediate braces. Helwig et. al. (1993) have shown that the shape of the initial imperfection should generally contain one less wave than the buckled shape between brace points to produce the largest possible brace moment. Hence for Sections #4 & #5 with one intermediate brace, the maximum imperfection was again applied at midspan where the brace was located, creating a half sine curve deflected profile. To maximize probable brace forces for systems with two intermediate braces Wang and Helwig (2003 “Cross frame and diaphragm behavior for steel bridges with skewed supports” TxDOT Research Report # 1772-1) showed that the maximum twist generally must occur at the brace closest to the point of maximum bending moment on the beam and the change in twist between this brace point and the adjacent braces should be equal to the initial imperfection θ_0 , which is calculated by the following expression:

$$\theta_0 = \frac{L_b}{500d} \quad (3.1)$$

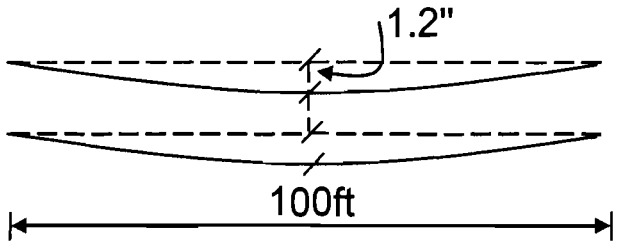
where: d is the depth of the cross section and L_b is the spacing between discrete torsional restraints (cross-frames).

Figure 3.6 shows a plan view of the shape and magnitude of the initial lateral imperfections in the top flanges used in the FEA studies presented in Chapter 8. The bottom flanges were essentially straight.

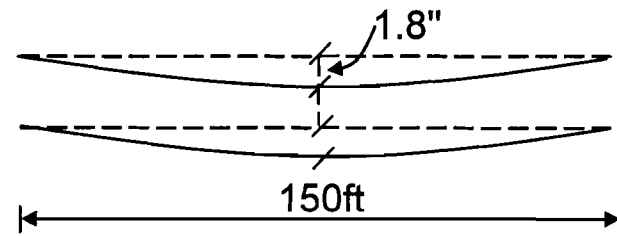
Some results from the FEA models are compared with test results in Chapter 6 and 7 to demonstrate the accuracy of the models. Chapter 8 focuses on the results from the parametric studies on the FEA models to help demonstrate the behavior of PMDF braced systems.



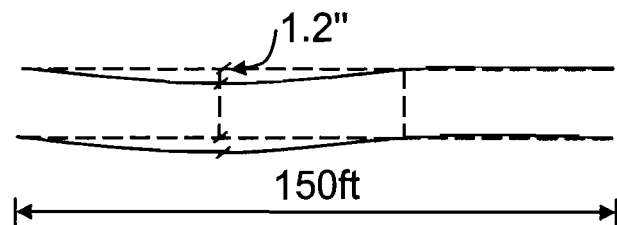
(a) W30x119, W18x71 and Section #3



(b) Sections #4 with one intermediate brace



(c) Sections #5 with one intermediate brace



(d) Sections #5 with two intermediate brace

Figure 3.6 Shape and Magnitude of the Initial Imperfections in FEA Studies

This page replaces an intentionally blank page in the original.

-- CTR Library Digitization Team

Chapter 4

Laboratory Test Set-ups

4.1 Overview

This investigation included laboratory experiments in conjunction with finite element analyses. The laboratory tests were divided into three phases. The first phase of testing focused on the determination of the shear properties for bridge deck forms. Tests were conducted on existing connection details as well as improved details that substantially increase the stiffness and strength of PMDF systems used in the bridge industry.

The first phase of laboratory tests was conducted in a testing frame that was fabricated so that the shear properties of the PMDF systems could be measured. The frame was utilized to subject the PMDF specimens to a pure shear deformation so that the shear stiffness and strength of the panels could be measured.

The second phase of testing focused on measuring the stiffness and strength characteristics of the PMDF in a system very similar to the actual conditions of the forms in field applications. PMDF specimens with the same connection configurations to those tested in the shear frame were attached to the top flanges of a twin girder test set-up with a 48 ft. span. The twin girder system was subjected to a variety of lateral deformation profiles so that the stiffness characteristics of the PMDF systems could be measured. The laboratory test results from this phase of the investigation were then compared with analysis results using different finite element analysis (FEA) models of the deck system. The purpose of the comparisons between the FEA models and the test results was to improve the understanding of the actual bracing behavior of PMDF systems.

The third phase of this program involved buckling tests and analyses for PMDF-braced girders. The twin girder system was loaded using gravity load simulators. The same PMDF specimens and connection configurations tested in the lateral displacement experiments were used. The lateral displacements of the girders were recorded at both the top and bottom of the web in order to calculate the twist of the cross section. The buckling test results were then compared to FEA results that utilized finite element models developed from the second phase of the investigation.

This chapter will provide a thorough overview of the experimental testing program and a description of the test set-ups, the PMDF specimens, and the connection details for each of the three phases of testing.

4.2 Shear Tests

4.2.1 Shear Frame Test Set-Up

As mentioned in Chapter 2, one of the important properties of a shear diaphragm that reflects its bracing behavior is the effective shear modulus, G' . Shear tests were conducted for this study using a relatively rigid frame to develop modifications to the connection details that improve the stiffness and strength of eccentrically connected PMDF systems.

The primary function of the shear test frame was to apply pure shear deformations to the PMDF specimens. Therefore an essential characteristic for the members of the frame is that they were sufficiently rigid against flexural and torsional deformations during testing. The support conditions of the frame were designed so that the frame was relatively free to experience panel shearing in the plane of the deck. Efforts were therefore made in the frame design to minimize the internal friction so that the primary resistance to deformation was provided by the PMDF specimen.

Figure 4.1 shows the scaled plan and elevation of the test frame constructed for this study. The primary members of the frame consisted of two parallel beams that simulated the top flanges of adjacent girders and an adjustable strap at the loading end of the frame to allow easy adjustment on the panel dimensions. Rolled W24x104 sections were used to support the test frame and cantilever loading frame. The support beams were placed on W12x50 segments to position the supporting beams at the correct elevation. Threaded, 1-1/16 inch diameter rods were used to anchor the W24x104 support beams by pre-stressing each rod to approximately 30 kips. The loads were applied to the frame using a hydraulic actuator that was connected to a loading beam that was anchored to the floor. Twenty rods were used to anchor the test frame and twelve rods anchored the loading beam to the laboratory's reaction slab. By anchoring the support beam to the reaction slab, translations at the supports of the test frame were essentially eliminated.

The members of the shear test frame included two "rigid" beams that simulated girder top flanges and an adjustable connecting strap. In order to achieve flexural and torsional rigidity, the beams for the test frame were built-up cross sections; each composed of a rolled W12x50 and an 18x1 inch steel plate. The W12x50 was oriented with the web in the plane of loading (parallel to the reaction slab) and the steel plate was welded to the flange tips on the topside creating a box-section. The torsional stiffness of the box section was substantially higher than the original W12x50 section.

The "rigid" beams were connected to the support beam by a clevis through which a 2-1/2 inch diameter pin passed through two needle bearings utilized to minimize the rotational restraint at the supports. The bearings were contained in a housing that was set with steel-filled epoxy and bolted with 1/2 inch diameter A325 bolts to prevent joint slippage. Doubler plates were welded to the W12x50 web at each connection to reinforce

the joints. The same pin and needle bearing assembly was used to connect the rigid beams to the adjustable connecting strap. As shown in Figure 4.1, the rigid beams were 16 ft long from support pin to strap pin.

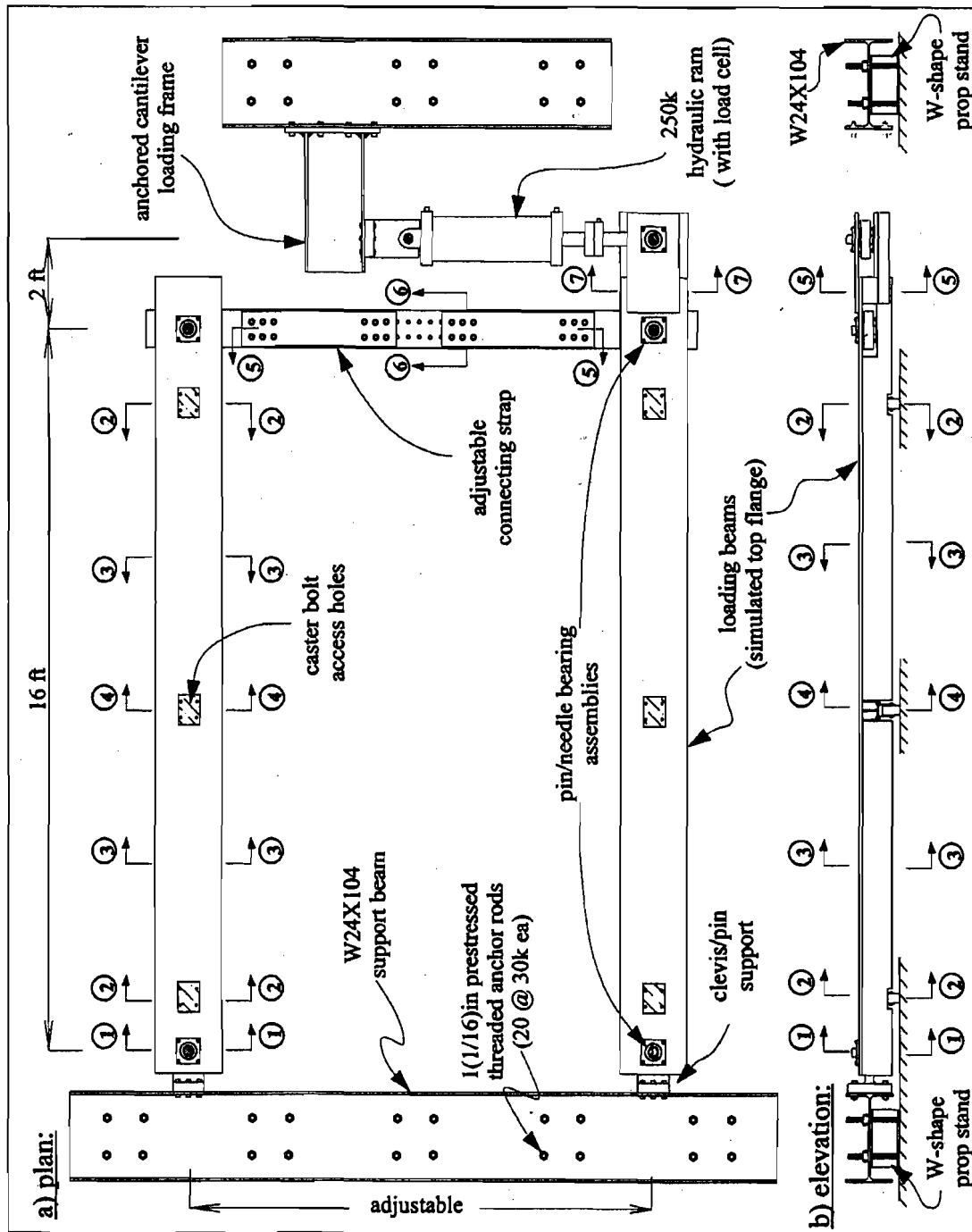


Figure 4.1 Shear Test Frame

The internal friction of the shear test frame was further reduced by bolting heavy-duty, industrial casters to the bottom of the loading beams. Single casters were placed at the ends of the loading beams and a pair of casters was used to provide additional stability near the middle of the beams. The positioning of the four casters on each support beam ensured that each of the test-frame beams were stable on their own and could be easily rolled into place to facilitate assembly of the frame. The positioning of the casters also reduced the torsional load on the pinned connections at the ends of the beams. A four-inch long, one-inch fender was trimmed off of the W12x50 flange tips on either side of the single casters to allow the casters to swivel without interference. At the double caster locations, four inches of the flange were removed below the web and replaced by extension plates to facilitate the caster seats. The extension plates were reinforced with three stiffeners on each side of the cross-section. Caster bolt access holes were also cut into the top plate so that the casters could be bolted to the horizontal web of the W12 X 50. To evenly distribute the weight of the test frame, steel plates were set to the same elevation on the test floor and leveled with hydrostone under each caster position.

The shear test frame was constructed so a variety of PMDF specimen dimensions could be tested. The adjustable connecting strap member at the loading end of the frame permitted easy adjustments to the frame so that different PMDF spans could be tested. The adjustable strap member was composed of three, 2-½ inch thick, 10 inch wide steel plates and four, 42-inch long, rolled C10x25 channel sections. The channels and plates were bolted with a total of twenty-four A490 7/8-inch diameter bolts (4 bolt groups @ 6 bolts ea). The outer bolt groups connected the channels to exterior plates that were in turn pinned to the loading beams while the inner bolt groups connected the channels to the interior plate. A single caster was mounted to the bottom of each channel on the underside of the strap and placed over a leveled steel plate.

Loading was applied to the shear test frame with a hydraulic actuator. One of the rigid beams was extended by welding two, 16x1 inch plates to its far end. The top extension plate was welded directly to the 18x1 inch plate. The bottom extension was accomplished by welding two L3x3x(3/8) angles to either side of the W12x50, then the 16x1 inch plate was welded to the horizontal angle legs. The same needle bearing assembly and pin connection was used to attach the 2-½ inch loading clevis to the loading beam as was used for the test frame supports and member connections. The use of the needle bearings and supporting casters significantly reduced the internal and external friction on the frame. A discussion is given below of the results from friction tests that were conducted on the frame system.

4.2.2 Shear Frame Friction Tests

After construction of the shear test frame was completed, friction tests were performed to determine the load required to break static internal friction. Although the test frame (loading beams and connecting strap) weighed approximately 5,000 lbs, friction tests revealed that only 30~60 lbs was necessary to displace the frame. This

relatively small magnitude of load was considered negligible and was not removed from shear test results.

4.2.3 Shear Test Instrumentation

Loading was applied to the shear test frame with a hydraulic actuator. A 100k capacity load cell was attached to the shaft of the ram. Deflections were measured with two-inch and four-inch linear, spring potentiometers. Four-inch potentiometers (4" pots) were positioned toward the free end of the loading beams while two-inch potentiometers (2" pots) were positioned closer to the supports.

4.2.4 PMDF Specimens and Connection Details (Shear Tests)

The deck panel specimens tested during this study were pre-closed, 3x8 (3-inch depth, 8-inch pitch) bridge deck forms with a 2 ft cover width and metal thickness of 16, 18, 20 and 22-gage. Figure 4.2 shows the cross-section profile for the PMDF specimens tested for this investigation. PMDF spans of 7'-11" and 8'-11" were considered that will be henceforth referred to as 8 ft and 9 ft, respectively.

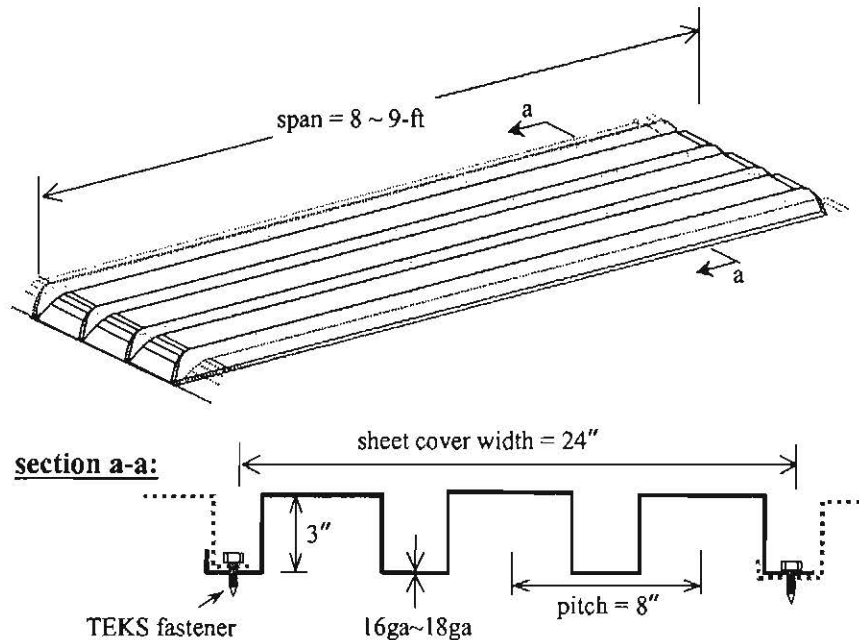


Figure 4.2 PMDF Profile

Deck form sheets spanned between the loading beams of the test frame, and were supported on cold-formed, L3x2x10 gage, galvanized angles, which are typical of those employed in bridge construction. TxDOT (TxDOT-1998) compression flange standards were followed for PMDF support angle attachment details. The support angles were welded directly to the top plate of the shear test frame loading beams with 1/8" fillet welds that were 1-1/2" long intermittently spaced 12 in on center. Three-inch long, 1/8" fillet welds were applied at the ends of the individual support angles.

The forms were fastened to the support angles in every trough by $\frac{3}{4}$ " long, $\frac{1}{4}$ " diameter TEKS screws. TEKS screws were also used to fasten adjacent sheets along side-laps with a maximum 18 inch, center-to-center spacing between fasteners. Special attention was paid to ensure that TxDOT standards were followed in regard to maintaining the minimum $\frac{1}{2}$ inch fastener edge distance on forms and support angles as shown in Figure 4.3.

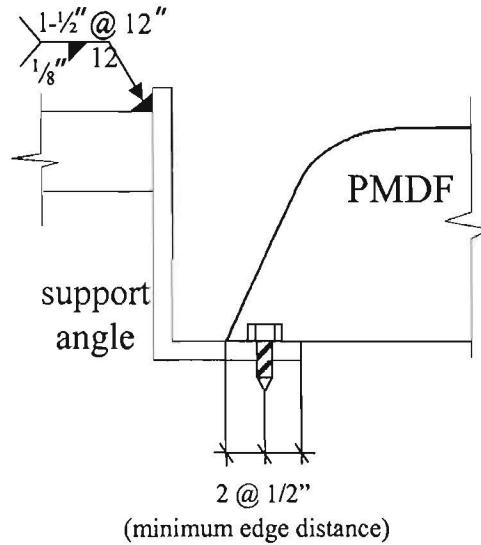


Figure 4.3 Support Angle-PMDF Connection

When a PMDF specimen is subjected to deformations in a shear test frame, the state of stress produces diagonal tension and compression fields within the panel as shown in Figure 4.4.

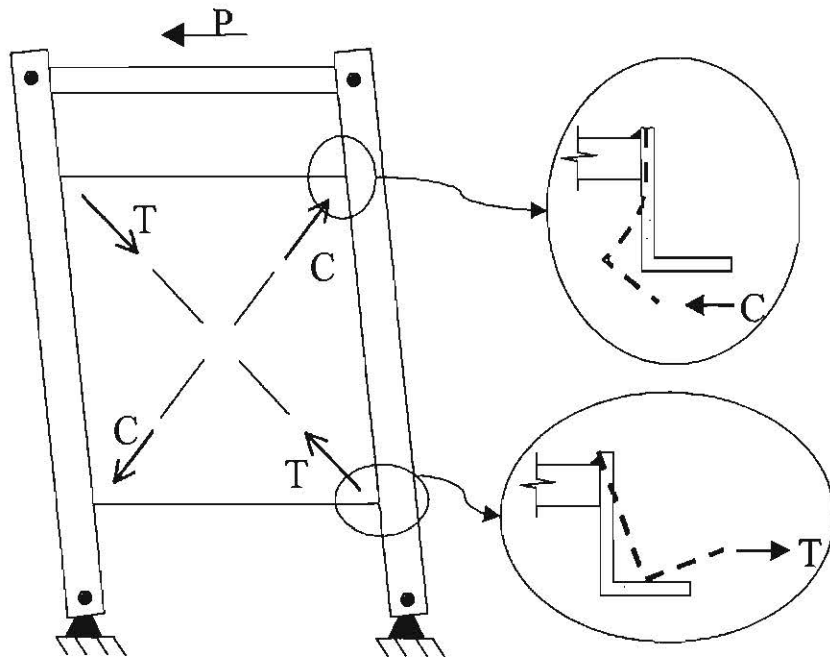


Figure 4.4 Diagonal Tension and Compression Fields on Sheared PMDF Specimen

As depicted in Figure 4.4, at the corners of the panel under diagonal compression, the support angle is pushed under the flange plate when the connection detail is eccentric. Conversely, at the corners of the panel under diagonal tension, the support angle is simply pulled away from the flange plate and generally rotates about the fillet weld. Depending on the magnitude of the eccentricity in the connection, the stiffness of the system is often dominated by the flexibility of the support angle. This is because the stiffness of PMDF systems is governed by the equation for springs in series as given in the following expression:

$$\frac{1}{\beta_{total}} = \frac{1}{\beta_{deck}} + \frac{1}{\beta_{conn}} \quad (4.1)$$

where: β_{total} = actual system stiffness; β_{deck} = stiffness of the PMDF and β_{conn} = stiffness of the connection (support angle included). The total system stiffness in Eq. (4.1) must be smaller than the least of either the deck or connection stiffness. In addition, the failure of the deck panel for cases with maximum eccentricity typically involves a severe deformation of the support angle at the corners of the panel as demonstrated by the photo in Figure 4.5.

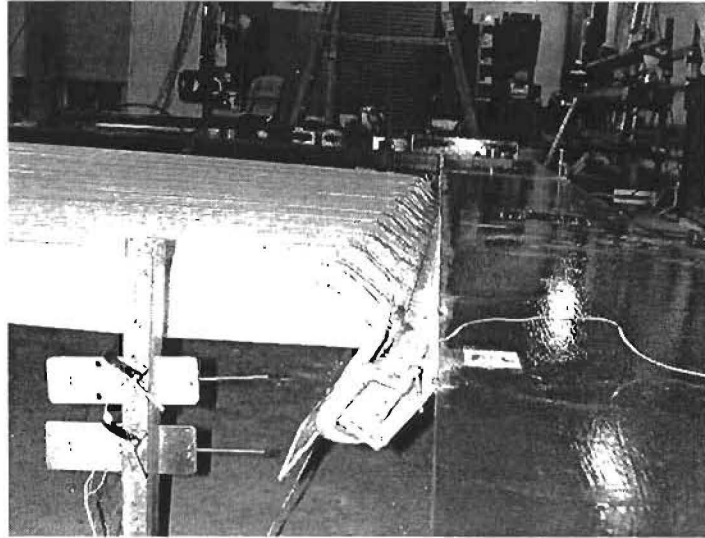


Figure 4.5 Failure Mode of Unstiffened Eccentric Connection

A number of modified connection details were tested to control the angle deformation, however one proved to be both practical and effective. This proposed modification involves a transverse stiffening angle that spans between adjacent girder flanges as shown in Figure 4.6.

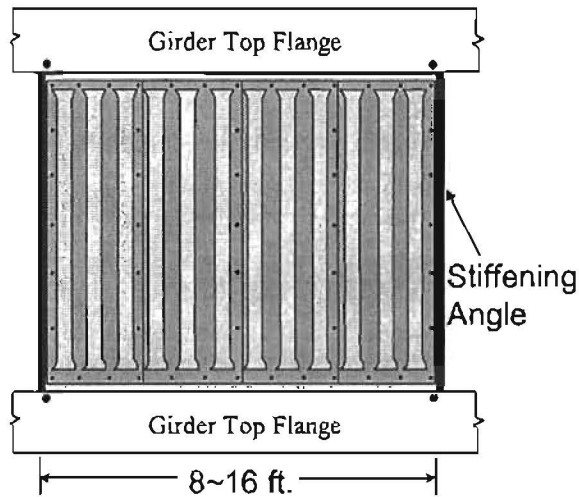


Figure 4.6 Transverse Stiffening Angle to Control Support Angle Deformation

The stiffening angles were positioned to coincide with a side-lap seam so the deck could be fastened directly to the angle. So as to have the same eccentricity of the stiffening angle and the support angle, the ends of the stiffening angle were welded to the

webs of fabricated T-stubs (2-½ inch, L3x2x10ga, long leg back-to-back) that were bolted to the underside of the top flange plate as shown in Figure 4.7.

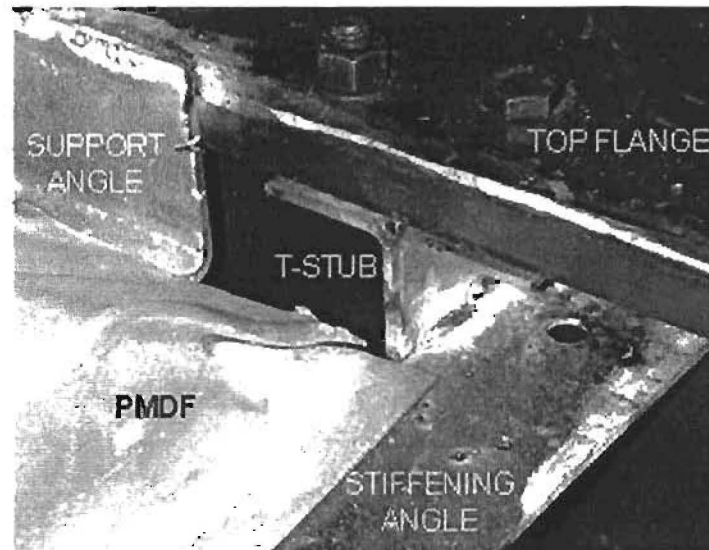


Figure 4.7 Eccentric T-Stub – Stiffening Angle Connection

A variety of prefabricated sections (hot-rolled or cold-formed) could also be used for this purpose. In most field applications where welding is permitted to the top flange, the T-stub would often be welded to the flange. To provide more flexibility in adjusting the location of the stiffening angles, bolted connections were used in this study. In addition to providing the flexibility in positioning the T-stubs, these tests would simulate potential connections that could be used in cases in which welding to the top flange may not be permitted. Welding the T-stubs would generally provide a better connection to the flange. While the purpose of the stiffening angles is to control the deformation of the support angles, they also provide support to the deck at the ends of the panel. (Figure 4.6). Since the deck is fastened on all four sides, the stiffening angle should provide a stronger and more redundant system. Utilizing the conventional connection details (with no stiffening angles), the failure of a PMDF bracing system may result in an unzipping of the fasteners along the length of the beam. However with the stiffening angle, all of the side lap fasteners must fail before the bracing system can fail.

Four types of PMDF support configurations were the focus of the first phase of the research:

- 1) no eccentricity, unstiffened
- 2) no eccentricity, stiffened
- 3) maximum eccentricity, unstiffened
- 4) maximum eccentricity, stiffened

Figure 4.8 illustrates these four configurations. The symbol “X” indicates a stiffened connection with the approximate eccentricity indicated by the vertical position of the “X”.

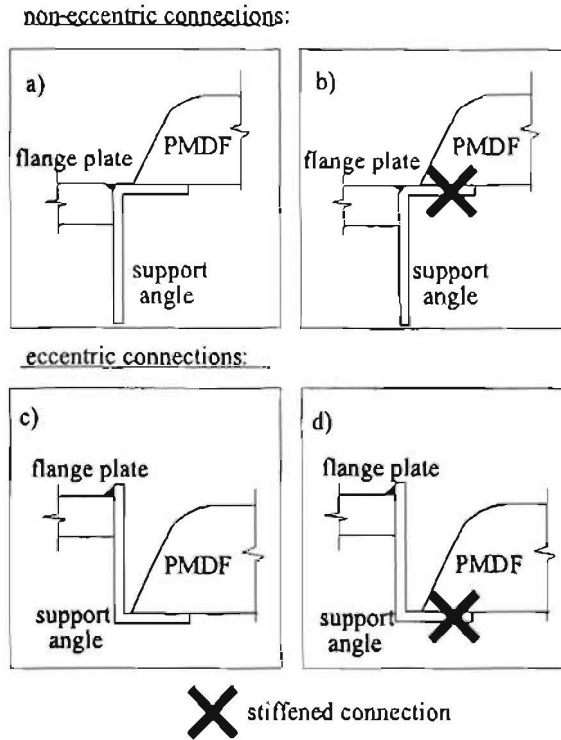


Figure 4.8 Connection Detail Symbol Illustration

For tests performed without eccentricity, the long leg of the support angle was oriented vertically downward and the short leg was placed flush with the level of the top flange plate. For tests with maximum eccentricity, the long leg of the support angle was oriented vertically upward with its edge extending 1/8" above the top flange plate of the loading beam.

Four basic parameters were investigated on PMDF shear specimens tested for this study:

1. Panel span
2. Panel width
3. Stiffener spacing
4. Support angle eccentricity

Each test was coded with a file name to identify the metal gage, connection detail and parameters for that particular specimen as demonstrated by the following example:

Test file name: 18ga. 9ds. 16pw. 8ss/us. ecc/noecc

(1) (2) (3) (4) (5)

- (1) Metal gage
- (2) Deck span (feet)
- (3) Panel width (feet)
- (4) Stiffener angle spacing
 - ss = stiffening angles spaced (feet)
 - us = unstiffened connection detail
- (5) Connection eccentricity
 - ecc = eccentric
 - noecc = no eccentricity

The naming scheme was employed so that key variables in each test could be identified in a single name. However, the naming scheme may be difficult for readers to follow and efforts will be made in the results chapters to identify the key variables for each test.

4.3 Lateral Displacement Tests

4.3.1 Twin Girder Set-Up

The first phase of testing focused on determining the stiffness and strength of the PMDF systems subjected to pure shear deformation. Laboratory tests conducted at the University of Texas at Austin (Soderberg 1995) produced results that indicated that the bracing behavior of PMDF might be more effective than what would be predicted by a shear diaphragm model. The bracing behavior of PMDF systems may be underestimated because the in-plane flexural contributions to the system are generally neglected by the shear diaphragm model. Until now, only in-plane shear contributions to deck form system behavior have been considered. To more accurately predict the actual behavior of PMDF systems, both shear and flexural components should be isolated.

The bracing contributions of the shear and flexural components dominate at different locations along the length of the girders. In an actual deflected profile of the buckled girders, the shear stiffness of PMDF will provide the greatest bracing contribution in regions with the largest shear deformation (Figure 4.9a). This will occur around discrete braces such as torsional cross-frames and diaphragms or other brace points. On the other hand, shear stiffness of the forms is relatively ineffective at locations near the midpoint between discrete braces since the top flange shear deformation of the buckled girder is essentially zero (Figure 4.9b). Although the bracing contribution from the shear component in these regions is small, the in-plane flexural stiffness will generally be most effective since this is the point with the largest lateral displacement.

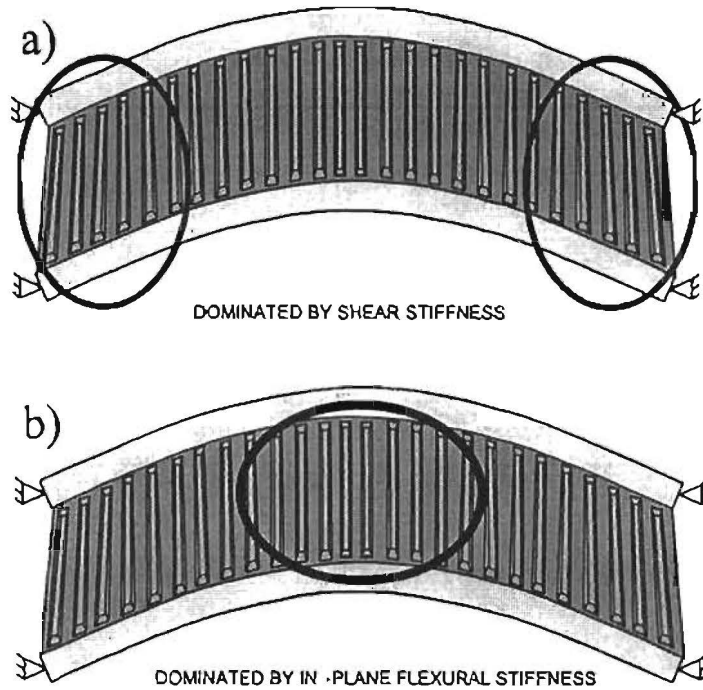
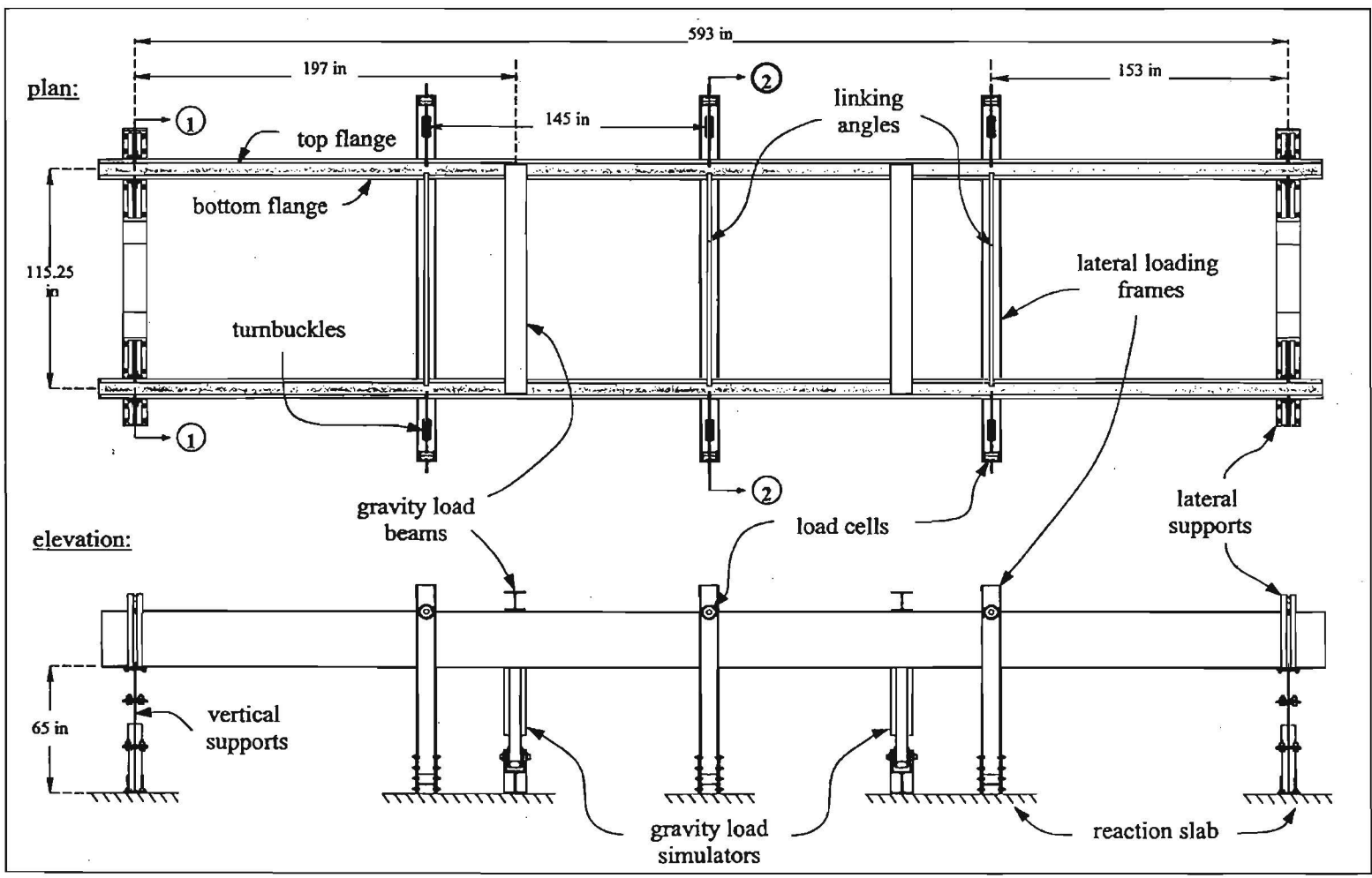


Figure 4.9 Regions of Shear and Flexural Contribution to Lateral Stiffness

To measure the behavior of the PMDF systems in actual applications, a twin girder test set-up was fabricated for use in lateral displacement and buckling tests. Two hot-rolled, ASTM 992, Grade 50, W30x90 beams were used for the girders in this set-up. The girders spanned a little under 50 ft (593 inches). The top flange of each girder was reduced to a width of 6.25 inches (from 10.4 inches) to produce a singly-symmetric section with $\rho = I_{yc}/I_y = 0.18$, which is near the lower bound of the AASHTO limitation of $\rho = 0.1$ and typical of the plate girder shapes employed in composite bridge construction. The girders were spaced web-to-web at 115.25 inches to accommodate placement of PMDF specimens with a 9 ft span. Figure 4.10 shows the scaled plan and elevation views of the twin-girder system constructed for this study. A photo of the twin girder setup is shown in Figure 4.11.

Figure 4.10 Twin Girder Test Set-Up



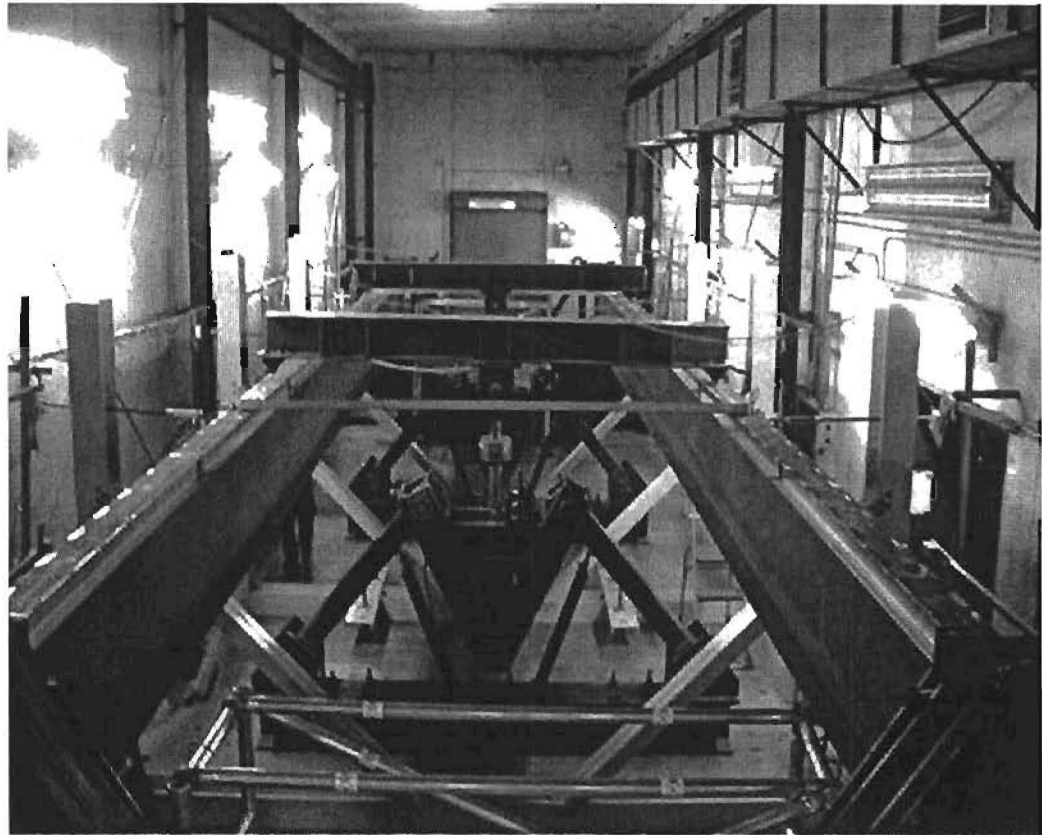


Figure 4.11 Twin Girder Lateral Displacement Test Set-Up

Figure 4.12 shows the elevation view of the twin-girder support system to scale (section 1-1 of Figure 4.10). Vertical support was provided by placing the girders atop stacked wide-flange sections (two W24x104 and one W16x67), which were anchored to the laboratory reaction slab. The purpose of these support details was to elevate the beams so that they did not interfere with the gravity load simulators, while also simulating simple support conditions. The flexibility of the webs in the support sections permitted the supports to “breathe” in the longitudinal direction. However, the system was too flexible in the longitudinal direction of the girders so transverse stiffeners were welded to the bottom support sections to increase the stiffness of the supports in the longitudinal direction of the girders. Lateral movement and twist of the girders were prevented at the supports, however the flanges were free to warp. Lateral support was provided to the girders by framing that clamped the top flanges with threaded rods that had rounded ends to minimize the warping restraint. Bearing brackets were welded above and below the top flanges at the lateral supports as a safety precaution against misalignment to the clamping rods during a loading sequence. Thrust bearings were utilized at the support contact points on the bottom flanges to minimize warping restraint caused by friction.

section 1-1:

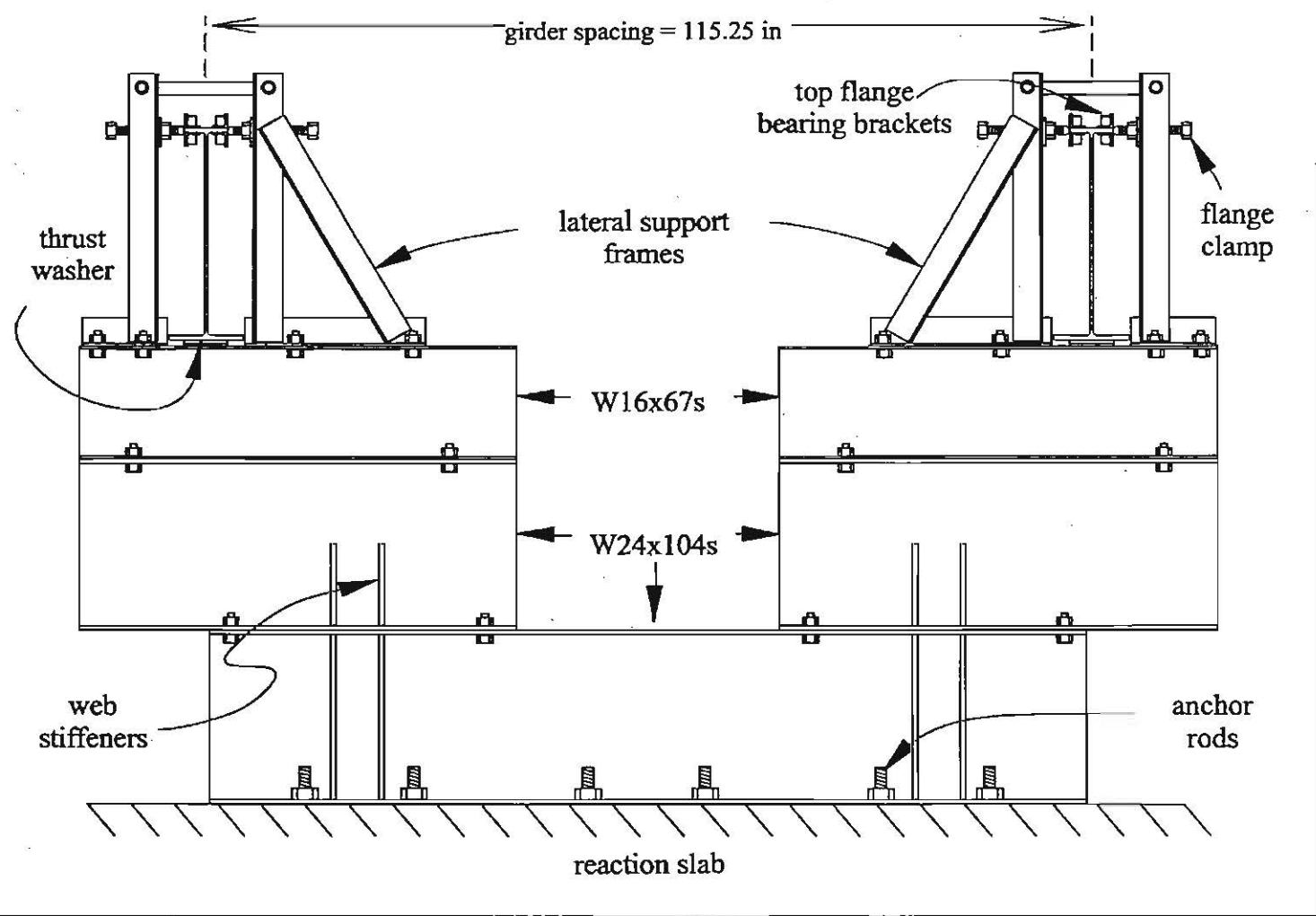


Figure 4.12 Twin Girder Supports

4.3.2 Lateral Loading Frames

To measure the lateral stiffness of the system, combinations of lateral displacements were applied at the quarter points and midspan along the girder length using turnbuckles connected to the loading frames that were anchored to the reaction floor as shown in Figure 4.13 (section 2-2 of Figure 4.10). The girders were linked together by L3x2x10ga galvanized angle at the lateral load points so the top flanges experienced the same horizontal movement. Three lateral loading frames were constructed for this project (one at each quarter point and one at midspan). Each loading frame could be used to apply loads to either girder so lateral displacements could be imposed on the system in two directions. Each lateral loading frame was built from a total of seven hot-rolled, steel members consisting of a base beam, two vertical columns and four knee braces. The base beam consisted of a 16-ft long W10x45 section that was oriented with its web parallel to the floor and bolted to the reaction slab. The columns were also W10x45 sections that were 10 ft long and bolted vertically, with flanges flush, to the flanges of the base beam. Sixteen A325 5/8 in diameter bolts and two 3/8 in thick gusset plates were used for each vertical member connection. The knee braces consisted of two 3x3x(3/8) angles that were used as struts with a 45-degree angle to the W10 x 45 columns and base beam. The struts provided the lateral bracing of the vertical W10x45 sections so that lateral loads could be applied to the test beams and PMDF systems.

Loads were applied to the top flanges of the girders by adjusting a turnbuckle as illustrated in Figure 4.13. The turnbuckle was attached to the girder on one side through an eyebolt that was linked to the girder by an eyehook. On the other side of the turnbuckle a 3/4 in diameter, passed through a hole in the web of the vertical W10 x 45 and provided anchorage to the turnbuckle. The turnbuckle also passed through the middle of a load cell that reacted on the web of the W10x45 so that forces could be measured.

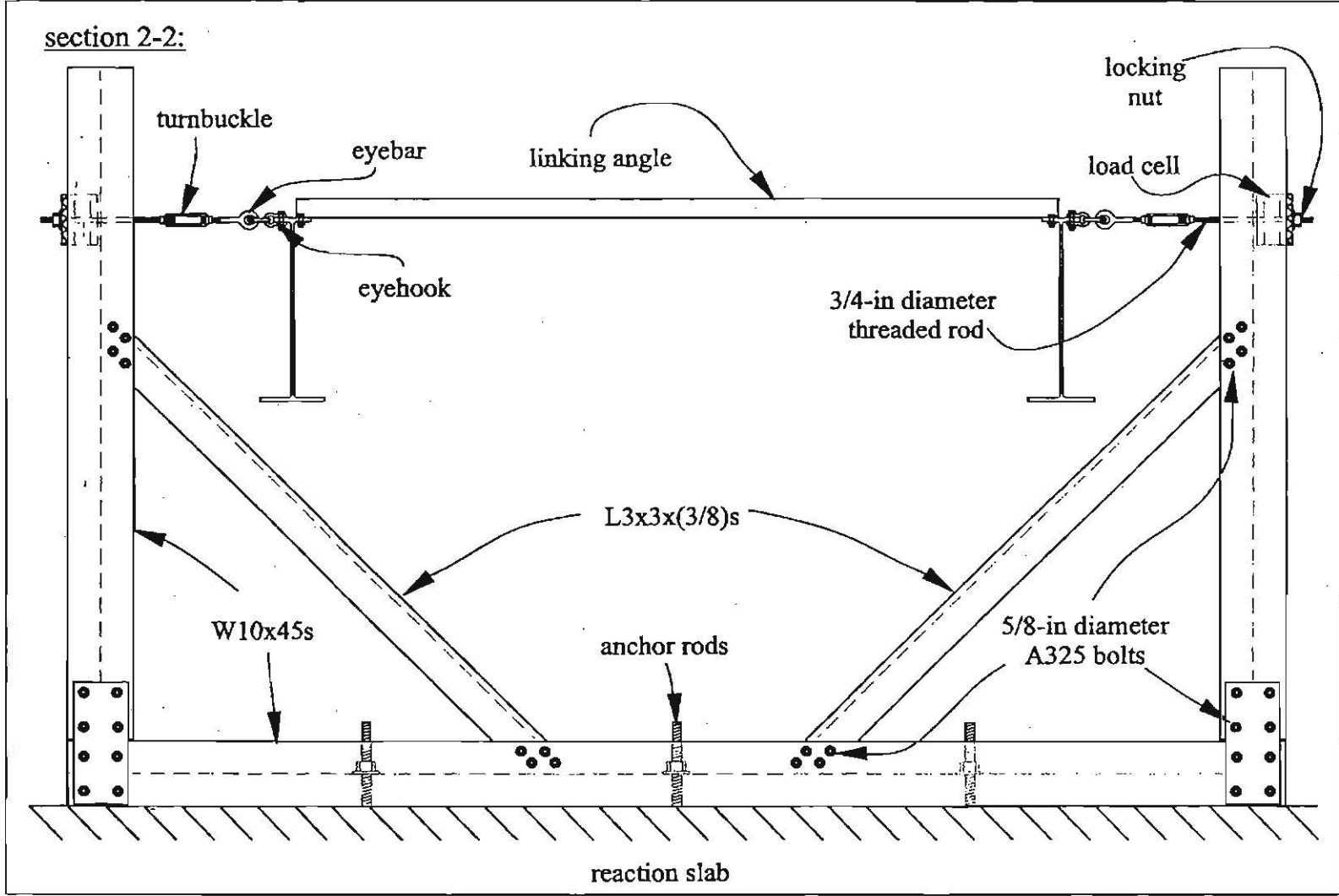


Figure 4.13 Lateral Loading Frame and Linking Member



Figure 4.14 Lateral Loading Frame with Turnbuckle to Load Cell Attachment

4.3.3 Lateral Displacement Test Instrumentation

As mentioned above, the threaded rods ($3/4$ in diameter) from the turnbuckle passed through load cells mounted on the outside of the lateral loading frames. These load cells were used to monitor forces in the turnbuckles (Figure 4.14). Rotary-string, linear potentiometers were used to measure displacements of the supports at top and bottom flanges. Strain gages were applied to the girders' top flange tips at midspan so that the maximum flange stresses could be monitored.

4.3.4 PMDF Specimens and Connection Details (Lateral Displacement Tests)

The PMDF specimens and connection details outlined for shear tests in section 4.2.4 are fundamentally the same as those investigated for lateral displacement tests. One primary difference is that specimens for lateral displacement tests were attached to the top flanges of a twin-girder system rather than the relatively rigid loading beams of the shear frame. Since the flange thickness of the test beams were thinner than the 1 inch plates that were used in the shear frame, the stiffness of the support angle connections differed slightly between the shear frame and the twin girder tests. This difference will

be discussed in Chapter 5. Three basic parameters of the PMDF specimens were investigated in the twin-girder lateral displacement tests:

1. Panel width
2. Stiffener spacing
3. Deck gage

16ga, 18ga and 20ga PMDF specimens, connected with maximum eccentricity and deck spans of 9 ft were considered. The deck stiffness was evaluated using three loading conditions: 1) lateral loading by the turn buckles at only the girder quarter-points, 2) lateral loading at midspan, and 3) loading at the quarter points and midspan. When the beams were loaded laterally at all three load points, the deformations that were imposed simulated a half-sine curve.

Similar to the naming scheme for the shear tests, a file naming scheme was employed in the twin girder tests to identify the gage type, panel width, stiffener spacing and displacement profile for that particular specimen as follows:

Test file name: 18ga.16ft.st8ft/unst.qp/ms/sine

(1) (2) (3) (4)

- (1) Gage type
- (2) Panel width (feet)
- (3) Stiffener spacing
 - st = stiffening angle spacing (feet)
 - unst = unstiffened connection detail
- (3) Displacement profile
 - qp = both quarter points
 - ms = midspan
 - sine = half-sine curve

The naming scheme was employed so that key variables in each test could be identified in a single name. However, the naming scheme may be difficult for readers to follow and efforts will be made in the results chapters to identify the key variables for each test.

Specimens were attached in panel increments, working from the supports towards midspan. The tests were conducted by first placing PMDF panels on only the 8 ft region adjacent to the support, followed by 12 ft and 16 ft panels adjacent to the support, and finally decking the entire 48 ft length.

4.4 Buckling Tests

4.4.1 Test Set-Up

The third phase of testing focused on the buckling behavior of the girders braced with PMDF. As mentioned previously in Section 4.3.1 the test set-up fabricated for the lateral displacement tests was utilized for the buckling tests. The loading was applied using two gravity load simulators. In the buckling tests, the lateral load frames that were used in the 2nd phase of testing were relied upon as lateral stops to limit the amount of lateral displacement of the girders during the buckling test. In this regard, the turnbuckles were set to remain slack for a precalculated amount of deformation. Should the girders buckle, the turnbuckles would prevent excessive lateral deformation that might yield the members. Gravity load simulators apply transverse load to the system without restraining lateral movement. Figure 4.15 shows a photo of the gravity load simulator.

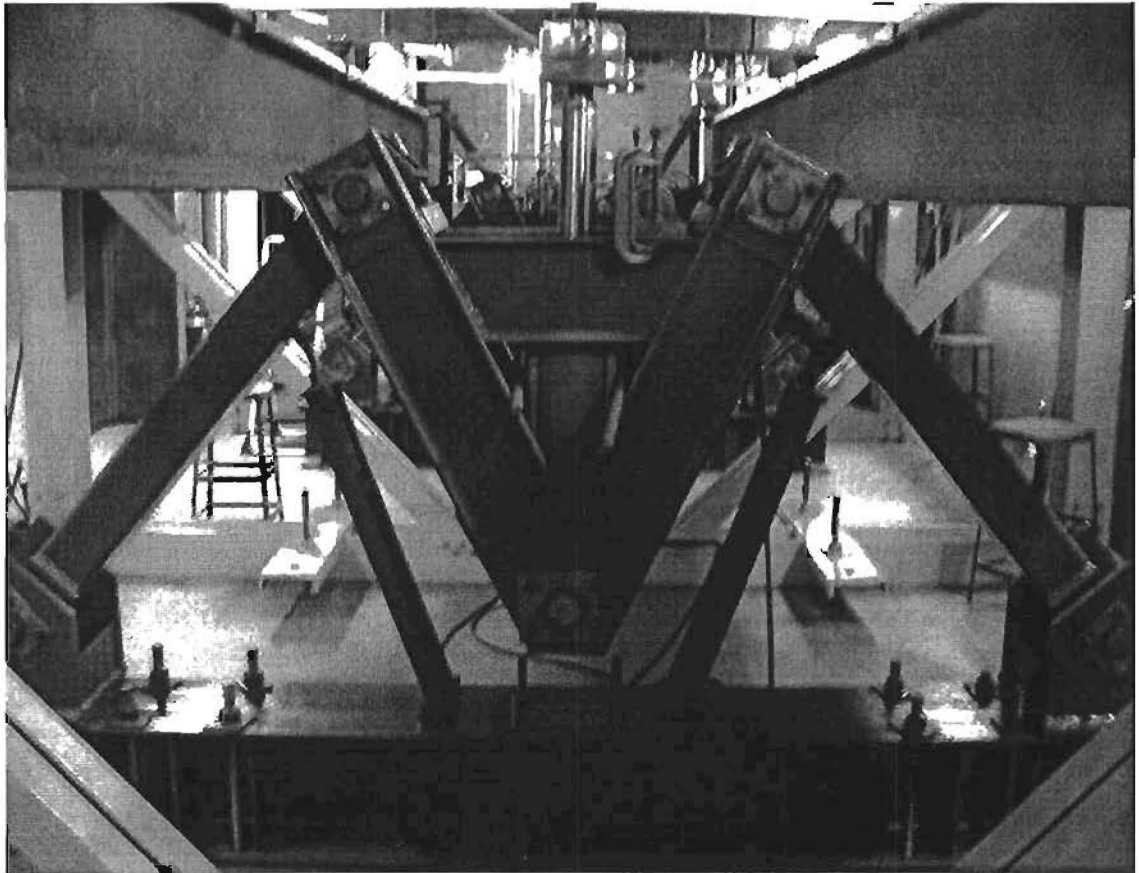


Figure 4.15 Gravity Load Simulator

As can be seen in Figure 4.15 the gravity load simulator consisted of an unstable truss system with four members. The four members consist of a W10x33 base beam that was anchored to the laboratory reaction slab. Two 6 ft long HSS8x6x3/8 tubes were pin connected to each end of the W10x33 beam. The other ends of those 6 ft long tubes were

pin connected to a rigid triangular frame. A 200 kip capacity hydraulic actuator was also connected to the bottom joint in the rigid triangular frame. The other end of the actuator was bolted to the loading beams, which spanned on top of the two W30x90 girders. Figure 4.16 shows a photo of the gravity load simulator beams.

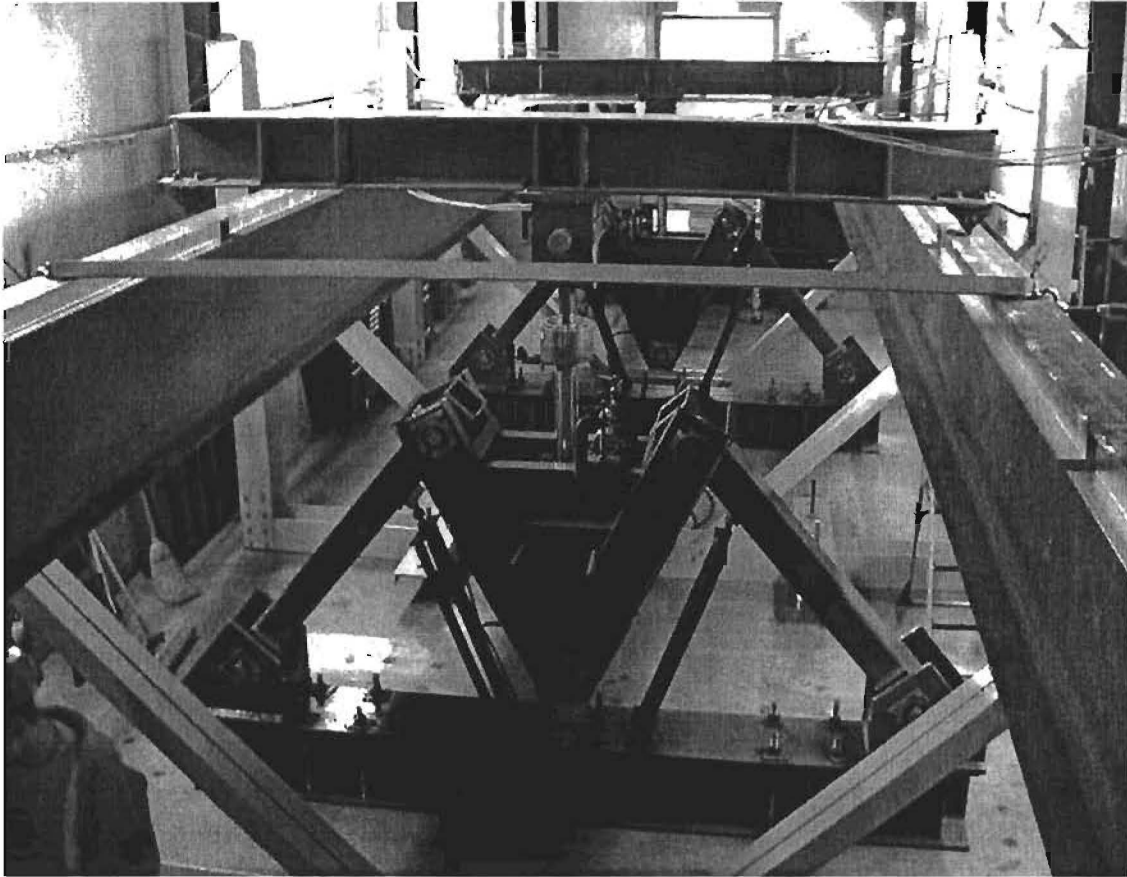


Figure 4.16 Gravity Load Simulator Beam

The loading beams essentially evenly distribute the load from the gravity load simulators between the two girders. These beams enable the load applied by the hydraulic ram to be evenly distributed to the girders as point loads. Knife-edges were bolted to the ends of the gravity load simulator beams in order to eliminate tipping restraint to the top flange of the test girders. Figure 4.17 shows a photo of the knife edge.

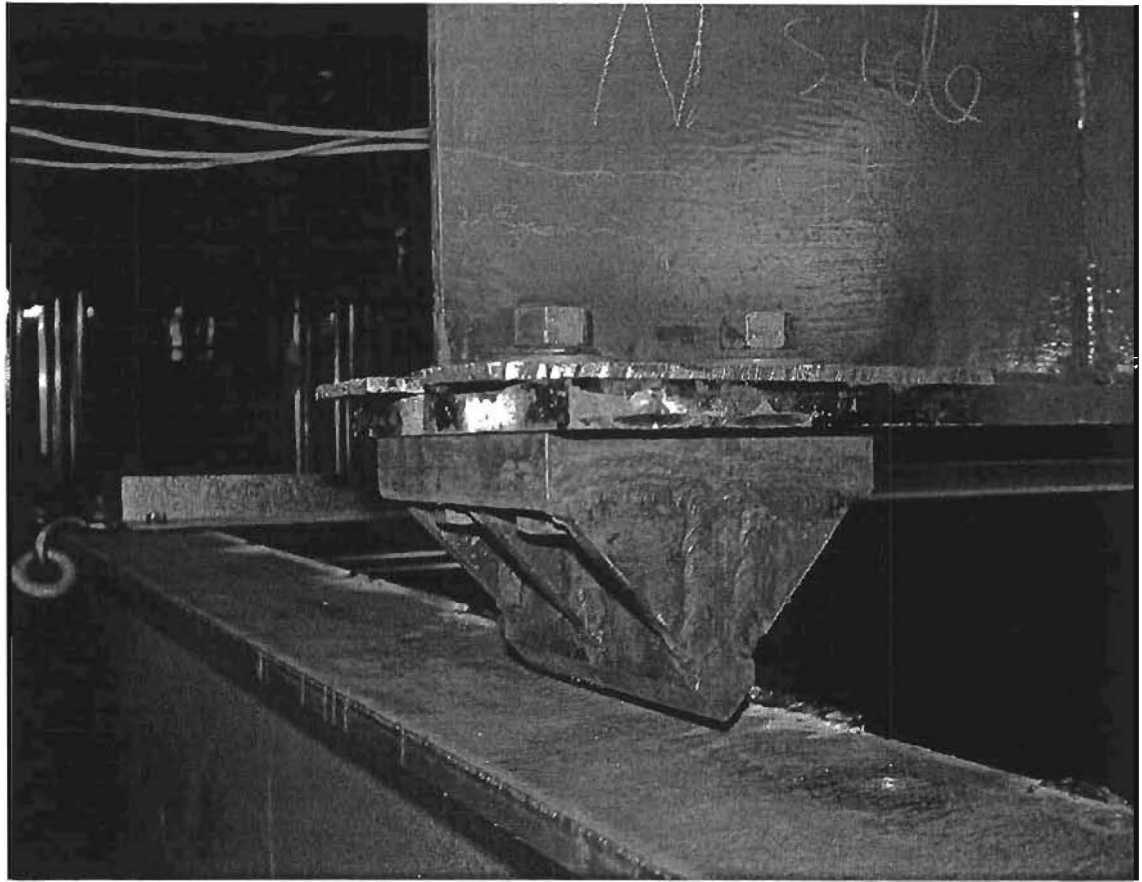


Figure 4.17 Knife Edges

The gravity load simulators were positioned at the third points along the girder length so that a constant moment region could be achieved around midspan during the buckling tests. This type of a moment diagram provides a reasonable simulation of a moment diagram that may result from a uniformly distributed top flange load, which is the typical loading for bridge girders during construction.

4.4.2 Buckling Test Instrumentation

Two lateral displacement measurements were recorded at the lateral loading frame locations (quarter points and midspan) by means of 4 in linear spring potentiometers (linear pots). One potentiometer was placed at the bottom of the web and the other 20 in above. Figure 4.18 shows a photo of the linear pots.

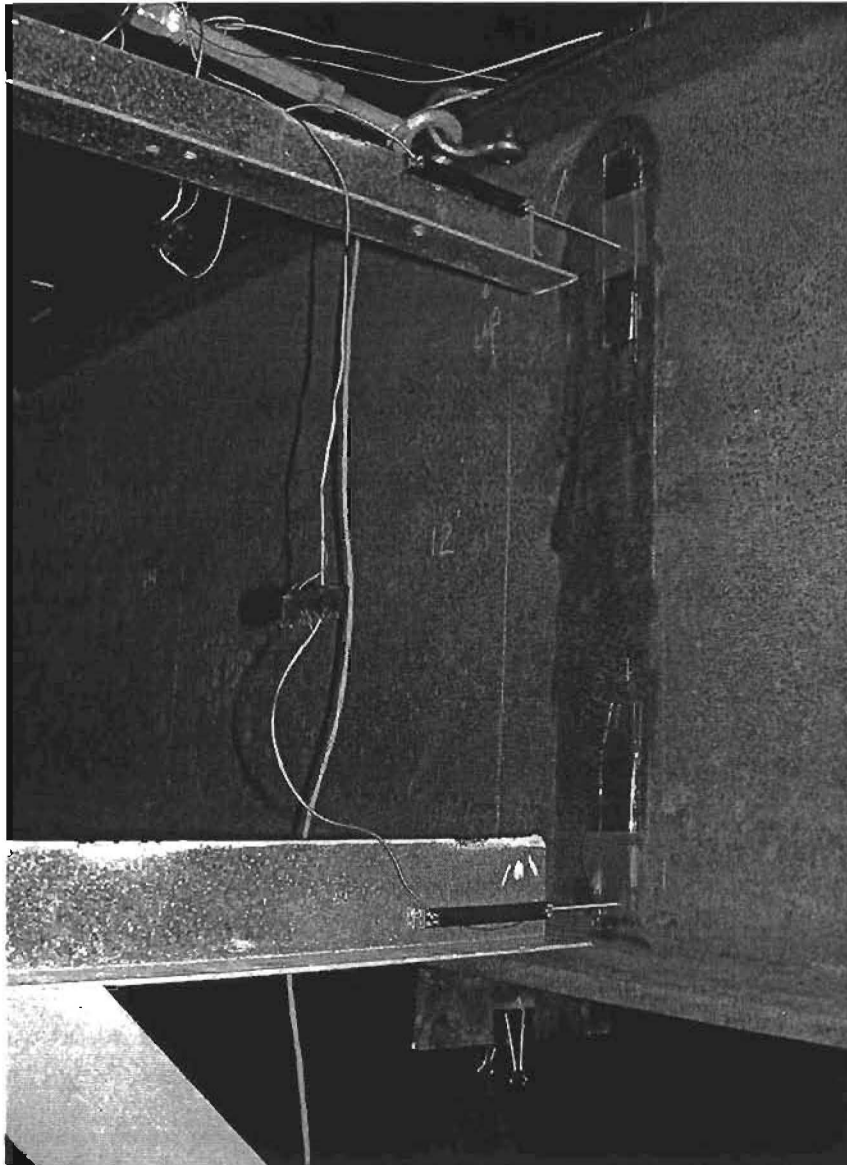


Figure 4.18 Linear Spring Potentiometers

At the contact point of each linear pot to the web, 7 in x 1.5 in pieces of glass were attached to the web surface using an epoxy adhesive. The glass minimized the friction between the linear pot and the sliding surface. Wax paper was placed in between the glass surface and the linear pot in order to further minimize the friction.

The inclination of the glass surfaces was measured using a digital level before each test. This measurement was necessary for the correction of the lateral displacement readings since the girders displaced vertically and the angle of the glass resulted in an “apparent” lateral deformation. Once the lateral displacement readings were corrected according to the inclination of the glass surfaces, these corrected lateral displacement values were used to calculate the twist of the cross section.

Rotary-string, linear potentiometers (rotary pots) were used to measure the vertical displacement of the girders. These rotary pots were attached to the middle of the bottom flange at the quarter points and midspan (Figure 4.19).

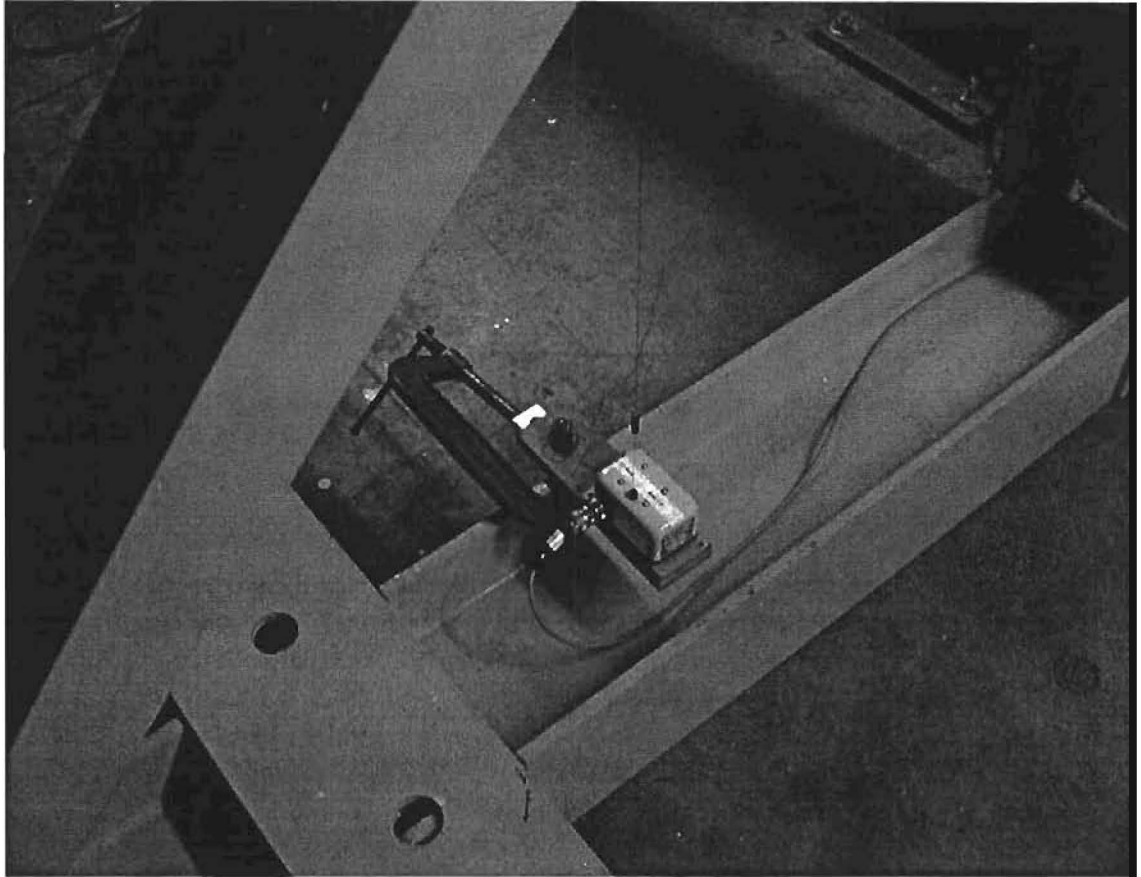


Figure 4.19 Rotary String Linear Potentiometers

Loads were monitored by load cells attached to the two hydraulic actuators. Strain gages were applied to the girder top flange tips at midspan in order to monitor the maximum top flange stresses.

4.4.3 PMDF Specimens and Connection Details (Buckling Tests)

The PMDF specimens and connection details outlined for the lateral displacement tests in Section 4.3.4 are fundamentally the same as those investigated for the buckling tests. The twin girder system in these tests was fully decked with 20 ga. PMDF forms. Three different sets of deck forms were placed on the girders.

The measured imperfection in the test girders was smaller than the imperfection that could be reasonably expected in field applications. As discussed in Chapter 3 most beam bracing design formulations are based upon an initial imperfection consisting of a twist of:

$$\theta_0 = \frac{L_b}{500d} \quad (4.2)$$

where: L_b is the spacing between points of zero twist and d is the depth of the girder. This imperfection comes from assuming that one flange has an out-of-straightness of $L_b/500$ while the other flange is straight. In order to test the deck under conditions that might be expected in field applications, the load was offset from the centerline of the flange to impose a torque that would simulate the maximum imperfection. Laboratory results were compared with FEA results on a girder with an imperfection matching the initial twist given in Eq. (4.2).

Each test was coded with a file name to identify the metal gage and the set number, stiffening angle spacing and the offset of load point (the knife edge) from the center line of the top flange as follows:

Test file name: $\underbrace{20\text{ga.}}_{(1)} \underbrace{01.}_{(2)} \underbrace{\text{st}8\text{ft}/\text{unst}}_{(3)} \underbrace{\text{.sg}0,5\text{ino ng}0,5\text{ino}}_{(4)}$

- (1) Gage type
- (2) Test set number
- (3) Stiffener spacing
 - st = stiffening angles spaced (feet)
 - unst = unstiffened connection detail
- (4) Load offset from center line of top flange
 - sg = south girder
 - ng = north girder
 - 0,5ino = offset amount (inch)
 - no = no offset

The naming scheme was employed so that key variables in each test could be identified in a single name. However, the naming scheme may be difficult for readers to follow and efforts will be made in the results chapters to identify the key variables for each test.

The results for the three different phases of the testing are presented in Chapters 5, 6, and 7. As mentioned earlier, comparisons are made between some of the test results and the FEA results. This was done to confirm that the FEA models provided reasonable estimates of the behavior of PMDF braced girders so that parametric studies could be done on the bracing systems.

This page replaces an intentionally blank page in the original.

-- CTR Library Digitization Team

Chapter 5

Shear Tests

5.1 Overview

The PMDF shear panels that were tested for this research were described in Section 4.2.4 of this report. Once each deck panel specimen was assembled into the shear test frame, specimens were subjected to three phases of loading:

- Phase 1 – elastic, reversed, cyclic loading without dead load (E-NDL)
- Phase 2 – elastic, reversed, cyclic loading with dead load (E-DL)
- Phase 3 - ultimate capacity, unidirectional loading with dead load (U-DL)

The goal of the first two phases of the testing was to obtain a measure of the shear stiffness of the PMDF system with and without superimposed dead load. The third phase of testing permitted the stiffness to be determined at higher load levels while also providing a measure of the shear strength. The following two subsections will provide an overview of the testing procedures for the elastic cyclic loading and the ultimate stage of loading.

5.2 Shear Test Phases 1 & 2: Elastic, Cyclic Loading and Initial Stiffness

Two phases of reversed, cyclic loading were applied to each specimen to determine the initial elastic stiffness ($G'_{0(E-NDL)}$ & $G'_{0(E-DL)}$). The first phase of cyclic loading was conducted on the deck alone, without any superimposed dead load. For the second phase of cyclic loading, steel plates weighing approximately 650 lbs each were placed on the specimens to simulate the effect of wet concrete on the system stiffness. Figure 5.1 shows a typical test setup with the superimposed dead load. As outlined in Chapter 4, panel widths of 8 ft, 12 ft, and 16 ft were tested. The panel in Figure 5.1 has a width of 12 ft.

One complete cycle of loading for the first two phases of elastic shear testing involved four load steps listed as follows:

- Load step 1) – loaded to $\tau' = 0.01$ (k/in)
- Load step 2) – unloaded to $\tau' = 0$
- Load step 3) – loaded to $\tau' = -0.01$ (k/in)
- Load step 4) – unloaded to $\tau' = 0$

Data was typically recorded for several load levels within a given cycle. Three cycles of loading were applied to the PMDF shear specimens for testing Phases 1 and 2. A data acquisition system running Lab View was used to record the incremental loads and corresponding deflections throughout the test.

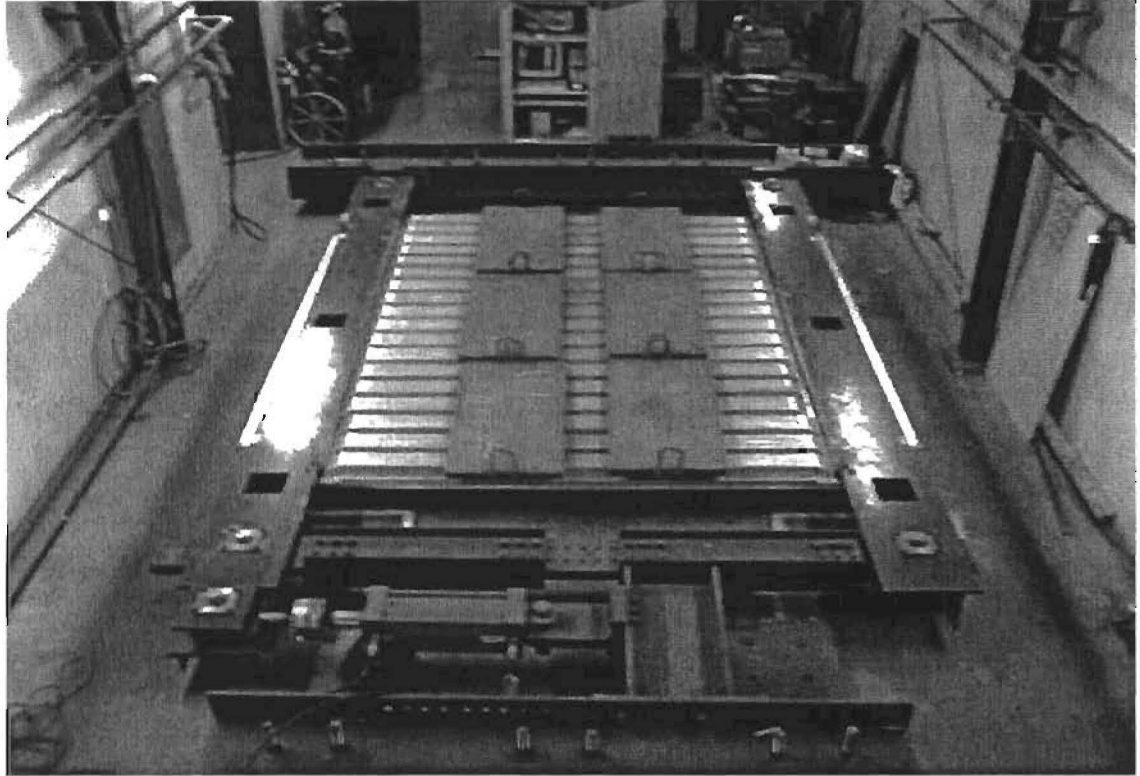


Figure 5.1 Shear Test Frame and Specimen with Simulated Concrete Load

These values were then transferred to Microsoft EXCEL spreadsheet for data processing and graphing. The data processing consisted of converting loads and deflections into effective shear stresses (τ') and shear strains (γ) respectively. A linear regression was performed on the data to obtain the average ratio of τ' / γ , thus giving the initial shear modulus, G'_0 . Figure 5.2 shows the data from Test 8, specimen (18ga.9ds.16pw.16ss.ecc). Recalling the naming scheme from Chapter 4 and reading from left to right in the name, this system was an 18 gage deck panel with a 9 ft deck span and a 16 ft panel width. The system had stiffening angles that were spaced at 16 ft (ie. only at the panel ends) and had the maximum eccentricity.

The graphs of the phase 1 and phase 2 loading show that the system stiffness is slightly higher for the Phase 2 test with superimposed dead load. The increase in stiffness for the loaded specimens most likely comes from the increase in friction forces between adjacent deck sheets along side lap seams as well as the support angle.

TEST 8: (18ga.9ds.16pw.16ss.ecc)

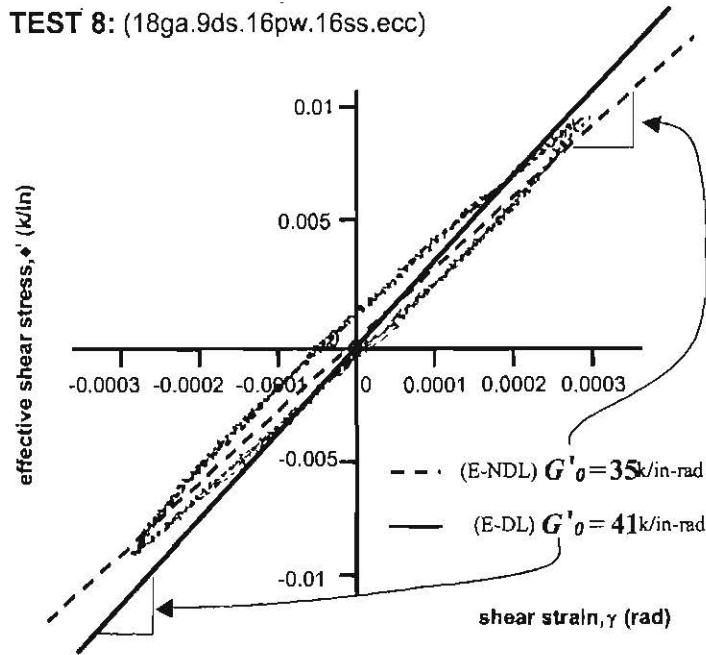


Figure 5.2 Elastic, Reversed Cyclic Loading (Initial Stiffness)

5.3 Shear Test Phase 3: Ultimate Capacity and Secant Stiffness

After the first two phases of cyclic loading were completed, specimens were racked (displaced) in one direction for Phase 3 of the shear testing until the ultimate load capacity, P_{ult} , was obtained. Similar to the first two phases of elastic, cyclic loading, the Phase 3 magnitudes of load and deflection recorded by the data acquisition system were transferred to spreadsheets for analysis and graphic interpretation.

In addition to determining the system ultimate shear strength (S'_{ult}) and rotational capacity (M'_{ult}), values of the secant stiffness at 40% and 80% of P_{ult} were also extracted from the Phase 3 tests, which will be referred to as $G'_{.4}$ and $G'_{.8}$ respectively. The secant stiffness $G'_{.4}$ is recommended by the Steel Deck Institute for design values of deck form stiffness when obtained from laboratory shear tests (Luttrell, L. D., *Steel Deck Institute Diaphragm Design Manual*, 2nd Ed., Canton, Ohio, 1995). Figure 5.3 shows the data from Phase 3 of Test 8, specimen (18ga.9ds.16pw.16ss.ecc), which was an 18-gage deck with a 9 ft deck span, a 16 ft panel width, had stiffening angles spaced at 16 ft and the maximum angle eccentricity. Values of the stiffness are shown at the initial cyclic loading stage (G'_0), secant stiffness at 40% of the ultimate load ($G'_{.4}$), and the secant stiffness at 80% of the ultimate load ($G'_{.8}$). As mentioned earlier, the Steel Deck Institute uses the stiffness at 40% of the ultimate load to identify the diaphragm stiffness. Comparing all three values provides an indication to the change in stiffness with increasing load. For this particular test, the system secant stiffness, $G'_{.8}$ (U-DL) = 11(k/in-rad), is 27% of its initial elastic stiffness, G'_0 (E-DL) = 41(k/in-rad).

Test 8: (18ga.9ds.16pw.16ss.ecc)
Phase 3 - ultimate with dead load (U-DL)

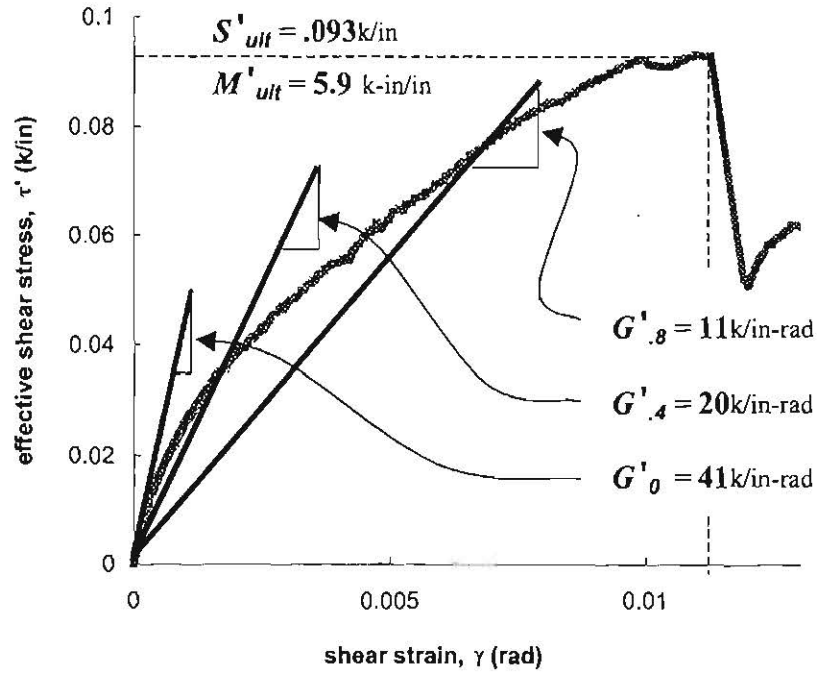


Figure 5.3 Phase 3 Loading Stress vs. Strain Behavior

5.4 Results

Results are presented in this section for the shear tests on the 16 gage, 18 gage, and 20 gage PMDF specimens. Since the behavior for the PMDF systems with the three different metal gages were very similar, much of the discussion will focus on the 18 gage deck. Although most of the tests were conducted with the maximum support angle eccentricity, tests were also conducted on systems with zero eccentricity to provide an indication of effect of the eccentricity on the stiffness and strength. Since the angle eccentricity in a real bridge will typically vary substantially along the girder length, the different support angle geometries also provide an indication of the range of stiffness values that may be encountered in the field. As outlined in Chapter 4, stiffening angles were incorporated into the deck system to improve the connection performance of the PMDF system. Tests will therefore be presented with and without the stiffening angles. Figure 5.4 shows a graph of the effective shear stress versus shear strain for Tests 1, 2, 3 and 4, which were tests on the 18-gage deck. The panels in these tests were all square with deck spans and panel widths of 8 ft. The effect of the eccentricity on the behavior of the unstiffened connections can be observed by comparing the curves for Tests 1 and 2. Test 1 had zero eccentricity while Test 2 had the maximum eccentricity. Although Test 2

possessed essentially the same ultimate capacity as Test 1, the corresponding stiffness is drastically reduced due to excessive support angle deformation. Figure 5.5 shows a picture of the severe angle deformation that reduces the stiffness of the eccentric connections. The picture was taken at the ultimate load on the panel. Also shown on the graphs are curves from tests demonstrating the beneficial effects of the stiffened connection details on the PMDF system behavior. Tests 3 and 4 have the same respective geometries as Tests 1 and 2, however the panels had stiffening angles at the ends. The presence of the stiffening angles is denoted by an X on the support angle. A comparison of Tests 2 and 4 reveals the improvement that stiffening angles have on eccentric connections. The graphs show that the stiffening angles can improve the strength of PMDF systems as well as the stiffness. Although the Test 3 had a higher stiffness and strength than Test 4, the effect of the eccentric support angle is not nearly as significant as with the cases with the unstiffened connections. Figure 5.6 shows a system with the stiffened support angle at the ultimate load. The stiffening angle prevents the support angle from pulling away from the flange. The failure of this system was actually caused by excessive bearing deformation along a sidelap fastener as well as buckling of the stiffening angle. Although Test 4 had an eccentric connection, the behavior of the system was very similar to the Test 1 curve, which had zero eccentricity.

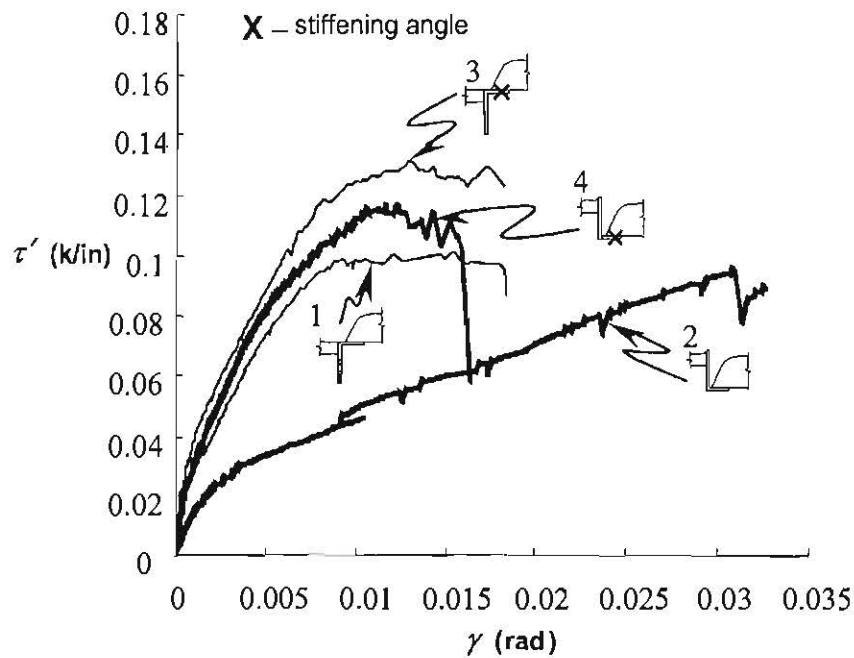


Figure 5.4 Effect of Stiffened Connections on PMDF Stress vs. Strain Behavior

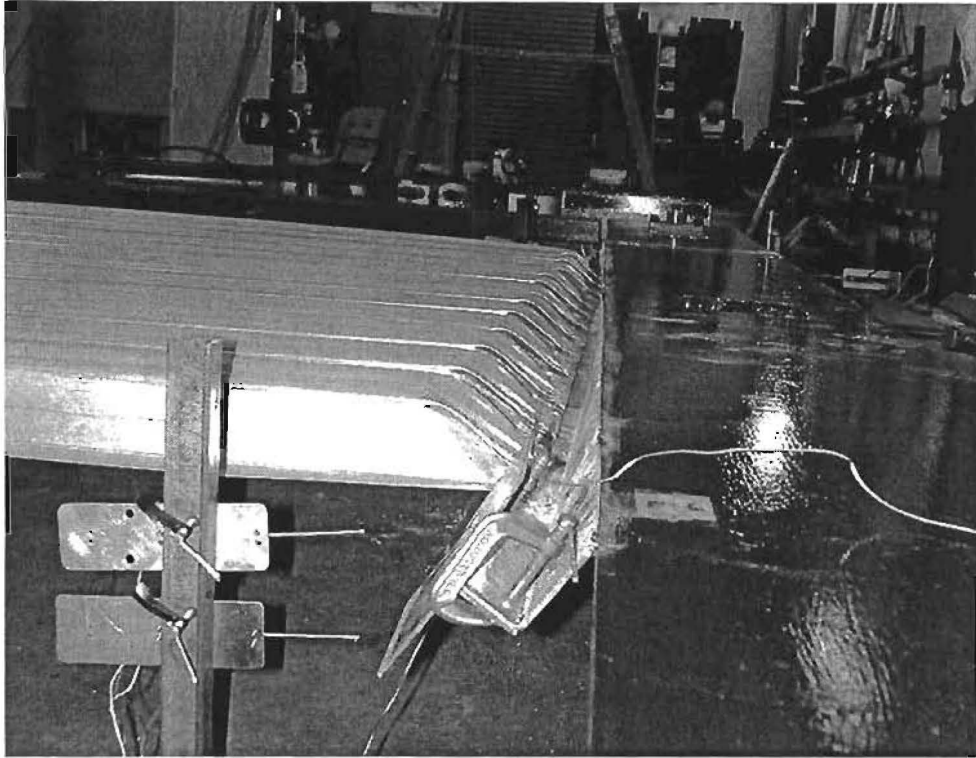


Figure 5.5 Support Angle Eccentricity Reduces the Stiffness of Unstiffened Deck Panels

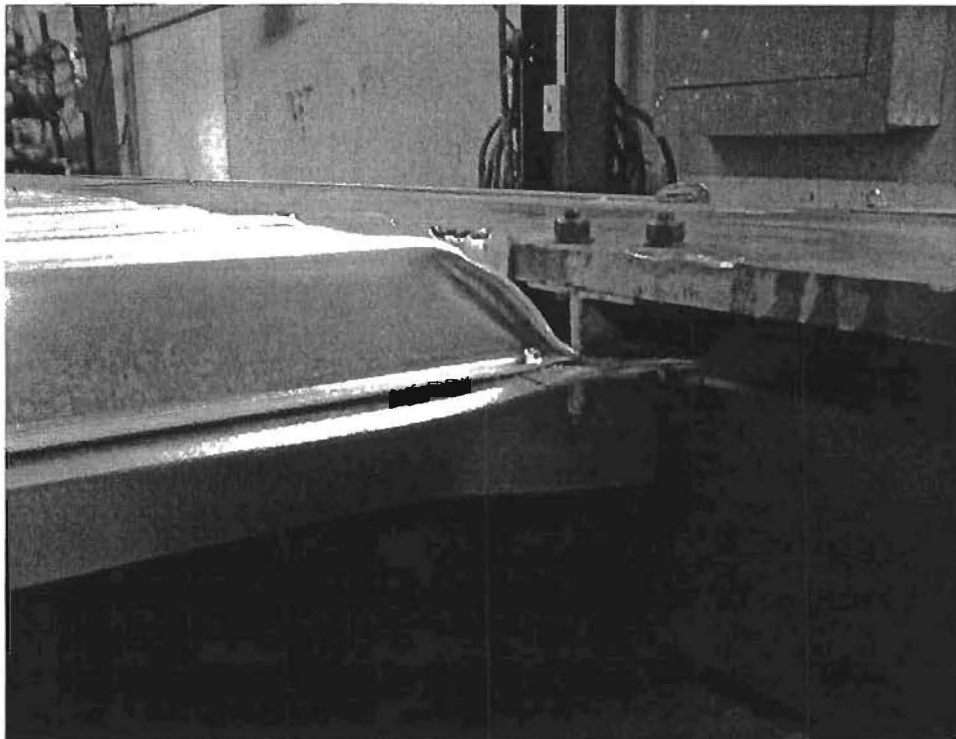


Figure 5.6 Failure of PMDF Systems with Stiffening Angles do not Result in Large Deformations at the Support Angle

Table 5.1 Shear Test Results for 18 ga. PMDF Specimens

	1	2	3	4	5	6	7	8	9
	Test # and Detail	span (ft)	width (ft)	stiffener spacing (ft)	$G'_{0(E-DL)}$ k/(in-rad) ($G'_{0(E-NDL)}$)	$G'_{.4(U-DL)}$ k/(in-rad) (% $G'_{0(E-DL)}$)	$G'_{.8(U-DL)}$ k/(in-rad) (% $G'_{0(E-DL)}$)	S'_{ult} k/in	M'_{ult} k-in/in
unstiffened (I)	1	8	8	NA	41 (31)	19 (46%)	14 (34%)	0.101	6.4
	2	8	8	NA	11 (36)	6 (55%)	4 (32%)	0.095	6
stiffened (II)	3	8	8	8	60 (33)	27 (45)	16 (27%)	0.132	8.4
	4	8	8	8	36 (35)	22(61%)	14 (40%)	0.116	7.4
	5	9	8	8	36 (27)	23 (64%)	14 (38%)	0.109	6.9
stiffened (III)	6	9	16	8	44 (37)	18 (41%)	17 (39%)	0.111	7
	7	9	12	12	39 (35)	22 (56)	13 (33%)	0.103	6.5
	8	9	16	16	41 (36)	20 (49%)	11 (27%)	0.093	5.9

Table 5.1 presents a summary of the results for the 18-gage deck. The first column labels the test number and illustrates the connection detail that was used between the deck and the top flange. The symbol “X” on the detail represents a stiffened connection with the approximate stiffening angle eccentricity indicated on the support angle. The diaphragm dimensions and stiffening angle spacing are also tabulated in the second, third and fourth columns.

Values for the effective shear modulus, G' , are tabulated in the fifth, sixth and seventh columns. In the fifth column, the initial “elastic, effective shear modulus” is the initial stiffness of the diaphragm with superimposed dead load from the Phase 2 of testing. The value shown in parentheses is the initial diaphragm stiffness from the phase 1 testing with no superimposed dead load. As mentioned in the last section, the Steel Deck Institute recommends a secant stiffness at a load level of 40% of the ultimate capacity, $G'_{.4}$. The value shown in column six of the table is the value of $G'_{.4}$ from the Phase 3 testing. The percentage of the initial elastic stiffness G'_{0} is given in parentheses. The ultimate effective shear strength, S'_{ult} , and ultimate rotational capacity, M'_{ult} , are provided in columns eight and nine respectively.

In addition to improving the connection details currently employed in bridge construction, this stage of the research also investigated the effects that the shear panel dimensions and stiffener spacing have on the overall strength and stiffness of PMDF systems. For this reason Table 5.1 is divided into three categories: Category I (Tests 1 & 2) represent the details commonly found in current practice, including both the non-eccentric and eccentric unstiffened connections; Category II (Tests 3, 4 & 5) consists of the results for the stiffened diaphragms having roughly the same square dimensions and eccentricities as those in Category I; Category III (Tests 6, 7 & 8) consist of the eccentric, stiffened connections with rectangular diaphragm dimensions and varied stiffener spacing.





The results for the Category 1 of Table 5.1 tests show that the eccentric connection (Test 2) only has about 25% of the initial stiffness of the connection without eccentricity (Test 1). Although the reduction in stiffness is considerable, the reduction in strength between these systems is not remarkable. Tests 3 & 4 had stiffened connections that have the same panel dimensions and eccentricities as the respective Tests 1 & 2. The reductions in the initial stiffness, G'_0 , due to the connection eccentricity between the systems in Category II is of the same relative magnitude as those in Category I. However, the percent reduction is not nearly as substantial (i.e., approximately 50% Category II reduction compared to a 75% Category I reduction). For the secant stiffness values at 40 % and 80% of the ultimate load with the stiffening angles, the eccentricity has very little affect on the measured values. Comparing the strengths of the panels with the maximum eccentricity (Tests 4 and 5 – stiffened to Test 2 – unstiffened), the stiffening angles increased the diaphragm strength by approximately 15% to 22% depending on the deck span. The significance of comparison between Tests 3 & 4 is that the stiffness and strength have been markedly improved with respect to Category I. In fact, the strength of the eccentric, stiffened detail in Test 4 is nearly 15% greater than that of the unstiffened detail with zero eccentricity (Test 1) while the initial stiffness is nearly the same. The secant stiffness at 40% of the ultimate load is actually higher for Test 4 than Test 1. The results in Category II show that slightly different deck spans had virtually no impact on the PMDF panel performance (Test 4 & 5).

The tests from Category III of Table 5.1 as well as Test 5 demonstrate the effects that the stiffening angle spacing and panel width have on the system performance. The correlation between Tests 5, 7 and 8 is that these systems share the same span while the respective panel widths were incrementally increased by four feet and that they were stiffened only at the ends of the panel. From this perspective it can be observed that increasing the stiffening angle spacing did not significantly change the panel performance. Although the panel width of Test 6 was twice that of Test 5, the two panels had the same spacing between stiffening angles. A comparison of these two tests indicates that the stiffness and strength were not substantially impacted by the panel width.

Table 5.2 and Table 5.3 show the corresponding results for the 16 gage and 20 gage specimens respectively. The behavior of the deck forms with these other metal

gages did not differ significantly from the 18 gage deck. The cases that were tested for the 16 gage deck all had stiffening angles positioned at the maximum eccentricity. Similar to the 18 gage tests, the panel widths that were considered ranged from 8 ft to 16 ft with stiffeners only at the ends (Tests 9, 11, and 12) as well as the case of 3 stiffening angles in Test 10. Despite significant changes in the panel geometry, the results were relatively similar to each other with G'_0 varying from 37 to 45, $G'_{0.4}$ varying from 17 to 23, and $G'_{0.8}$ varying from 14 to 17.

Table 5.2 Shear Test Results for 16ga PMDF Specimens

1	2	3	4	5	6	7	8	9
Test # and Detail	span (ft)	width (ft)	stiffener spacing (ft)	$G'_{0(E-DL)}$ k/(in-rad) ($G'_0(E-NDL)$)	$G'_{.4(U-DL)}$ k/(in-rad) ($\%G'_0(E-DL)$)	$G'_{.8(U-DL)}$ k/(in-rad) ($\%G'_0(E-DL)$)	S'_{ult} k/in	M'_{ult} k-in/in
9 	9	8	8	36 (32)	21 (58%)	15 (42%)	0.109	6.9
10 	9	16	8	45 (38)	23 (51%)	17 (38%)	0.103	6.5
11 	9	12	12	40 (37)	17 (43%)	14 (35%)	0.115	7.3
12 	9	16	16	37 (34)	22 (59%)	15 (41%)	0.088	5.6

The results for the 20 gage (Table 5.3) deck show tests for cases with conventional connection details as well as the stiffened connections. The comparisons between the stiffened connections and the unstiffened connections are very similar to those observed for the 18 gage deck. The stiffening angle substantially increases the stiffness of the PMDF system. The stiffened eccentric connection (Test 16) provided higher values of the stiffness than the unstiffened system with zero eccentricity.

Table 5.3 Shear Test Results for 20ga PMDF Specimens




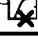
1	2	3	4	5	6	7	8	9
Test # and Detail	span (ft)	width (ft)	stiffener spacing (ft)	$G'_{0(E-DL)}$ k/(in-rad) ($G'_0(E-NDL)$)	$G'_{.4(U-DL)}$ k/(in-rad) ($\%G'_0(E-DL)$)	$G'_{.8(U-DL)}$ k/(in-rad) ($\%G'_0(E-DL)$)	S'_{ult} k/in	M'_{ult} k-in/in
13 	8	8	NA	29 (21)	12 (42%)	10 (32%)	0.08	4.3
14 	8	8	NA	9 (7.3)	6 (62%)	NA	0.06	3.4
15 	8	8	8	46 (41)	26 (56%)	16 (33%)	0.09	5.1
16 	8	8	8	29 (31)	15 (50%)	12 (40%)	0.08	4.5

Table 5.4 groups the sets of tests performed on 20 ga, 18 ga and 16 ga PMDF specimens. Figure 5.7 to Figure 5.10 show the graphs of the shear stress versus the shear strain for the ultimate loading stage for the 18 and 16 gage deck with stiffened connections. The curves show that the 18 gage deck did provide a little higher ductility than the 16 gage deck, however neither metal gage would exhibit behavior that would be categorized as highly ductile. As a result, care should be taken in utilizing the PMDF systems to ensure that the forms have a relatively high factor of safety.

Table 5.4 Shear Test Results for 20ga 18ga and 16ga PMDF Specimens

1	2	3	4	5	6	7	8	9
Test # and gage	span (ft)	width (ft)	stiffener spacing (ft)	$G'_{0(E-DL)}$ k/(in-rad) ($G'_{0(E-NDL)}$)	$G'_{.4(U-DL)}$ k/(in-rad) (% $G'_{0(E-DL)}$)	$G'_{.8(U-DL)}$ k/(in-rad) (% $G'_{0(E-DL)}$)	S'_{ult} k/in	M'_{ult} k-in/in
16 (20ga)	9	8	8	29 (31)	15 (50%)	12 (40%)	0.08	4.5
5 (18ga)	9	8	8	36 (31)	23 (64%)	14 (38%)	0.109	6.9
9 (16ga)	9	8	8	36 (32)	21 (58%)	15 (42%)	0.109	6.9
6 (18ga)	9	16	8	44 (36)	18 (41%)	17 (39%)	0.111	7
10 (16ga)	9	16	8	45 (38)	23 (51%)	17 (38%)	0.103	6.5
7 (18ga)	9	12	12	39 (33)	22 (56%)	13 (33%)	0.103	6.5
11 (16ga)	9	12	12	40 (37)	17 (43%)	14 (35%)	0.115	7.3
8 (18ga)	9	16	16	41 (35)	20 (49%)	11 (27%)	0.093	5.9
12 (16ga)	9	16	16	37 (34)	22 (59%)	15 (41%)	0.088	5.6

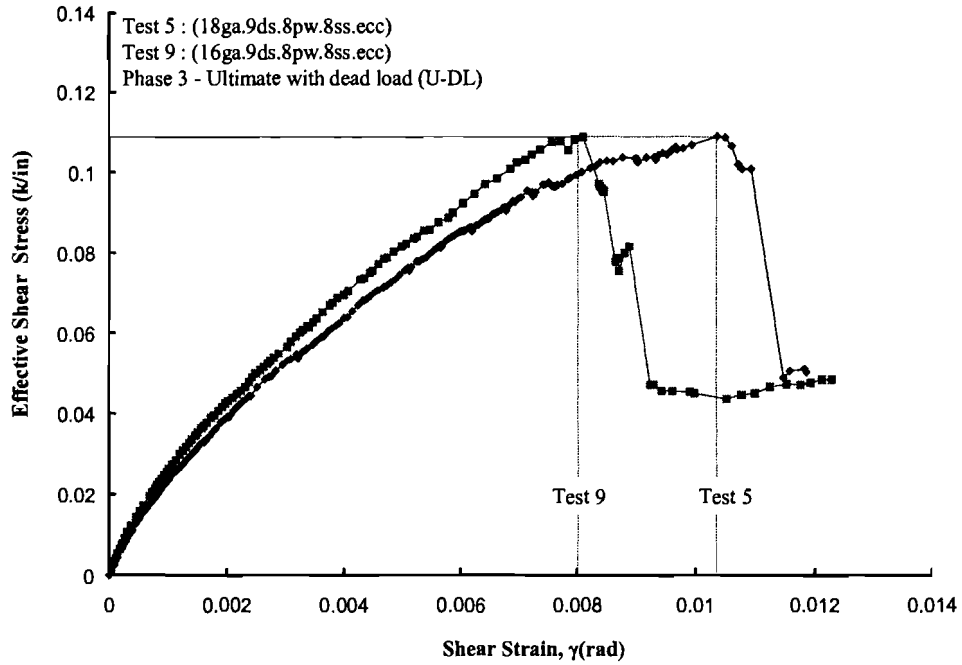


Figure 5.7 Ductility of 18ga and 16ga PMDF Systems with Stiffened Connection Details (8 ft Panel Width and Stiffener Spacing)

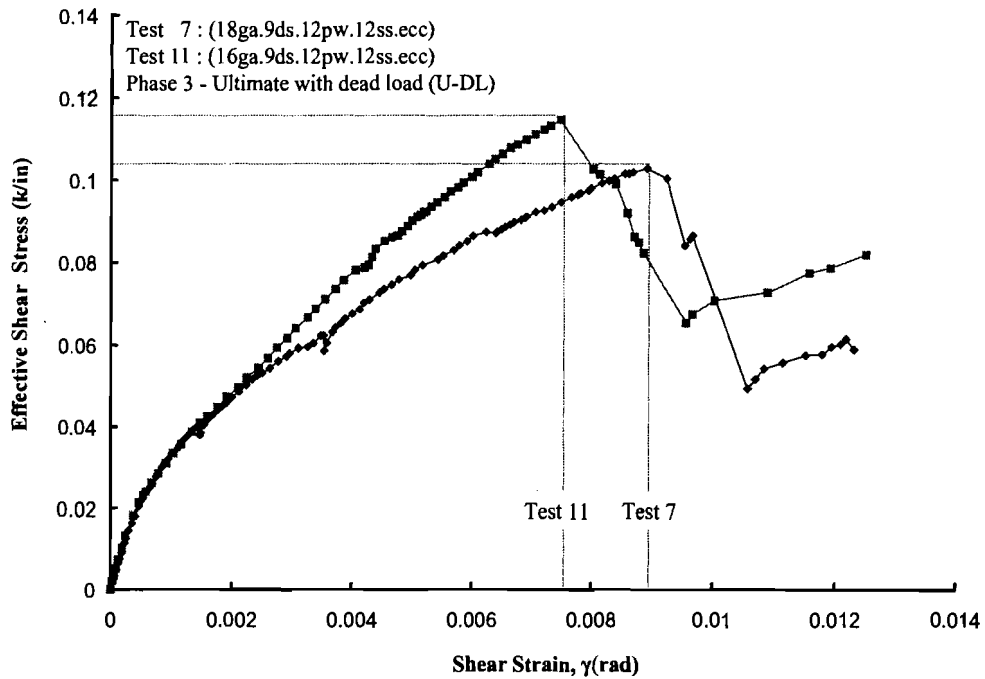


Figure 5.8 Ductility of 18ga and 16ga PMDF Systems with Stiffened Connection Details (12 ft Panel Width and Stiffener Spacing)

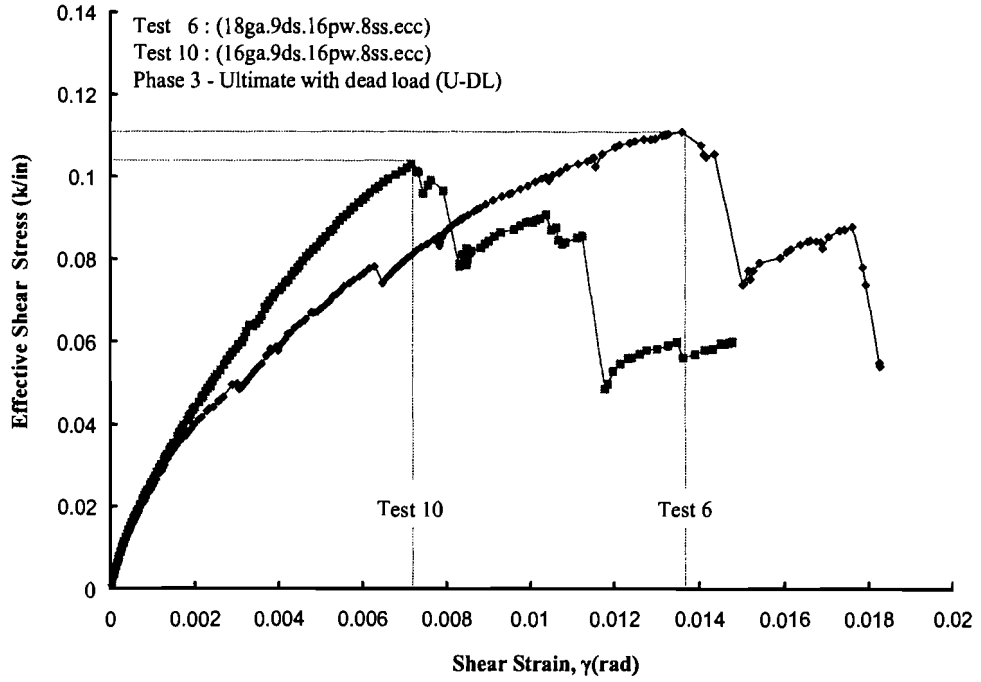


Figure 5.9 Ductility of 18ga and 16ga PMDF Systems with Stiffened Connection Details (16 ft Panel Width – 8 ft Stiffener Spacing)

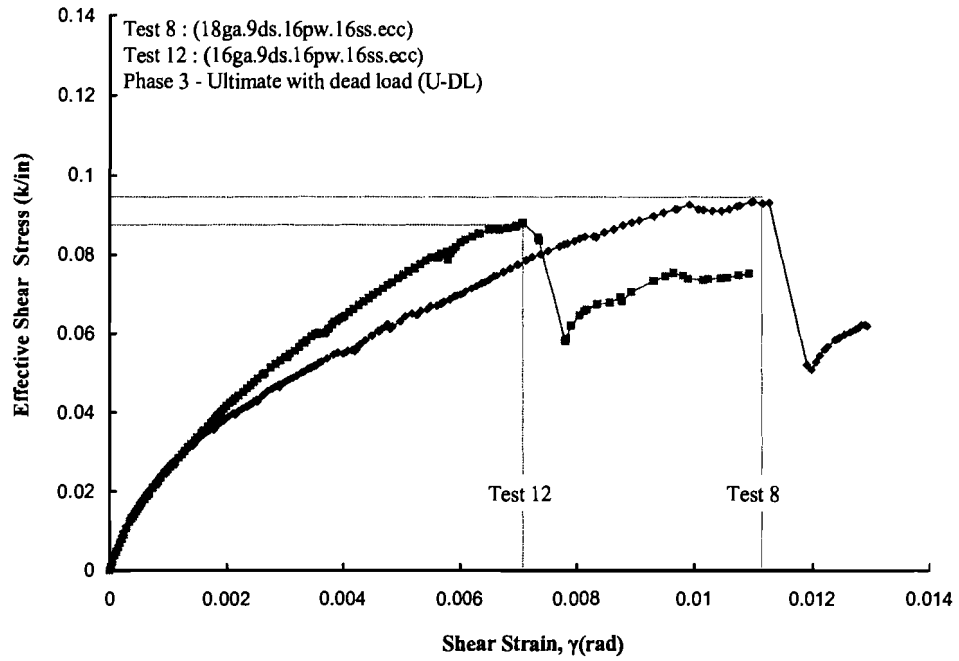


Figure 5.10 Ductility of 18ga and 16ga PMDF Systems with Stiffened Connection Details (16 ft Panel Width and Stiffener Spacing)

Chapter 6

Twin Girder Lateral Displacement Tests

6.1 Overview

The objective of this phase of the testing was to determine the lateral stiffness of PMDF systems subjected to deformations similar to the deflected top flange profile of buckled girders. In the shear tests that were discussed in Chapter 5, the test frame forced the PMDF to deform in a mode of pure shear. In actual applications the forms are bent in their plane. As a result, the shear stiffness contributes the most near the ends and around cross-frames or diaphragms. Near the middle between these discrete bracing points, the in-plane flexural stiffness contributes to the lateral stiffness. To measure the behavior, a twin girder setup was designed and constructed. The 50 ft long twin girder and PMDF specimens tested in this phase of the research were described in Section 4.3.4 of this report. A total of 5 PMDF systems were tested:

1. 18 gage
2. 16 gage
3. 20 gage first set (20ga01)
4. 20 gage second set (20ga02)
5. 20 gage third set (20ga03)

The reason three 20 gage decks were laterally tested was because these were the primary systems on which buckling tests were conducted. So as to ensure that equal quality was achieved between the different systems, lateral load tests were conducted prior to the buckling tests.

Shear strains during lateral displacement tests were limited to the elastic range as determined from the shear tests.

For the 18 gage series of tests PMDF panels were tested with and without superimposed dead load that was applied with 4ft x 4ft x 0.5ft concrete blocks (~1000 lbs ea). For the 16ga, 20ga01, 20ga02 and 20ga01 series of tests PMDF panels were tested only with the superimposed dead load.

6.2 Partially Decked Tests

As explained earlier in Section 4.3.4 specimens were attached in panel increments, working from the supports towards midspan. The tests were conducted by first placing PMDF panels on only the 8 ft region adjacent to the support, followed by 12 ft and 16 ft panels. Tests conducted with panels only near the support region should be dominated by the in-plane shear stiffness of the PMDF.

Companion finite element analyses (FEA) were done on girders with a shear diaphragm for bracing. Isolated comparisons were made between the test results and the

FEA results to demonstrate the bracing behavior. The shear diaphragm truss panel model described in Section 3.2 was used in the FEA studies. For the unstiffened deck, the effective shear modulus, G' , was determined using the laboratory test results with PMDF installed only over the 12 ft region (up to the quarter-point lateral loading frames) near the two supports as depicted in Figure 6.1. The area of the FEA shear diaphragm truss panels was adjusted to acquire the same lateral stiffness as the laboratory tests conducted on the 12 ft PMDF specimens.

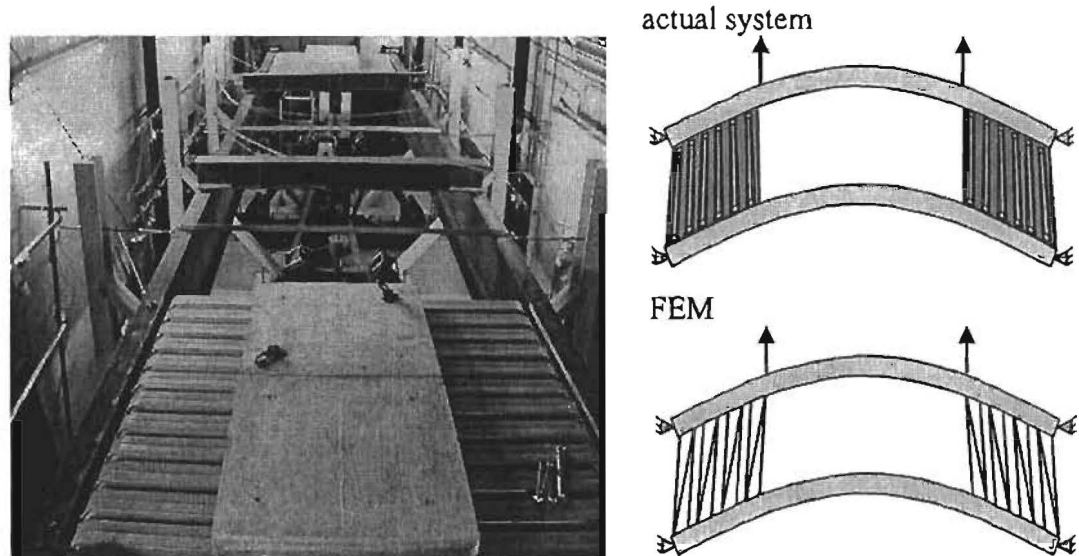


Figure 6.1 Left- Partially Decked (12ft) PMDF Specimen with Concrete Dead Load; Right- Calibration of FEA from Unstiffened Partially Decked System

To capture the behavior of PMDF systems with stiffening angle connection details, a stiffening truss model was developed as explained in Section 3.2. This model was achieved by attaching a stiffening truss system as depicted in Figure 6.2. Two rigid beam elements with pinned ends were used to simulate the stiffening angles to which the stiffening trusses were connected. In this phase of the analysis, the elements labeled “shear diaphragm truss elements” in Figure 6.2 had the same cross-sectional area from the unstiffened model for each deck type. Laboratory tests with 8 ft and 16 ft of decking at the ends of the girders (spacing between stiffening angles = 8 ft and 16 ft respectively) were performed. The areas of the stiffening truss elements were then adjusted in the FEA model so that the lateral stiffness of the computer solution and test results matched. Since the deck panels near the supports primarily provide bracing due to the shear stiffness, the partially decked tests provided results that indicated the bracing contributions primarily due to the diaphragm action in the PMDF system. These results had reasonable agreement with the shear frame tests, however the deck system was not quite as stiff since the flange thickness of the test beams was less than the thickness of the flanges on the shear frame beams. As a result, regions along the support angle that were subjected to compression-type forces were not as stiff as in the shear frame tests.

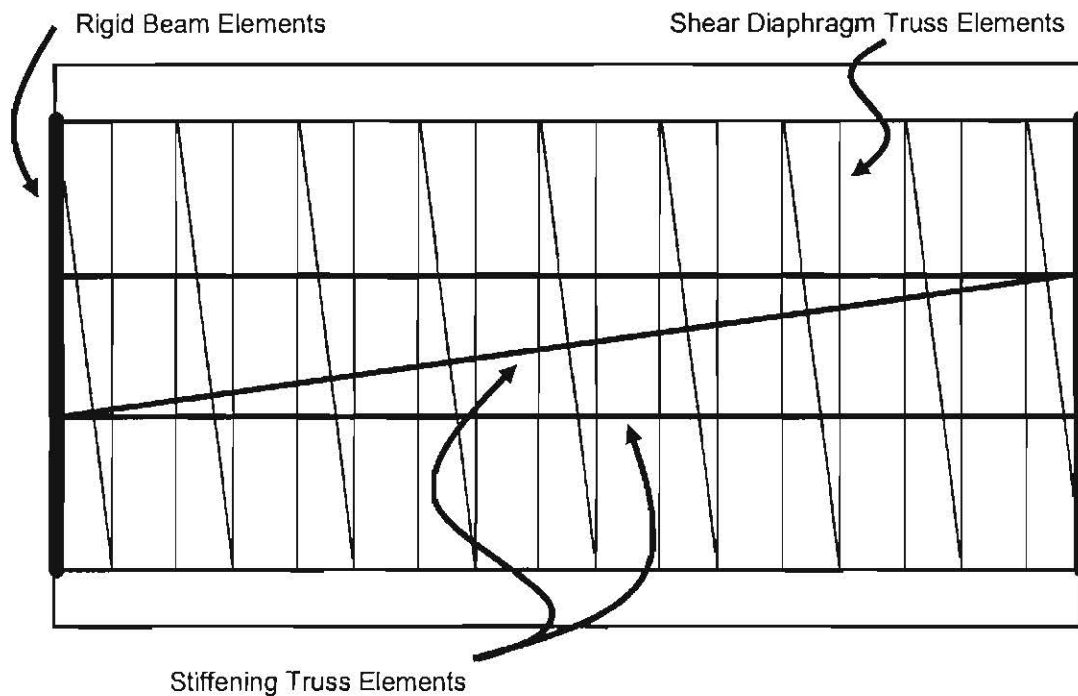


Figure 6.2 FEA Stiffening Angle Truss

6.3 Fully Decked Tests

Utilizing the results from the partially decked tests provided information as to the shear stiffness of the PMDF system. However when comparisons were made between the laboratory test results and FEA results for the fully deck systems, the FEA solutions tended to underestimate the stiffness of the PMDF system. The larger stiffness of the actual system was attributed to the in-plane flexural stiffness of the deck forms. Although the shear stiffness provides significant restraint to the top flange near the ends of the member, the contributions of the shear stiffness near midspan are essentially zero since there is very little shear deformation in this region. Therefore one of the goals of this phase of the research was to compare the laboratory and FEA results of the fully decked system and identify the additional contribution to unstiffened PMDF systems that is not captured by a shear diaphragm model. For systems without stiffening angle connection details, two beam elements coupled laterally to the top flange of both of the girders was used to study the effect of the in-plane stiffness of the decking as shown in Figure 6.3. The moment of inertia of the FEA beam elements was adjusted to acquire the same lateral stiffness measured in the laboratory tests.

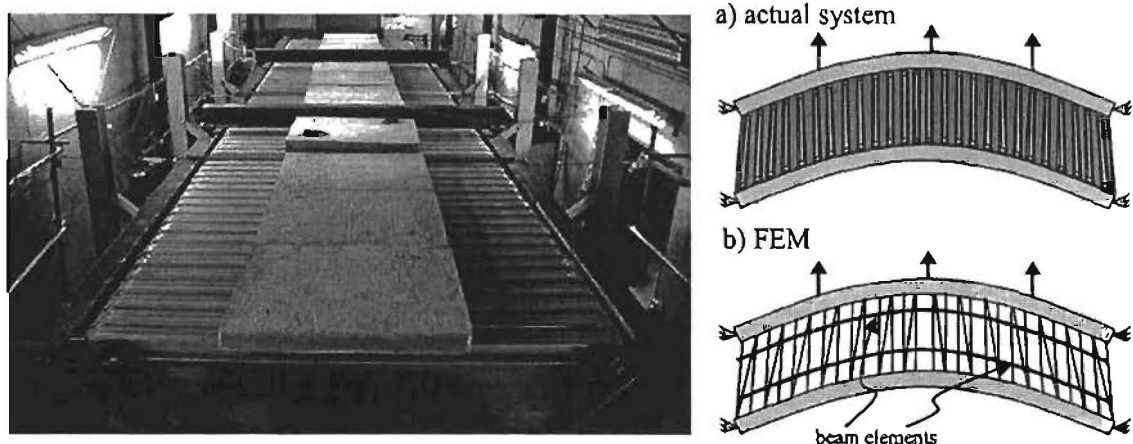


Figure 6.3 Left- Fully Decked (24ft) PMDF Specimen with Concrete Dead Load; Right- Calibration of Beam Element from Unstiffened Fully Decked System

With the fully decked system 8 ft, 16 ft and 24 ft spaced stiffened tests were also performed. The 8 ft and 16 ft spaced stiffened laboratory test results were compared with FEA results that used the stiffening truss element areas calculated from the partially decked stiffened systems. For the 24 ft stiffened system, the FEA model was calibrated using the fully decked system.

6.4 Results

Table 6.1 through Table 6.17 provide values for the lateral stiffness from both laboratory and FEA results for 18ga, 16ga, 20ga01, 20ga02 and 20ga03 deck systems, respectively. The tabulated values are the lateral stiffness (k/in) of the PMDF system measured at the respective turnbuckle locations. A measure of the lateral stiffness of the system was obtained by dividing the turnbuckle or FEA force by the corresponding lateral deflection at the point.

The second column of values in Table 6.1 through Table 6.5 shows results for the 12 ft panel, unstiffened system. Results in this column are identical because the FEA shear diaphragm was calibrated to this case. Based on the laboratory measurements, the 18 ga unstiffened deck had a $G' = 8.5$ k/(in-rad), shown in second row in parenthesis. This value was less than the value of $G' = 11$ k/(in-rad) shown in Table 5.1 from the shear tests on the same deck system (Test 2 – unstiffened deck). The primary reason for the lower stiffness in the twin girder tests was most likely due to the difference in the flange thickness between the shear test frame and the flanges of the twin-girder setup. The W30x90 beams had a top flange thickness of approximately 0.60 in compared with the 1 in plate thickness in the shear frame. Figure 4.4 that was presented earlier discussed the effect of the flange thickness on the stiffness of parts of the connection that are subjected to compression.

Based on the laboratory tests, the 16 ga unstiffened deck had a $G' = 7.1$ k/(in-rad). This value was less than the value of $G' = 8.5$ k/(in-rad) for the thinner 18 ga deck

system. However, the eccentricity of the support angles welded to the top flange of the 16 ga deck system was slightly higher than the eccentricity of the support angles used in the 18 ga deck system, which led to a lower system stiffness for the thicker deck. Since the PMDF systems follow the behavior of springs in series as outlined in Eq. 4.1, the lower stiffness of either the connection or the deck often controls the system stiffness. For the 20 gage systems, 20ga01, 20ga02 and 20ga 03 unstiffened decks had G' values of 6.8, 7.3 and 6.8 k/(in-rad) respectively. As discussed above these values were lower than $G' = 9.5$ k/(in-rad) from the shear tests on the same deck system due to the flange thickness difference between the test beams and the shear frame.

The third and fourth columns of values in Table 6.1 through Table 6.5 provide results for the fully decked systems displaced at the quarter-points and midspan, respectively. The numbers in parentheses in the forth row show the moment of inertias used for the beam elements which simulated the in-plane flexural stiffness of the fully decked system. For both quarter point and midspan loading, the shear diaphragm model underestimated the lateral stiffness of the actual PMDF system of 18ga, 16ga, 20ga01, 20ga02 and 20ga03 by the ratio of $(8.6)/(6.7) = 1.28$, $(10.7)/(5.9) = 1.28$, $(6.8)/(5.6) = 1.21$, $(7.7)/(6.0) = 1.28$ and $(6.5)/(5.6) = 1.16$ respectively for quarter point loading and $(11.4)/(7.0) = 1.63$, $(10.7)/(5.9) = 1.81$, $(8.1)/(5.8) = 1.40$, $(10.0)/(6.2) = 1.61$ respectively for midspan loading.

The fifth and sixth columns in the tables provide results for the fully decked systems displaced with a half-sine loading. Making a meaningful comparison between the lateral stiffness values from the measured and FEA results with the sine loading can be difficult since the behavior at the quarter points and midspan are quite different. The fifth column corresponds to the lateral stiffness at midspan and the sixth column corresponds to the lateral stiffness at the quarter points. At midspan the shear diaphragm model underestimated the lateral stiffness of the actual PMDF system by the ratio of 2.1, 2.7, 1.8, 1.7 and 2.0 respectively. However, at the quarter points the shear diaphragm model *overestimated* the lateral stiffness of the actual PMDF system by the ratio of 1.1, 1.8, 1.2, 1.3 for 18ga, 16ga, 20ga01 and 20ga03 deck systems, respectively. For the 20ga02 deck system, the shear diaphragm model underestimated the lateral stiffness of the actual PMDF system by the ratio of 1.1 for the 20ga02 deck system at midspan.

Lateral loading only at the quarter points or at midspan showed that the shear diaphragm model underestimated the lateral stiffness of the bracing. However for the half sine curve loading, the indication of these stiffness comparisons can be difficult to comprehend since for all but one of the decks tested the FEA shear diaphragm model underestimated the stiffness at midspan but overestimated the stiffness at the quarter points. However a comparison between the midspan stiffness values between the cases for the half sine curve loading and the midspan lateral loading (column 3) provide an indication that the stiffness is underestimated by the shear diaphragm model even for the sine curve loading. For example, for the 18 ga tests shown in Table 6.1, the measured midspan stiffness was 8.2 k/in for the half sine loading. Using the sine curve loading in the FEA analysis with only a midspan load provided a stiffness of only 7 k/in. A larger

stiffness was achieved at the midspan location even though loads were also applied at the quarter points in the half sine curve loading.

Table 6.1 18ga Tests Unstiffened, Comparison of Laboratory and FEA Results

LATERAL STIFFNESS (k/in)	12 ft end panel unstiffened quarter point loading	Fully decked unstiffened midspan point loading	Fully decked unstiffened quarter point loading	Fully decked unstiffened half sine loading	
				midspan	quarter point
Laboratory	6.3	11.4	8.6	8.2	3.2
FEA shear diaphragm	6.3 (G'=8.5 k/in)	7 (G'=8.5 k/in)	6.7 (G'=8.5 k/in)	3.9 (G'=8.5 k/in)	3.6 (G'=8.5 k/in)
FEA shear diaphragm & beam element	NA	11.3 (I=260 in ⁴)	8.6 (I=110 in ⁴)	5.4 (I=170 in ⁴)	4.5 (I=170 in ⁴)

Table 6.2 16ga Unstiffened Tests, Comparison of Laboratory and FEA Results

LATERAL STIFFNESS (k/in)	12 ft end panel unstiffened quarter point loading	Fully decked unstiffened midspan point loading	Fully decked unstiffened quarter point loading	Fully decked unstiffened half sine loading	
				midspan	quarter point
Laboratory	5.5	10.7	7.3	9.1	1.7
FEA shear diaphragm	5.5 (G'=7.1 k/in)	5.9 (G'=7.1 k/in)	5.7 (G'=7.1 k/in)	3.4 (G'=7.1 k/in)	3.1 (G'=7.1 k/in)
FEA shear diaphragm & beam element	NA	10.5 (I=280 in ⁴)	7.5 (I=100 in ⁴)	4.9 (I=170 in ⁴)	3.9 (I=170 in ⁴)

Table 6.3 20ga(01) Unstiffened Tests, Comparison of Laboratory and FEA Results

LATERAL STIFFNESS (k/in)	12 ft end panel unstiffened quarter point loading	Fully decked unstiffened midspan point loading	Fully decked unstiffened quarter point loading	Fully decked unstiffened half sine loading	
				midspan	quarter point
Laboratory	5.4	8.1	6.8	5.9	2.6
FEA shear diaphragm	5.4 (G'=6.8 k/in)	5.8 (G'=6.8 k/in)	5.6 (G'=6.8 k/in)	3.3 (G'=6.8 k/in)	3 (G'=6.8 k/in)
FEA shear diaphragm & beam element	NA	8.1 (I=140 in ⁴)	6.8 (I=65 in ⁴)	3.9 (I=65 in ⁴)	3.4 (I=65 in ⁴)

Table 6.4 20ga(02) Unstiffened Tests, Comparison of Laboratory and FEA Results

LATERAL STIFFNESS (k/in)	12 ft end panel unstiffened quarter point loading	Fully decked unstiffened midspan point loading	Fully decked unstiffened quarter point loading	Fully decked unstiffened half sine loading	
				midspan	quarter point
Laboratory	5.7	10	7.7	5.9	3.6
FEA shear diaphragm	5.7 (G'=7.3 k/in)	6.2 (G'=7.3 k/in)	6 (G'=7.3 k/in)	3.5 (G'=7.3 k/in)	3.2 (G'=7.3 k/in)
FEA shear diaphragm & beam element	NA	10 (I=240 in ⁴)	7.7 (I=80 in ⁴)	4.9 (I=170 in ⁴)	4 (I=170 in ⁴)

Table 6.5 20ga(03) Unstiffened Tests, Comparison of Laboratory and FEA Results

LATERAL STIFFNESS (k/in)	12 ft end panel unstiffened quarter point loading	Fully decked unstiffened midspan point loading	Fully decked unstiffened quarter point loading	Fully decked unstiffened half sine loading	
				midspan	quarter point
Laboratory	5.3	9.1	6.5	6.5	2.3
FEA shear diaphragm	5.3 (G'=6.8 k/in)	5.8 (G'=6.8 k/in)	5.6 (G'=6.8 k/in)	3.3 (G'=6.8 k/in)	3 (G'=6.8 k/in)
FEA shear diaphragm & beam element	N/A	9.1 (I=180 in ⁴)	6.5 (I=45 in ⁴)	4.1 (I=65 in ⁴)	3.4 (I=65 in ⁴)

Table 6.6 through Table 6.9 provide values for the lateral stiffness from both laboratory and FEA results for the 8 ft stiffened tests for the 18ga, 16ga, 20ga01 and 20ga02 deck systems, respectively. Stiffened tests were not performed on the 20ga03 deck system. The second column of values in Table 6.6 through Table 6.9 show results for the 16 ft end panel, unstiffened system quarter point loading. The third column of values tabulates results for the 16ft end panel with stiffeners spaced at 8ft. It can be observed from the results that the 8 ft stiffened system is stiffer than the unstiffened system with a ratio of $(17.4)/(9.4) = 1.85$, $(14.0)/(7.6) = 1.84$, $(10.8)/(6.9) = 1.57$ for 18ga, 16ga and 20ga01 deck systems respectively. Partially decked tests were not performed on 20ga02 deck system. The shear diaphragm model underestimated the lateral stiffness of the 16 ft end panel tests with stiffening angles spaced at 8 ft by the ratio of 2.60, 2.46 and 1.92 for 18ga, 16ga and 20ga01 deck systems, respectively.

The fourth and fifth columns of values in Table 6.6 through Table 6.9 provide results for the fully decked 8 ft stiffened systems displaced at the midspan and quarter-points, respectively. The sixth and seventh columns of values in Table 6.6 through Table 6.9 provide results for the fully decked 8 ft stiffened systems displaced with a half sine loading. The sixth column corresponds to the lateral stiffness at midspan and the seventh

column corresponds to the lateral stiffness at quarter points. The numbers in parentheses show the areas of the stiffened truss elements used in the FEA models. In 18ga and 16ga tests the FEA model's stiffened truss elements had to be recalibrated since the model calibrated from the 16 ft end panel with 8 ft stiffeners overestimated the stiffness of the fully decked systems. However for the 20ga01 test this recalibration was not needed as can be seen in Table 6.8. As stated earlier no partially decked tests were conducted on the 20ga02 deck system, hence the model was calibrated according to the fully decked tests.

Table 6.6 18ga Stiffened 8ft Tests, Comparison of Laboratory and FEA Results

LATERAL STIFFNESS (k/in)	16 ft end panel unstiffened quarter point loading	16 ft end panel stiffened 8ft quarter point loading	Fully decked stiffened 8ft mid point loading	Fully decked stiffened 8ft quarter point loading	Fully decked stiffened 8ft half sine loading	
					midspan	quarter point
Laboratory	9.4	17.4	19.3	17	11.7	9.2
FEA shear diaphragm	6.7	6.7	6.9	6.7	4	3.6
FEA shear diaphragm & stiff. element	NA	17.9 (A=3.0 in ²)	19.4 (A=1.7 in ²)	17.4 (A=1.6 in ²)	12 (A=1.6 in ²)	8.3 (A=1.6 in ²)

Table 6.7 16ga Stiffened 8ft Tests, Comparison of Laboratory and FEA Results

LATERAL STIFFNESS (k/in)	16 ft end panel unstiffened quarter point loading	16 ft end panel stiffened 8ft quarter point loading	Fully decked stiffened 8ft mid point loading	Fully decked stiffened 8ft quarter point loading	Fully decked stiffened 8ft half sine loading	
					midspan	quarter point
Laboratory	7.6	14.0	16.9	13.3	12.6	5.2
FEA shear diaphragm	5.7	5.7	5.9	5.7	3.4	3.1
FEA shear diaphragm & stiff. element	NA	14.0 (A=1.2 in ²)	16.6 (A=1.3 in ²)	13.5 (A=0.9 in ²)	9.3 (A=1.0 in ²)	7 (A=1.0 in ²)

Table 6.8 20ga(01) Stiffened 8ft Tests, Comparison of Laboratory and FEA Results

LATERAL STIFFNESS (k/in)	16 ft end panel unstiffened quarter point loading	16 ft end panel stiffened 8ft quarter point loading	Fully decked stiffened 8ft mid point loading	Fully decked stiffened 8ft quarter point loading	Fully decked stiffened 8ft half sine loading	
					midspan	quarter point
Laboratory	6.9	10.8	11.3	9.9	8	3.9
FEA shear diaphragm	5.6	5.6	5.8	5.6	3.3	3
FEA shear diaphragm & stiff. element	NA	10.8 (A=0.5 in ²)	11.6 (A=0.5 in ²)	11 (A=0.5 in ²)	5.9 (A=0.3 in ²)	5 (A=0.3 in ²)

Table 6.9 20ga(02) Stiffened 8ft Tests, Comparison of Laboratory and FEA Results

LATERAL STIFFNESS (k/in)	16 ft end panel unstiffened quarter point loading	16 ft end panel stiffened 8ft quarter point loading	Fully decked stiffened 8ft mid point loading	Fully decked stiffened 8ft quarter point loading	Fully decked stiffened 8ft half sine loading	
					midspan	quarter point
Laboratory	NA	NA	15.3	13.3	9.4	6.2
FEA shear diaphragm	NA	NA	6.2	6	3.5	3.2
FEA shear diaphragm & stiff. element	NA	NA	15.3 (A=1.0 in ²)	13.3 (A=0.8 in ²)	8.6 (A=0.8 in ²)	6.7 (A=0.8 in ²)

Table 6.10 through Table 6.13 provides values for the lateral stiffness from both laboratory and FEA results for the 16 ft stiffened tests for 18ga, 16ga, 20ga01 and 20ga02 deck systems respectively. Stiffened tests were not performed for 20ga03 deck system and for 20ga02deck system partially decked tests were not carried. The second column of values shows results for the 16 ft end panel, unstiffened system quarter point loading. The third column shows results for the 16 ft end panel 16 ft stiffened tests. The numbers in parentheses show the areas of the stiffened truss elements used in the FEA model. It can be observed from the results that the 16 ft stiffened system was stiffer than the unstiffened system with a ratio of $(14.9)/(9.4) = 1.59$, $(13.1)/(7.6) = 1.72$ and $(10.3)/(6.9) = 1.49$ for 18ga, 16ga and 20ga01 deck systems respectively. The shear diaphragm model underestimated the lateral stiffness of the 16 ft end panel stiffened 16 ft system by the ratio of $(14.9)/(6.7) = 2.22$, $(13.1)/(5.7) = 2.29$ and $(10.3)/(5.6) = 1.84$ for 18ga, 16ga and 20ga01 deck systems respectively. The area of the stiffened truss element for the partially decked 16ga deck system (18 in²) was not only 4 times higher than the area calculated for the partially decked 18ga and 20ga01 deck systems, but also more than 4 times higher than the area calculated for the fully decked 16ga deck system. Hence this higher area was not used in any of the FEA.

The fourth and fifth columns of values in Table 6.10 through Table 6.13 provide results for the fully decked 16 ft stiffened systems displaced at the midspan and quarter-points respectively. The sixth and seventh columns of values in Table 6.10 through Table 6.13 provide results for the fully decked 16 ft stiffened systems displaced with a half sine loading. The sixth column corresponds to the lateral stiffness at midspan and the seventh column corresponds to the lateral stiffness at quarter points.

Table 6.10 18ga Stiffened 16ft Tests, Comparison of Laboratory and FEA Results

LATERAL STIFFNESS (k/in)	16 ft end panel unstiffened Quarter point loading	16 ft end panel stiffened 16ft Quarter point loading	Fully decked stiffened 16ft mid point loading	Fully decked stiffened 16ft quarter point loading	Fully decked stiffened 16ft half sine loading	
					midspan	quarter point
Laboratory	9.4	14.9	15	16.4	10.1	8.9
FEA shear diaphragm	6.7	6.7	6.9	6.7	4	3.6
FEA shear diaphragm & stiff. element	NA	11.2 (A=4.0 in ²)	14.9 (A=5.0 in ²)	15.5 (A=5.5 in ²)	8.8 (A=4.5 in ²)	9.5 (A=4.5 in ²)

Table 6.11 16ga Stiffened 16ft Tests, Comparison of Laboratory and FEA Results

LATERAL STIFFNESS (k/in)	16 ft end panel unstiffened quarter point loading	16 ft end panel stiffened 16ft quarter point loading	Fully decked stiffened 16ft mid point loading	Fully decked stiffened 16ft quarter point loading	Fully decked stiffened 16ft half sine loading	
					midspan	quarter point
Laboratory	7.6	13.1	12.5	12.1	9.6	6.6
FEA shear diaphragm	5.7	5.7	5.9	5.7	3.4	3.1
FEA shear diaphragm & stiff. element	NA	13 (A=18 in ²)	12.8 (A=4.0 in ²)	12.3 (A=3.5 in ²)	7.5 (A=3.5 in ²)	8 (A=3.5 in ²)

Table 6.12 20ga(01) Stiffened 16ft Tests, Comparison of Laboratory and FEA Results

LATERAL STIFFNESS (k/in)	16 ft end panel unstiffened quarter point loading	16 ft end panel stiffened 16ft quarter point loading	Fully decked stiffened 16ft mid point loading	Fully decked stiffened 16ft quarter point loading	Fully decked stiffened 16ft half sine loading	
					midspan	quarter point
Laboratory	6.9	10.3	10	9.9	6.2	5.5
FEA shear diaphragm	5.6	5.6	5.8	5.6	3.3	3
FEA shear diaphragm & stiff. element	NA	10.2 (A=4.0 in ²)	10 (A=1.8 in ²)	9.8 (A=1.8 in ²)	5.9 (A=1.8 in ²)	6.1 (A=1.8 in ²)

Table 6.13 20ga(02) Stiffened 16ft Tests, Comparison of Laboratory and FEA Results

LATERAL STIFFNESS (k/in)	16 ft end panel unstiffened Quarter point loading	16 ft end panel stiffened 16ft Quarter point loading	Fully decked stiffened 16ft mid point loading	Fully decked stiffened 16ft quarter point loading	Fully decked 0 half sine loading	
					midspan	quarter point
Laboratory	NA	NA	13.2	12.9	6.8	9.1
FEA shear diaphragm	NA	NA	6.2	5.9	3.5	3.2
FEA shear diaphragm & stiff. element	NA	NA	13.2 (A=4.0 in ²)	12.9 (A=4.0 in ²)	8 (A=4.0 in ²)	8.6 (A=4.0 in ²)

Table 6.14 through Table 6.17 provides values for the lateral stiffness from both laboratory and FEA results for the 24 ft stiffened tests. The second and third columns of values provide results for the fully decked 24 ft stiffened systems displaced at the midspan and quarter-points respectively. The fourth and fifth columns of values in Table 6.14 through Table 6.17 provide results for the fully decked 24 ft stiffened systems displaced with a half sine loading. The fourth column corresponds to the lateral stiffness at midspan and the fifth column corresponds to the lateral stiffness at quarter points.

Table 6.14 18ga Stiffened 24ft Tests, Comparison of Laboratory and FEA Results

LATERAL STIFFNESS (k/in)	Fully decked stiffened 24ft mid point loading	Fully decked stiffened 24ft quarter point loading	Fully decked stiffened 24ft half sine loading	
			midspan	quarter point
Laboratory	17.3	16.1	11.8	8.1
FEA shear diaphragm	6.9	6.7	4	3.6
FEA shear diaphragm & stiff. element	17.8 (A=7.0 in ²)	13.7 (A=30 in ²)	22.2 (A=12 in ²)	2.9 (A=12 in ²)

Table 6.15 16ga Stiffened 24ft Tests, Comparison of Laboratory and FEA Results

LATERAL STIFFNESS (k/in)	Fully decked stiffened 24ft mid point loading	Fully decked stiffened 24ft quarter point loading	Fully decked stiffened 24ft half sine loading	
			midspan	quarter point
Laboratory	15.9	11.5	11.8	4.5
FEA shear diaphragm	5.9	5.7	3.4	3.1
FEA shear diaphragm & stiff. element	15.3 (A=6.0 in ²)	11.6 (A=20 in ²)	15.9 (A=8 in ²)	2.6 (A=8 in ²)

Table 6.16 20ga(01) Stiffened 24ft Tests, Comparison of Laboratory and FEA Results

LATERAL STIFFNESS (k/in)	Fully decked stiffened 24ft mid point loading	Fully decked stiffened 24ft quarter point loading	Fully decked stiffened 24ft half sine loading	
			midspan	quarter point
Laboratory	11	9.9	7.1	4.9
FEA shear diaphragm	5.8	5.6	3.3	3
FEA shear diaphragm & stiff. element	11 (A=3.2 in ²)	9.9 (A=8.5 in ²)	11.3 (A=4.9 in ²)	2.8 (A=4.9 in ²)

Table 6.17 20ga(02) Stiffened 24ft Tests, Comparison of Laboratory and FEA Results

LATERAL STIFFNESS (k/in)	Fully decked stiffened 24ft mid point loading	Fully decked stiffened 24ft quarter point loading	Fully decked stiffened 24ft half sine loading	
			midspan	quarter point
Laboratory	14.6	12.8	8.7	6.9
FEA shear diaphragm	6.2	5.9	3.5	3.2
FEA shear diaphragm & stiff. element	14.6 (A=5.2 in ²)	12.1 (A=22 in ²)	16.1 (A=8 in ²)	2.7 (A=8 in ²)

Table 6.18 provides values for the properties of the FEA elements determined for the deck systems in ascending order with respect to deck stiffness G'. The first column of

values lists the deck type. The second and third columns of values list the stiffness and the rigidity of the deck system respectively.

The fourth column of values lists the moment of inertia of the flexural beam element used for the unstiffened models. It can be observed from Table 6.18 that as the deck system gets stiffer, the flexural elements used in the FEA gets stiffer.

The fifth, sixth and seventh columns of values list the areas of the stiffening truss elements used in the FEA for 8 ft, 16 ft and 24 ft stiffened deck systems respectively. The area of the truss element required for the 8 ft stiffened 18ga deck system with a G' of 8.5 (k/in) was 5.3 times greater than the area of the truss element required for the 8 ft stiffened 20ga01 deck system with a G' of 6.8 (k/in). A similar relationship was observed for the 16 ft and 24 ft stiffened systems.

Table 6.18 Properties of the FEA Elements

Deck Type	G' (k/in)	Q (k/rad)	Flexural Element (I) Sine Loading (in ⁴)	Stiffened 8ft Truss Area Sine Loading (in ²)	Stiffened 16ft Truss Area Sine Loading (in ²)	Stiffened 24ft Truss Area Sine Loading (in ²)
20(03)	6.8	371	65	NA	NA	NA
20(01)	6.8	371	65	0.3	1.8	4.9
20(02)	7.3	398	170	0.8	4	8
16	7.1	387	170	1	3.5	8
18	8.5	463	170	1.6	4.5	12

This page replaces an intentionally blank page in the original.

-- CTR Library Digitization Team

Chapter 7

Twin Girder Buckling Tests

7.1 Overview

This chapter focuses on the laboratory buckling tests on the twin girder system with PMDF for bracing. In addition to describing the procedures followed for laboratory tests, results from experiments and finite element analysis are compared and summarized. The purpose of the buckling tests was to improve the understanding of the buckling behavior of steel I-girders braced with PMDF as well providing results to check the accuracy of the FEA models that were used for parametric studies presented in Chapter 8.

7.2 Test Phases

The deck systems that were tested for buckling were described in Section 4.4.4. An important aspect of conducting the buckling tests was to subject the deck to conditions that might be expected in the field. As with the lateral load tests that were outlined in the last chapter, the support angles were placed with the maximum eccentricity (~2.88 in). In most situations the deck eccentricity will vary along the length and not be a constant maximum value, however it was desired to test the deck in the worst possible condition. A difficult feature of girders that might be encountered in the field that was difficult to simulate is the critical initial imperfection. Since the magnitude of the brace forces are directly dependent on the initial imperfection, it was desired to model the girders with the worst possible imperfection. However the initial out-of-straightness and twist of the girders generally did not match the magnitude or shape that is often assumed in bracing studies. Many brace provisions are based upon an initial imperfection in which the bottom flange is straight and the top flange is displaced an amount equal to $L_b/500$, where L_b is the spacing between points of zero twist. To simulate the imperfection, the applied load was offset in one direction. Therefore, the tests were conducted in three phases as follows:

- Phase 1 - No offset tests
- Phase 2 - Loads offset by 0.5 in. in one direction
- Phase 3 - Load offset to simulate the $L_b/500d$ initial twist imperfection

The phase 3 offset was determined by comparing the twist behavior of the girders with the offset load to FEA results on an imperfect girder with an imperfection equal to the critical value ($L_b/500d$). In the first two phases the moment level applied to the twin girder system was limited to 400 k-ft so that the applied stresses in the girders would not exceed 30 ksi, hence the girders would remain elastic. The stress of 30 ksi was deemed a safe level so that the members would not yield when the applied stress was combined with the residual stresses in the member. Keeping the system elastic enabled the comparison between the behaviors of the deck systems with different stiffening angle spacing. In the no offset tests the knife-edges that were bolted to the loading beams were

aligned with the centerline of the web of the girders. In the half inch offset tests the knife-edges were placed with an eccentricity of 0.5 in (in the same direction) with respect to the web centerline. The offset was applied in the direction that the twin girders tended to displace based upon the Phase 1 buckling tests with no offset.

The purpose of the third phase was to load the girder and PMDF bracing up to failure. However before the final loading phase was conducted the effect of imperfections to the buckling behavior had to be considered. As previously explained the two primary factors that affect the buckling behavior of girders are the brace stiffness and the magnitude and shape of the initial imperfection. Since other bracing provisions such as those in the AISC LRFD Specifications (2001) are based upon an initial imperfection/twist of $L_b/500d$ as shown in Figure 3.5 (Section 3.4), it was essential to load the girder system with an eccentricity that would represent a girder system with an initial twist of $L_b/500d$. Once the accuracy of the FEA models was confirmed with results from the first two phases of the buckling tests, large displacement analysis were performed on the FEA models with an initial imperfection of $L_b/500d$. The result of the analysis was compared with several FEA results that had the actual imperfections of the girders measured at the lab with different eccentricities in the applied load. Based upon these comparisons it was concluded that a 0.5 in eccentricity on the north girder and a 0.9 in eccentricity for the south girder was necessary to mimic the behavior of a girder system with an initial imperfection of $L_b/500d$.

7.3 Initial Imperfections

The initial imperfections of the girders were measured before each buckling test to facilitate companion large displacement buckling analyses using the FEA models. These measurements were taken by stretching a thin wire along both sides of the girders both on top and bottom of the web. The wire was offset from the web at the ends and essentially established a straight line that could be used to measure the imperfection in the girder along the length. The imperfections generally differed from one set of deck systems to another. The primary reason for this was the lateral displacement tests that were done before the buckling tests. Because of the internal friction of the system the initial and final positions of the girder flanges in the lateral displacements tests were generally not the same. The internal friction comes from the weight of the concrete blocks on the metal deck forms. During the lateral load tests, the individual panels in the formwork tended to displace relative to adjacent sheets as well as the support angle. This friction tended to “lock” deformations into the girder system. However, during the first two phases of the buckling tests, for each individual PMDF system the imperfections remained almost unchanged. In the third phase of buckling tests the girders were loaded beyond the elastic limit of the support angles which locked the deformations after the load was released. However when the concrete blocks, deck and the support angles were removed the two girders essentially came back to the initial position. Typical imperfection readings are shown in Figure 7.1 through Figure 7.3.

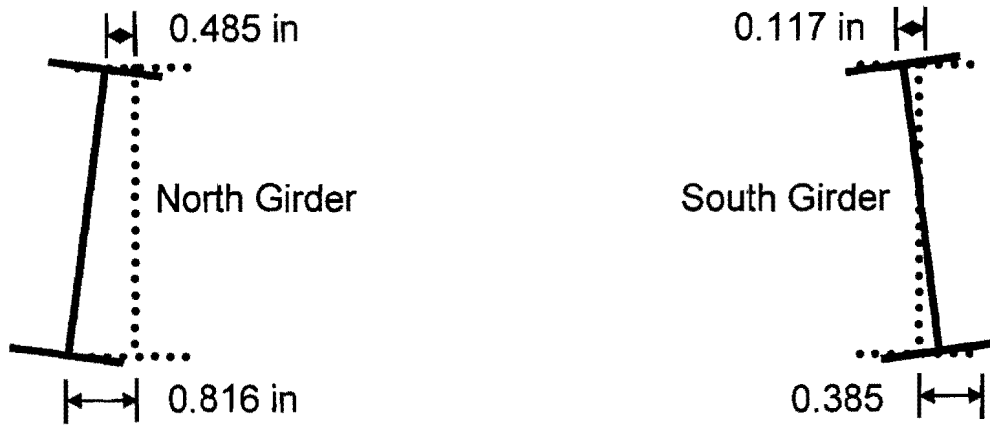


Figure 7.1 Initial Imperfections of 20ga01 Tests

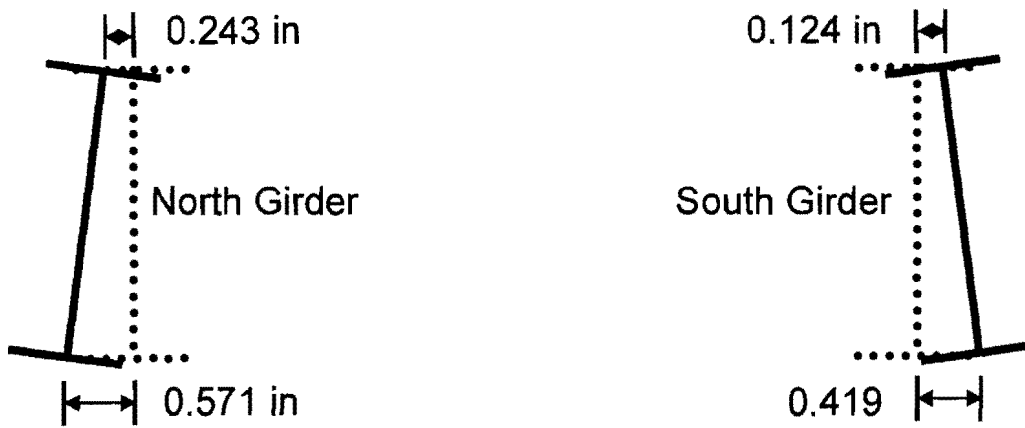


Figure 7.2 Initial Imperfections of 20ga02 Tests

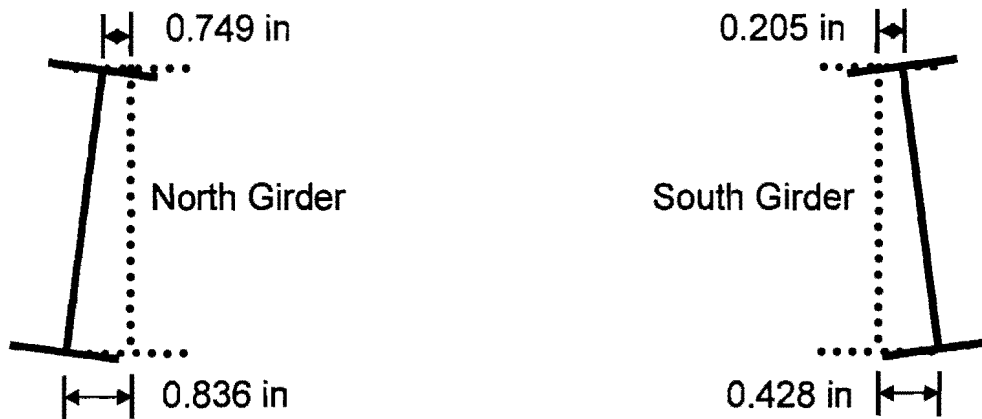


Figure 7.3 Initial Imperfections of 20ga03 Tests

7.4 Test Results

7.4.1 20ga01 Tests

Figure 7.4 and Figure 7.5 show the midspan moment vs. twist data for north and south girders respectively for the first test on the 20 gage deck (20ga01) with no offset and stiffener spacings of 8 ft, 16 ft and 24 ft as well as the case with no stiffening angles. Counter clockwise rotations are denoted as positive. For both of the girders 8 ft and 24 ft stiffened systems behave very similar up to a moment of approximately 300 k-ft. After this load level the system with the 24 ft stiffener spacing started to twist in the other direction. As expected the unstiffened system was the least stiff among the four systems. The 16 ft stiffened system was less stiff than both the 8 ft and 24 ft. The lower stiffness of the 16 ft stiffener spacing relative to the 24 ft spacing was generally not expected. The better behavior of the system with the 24 ft stiffener spacing is probably due to the presence of a stiffening angle at the location with the largest deformation (midspan). The 16 ft spacing put stiffening angles at the third points but not at midspan. In the stiffened tests almost all of the rotation was due to bottom flange lateral displacement. The top flange lateral displacements were about 0.03 in at the moment level of 400 k-ft for both of the girders, whereas bottom flange lateral displacements were in the range of 0.30-0.38 in for the north girder and approximately 0.2 in. for the south girder. This implies that the center of twist of the cross section was relatively close to the top flange. This is very similar to the behavior of diaphragm braced beams discussed by Helwig and Frank (1999 "Stiffness Requirements for diaphragm bracing of beams," J. of Structural Engineering, ASCE, Vol. 125, No. 11, pp. 1249-1256). For the unstiffened system, the top flange lateral displacements were about 0.2 in and the bottom flange lateral displacements were about 0.40 in at moment level of 400 k-ft.

A comparison of Figure 7.4 and Figure 7.5 show that the north girder twist was almost 3 times larger than the south girder. The primary reason for this was probably due to larger imperfections in the north girder.

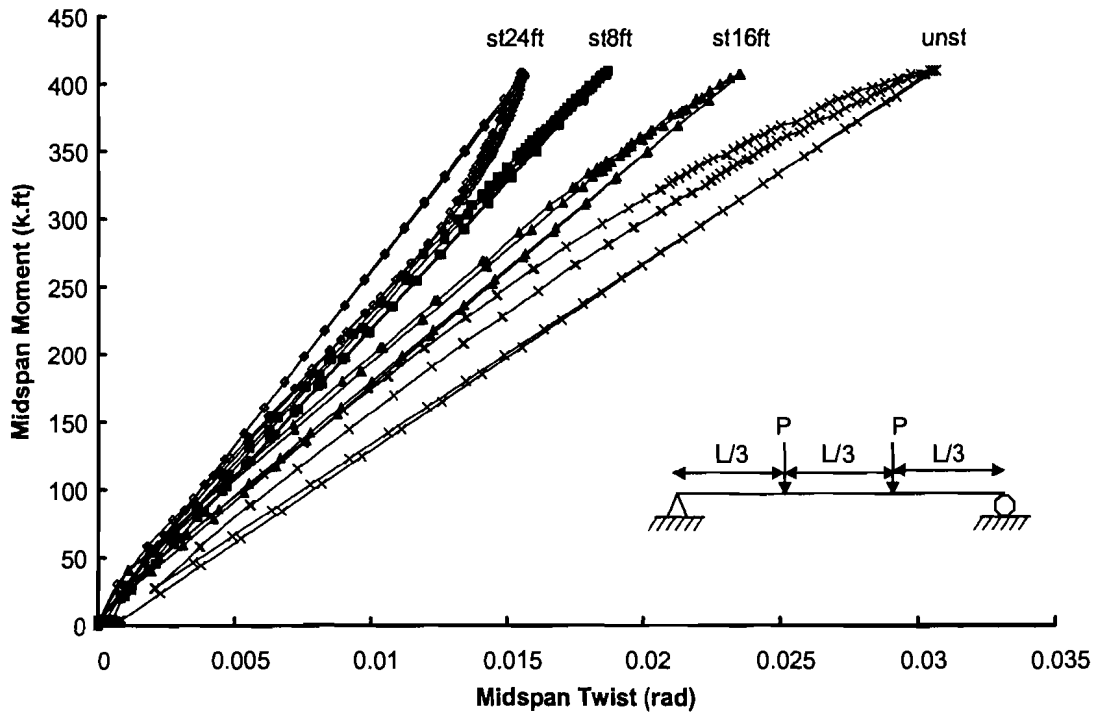


Figure 7.4 Midspan Moment vs. Twist Data (20ga01.no Test - North Girder)

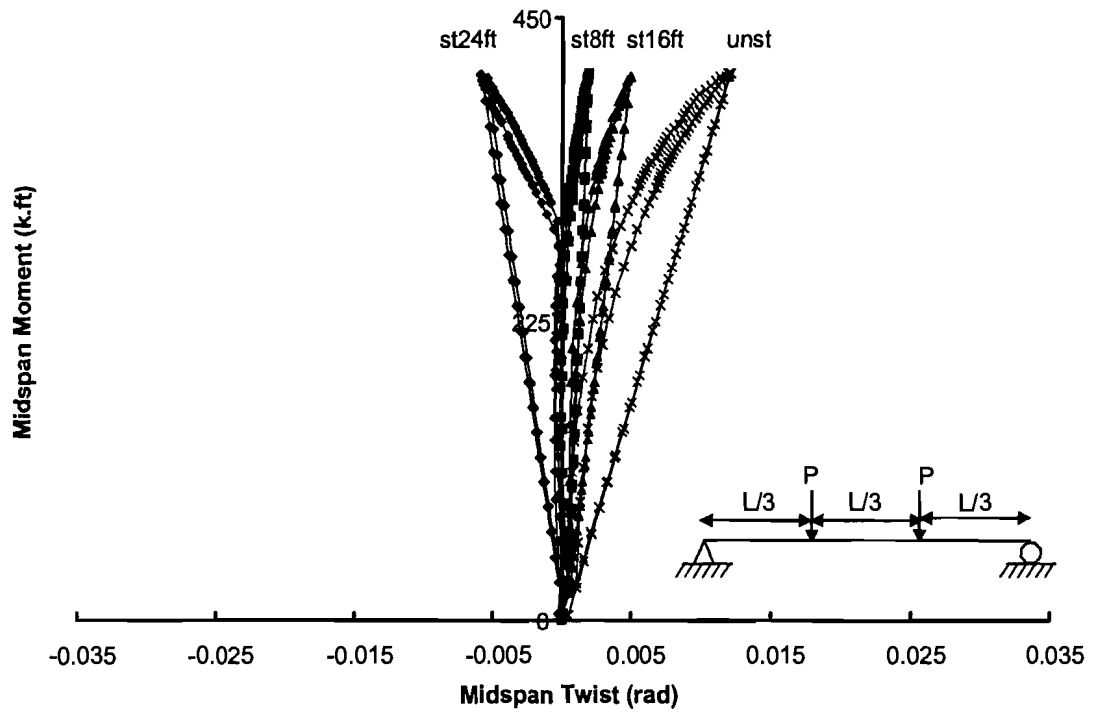


Figure 7.5 Midspan Moment vs. Twist Data for 20ga01.no Tests (South Girder)

Figure 7.6 and Figure 7.7 show a comparison of the measured test data relative to the predicted results from the FEA models. Although, the linear elastic FEA solution was taken to a higher load level, the behavior that is of interest is the slope of the curves since this represents the stiffness of the system. The figures show a graph of the midspan moment vs. twist for the 8 ft stiffened deck system with no offset for the north and south girders respectively. A 0.5 in^2 stiffening angle was used in the finite element model, which was determined based upon the lateral load test presented in Chapter 6. The FEA solution is very consistent with the test data for the north girder. For the south girder it gives conservative results.

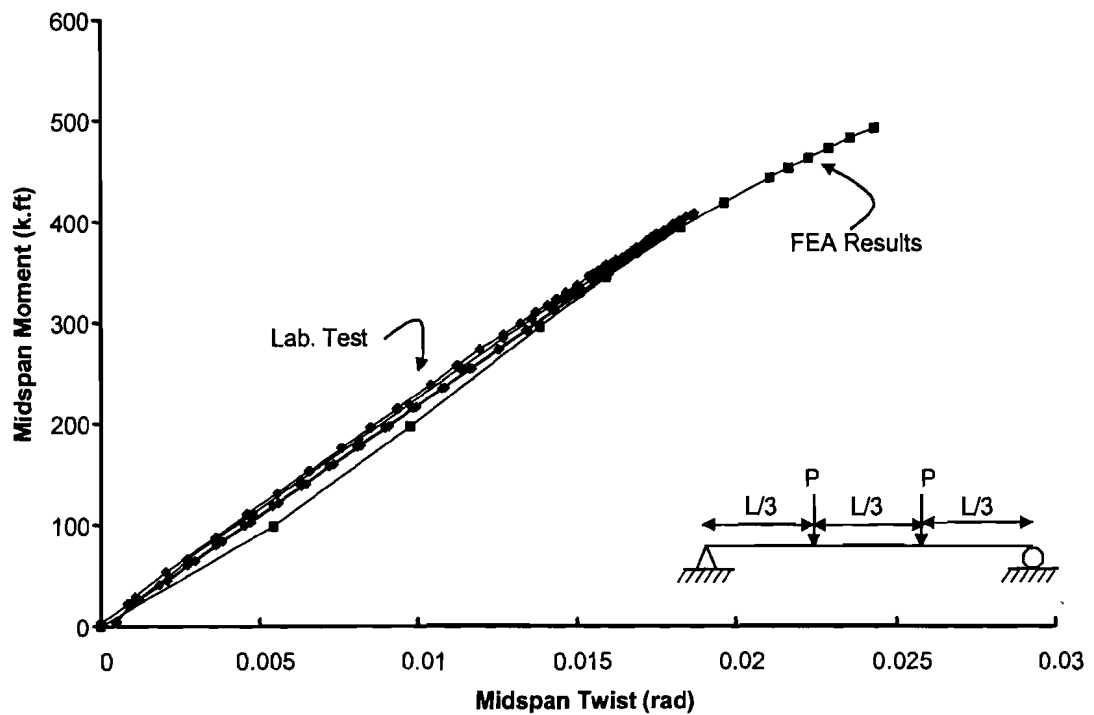


Figure 7.6 Comparison of Midspan Moment vs. Twist for 20ga01.st8ft.no (North Girder)

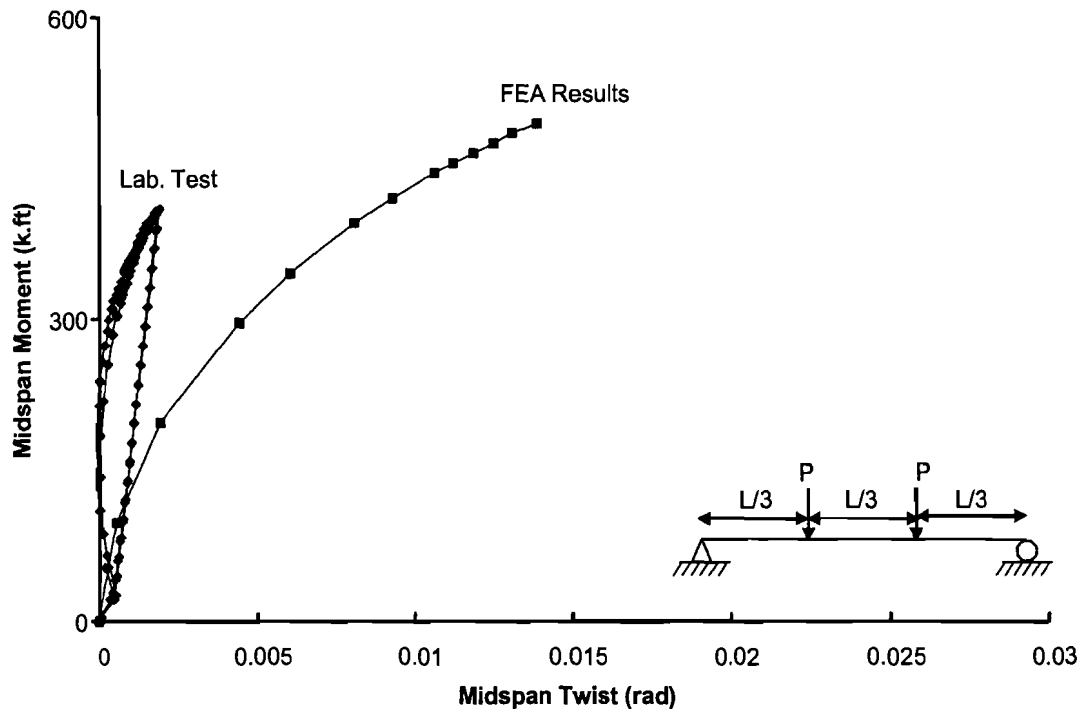


Figure 7.7 Comparison of Midspan Moment vs. Twist for 20ga01.st8ft.no (South Girder)

Similar agreement was obtained for the system with the 16 ft spacing between the stiffening angles as shown in Figure 7.8 and Figure 7.9 for the north and south girders respectively. The sizes of the stiffening angle truss in the FEA was based upon the lateral load tests discussed in Chapter 6. For the north girder, the FEA is slightly unconservative at larger moment levels. The solution is conservative relative to measured results for the south girder.

Figure 7.10 and Figure 7.11 show a comparison of midspan moment vs. twist data with the FEA results for the 24 ft stiffened deck system with no offset for the north and south girders respectively. The area of the stiffening truss was determined from the lateral load tests covered in Chapter 6. For both of the girders, the FEA solution is conservative, however as discussed earlier after about 300 k-ft of moment the girders started twisting in the other direction and this was not mimicked by the FEA Solution.

Figure 7.12 and Figure 7.13 show a comparison of midspan moment vs. twist for the test data and the FEA results for the unstiffened deck system with no offset for north and south girders respectively. A flexural beam element with a moment of inertia of 65 in^4 was suggested from the lateral load tests discussed in Chapter 6, however a flexural beam element with a moment of inertia of 10 in^4 gave better results. The FEA is unconservative for the north girder; however it gives good results for the south girder.

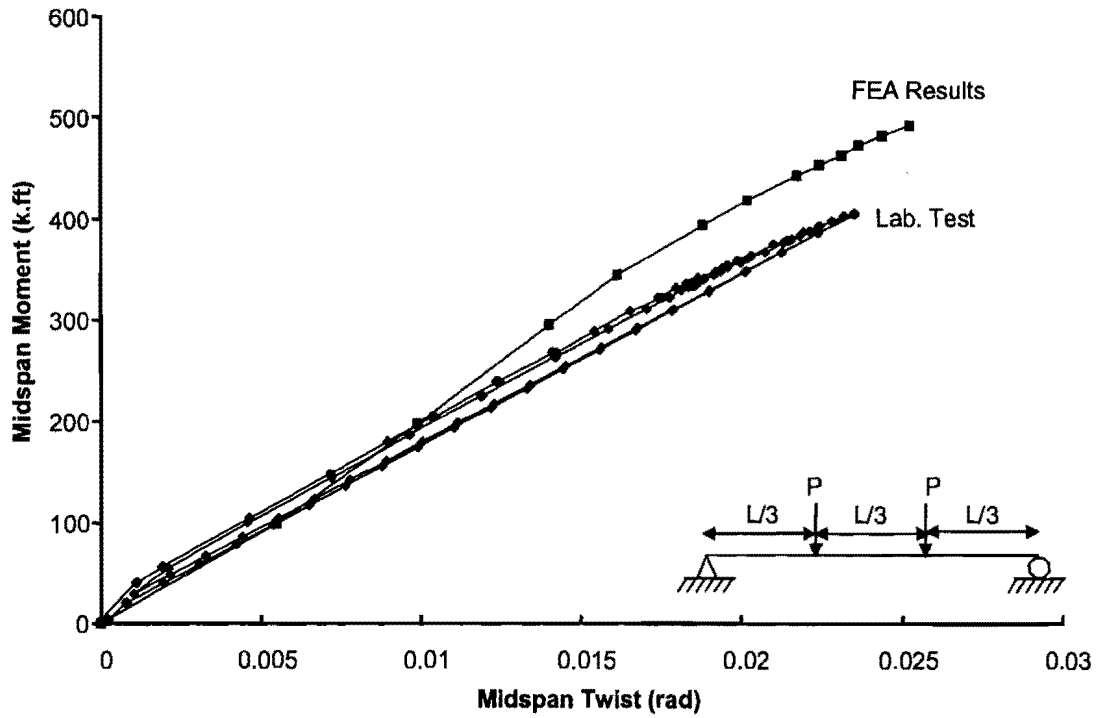


Figure 7.8 Comparison of Midspan Moment vs. Twist for 20ga01.st16ft.no (North Girder)

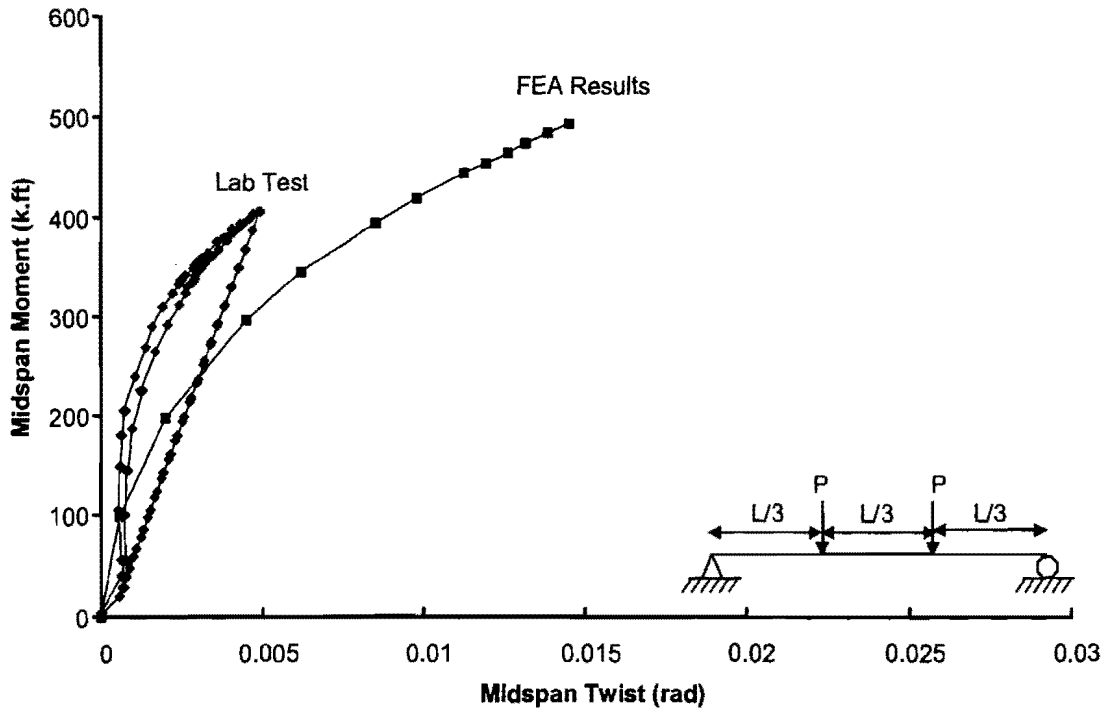


Figure 7.9 Comparison of Midspan Moment vs. Twist for 20ga01.st16ft.no (South Girder)

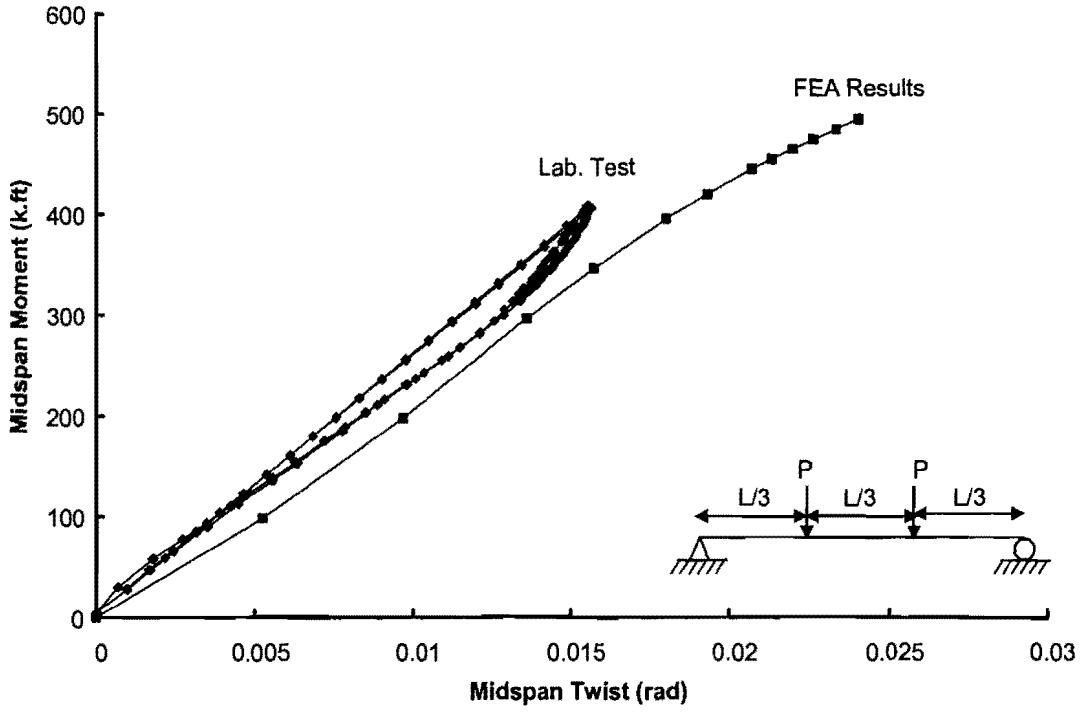


Figure 7.10 Comparison of Midspan Moment vs. Twist for 20ga01.st24ft.no (North Girder)

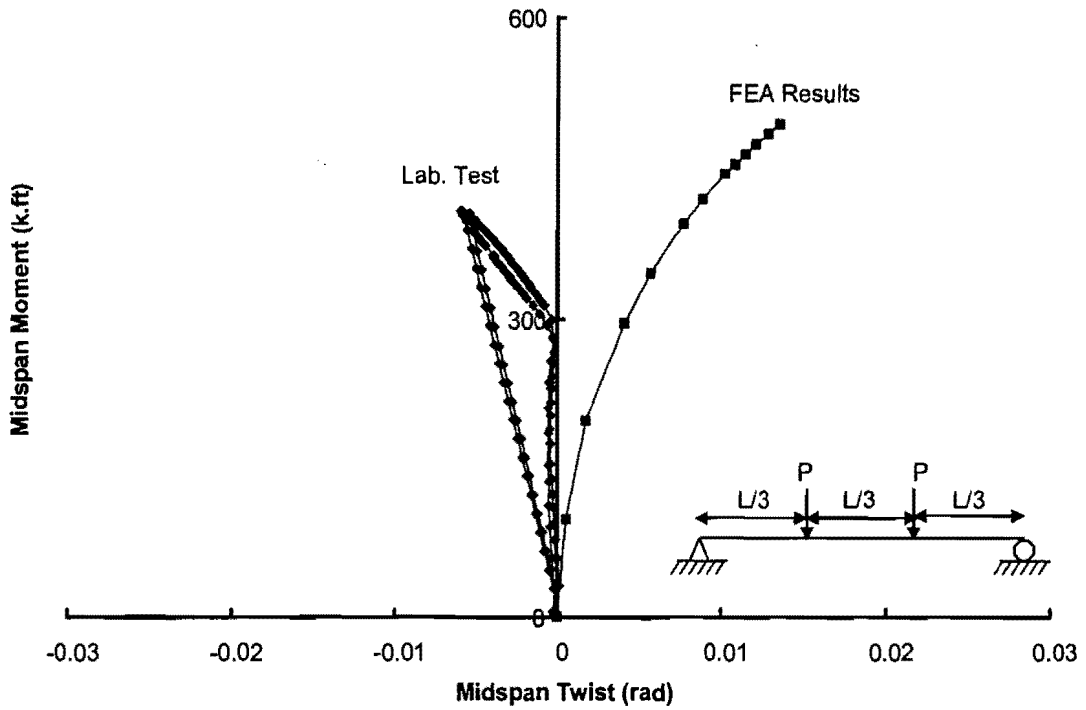


Figure 7.11 Comparison of Midspan Moment vs. Twist for 20ga01.st24ft.no (South Girder)

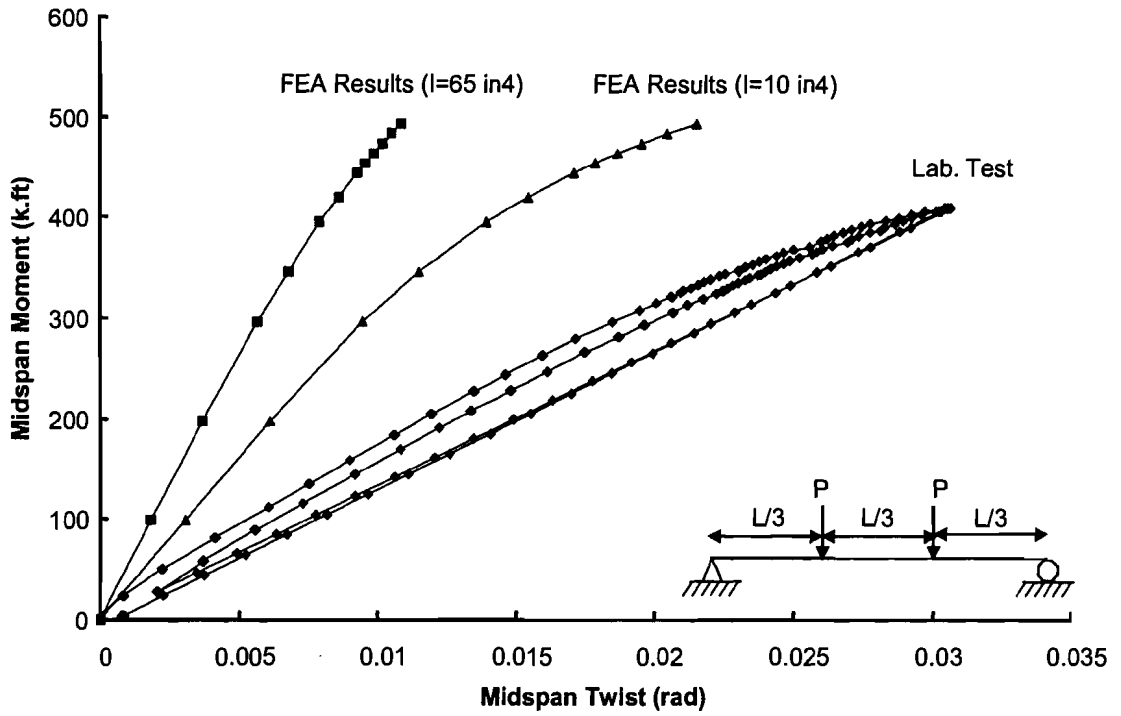


Figure 7.12 Comparison of Midspan Moment vs. Twist for 20ga01.unst.no (North Girder)

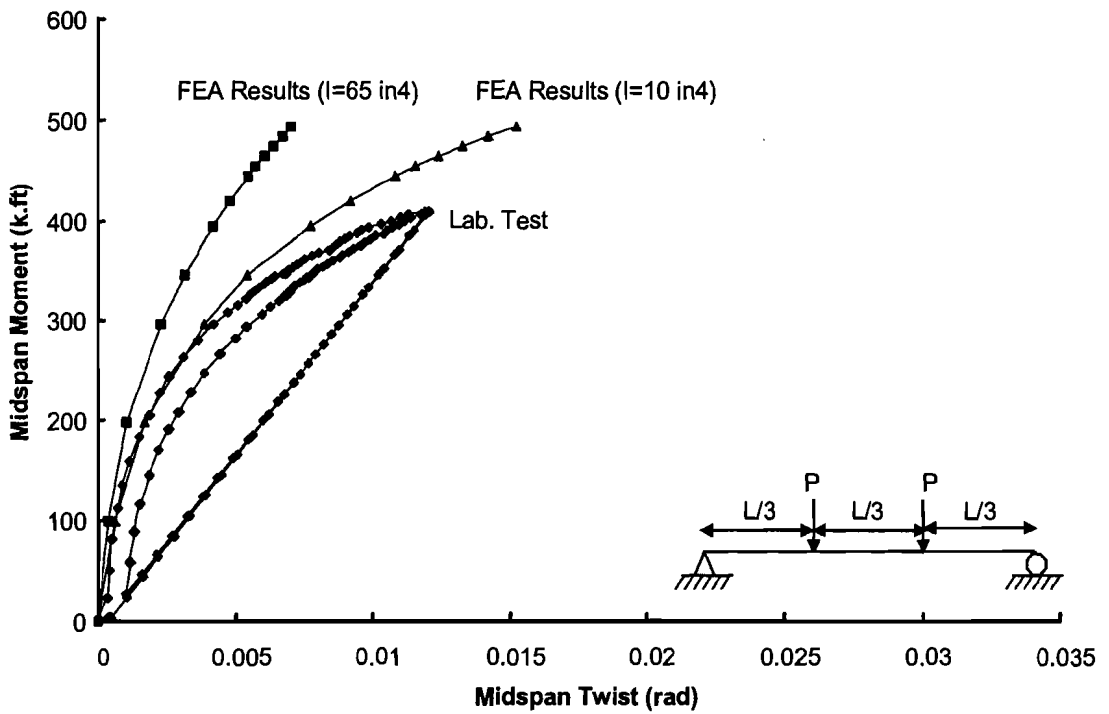


Figure 7.13 Comparison of Midspan Moment vs. Twist for 20ga01.unst.no (South Girder)

After the no offset tests were performed, half inch and one inch offset tests were carried out in order to obtain an indication of the offset needed to mimic an $L_b/500d$ initial twist imperfection. Figure 7.14 and Figure 7.15 show the actual midspan moment vs. twist data for north and south girders respectively from tests with the 20 gage deck and stiffener spacing of 8 ft, 16 ft, 24 ft and unstiffened. Counter clockwise rotation is positive. The 24 ft decked system was slightly stiffer than the 16 ft stiffened decked system. Both of these systems were stiffer than the unstiffened system and less stiff than the 8 ft stiffened system. The primary reason for the 24 ft stiffened system to be stiffer than the 16 ft stiffened system in both the no offset and half inch offset tests was probably due to the existence of a stiffening angle at midspan. The 16 ft stiffened system had one more stiffening angle than the 24 ft stiffened system however they were located at the third points instead of at midspan.

In the stiffened tests the top flange lateral displacements were about 0.15 in at the moment level of 400 k-ft, whereas bottom flange lateral displacements were about 0.70-0.80 in. These displacements were 2 to three times more than the displacements encountered in the no offset tests. This increase in the lateral deflections was due to the increase in initial imperfections by the half-inch offset of the load. Figure 7.16 shows a comparison of midspan moment vs. twist test data for 8 ft stiffened no offset and half inch offset tests for the north girder. At the moment level of 400 k-ft the twist of the half inch offset deck system was $(0.042)/(0.0186) = 2.26$ times more than the twist of the no offset deck system.

The top flange lateral displacement of the unstiffened half inch offset deck system was 0.30 in at the moment level of 400 k-ft for the north girder. As mentioned above this displacement was 0.15 in for the stiffened systems at the same moment level. However the bottom flange lateral displacement of the unstiffened deck system was only 10% greater than the stiffened deck systems. This implies that as the deck system becomes less stiff the center of twist moves toward bottom flange.

Figure 7.17 and Figure 7.18 show a comparison of midspan moment vs. twist data for the laboratory test and the FEA results for the 8 ft stiffened deck system with half inch offset for the north and south girders, respectively. For both of the girders the FEA is slightly conservative.

Figure 7.19 and Figure 7.20 show a comparison of midspan moment vs. twist data for the laboratory test and the FEA results for the 16 ft. stiffened deck system with half inch offset for the north and south girders, respectively. For both of the girders the FEA solution had good agreement with the test results.

Figure 7.21 and Figure 7.22 show a comparison of midspan moment vs. twist test data with the FEA results for 24 ft stiffened deck system with half inch offset for north and south girders respectively. The FEA solution was slightly conservative for both of the girders.

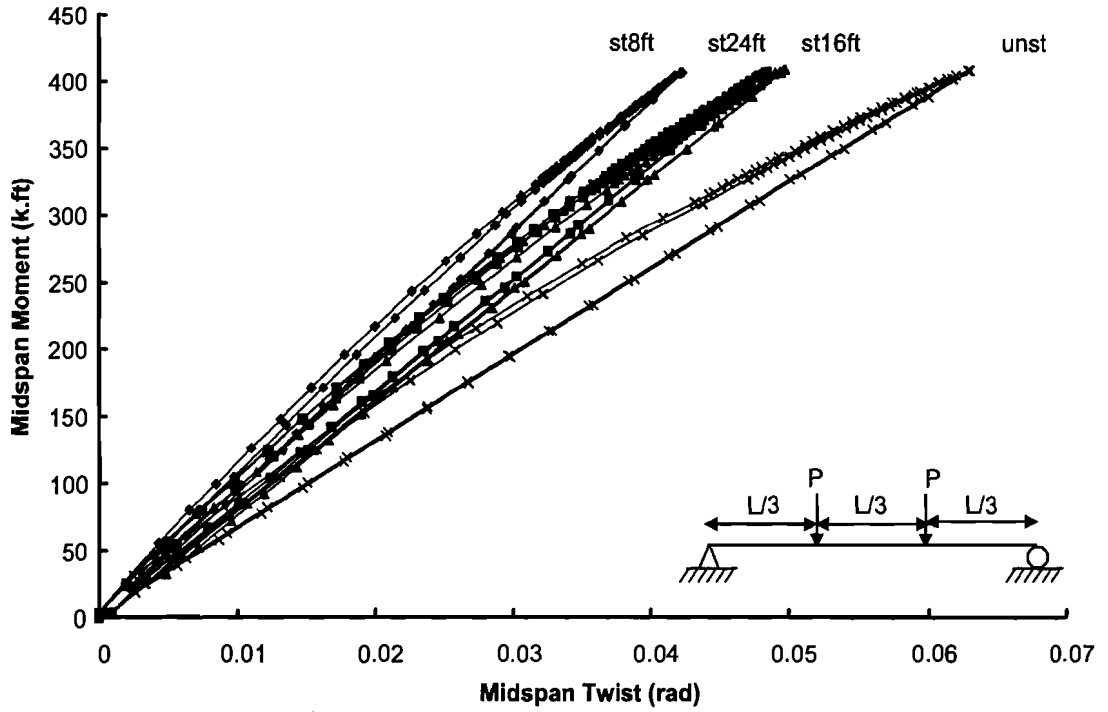


Figure 7.14 Midspan Moment vs. Twist Data for 20ga01.hio Tests (North Girder)

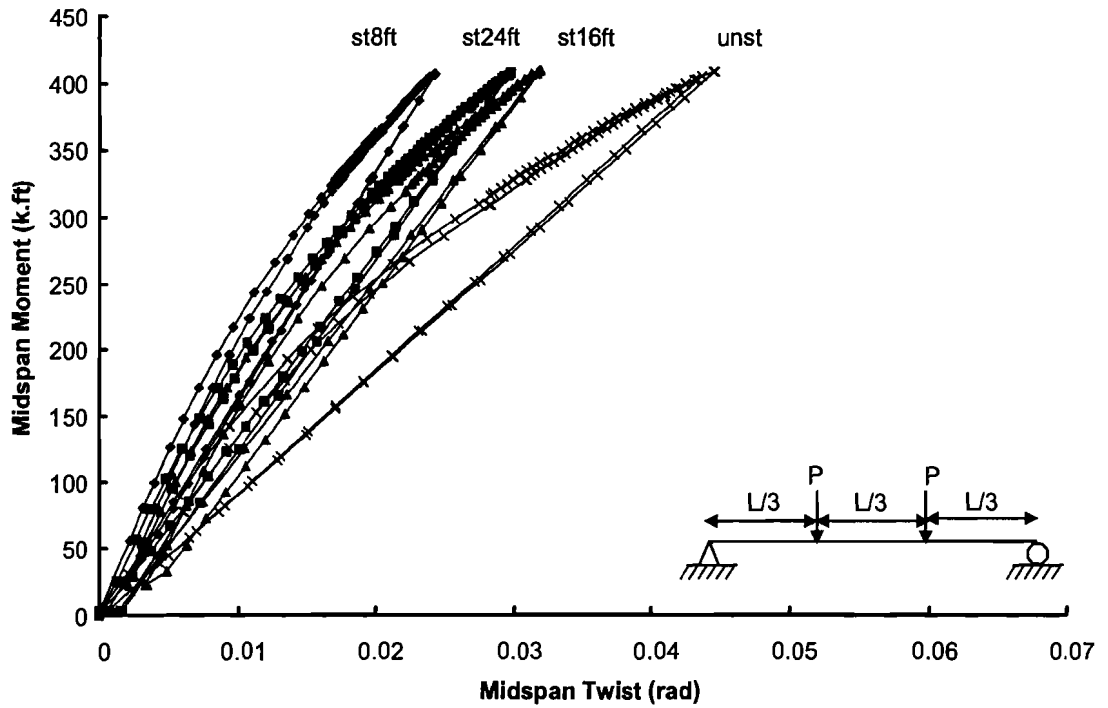


Figure 7.15 Midspan Moment vs. Twist Data for 20ga01.hio Tests (South Girder)

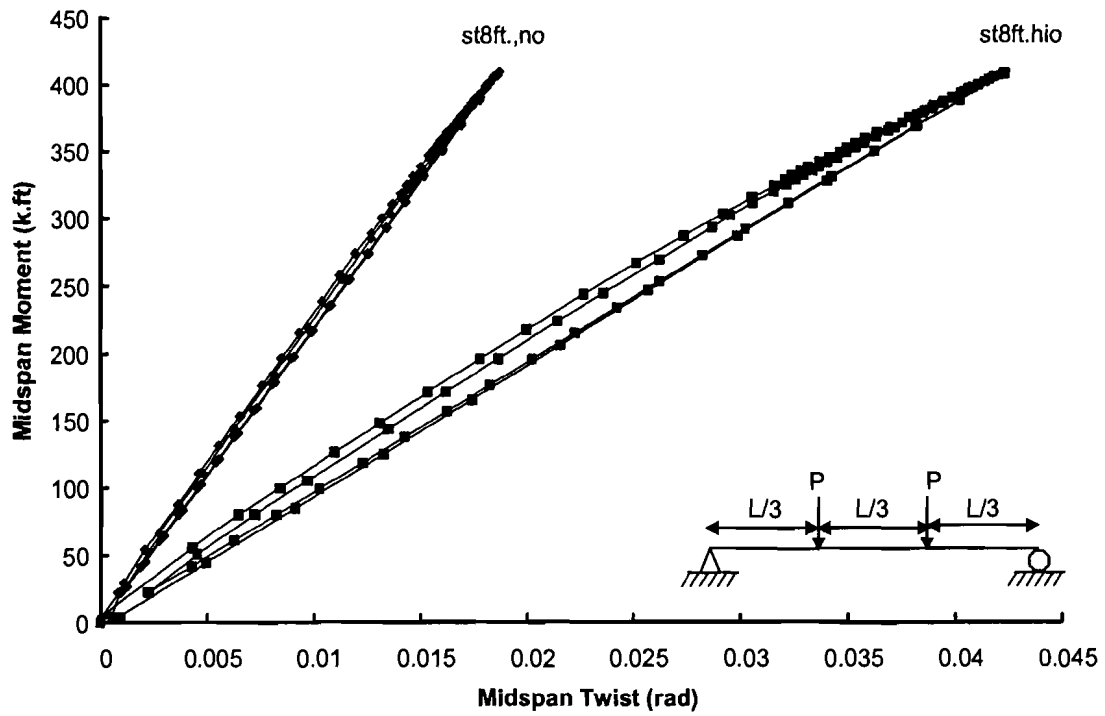


Figure 7.16 Comparison of Midspan Moment vs. Twist for 20ga01.st8ft.no & 20ga01.st8ft.hio (North Girder)

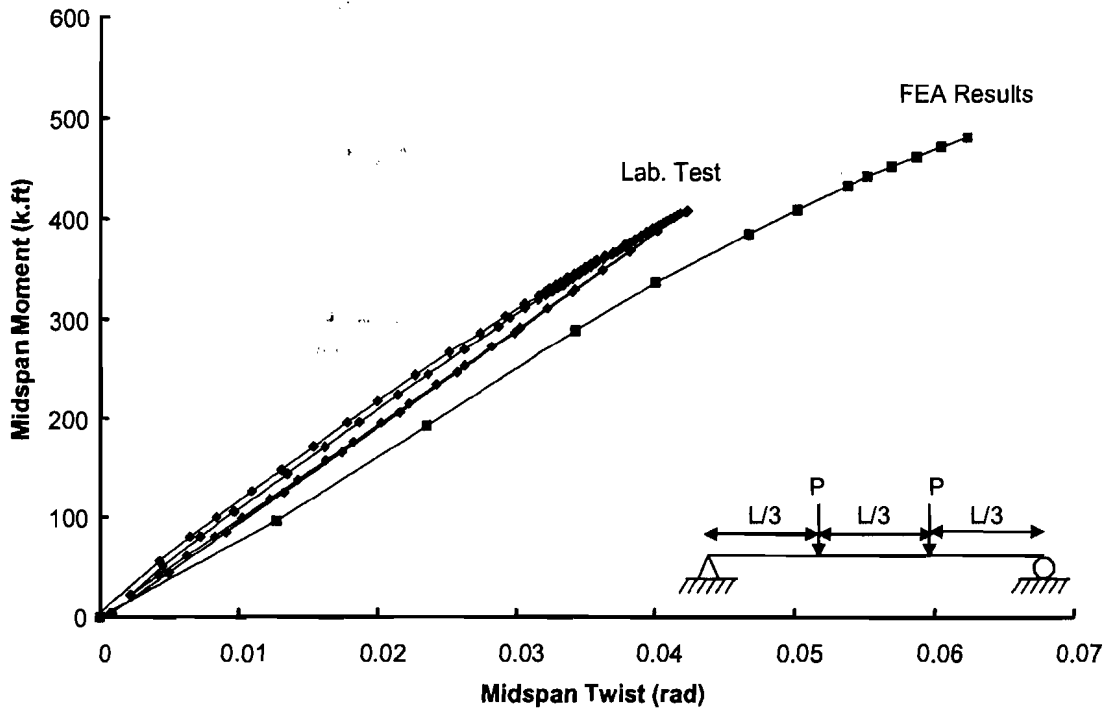


Figure 7.17 Comparison of Midspan Moment vs. Twist for 20ga01.st8ft.hio (North Girder)

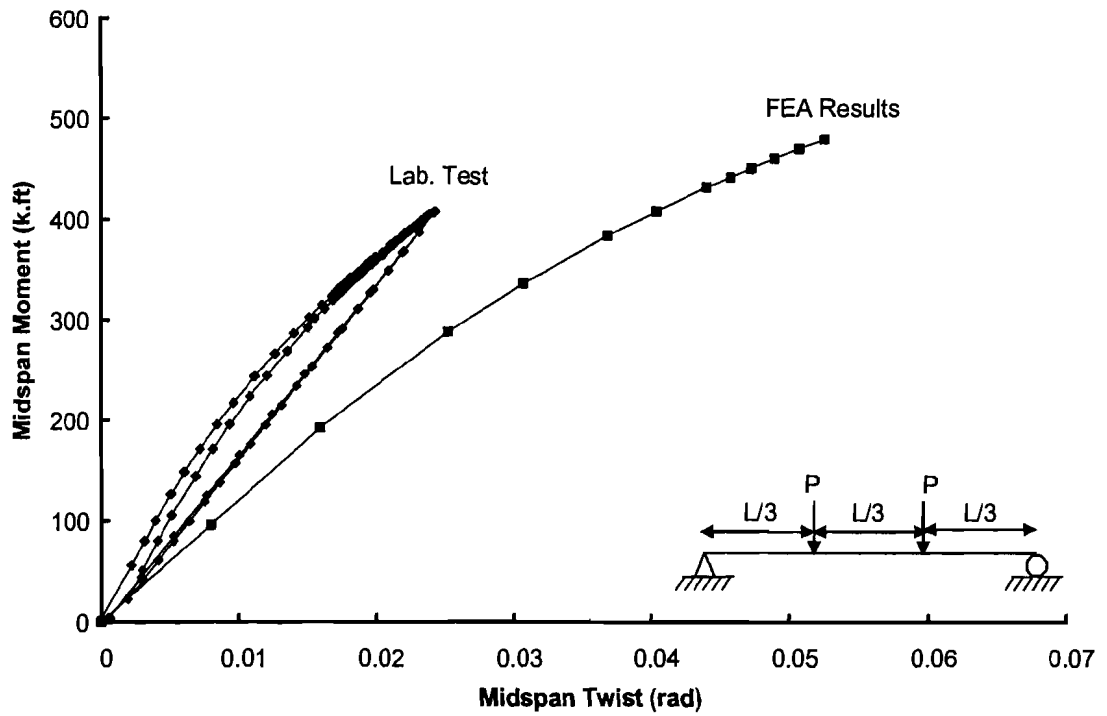


Figure 7.18 Comparison of Midspan Moment vs. Twist for 20ga01.st8ft.hio (South Girder)

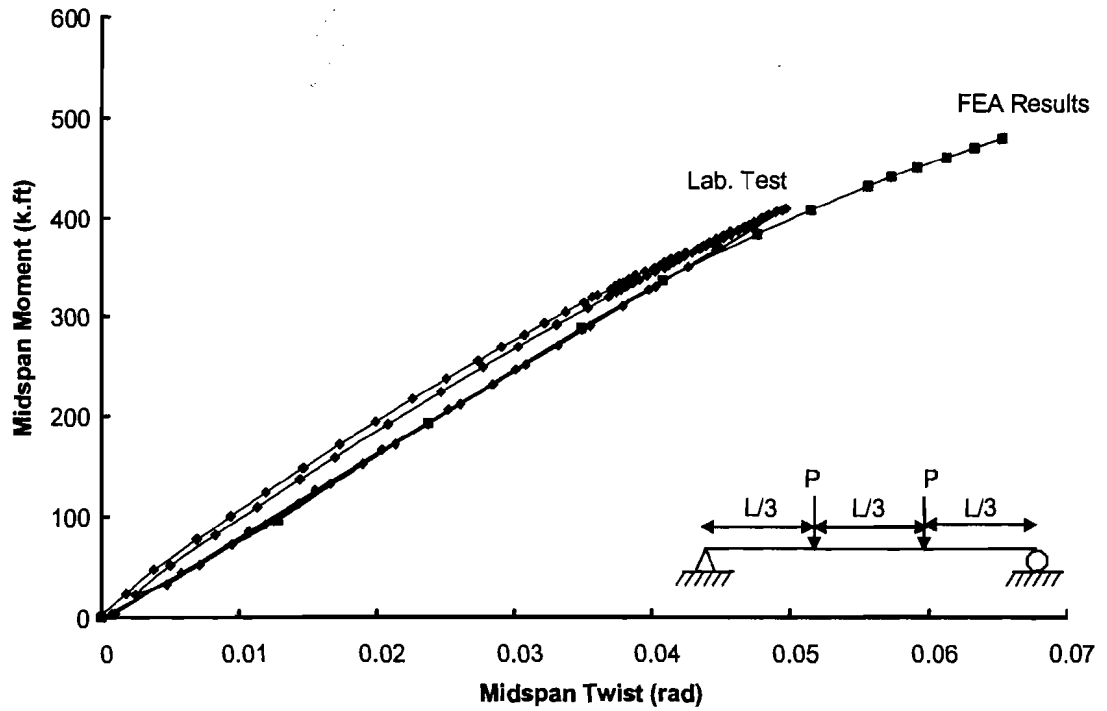


Figure 7.19 Comparison of Midspan Moment vs. Twist for 20ga01.st16ft.hio (North Girder)

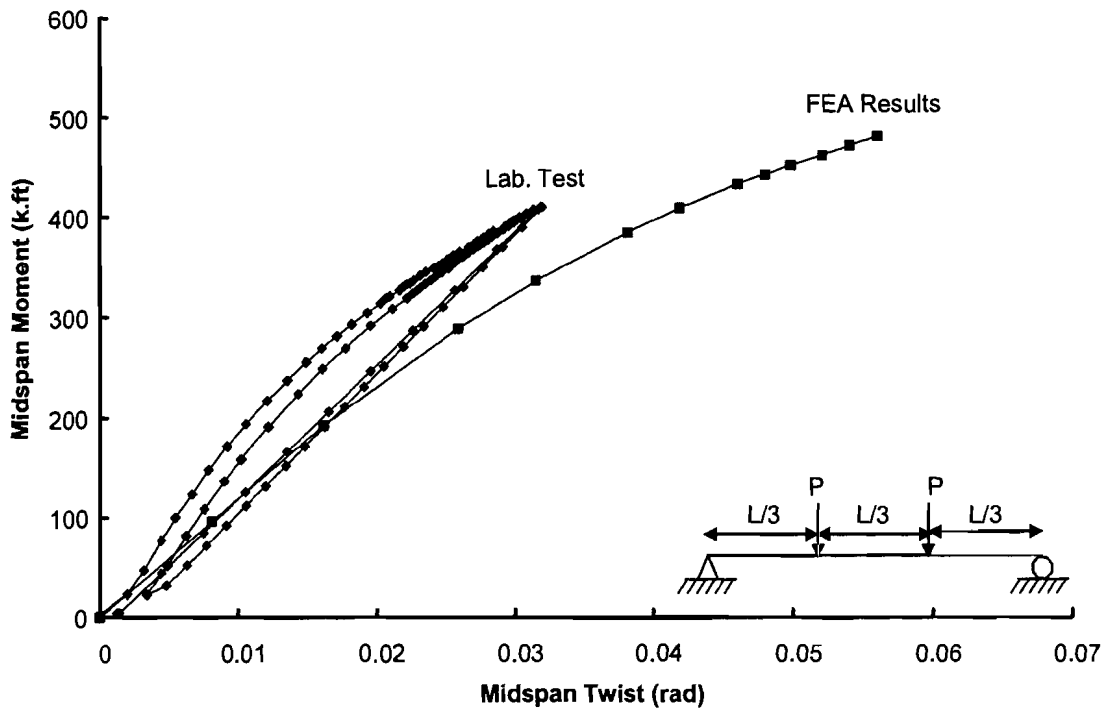


Figure 7.20 Comparison of Midspan Moment vs. Twist for 20ga01.st16ft.hio (South Girder)

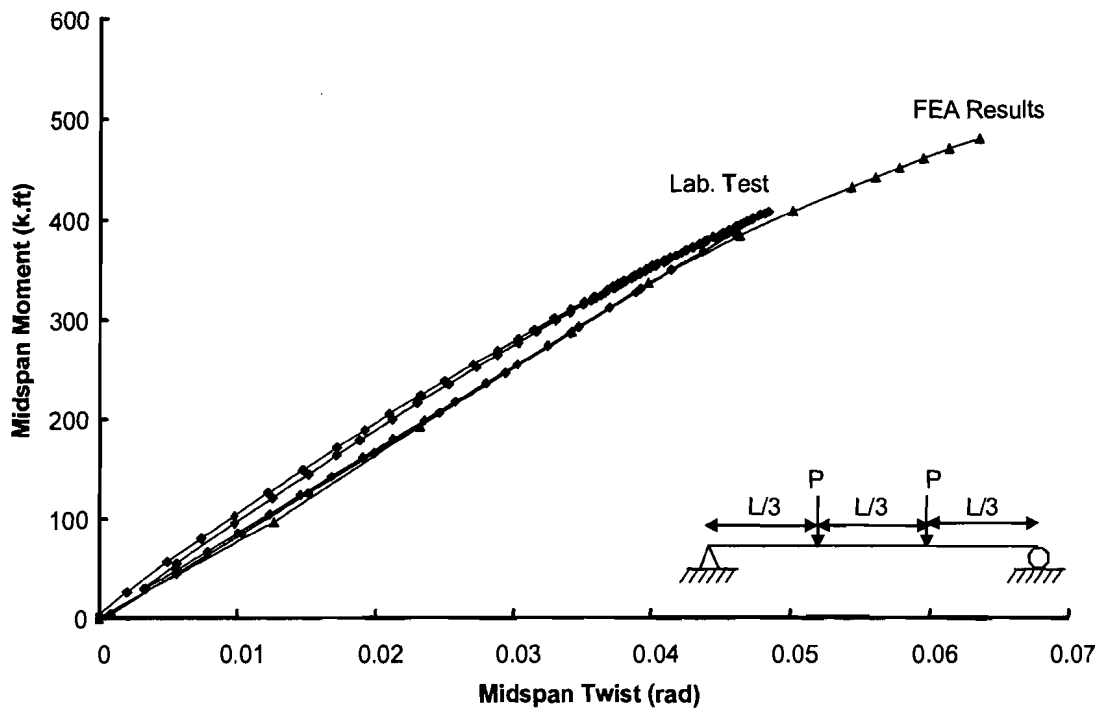


Figure 7.21 Comparison of Midspan Moment vs. Twist for 20ga01.st24ft.hio (North Girder)

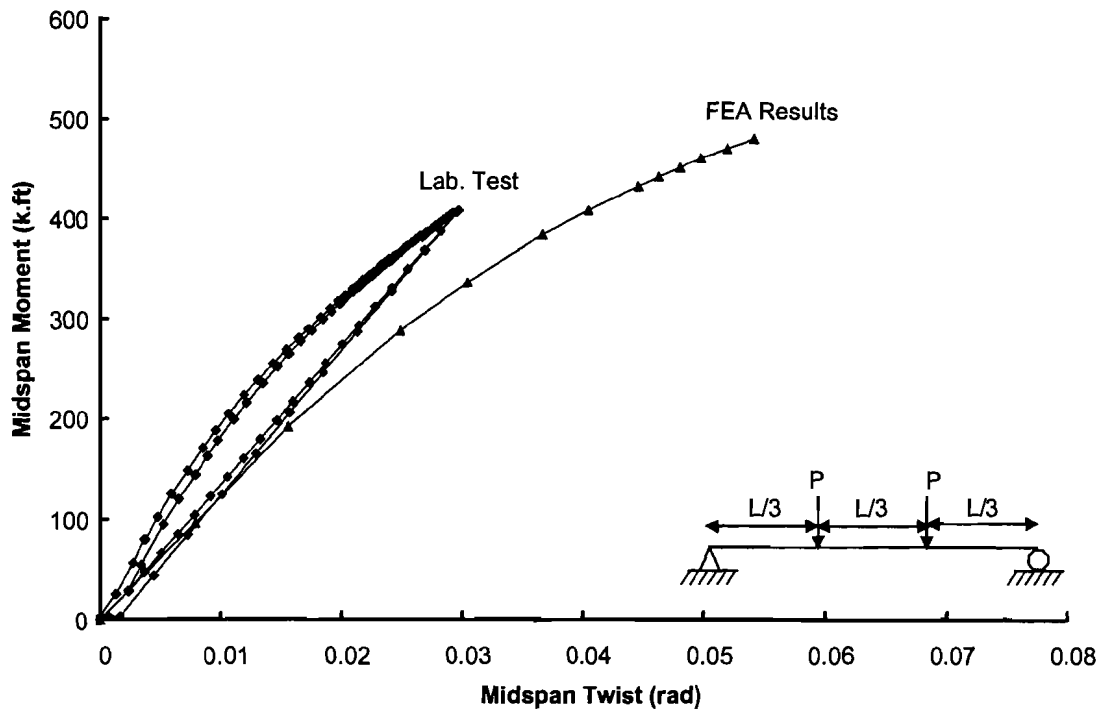


Figure 7.22 Comparison of Midspan Moment vs. Twist for 20ga01.st24ft.hio (South Girder)

Figure 7.23 and Figure 7.24 show a comparison of midspan moment vs. twist test data with the FEA results for the unstiffened deck system with half inch offset for north and south girders respectively. The FEA with a flexural beam element of 10 in^4 was stiffer than the actual system for both of the girders. The actual behavior of the unstiffened deck system was also compared with a shear diaphragm FEA. The shear diaphragm model was less stiff than the actual system for both of the girders.

After the completion of the half inch offset tests, the unstiffened deck was tested with a one inch offset. However the 400 k-ft moment level was high enough to yield the support angles. The girders were still elastic however the lateral stiffness of the system was decreased by about 30%. Therefore, the deck forms were replaced for further testing. The results from the next stage of testing are discussed in the following section.

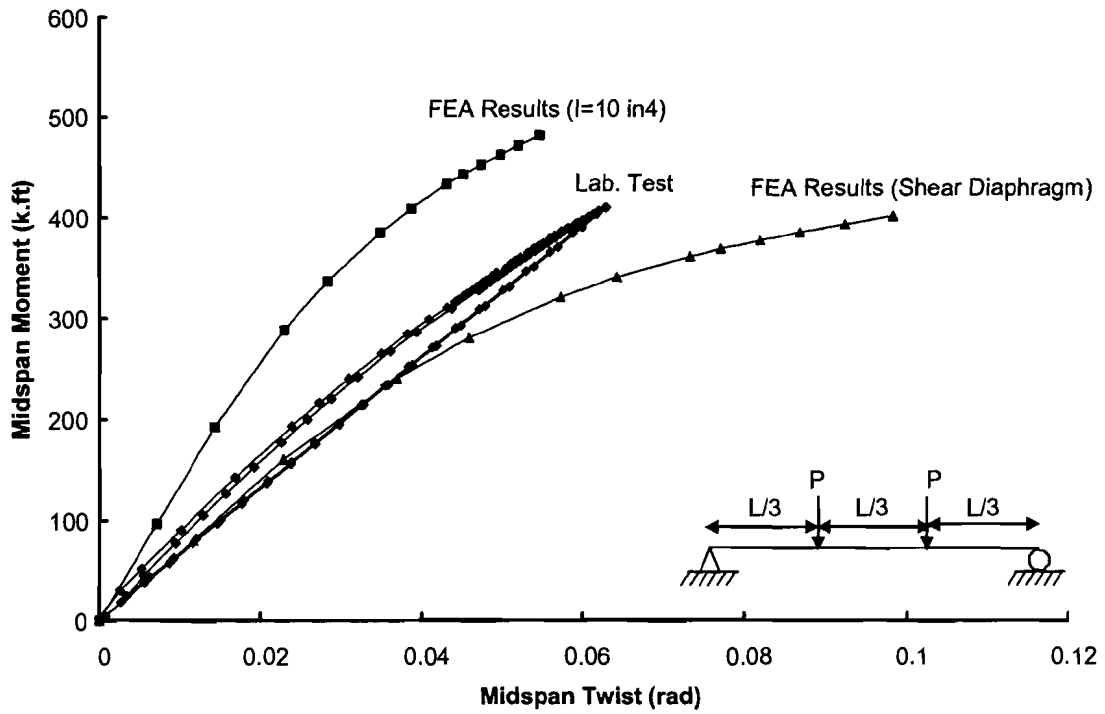


Figure 7.23 Comparison of Midspan Moment vs. Twist for 20ga01.unst.hio (North Girder)

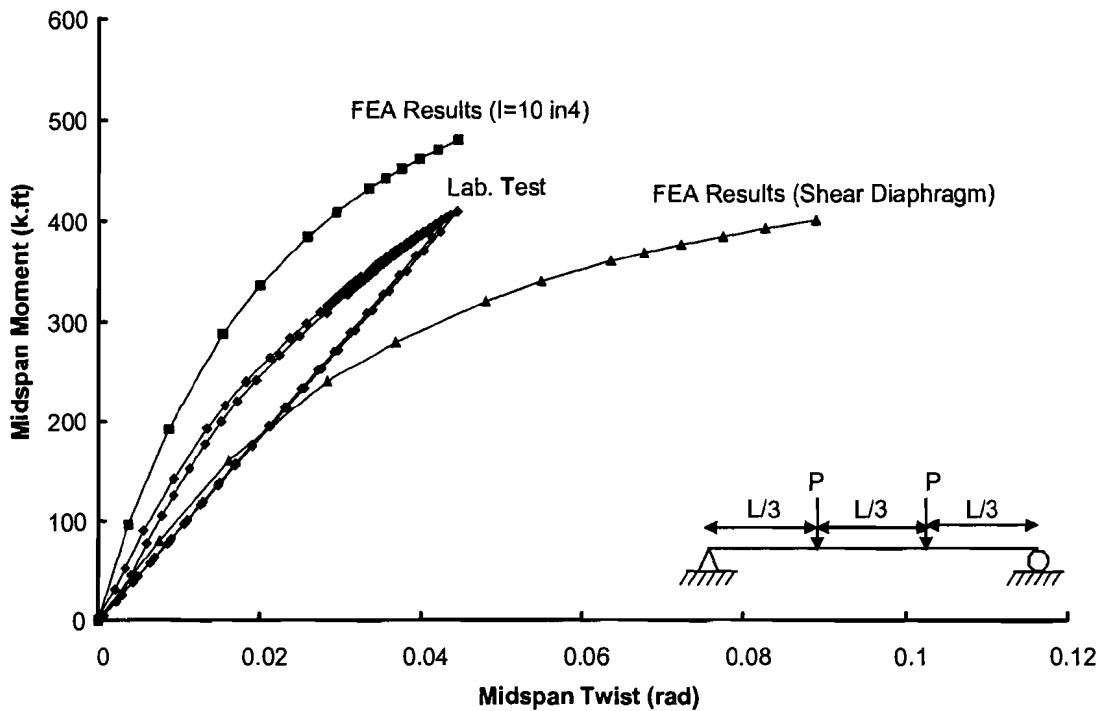


Figure 7.24 Comparison of Midspan Moment vs. Twist for 20ga01.unst.hio (South Girder)

7.4.2 20ga02 Tests

For this set of 20ga deck system only the stiffened systems were tested for buckling. The failure test was done on the 16 ft stiffened deck system. Figure 7.25 and Figure 7.26 show the midspan moment vs. twist data for the north and south girders respectively from tests with a stiffener angle spacing of 8 ft, 16 ft and 24 ft and no offset in the applied load. Counter clockwise rotations were taken as positive. Similar to the 20 gage test discussed in the last section, the 8 ft stiffened system was the stiffest system. Even though the 24 ft stiffened system had one less stiffening angle than the 16ft stiffened system, it was stiffer than the 16 ft stiffened system. As explained for 20ga01 tests the main reason for that was probably the existence of a stiffening angle at midspan. The north girder twisted in the counterclockwise direction. Unlike the 20ga01 tests the south girder twisted in the clockwise rotation, however the rate of twist was decreasing slightly as the moment level increased.

Similar to 20ga01 tests in the stiffened tests almost all of the rotation was due to bottom flange lateral displacement. The top flange lateral displacements were about 0.03 in at the moment level of 400 k-ft for both of the girders, whereas the bottom flange lateral displacements were about 0.25 in and 0.11 in for the north and south girders respectively. This shows that the center of twist of the cross section was closer to top flange.

Figure 7.27 and Figure 7.28 show a comparison of the midspan moment vs. twist test data with the FEA results for the 8 ft stiffened deck system with no offset for the north and south girders, respectively. The stiffening angle was sized based upon the lateral load tests discussed in Chapter 6. The FEA is conservative up to a moment level of 350 k-ft and then it becomes unconservative for the north girder. For the south girder the FEA gives conservative results. The model also twisted in the clockwise direction at a decreasing rate consistent with the laboratory test data.

Figure 7.29 and Figure 7.30 show a comparison of midspan moment vs. twist test data with the FEA results for 16 ft stiffened deck system with no offset for the north and south girders, respectively. The stiffening angle system was sized based upon the lateral load tests discussed in Chapter 6. The FEA solution is conservative up to a moment level of 270 k-ft and then it becomes unconservative for the north girder. For the south girder the FEA solution provided conservative results similar to the 8 ft stiffened model. The model also twisted in the clockwise direction at a decreasing rate consistent with the laboratory test data.

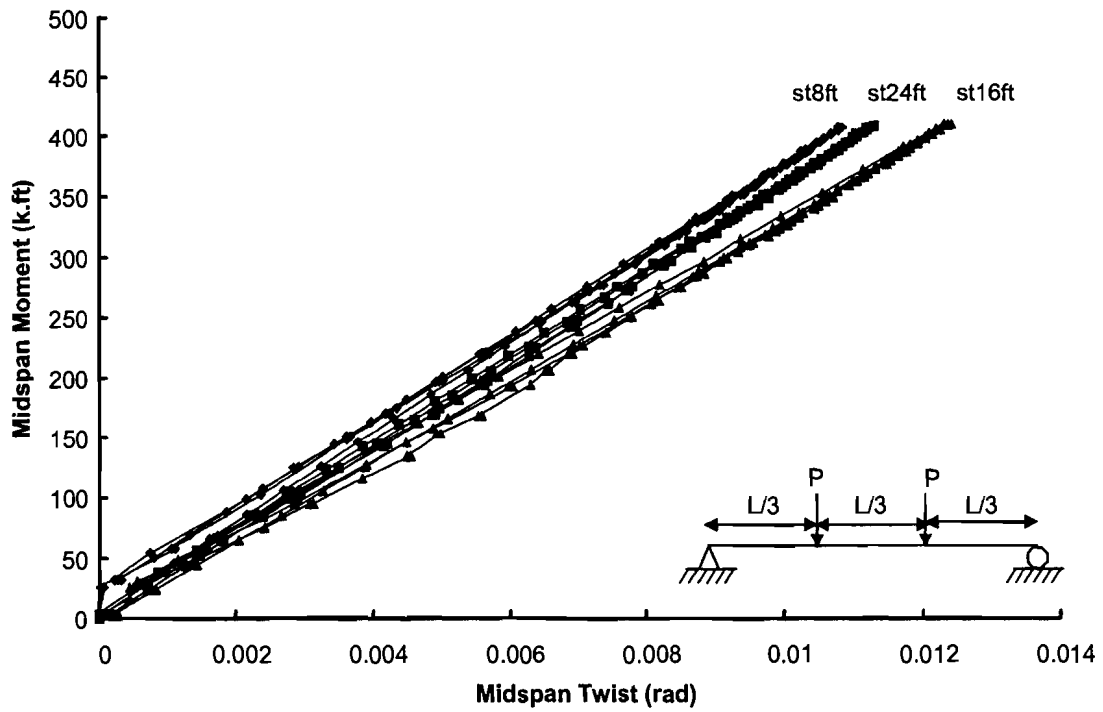


Figure 7.25 Midspan Moment vs. Twist Data for 20ga02.no Tests (North Girder)

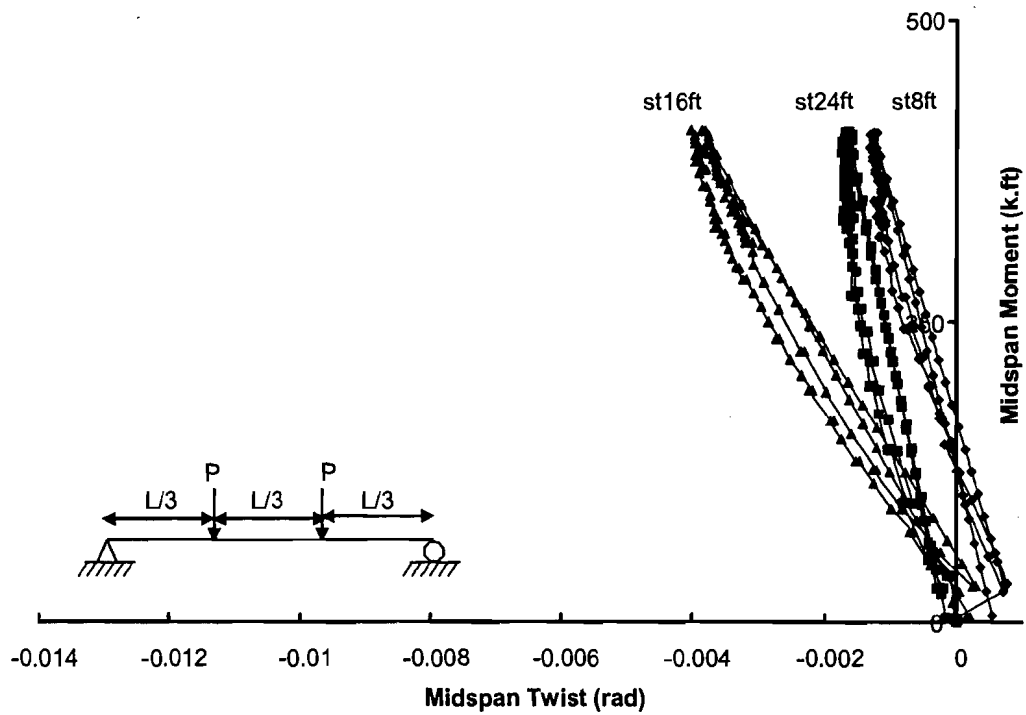


Figure 7.26 Midspan Moment vs. Twist Data for 20ga02.no Tests (South Girder)

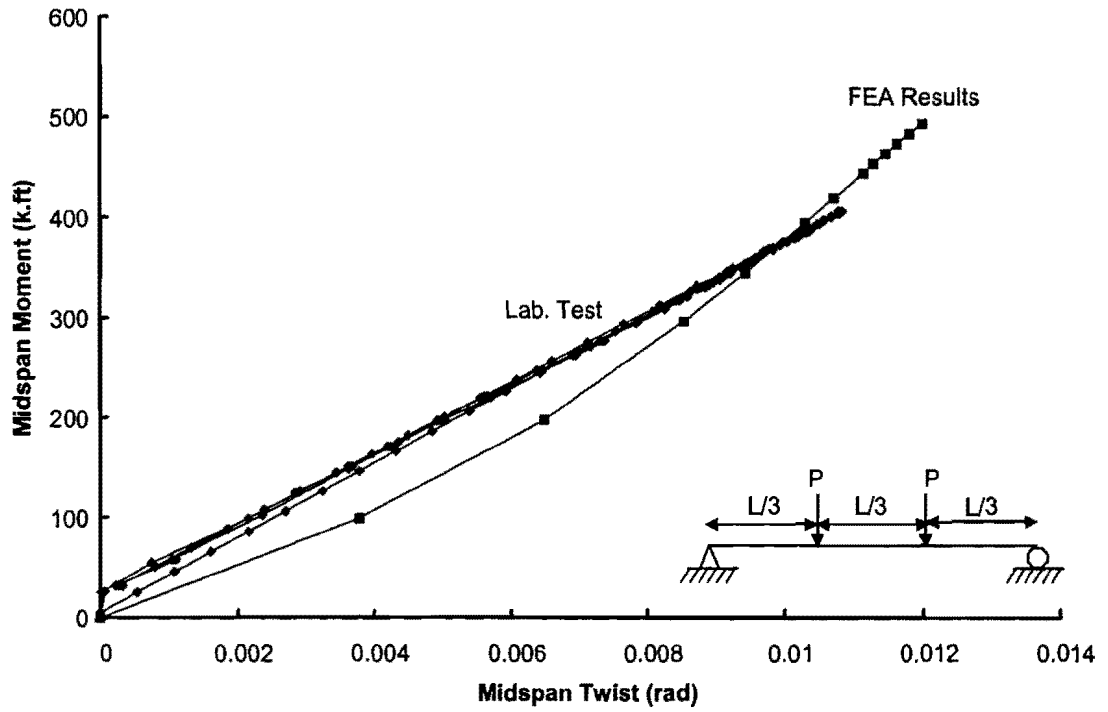


Figure 7.27 Comparison of Midspan Moment vs. Twist for 20ga02.st8ft.no (North Girder)

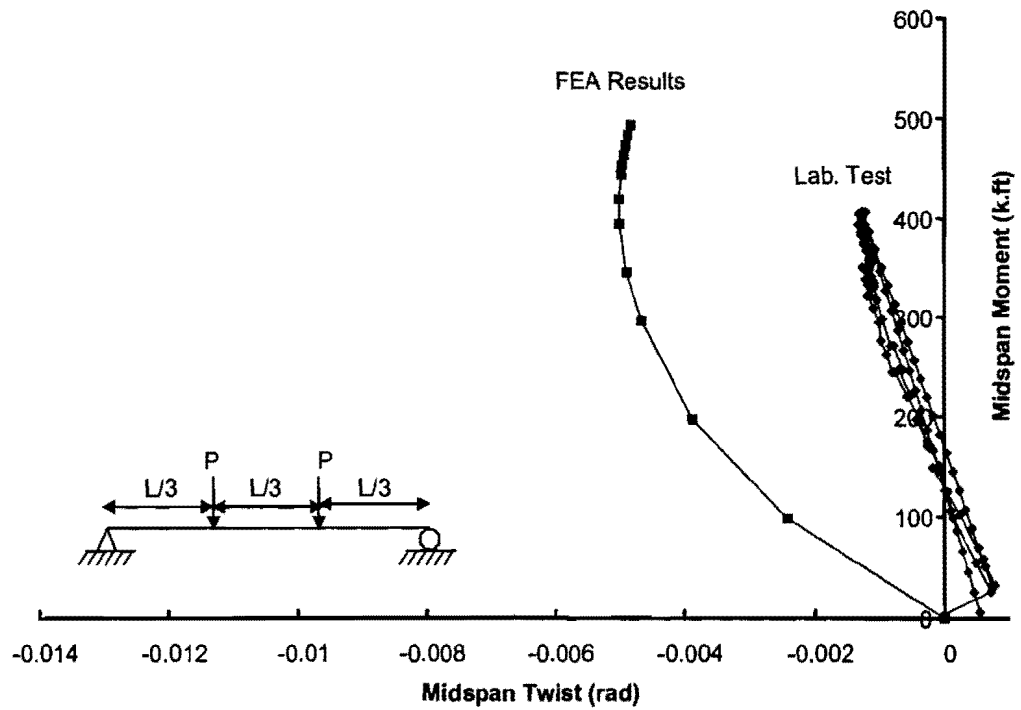


Figure 7.28 Comparison of Midspan Moment vs. Twist for 20ga02.st8ft.no (South Girder)

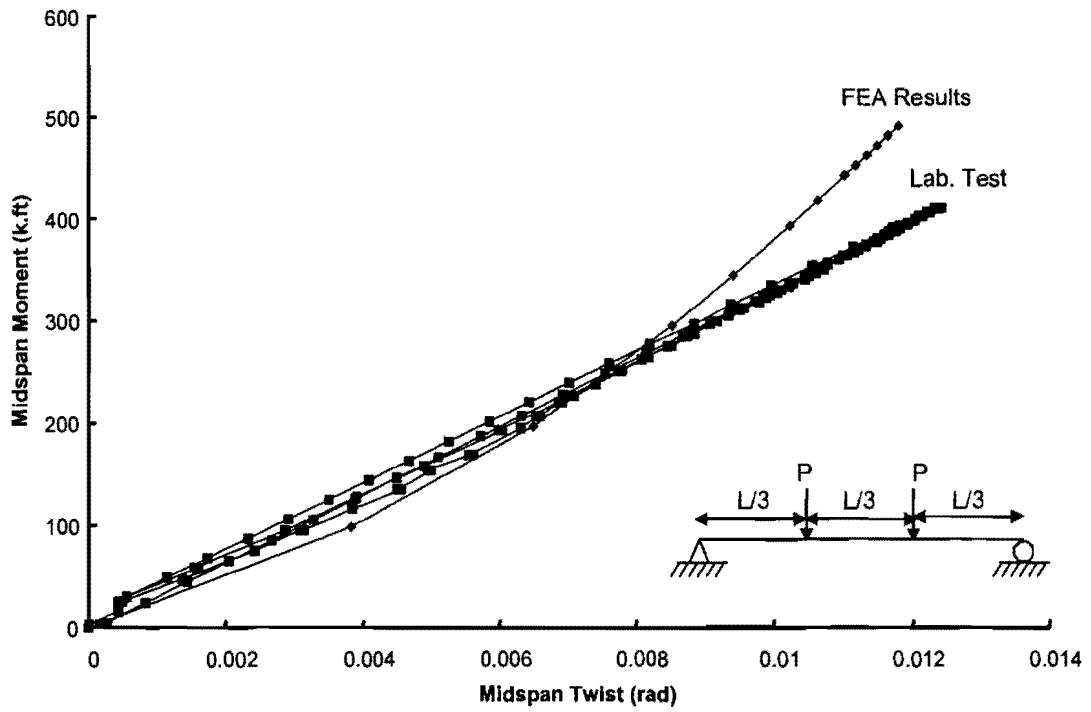


Figure 7.29 Comparison of Midspan Moment vs. Twist for 20ga02.st16ft.no (North Girder)

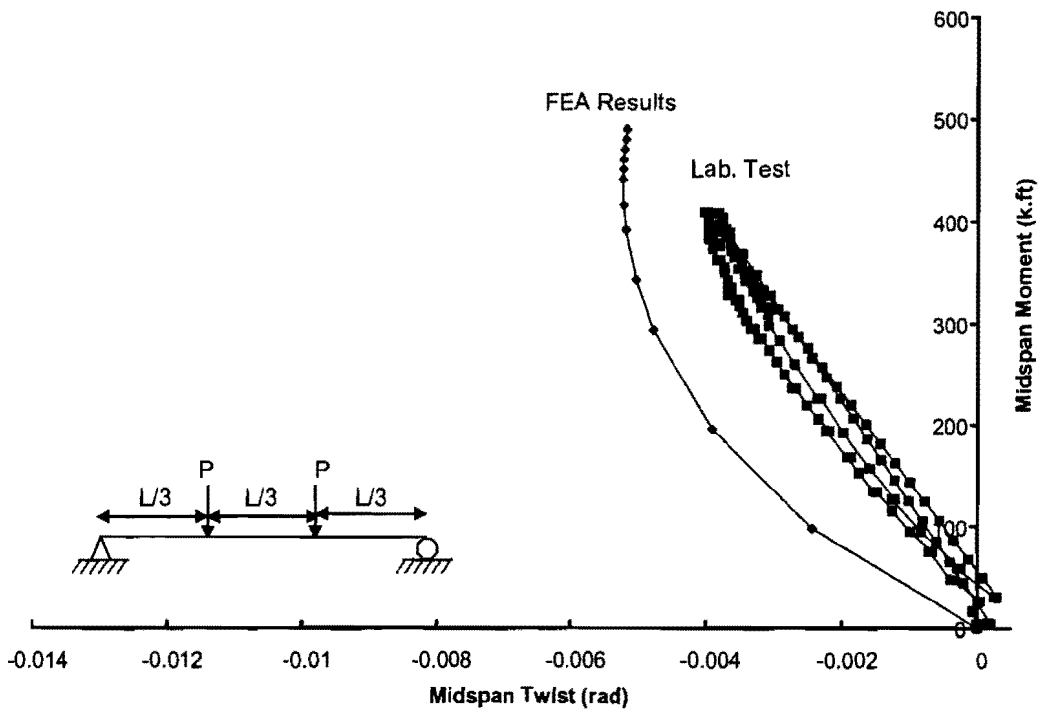


Figure 7.30 Comparison of Midspan Moment vs. Twist for 20ga02.st16ft.no (South Girder)

Figure 7.31 and Figure 7.32 show a comparison of the midspan moment vs. twist test data with the FEA results for the 24 ft stiffened deck system with no offset for the north and south girders, respectively. The area of the stiffening angles was based upon the lateral load tests that were discussed in Chapter 6. Similar to the 8 ft and 16 ft stiffened systems the FEA solution is conservative up to a moment level of 300 k-ft and then it becomes unconservative for the north girder. For south girder the FEA solution gives conservative results. The model twisted in the clockwise direction at a decreasing rate consistent with the laboratory measurements.

Figure 7.33 and Figure 7.34 show a comparison of the midspan moment vs. twist test data of tests with the no offset and the half-inch offset in the applied loads for the north and south girders, respectively. Results are shown for the cases with the 16 ft stiffener spacing and the 8 ft. stiffener spacing (half inch offset only). As discussed earlier applying the load with an offset is equivalent to increasing the imperfections. This can clearly be seen in Figure 7.33 and Figure 7.34. For the north girder the half-inch offset system is almost three times less stiff than the no offset system for the 20ga02 deck system. For the south girder the half-inch offset not only made the system less stiff but also caused the girder to twist in the other direction. Figure 7.33 and Figure 7.34 also compares the two half inch offset systems. 20ga01 deck system is less stiff than the 20ga02 deck system. The difference in the stiffness is due to the difference in the initial imperfections of the systems. From Figure 7.1 and Figure 7.2 it can be seen that 20ga01 deck system had bigger initial imperfections.

Figure 7.35 and Figure 7.36 show a comparison of midspan moment vs. twist for the laboratory tests and the FEA results for the 16 ft stiffened deck system with a half-inch offset for the north and south girders, respectively. Two finite element analyses were conducted. In the first analysis, the actual imperfections of the girders were modeled and the load was offset by half-inch offsets to the north of the centerline of the web just like the actual test. In the second analysis an initial imperfection of $L_b/500$ was applied to the top flange (straight bottom flange) and the load was applied with no offset. The FEA results with the actual imperfections had good agreement with the actual test results for both of the girders. The FEA results with the $L_b/500$ imperfection also had relatively good agreement with the north girder, however the model was about 5 times less stiff than the test results for the south girder. This implied that the half-inch offset applied to the north girder was satisfactory to mimic a $L_b/500$ imperfection for the north girder, however a larger offset was necessary for the south girder. Several FEA were performed by keeping the load at half inches to the north of the center of web for north girder, and changing the location of the load for south girder. The FEA results revealed that an offset of 0.9 in was necessary to mimic an initial imperfection of $L_b/500$ for the south girder. The FEA results can be seen in Figure 7.37 and Figure 7.38 for north and south girders, respectively.

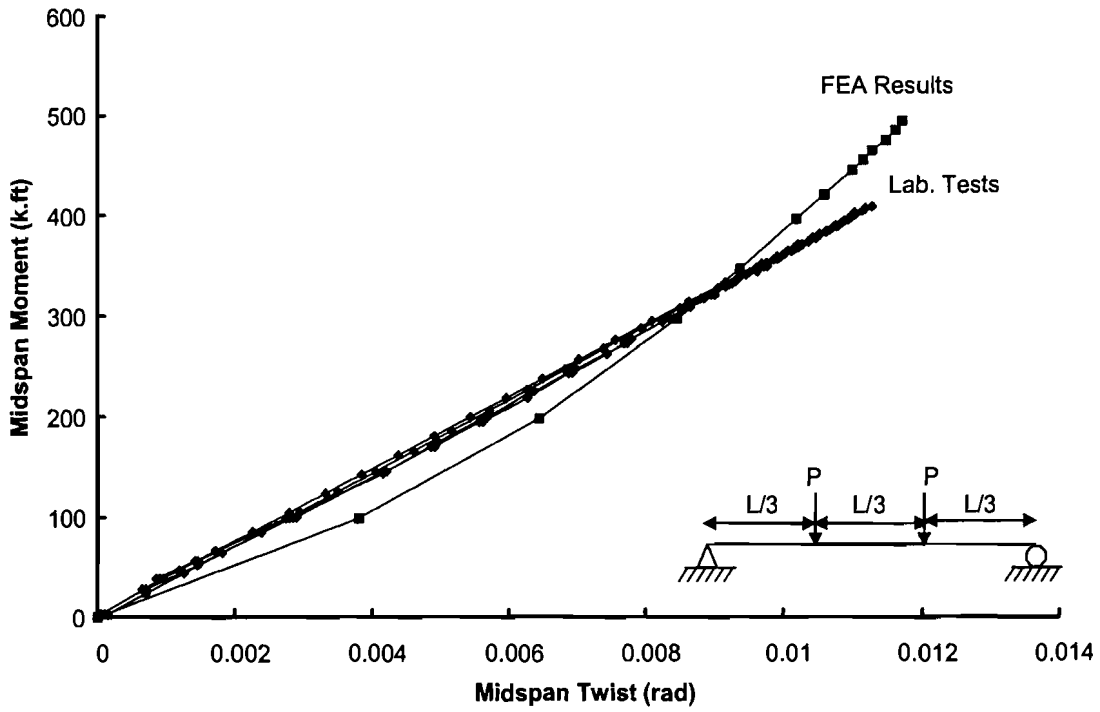


Figure 7.31 Comparison of Midspan Moment vs. Twist for 20ga02.st24ft.no (North Girder)

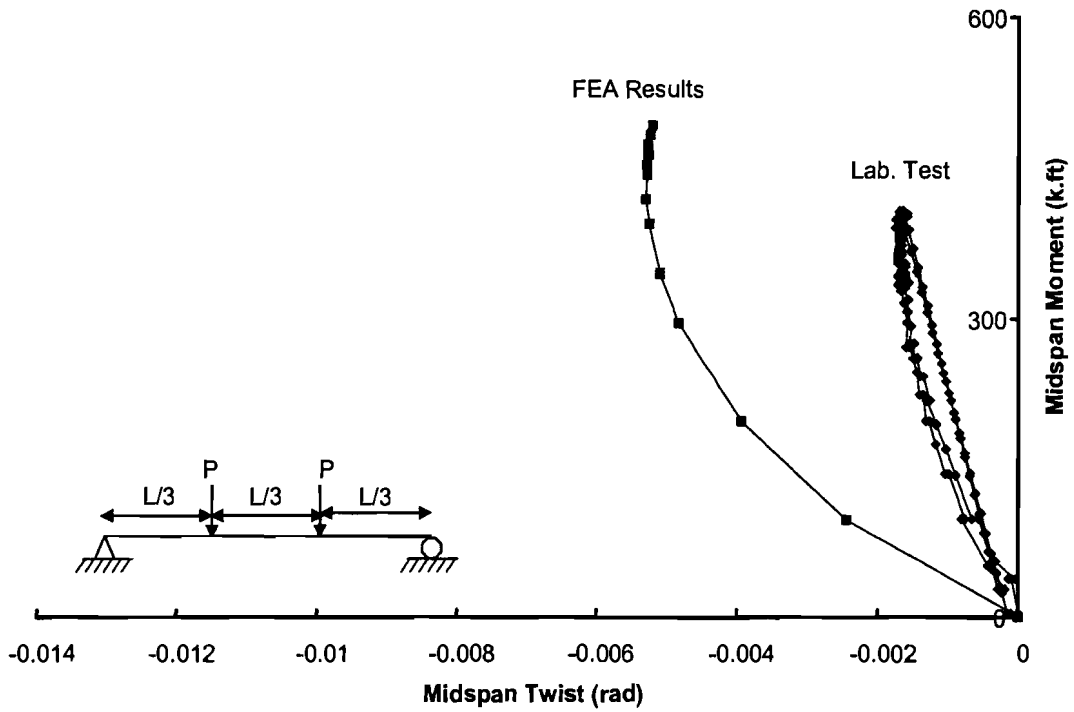


Figure 7.32 Comparison of Midspan Moment vs. Twist for 20ga02.st24ft.no (South Girder)

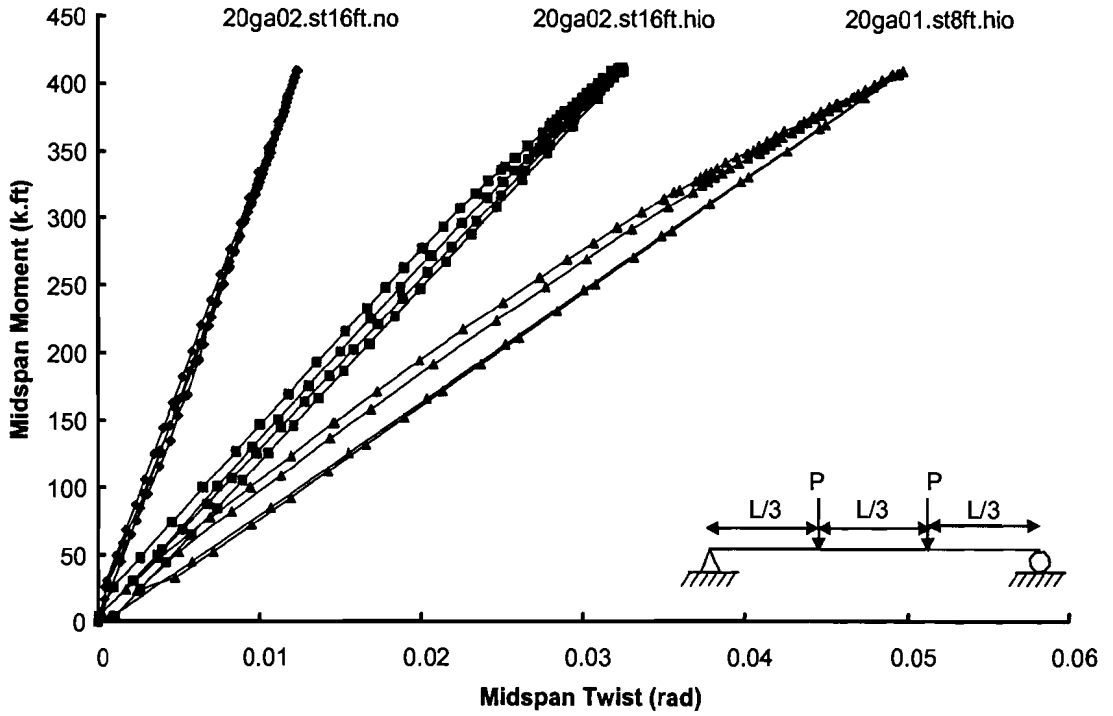


Figure 7.33 Comparison of Midspan Moment vs. Twist for 20ga02.st16ft.no, 20ga02.st16ft.hio and 20ga01.st16ft.hio Tests (North Girder)

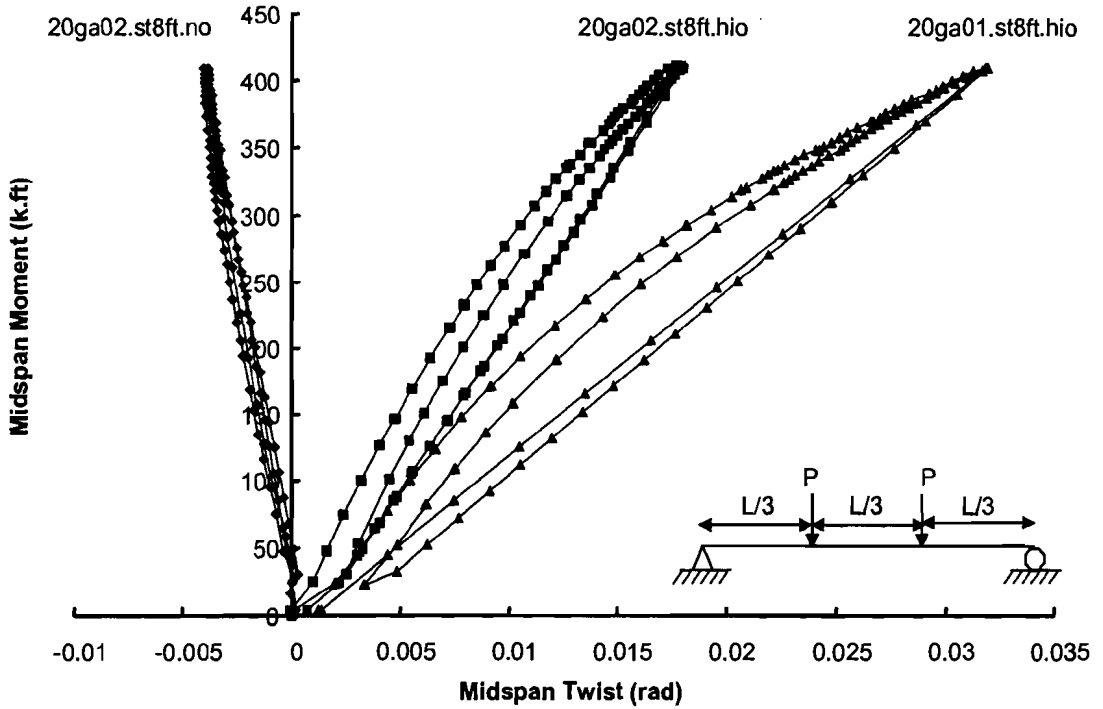


Figure 7.34 Comparison of Midspan Moment vs. Twist for 20ga02.st16ft.no, 20ga02.st16ft.hio and 20ga01.st16ft.hio Tests (North Girder)

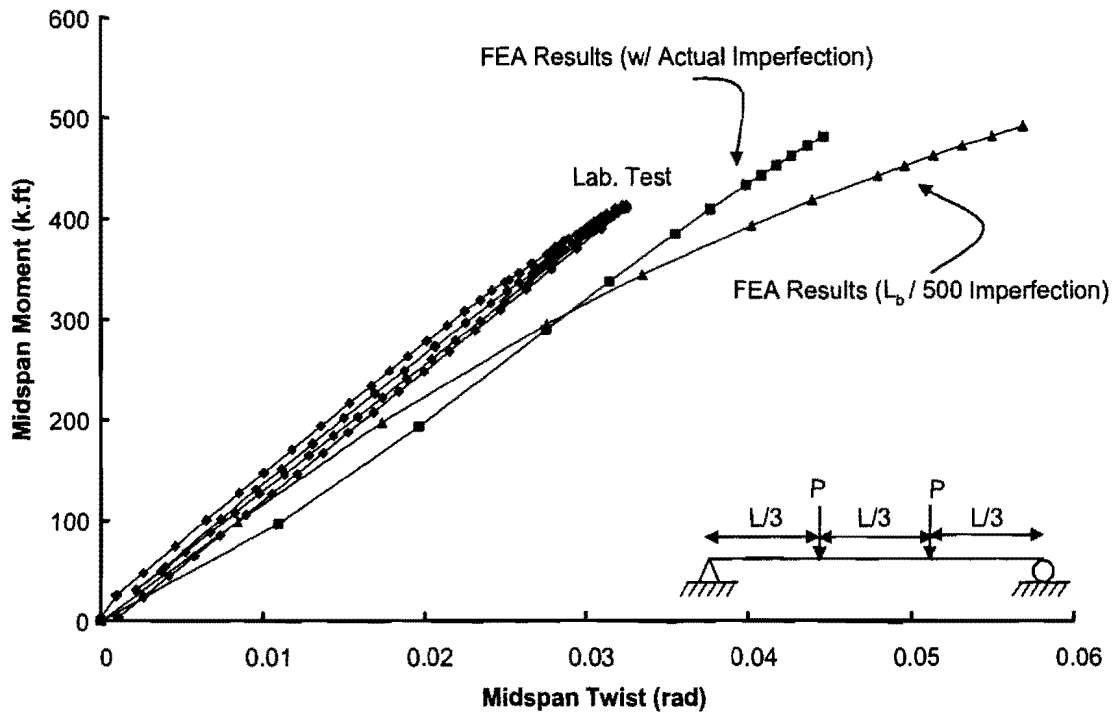


Figure 7.35 Comparison of Midspan Moment vs. Twist for 20ga02.st16ft.hio (North Girder)

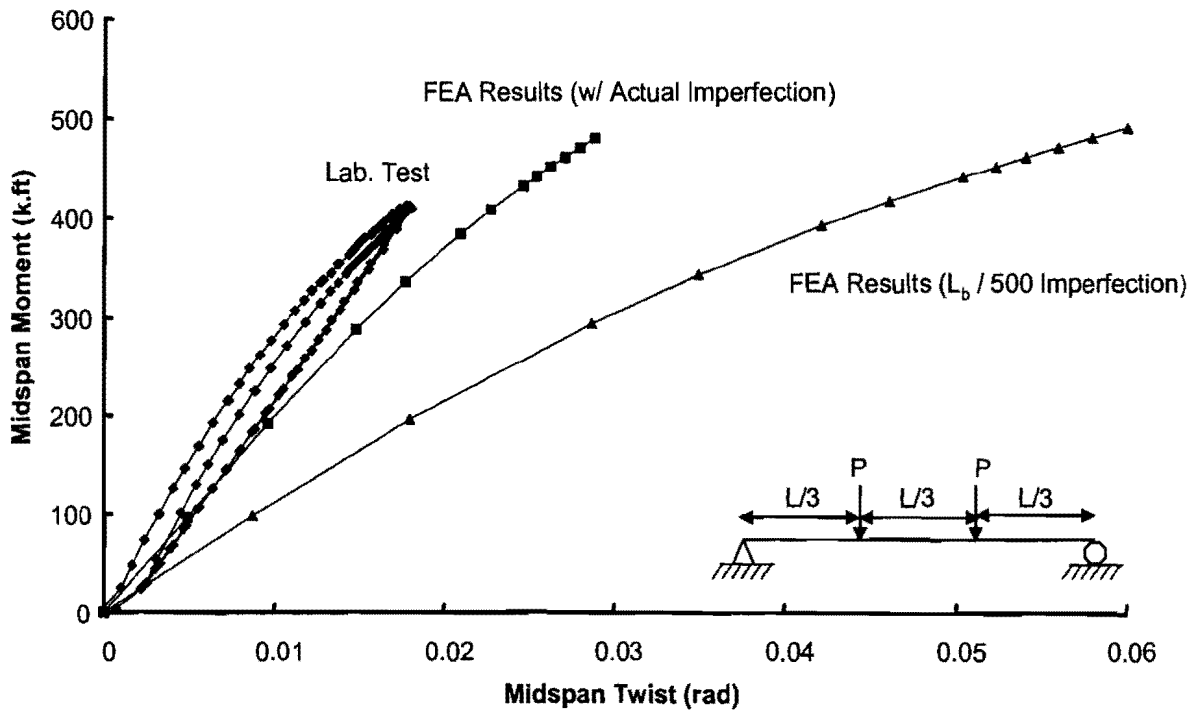


Figure 7.36 Comparison of Midspan Moment vs. Twist for 20ga02.st16ft.hio (South Girder)

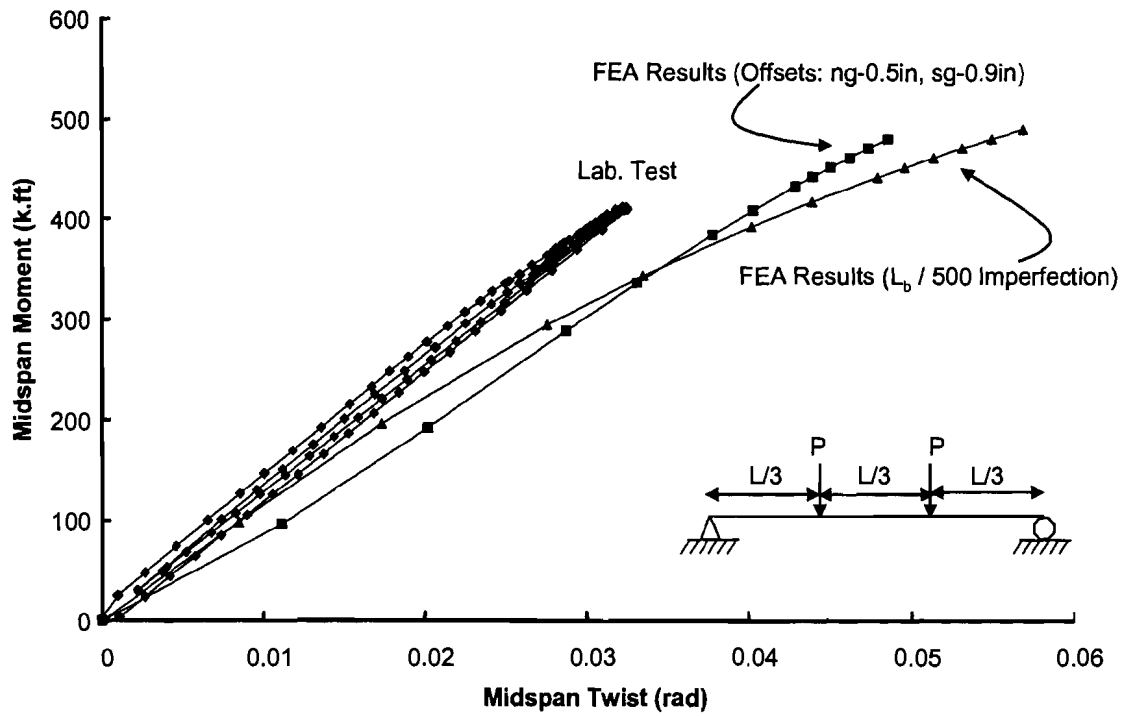


Figure 7.37 Comparison of Midspan Moment vs. Twist for 20ga02.st16ft.hio to Determine the Offset of the Applied Load (North Girder)

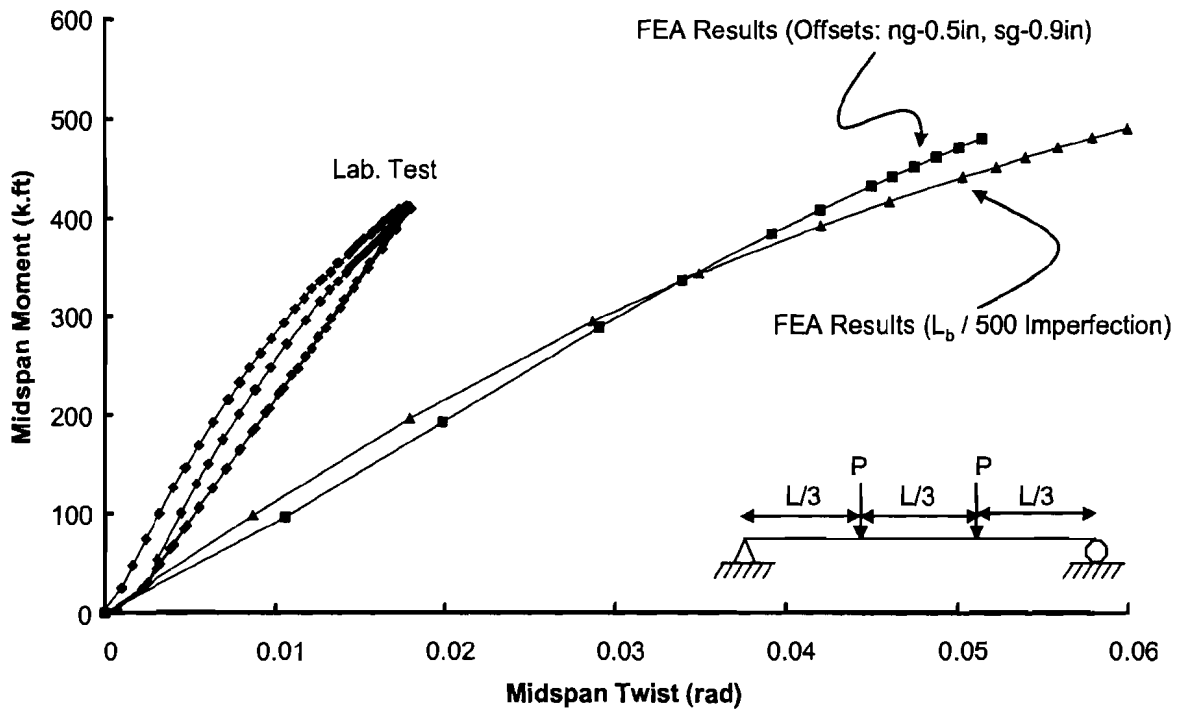


Figure 7.38 Comparison of Midspan Moment vs. Twist for 20ga02.st16ft.hio to Determine the Offset of the Applied Load (South Girder)

Eigenvalue buckling analyses were also performed, revealing the buckling capacity as 76 kips at each load point, assuming linear elastic materials. After the finite element analyses were completed the 16 ft stiffened 20ga02 deck system was loaded up to failure. As discussed above, the loads were offset by 0.5 in for the north girder and 0.9 in for the south girder.

Failure occurred due to a bearing failure in the PMDF around a TEK screw between the PMDF and the support angle approximately 12.3 ft away from the east support of the south girder. It was observed after the failure that one of the fasteners at the failure location was skipped during erection, hence creating the weakest location of the system. Figure 7.39 shows a photo of the failure location.



Figure 7.39 Photo of Failure of the Deck to Support Angle Connection

Figure 7.40 and Figure 7.41 show the midspan moment vs. total twist for the failure test for the north and south girders, respectively. The total twist has been normalized by the initial twist. Both of the curves flatten out at a moment level of about 500 k-ft. The ultimate load that was achieved was 32.5 kips corresponding to a moment level of 524 k-ft. The measured ultimate stresses from the strain gages on the girder

flanges were 32.3 ksi and 42.2 ksi for south and north girders respectively. At the failure moment the top flange lateral displacements were 0.83 in and 0.92 in and bottom flange lateral displacements were 1.05 in and 1.19 in for north and south girders respectively. As discussed earlier the philosophy for the design of bracing members is traditionally to achieve a desired load level while limiting the deformation of the system to be equal to the initial imperfection. At the moment level of 450 k-ft (Max. design construction load that would cause a stress of 30 ksi) the value of the total twist over initial twist was 2.37 (18% higher than the desired value of 2) for both of the girders and the measured stresses were 30.3 ksi and 33.1 ksi for north and south girders respectively. Top flange lateral displacements were 0.49 in and 0.55 in and bottom flange lateral displacements were 0.89 in and 0.90 in for north and south girders, respectively.

The value 2 that corresponds to the deformations of the system to be equal to the initial imperfections was achieved at a moment level of 403 k-ft. At this moment level the calculated stress was 26.7 ksi whereas the measured stresses were 28.1 ksi and 29.1 ksi for north and south girders respectively. Top flange lateral displacements were 0.11 in and 0.13 in and bottom flange lateral displacements were 0.68 in and 0.65 in for the north and south girders, respectively.

The permanent deformation observed at the graphs at the end of the test after the load was removed was mainly due to the deformed support angles. Once the deck and the support angles were removed, the girders recovered the deformations. Figure 7.42 shows a photo of the deformed support angle after the test. The deformation in the support angle occurred after the bearing failure around a TEK screw.

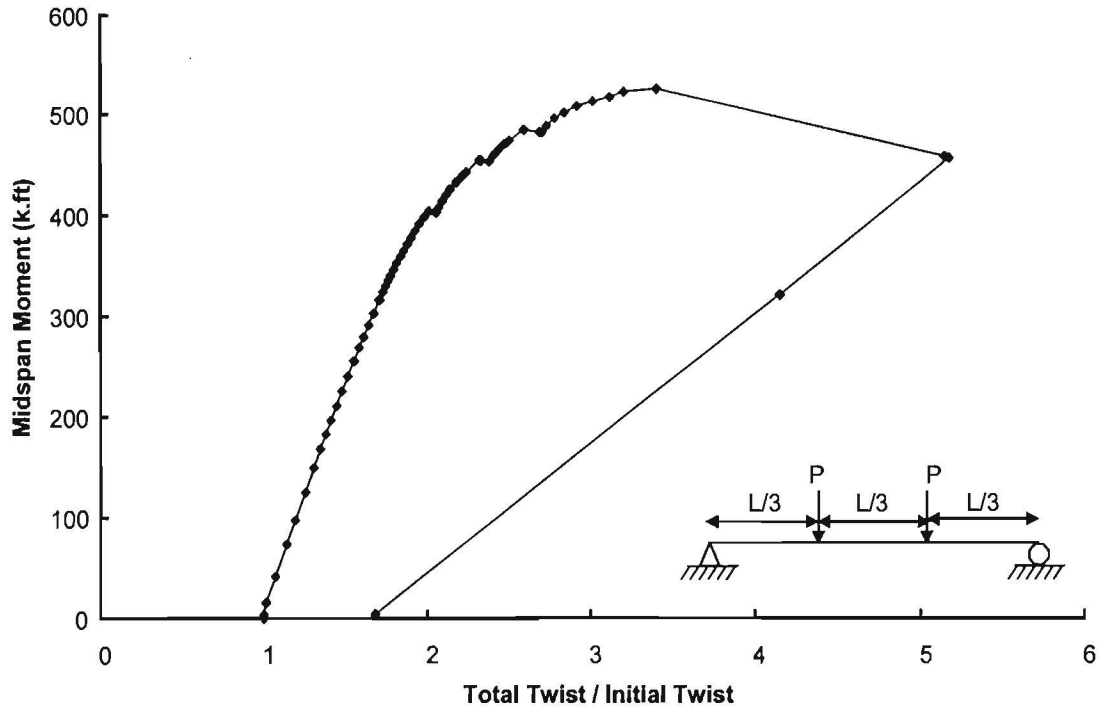


Figure 7.40 Midspan Moment vs. Total Twist / Initial Twist Test Data for 20ga02.st16ft Failure Test (North Girder)

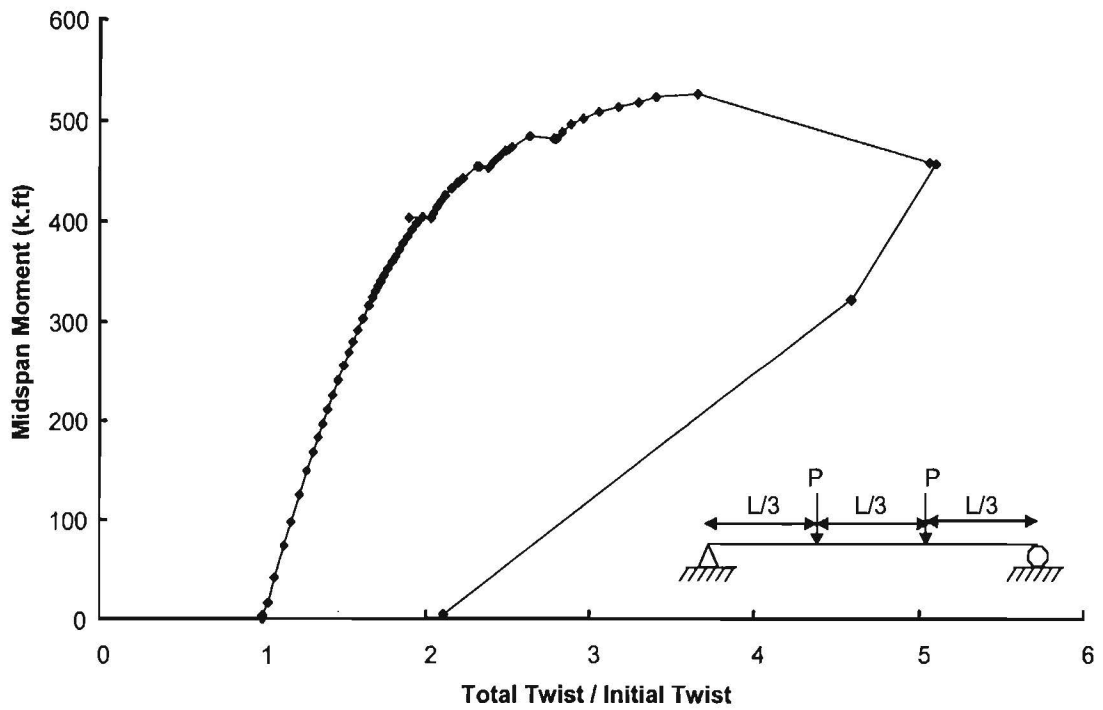


Figure 7.41 Midspan Moment vs. Total Twist / Initial Twist Test Data for 20ga02.st16f Failure Test (South Girder)

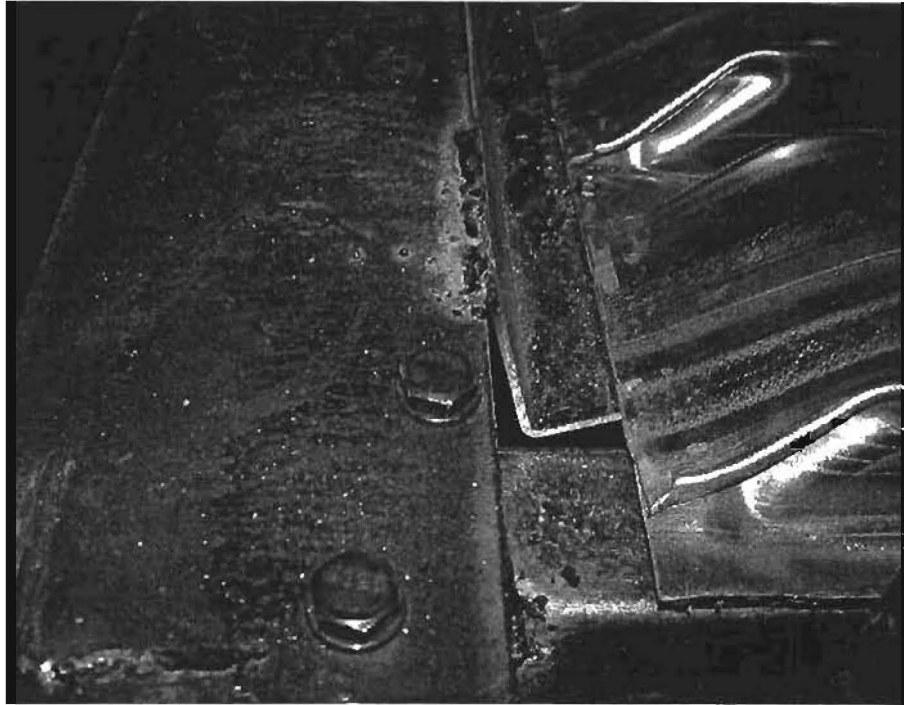


Figure 7.42 Photo of Deformed Support Angle after 20ga02.st16ft Failure Test

Figure 7.43 and Figure 7.44 show a comparison of midspan moment vs. the total twist from the laboratory tests and the FEA results. Up to a moment level of 450 k-ft the FEA results match very well with the behavior of the actual system for both of the girders. Therefore, the brace moments corresponding to this moment level were calculated by using the FEA results. Figure 7.45 show the distribution of the brace moments (per inch length) calculated from the shear diaphragm truss elements along the girder length at the moment level of 450 k-ft (14% less than the ultimate moment achieved). Since the brace moments were symmetric about midspan, only half of the graph is shown. It can be seen from this graph that the maximum brace moments occurred around 11.3 ft-15.3 ft away from the support, exactly where the failure took place.

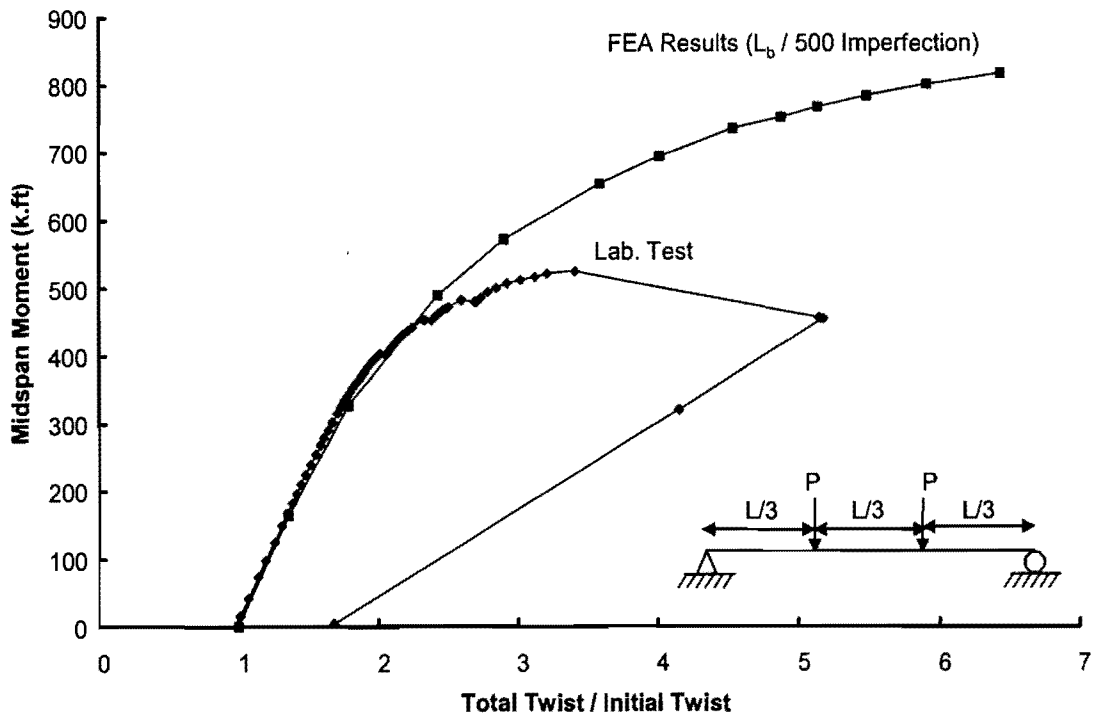


Figure 7.43 Comparison of Midspan Moment vs. Total Twist / Initial Twist Test Data for 20ga02.st16f Failure Test (North Girder)

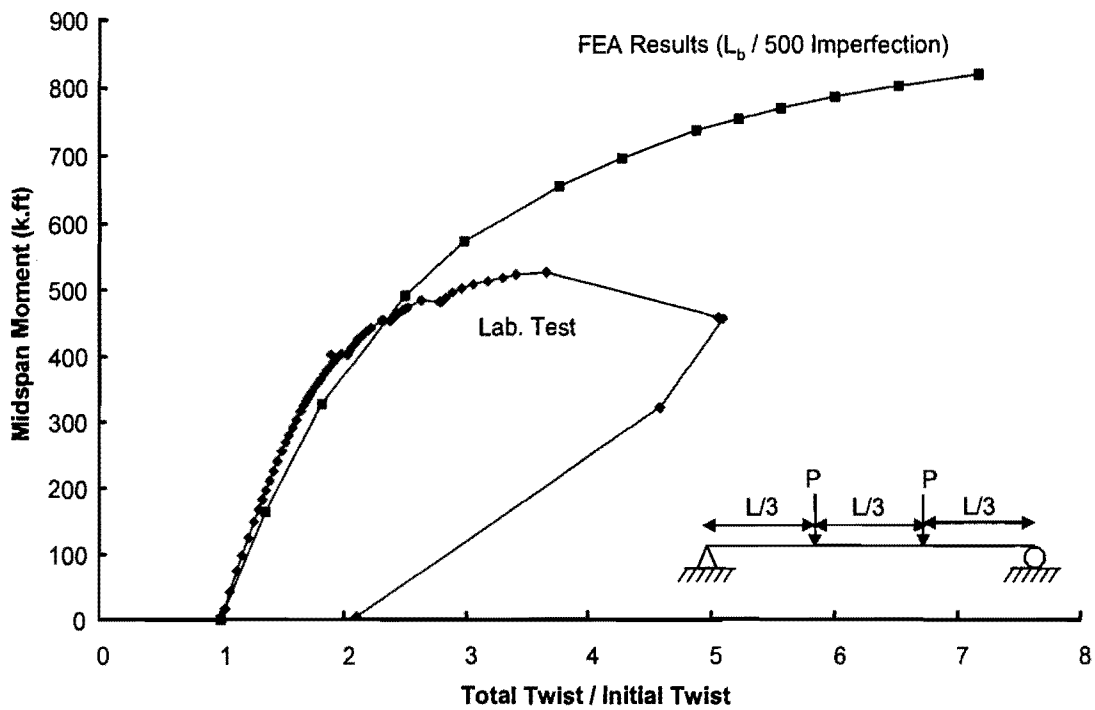


Figure 7.44 Comparison of Midspan Moment vs. Total Twist / Initial Twist Test Data for 20ga02.st16f Failure Test (South Girder)

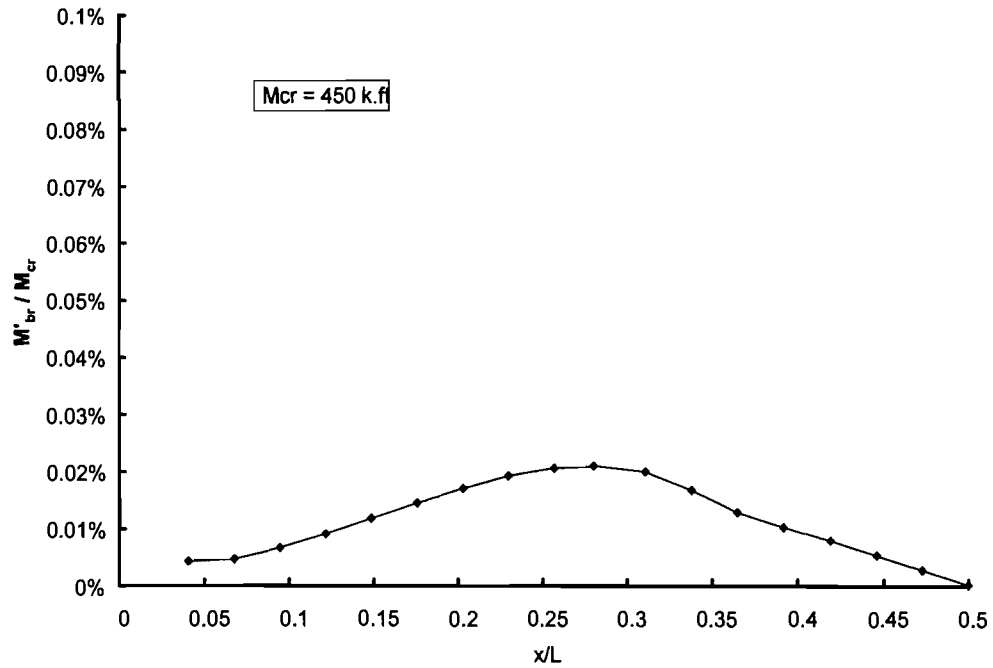


Figure 7.45 Distribution of Brace Moments along Girder Length

7.4.3 20ga03 Tests

For this set of 20ga deck system only the unstiffened system was tested for buckling. This test was done to get an indication of the buckling behavior of the PMDF system without the stiffening angles. Figure 7.46 and Figure 7.47 show a comparison of the midspan moment vs. twist for the laboratory data and FEA results for the unstiffened deck system with a half-inch offset for the north and south girders, respectively. A beam element with a moment of inertia of 10 in⁴ was used in the finite element model similar to the 20ga01 analyses. The FEA results with the actual imperfections had good agreement with the test results for the south girder and were unconservative for the north girder. Similar to test discussed in the last section, additional analyses were performed in order to determine the offset of the load to mimic a $L_b/500$ imperfection. It was concluded that 0.5 in and 0.9 in offset for the north and south girders respectively was necessary to mimic the behavior of a system with an initial imperfection of $L_b/500$ for the top flange with a straight bottom flange.

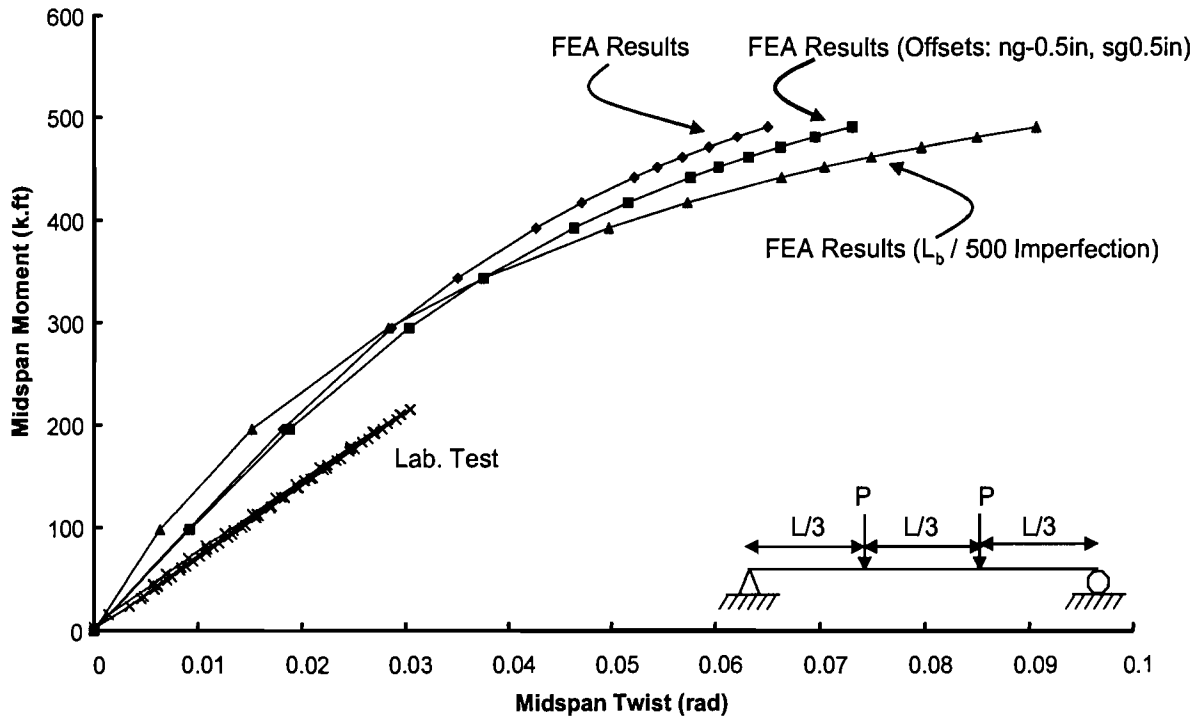


Figure 7.46 Comparison of Midspan Moment vs. Twist Test Data for 20ga02.st16f Failure Test (North Girder)

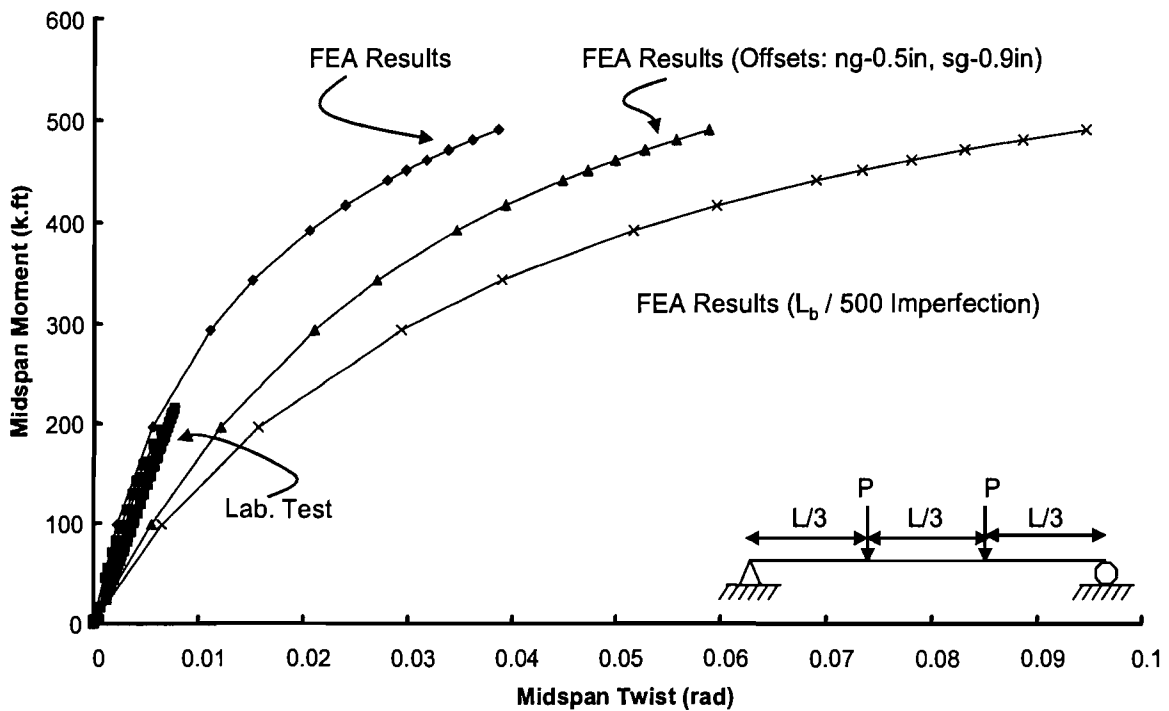


Figure 7.47 Comparison of Midspan Moment vs. Total Twist Test Data for 20ga02.st16f Failure Test (South Girder)

Figure 7.48 and Figure 7.49 show the comparison between the two failure tests, 20ga02.st16ft and 20ga03.unst for the north and south girders, respectively. The moment vs. total twist / initial twist behavior of an unbraced girder ($L_b = 50$ ft) and the eigenvalue buckling moment corresponding to $L_b = 25$ ft is also included in the figures. The unstiffened failure test was aborted at about 370 k-ft of moment when the curve started to flatten out. It can clearly be seen from the graphs that the 16 ft stiffened system did a much better job in controlling the deformations and carried approximately 35% more moment than the unstiffened system. It can also be seen from the graphs that a stiffened deck system can carry 6 to 7 times higher moments than an unbraced girder. If conventional methods of bracing were utilized for this 50 ft long girder, the designer would have put a cross frame at midspan reducing the unbraced length to 25 ft. The stiffened deck system carries at least twice the buckling moment capacity of the girder with a midspan cross frame and with no PMDF.

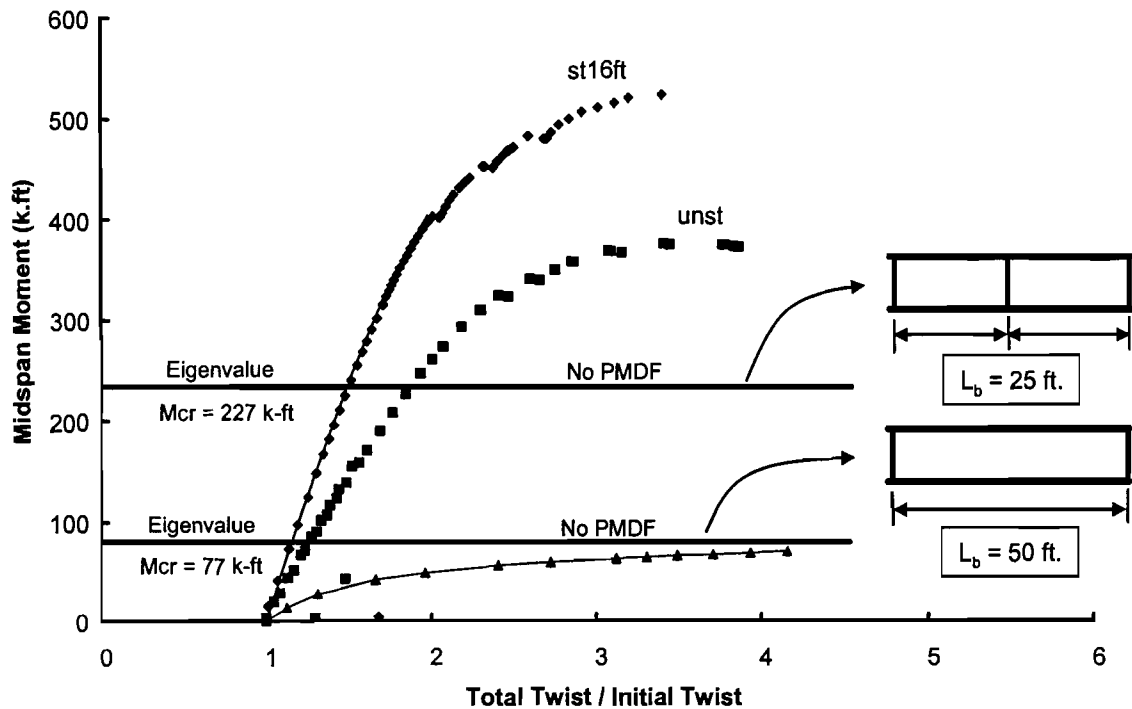


Figure 7.48 Comparison of Midspan Moment vs. Total Twist / Initial Twist Test Data for 20ga02.st16f and 20ga03.unst Failure Tests (North Girder)

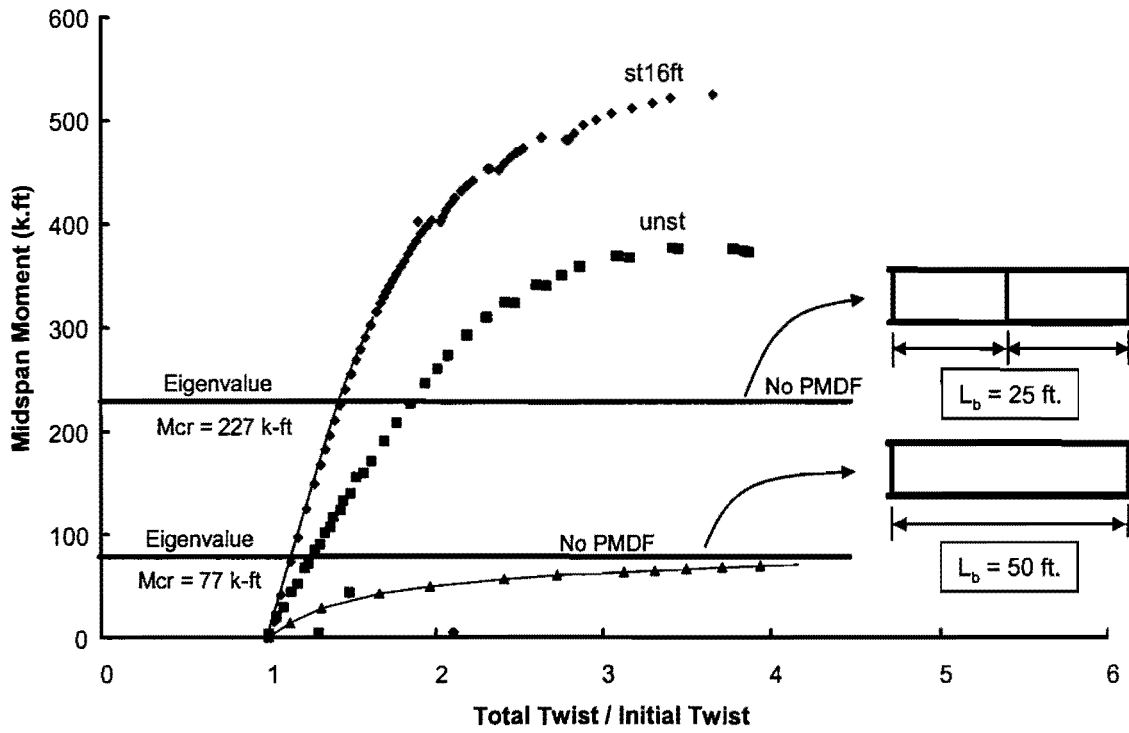


Figure 7.49 Comparison of Midspan Moment vs. Total Twist / Initial Twist Test Data for 20ga02.st16f and 20ga03.unst Failure Tests (South Girder)

This page replaces an intentionally blank page in the original.

-- CTR Library Digitization Team

Chapter 8

Parametric Studies

8.1 Overview

The previous chapter compared the finite element analysis results with the laboratory buckling tests. Finite element results are presented in this chapter for twin girders with normal supports braced with deck forms using stiffened connections. Results are shown for both the rolled beam and built-up sections that were shown in Figure 3.4.

Eigenvalue buckling analyses are presented in Section 8.2. Finite element results from the large displacement analyses for wide flange sections are shown in Section 8.3. These results are then used to calculate the brace forces. Some of the girders had intermediate cross-frames. Tension-only cross-frames that framed into the girders at the top and bottom flange locations were used in these situations. The results from the FEA analyses are summarized in Section 8.4.

Previous research studies have mostly focused on diaphragm-braced girder systems. The finite element analyses presented in this section show results for both diaphragm-braced girders and girders braced by PMDF systems with stiffened connections. For Section #3, which was the section used in the laboratory tests, 8 ft, 16 ft and 24 ft spaced stiffening angles were investigated. For all other sections 10 ft and 20 ft spaced stiffening angles were used in the analyses. Two types of loading were considered for Section #3, uniformly distributed load and concentrated loads at the third points. For all other sections a uniformly distributed load was considered. All transverse loads were applied at the top flange.

The spacing of the girders was 115.25 in. Therefore the deck shear rigidity Q was varied by changing the effective shear stiffness G' of the deck. This does not have any effect on the analyses of the girders braced with shear diaphragms. However the effect of girder spacing (deck span) on the contribution of bracing provided by the stiffening angles was not investigated. Twin girder systems were considered in the analysis. Most bridges have more than 2 girders and therefore the shear rigidity for each girder will tend to go up since there is more metal deck forms per girder that can provide bracing. For example, for the same PMDF system, bridges with 3, 4 and 5 girders will have respective increases in the shear rigidity of 33%, 50%, and 60% higher than a twin girder system.

The goal of these parametrical studies was to improve the understanding of the bracing behavior of the PMDF systems with stiffened and unstiffened connections. There are some basic assumptions that were necessary to make regarding how the trusses that simulate the stiffening angles were to be sized. The general approach that was adopted in the modeling of these systems was to maintain a conservative model. In addition, expressions that can be utilized to estimate the stiffness and strength

requirements for the PMDF systems are also presented. A conservative approach has also been adopted for these expressions.

8.2 Eigenvalue Buckling Analyses

A modified approximation to the buckling capacity of girders braced by a shear diaphragm was given by Eq. (2.14) and is repeated here for convenience:

$$M_{cr} = C_b^* M_g + mQd \quad (8.1)$$

The component of the deck in Eq. (8.1) is only a function of the girder depth and the deck shear rigidity as well as the constant m that depends on the type of loading, the presence of intermediate bracing, and the web slenderness. Values of m were given in Table 2.1. The graphs presented in this section are the comparison of FEA results and the buckling capacity from Eq. (8.1). Equation (8.1) was developed for girders braced by a shear diaphragm that was fastened on only two sides (ie. at the support angle). The results that will be presented in this chapter will also focus on the behavior of PMDF systems with stiffening angles. Since these systems have panels that are connected on 4 sides, they tend to be more effective than a shear diaphragm supported on only two sides. As a result these systems will provide more stability bracing than conventional diaphragms connected on two sides. The stability bracing contributions from the stiffening angles provide a quite different type of bracing than the restraint coming from the PMDF connection through the support angle. The term “ mQd ” in Eq. (8.1) represents the contribution from the PMDF/support angle connection. From a stability perspective, the contribution from the stiffening angle is different and is more similar to a discrete brace framing into the girders at a single point. Since the deck/stiffening angle system really provides restraint of two points relative to one another, the system is very similar to a “*relative bracing*” system. While there have been a number of previous studies on the behavior of relative bracing systems, very little has been done on combination systems such as the PMDF system with stiffened connections.

The lateral load tests that were presented in Chapter 6 showed that the stiffened connections provided a larger lateral stiffness than the unstiffened connection. Considering the cases with a lateral load at midspan for the 20 gage deck, the difference in the lateral stiffness between the unstiffened and stiffened systems ranged between 2 k/in and approximately 5.3 k/in. This increment in the lateral stiffness due to the stiffening angles can provide a significant increase in the buckling capacity, however accounting for the bracing is somewhat difficult. For many problems, this amount of bracing acting alone may be adequate to substantially reduce the unbraced length of the beams. As a simple estimate the bracing of the stiffening angles will be approximated by using 50% of the buckling moment computed by using $L_b/2$ to evaluate the buckling capacity, where L_b is the spacing between the cross-frames. This approach should be conservative for most problems since the stiffening angles probably provide significantly higher bracing, however this provides a simple solution that can be graphed along with the FEA solutions. Therefore, Eq. (8.1) becomes:

$$M_{cr} = \frac{C_b \cdot M_g(L_b/2)}{2} + mQd \quad (8.2)$$

In all of the graphs the key information about the girders is provided: the total span length (L), the unbraced length of the girder (L_b), the span to depth ratio (L/d), the web slenderness ratio (h/t_w), the plastic moment capacity (M_p) and the buckling capacity of the unbraced girder ($C_b \cdot M_g$) under the appropriate loading. In addition to the key girder information, the moment level corresponding to the service loads is also shown in the graphs. The service moment level was assumed to be the moment that would create a stress of 25 ksi at the extreme fiber of the cross section (M_{S25}). The stress level of 25 ksi is somewhat of an arbitrary stress, however this seemed to be a reasonable level of in-plane bending stress during construction. The stress of 25 ksi would be caused by the girder self-weight, the wet concrete and formwork, as well as a live load caused by the construction personnel and equipment.

Table 6.18 in Chapter 6 presented the properties of the stiffening truss elements used in the FEA of lateral displacement tests. It can be observed from this table that as the deck gets stiffer the stiffening truss elements also get stiffer. In all of the analyses with a stiffening truss, the size of the truss that was used corresponded to the values that were measured for the first test with the 20 gage deck and the sine loading/displacement and a G' of 6.8 k/in. Referring back to Table 6.18, this was the case that provided the lowest stiffness from the stiffening truss. This is a conservative assumption since the truss size for the stiffening angles would in reality increase with thicker/stiffer PMDF forms. No analyses were performed for Q values less than 370 k/rad and the relationship between Q = 0 and 370 k/rad was conservatively assumed to be linear. It should be noted that the effective shear stiffness of the decks used in the field will usually be greater than the least value obtained from laboratory test results. The tests in the laboratory used the largest possible eccentricity all along the girder length. In the field the eccentricities will often be smaller at several locations along the girder length, which will generally result in deck rigidities greater than 370 k/rad.

Figure 8.1 and Figure 8.2 show the comparison of FEA results and Eq. (8.2) for Section #3, which is the singly symmetric section used in the laboratory tests. Figure 8.1 is for third point loading case and Figure 8.2 is for the uniformly distributed load case. For the third point loading case, the 24 ft stiffened model gave the lowest buckling capacities and the 8 ft stiffened model gave the highest buckling capacities. Laboratory results from Chapter 7 revealed that the 24 ft stiffened deck system provided a higher buckling capacity than the 16 ft stiffened deck system. The FEA model for this case however doesn't show the benefit from the presence of a stiffening angle at midspan. The reason for the difference between the test results and the FEA solution is probably due to some stiffening affect in the actual sheeting of the PMDF that occurs when a stiffening angle is placed at midspan. The buckling capacity of the shear diaphragm model was well below the buckling capacity of all three stiffened models. Helwig and

Frank (1999) suggested an m value equal to $3/8$ for h/t_w ratios greater than 60 for Eq. (8.1).

For the uniformly distributed load case the 24 ft stiffened FEA predicted even higher buckling capacities than the 8 ft stiffened FEA, which is not realistic. It is not clear from the eigenvalue buckling solution why this is. The approximate solution given in Eq. (8.2) is conservative relative to the FEA solutions. The girder buckling contribution that is graphed in the figures is the full capacity using $L_b=25$ ft. The value that is specified in Eq. (8.2) is actually only half this moment. The moment levels that are predicted by the FEA solution for Q values equal to 390 k/rad, are actually higher than the yield moment for the beams assuming 50 ksi steel ($M_y = 752$ k-ft). As was presented in the last chapter, this system actually failed at a moment level a little higher than 500 k-ft. However it is important to recall that the eigenvalue solutions in this case do not reflect the effects of initial imperfections. These solutions essentially represent the ideal conditions. It can also be observed from both of the graphs that the service moment level could easily be reached by the stiffened deck systems.

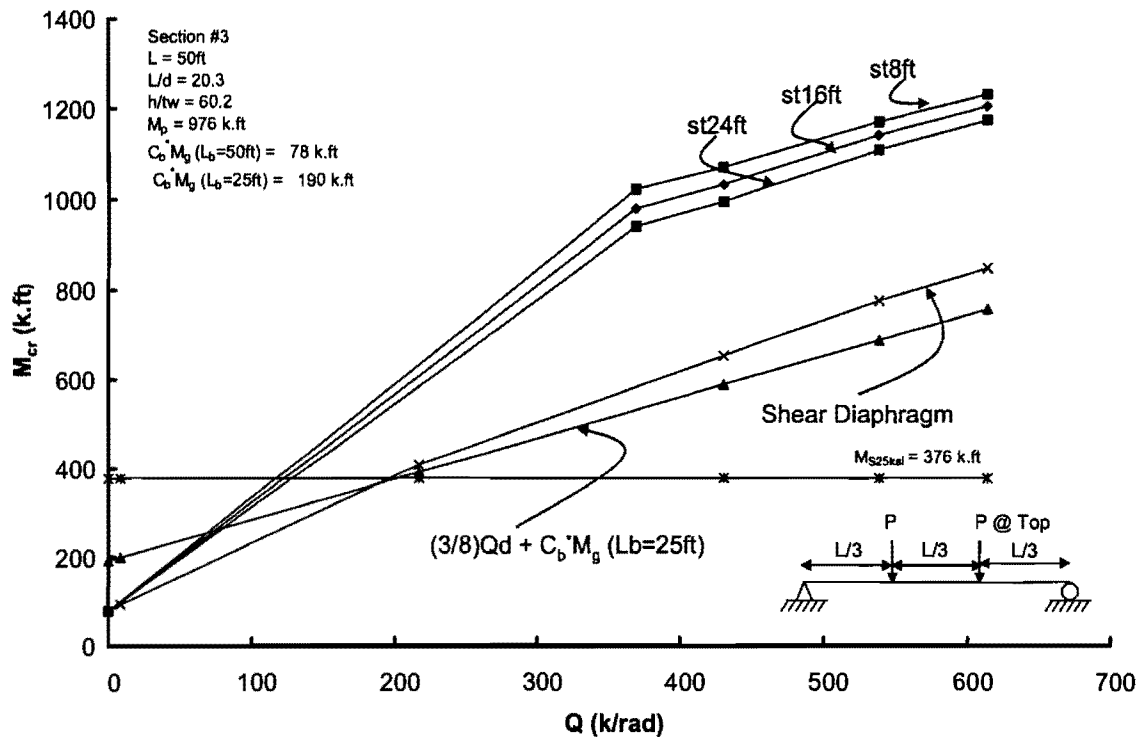


Figure 8.1 Comparison of FEA Results and Deck Component from Eq. (8.2) (Section #3, Third Point Loading)

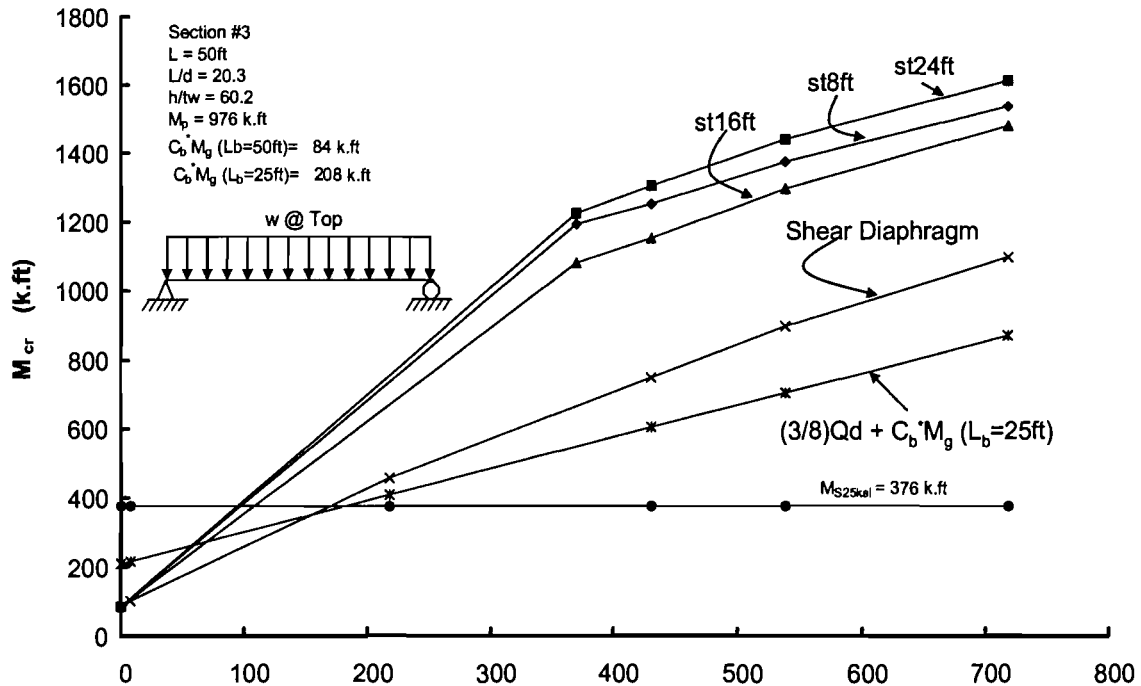


Figure 8.2 Comparison of FEA Results and Deck Component from Eq. (8.2) (Section #3, Uniformly Distributed Load)

For the rest of the cross sections studied, 10 ft and 20 ft values of the stiffening angle spacing were utilized. The areas of the stiffening angles that were used for the 10 ft and 20 ft system were the same as for the 8 ft and 16 ft models that were used for Section #3. This is a conservative approach since it can be seen from Table 6.18 in Chapter 6 that the stiffening truss elements get stiffer as the spacing of the stiffening beam elements increase.

For the 50 ft and 150 ft long spans, the stiffening angles cannot be evenly distributed if the spacing is 20 ft. The distribution of the 20 ft spaced stiffening angles is shown in Figure 8.3.

Figure 8.4 shows the comparison of FEA results and Eq. (8.2) for the W18x119. Helwig and Frank suggested an m value equal of $1/2$ for h/t_w ratios less than 60. The graphs show that Eq. (8.2) provides conservative estimates of the buckling behavior of the system. A very small deck is required to get to the moment corresponding to 25 ksi.

Figure 8.5 shows the comparison of FEA results and Eq. (8.2) for the W18x71. Similar to the W18x119 section, this equation was conservative than the FEA solution. In this case the full moment corresponding to an unbraced length of 25 ft ($L_b/2$) was used and the expressions are still conservative with respect to the FEA solution.

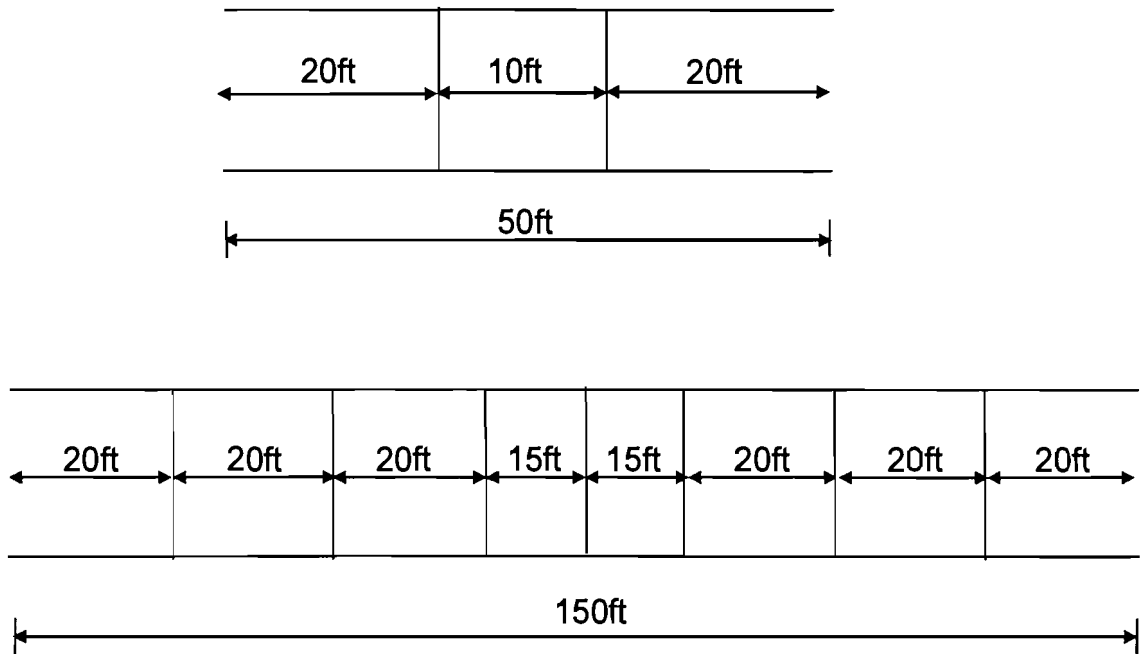


Figure 8.3 Distribution of 20ft Spaced Stiffening Angles (Plan View)

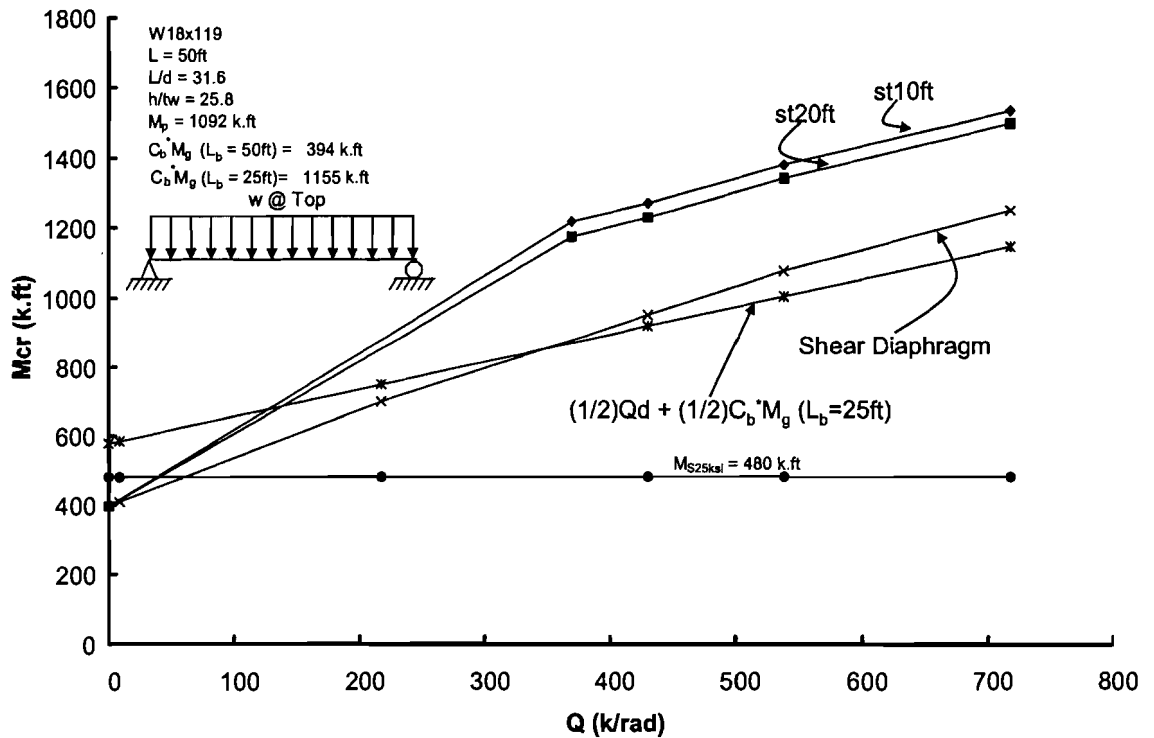


Figure 8.4 Comparison of FEA Results and Deck Component from Eq. (8.2) (W18x119)

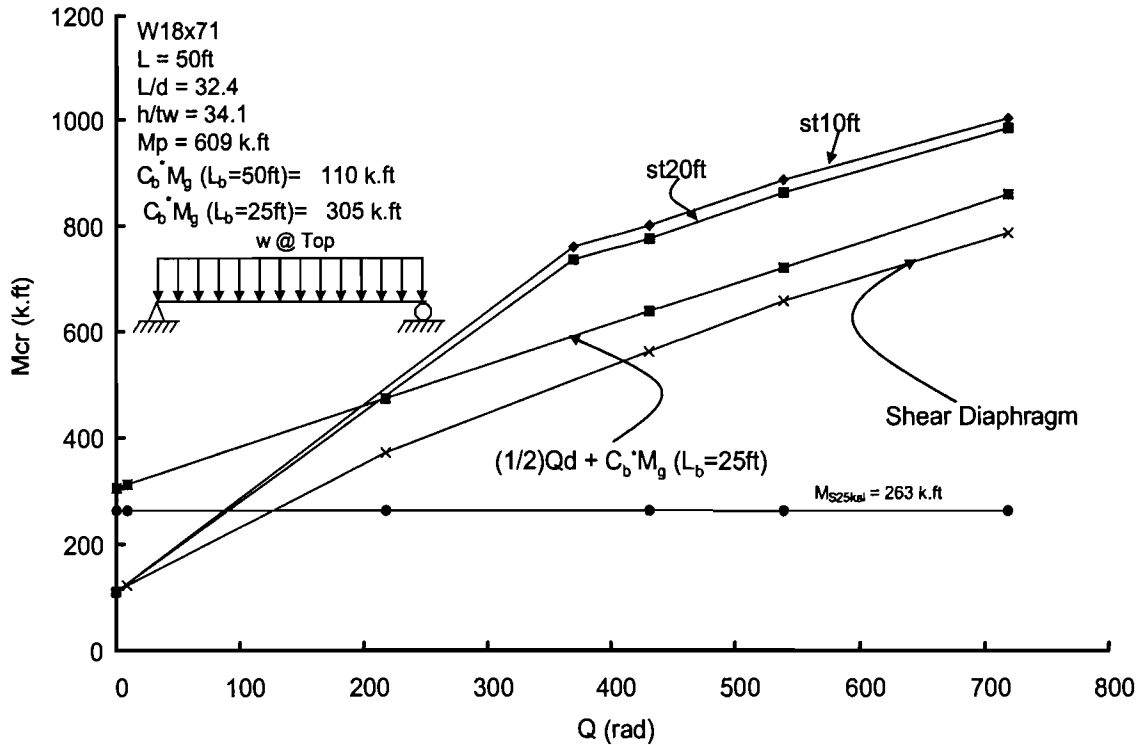


Figure 8.5 Comparison of FEA Results and Deck Component from Eq. (8.2) (W18x71)

Figure 8.6 shows the comparison of the FEA results and Eq. (8.2) for Section #4 with a spacing between cross-frames equal to the total beam length of 100 ft. Again the full moment term corresponding to $L_b/2$ was graphed instead of half the value as shown in Eq. (8.2). Using half of this moment term would provide conservative estimates. The buckling moment of the girders with no bracing is 281 k-ft while the moment due to the self weight of the girder is 219 k-ft. This implies that the girders alone may be able to support their own weight. If stiffened decks are used for bracing as shown in Figure 8.6 a Q value between 400 and 500 k/rad is required. The 100 ft spacing between the discrete twist restraints would probably make the sections a bit flexible. Therefore placing a cross-frame at midspan would probably be more practical.

Figure 8.7 shows the comparison of the FEA results and Eq. (8.2) for Section #4 with an intermediate cross frame at midspan. By the addition of this brace the unbraced length of the girders with the deck forms is reduced to 50 ft and the buckling capacity of the girders increases from 281 k-ft. to 1073 k-ft. The bracing provided by the stiffened PMDF was more effective as compared to the section with no intermediate cross frames and the service moment level was reached at Q values of approximately 120 k/rad. Since there was an intermediate cross frame, the value of m was taken as 5/8 as recommended by Helwig and Yura (2003).

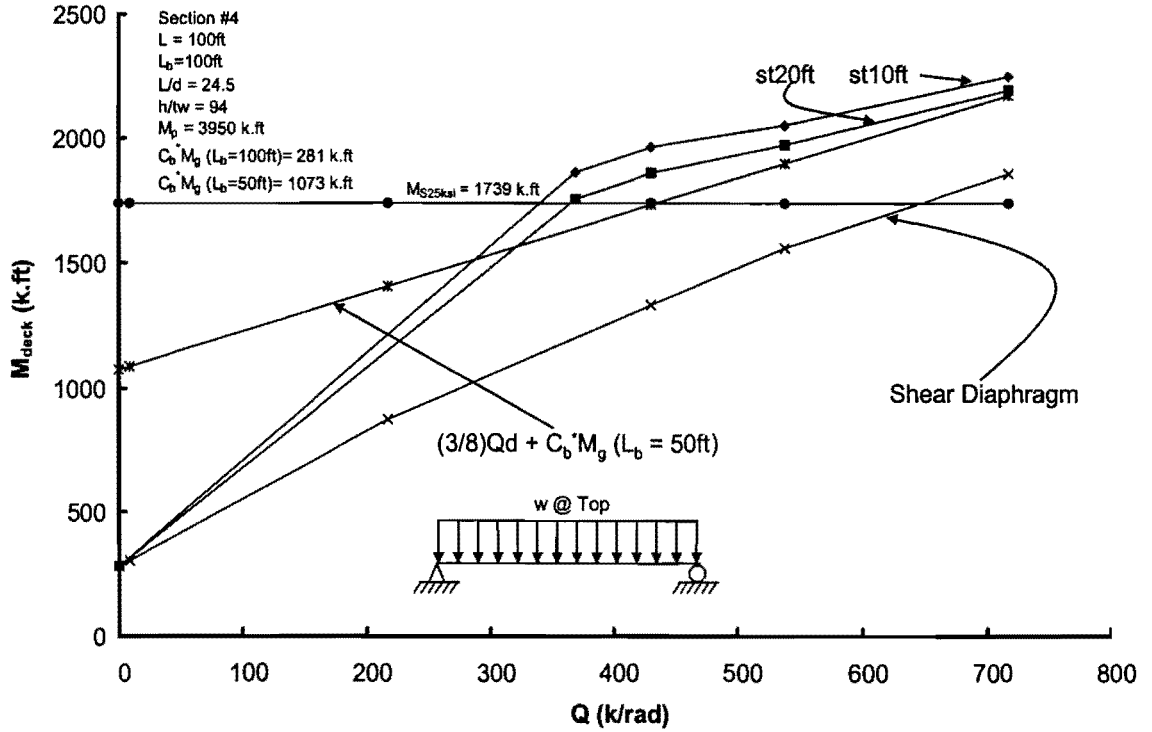


Figure 8.6 Comparison of FEM Results and Deck Component from Eq. (8.2) (Section #4, Unbraced)

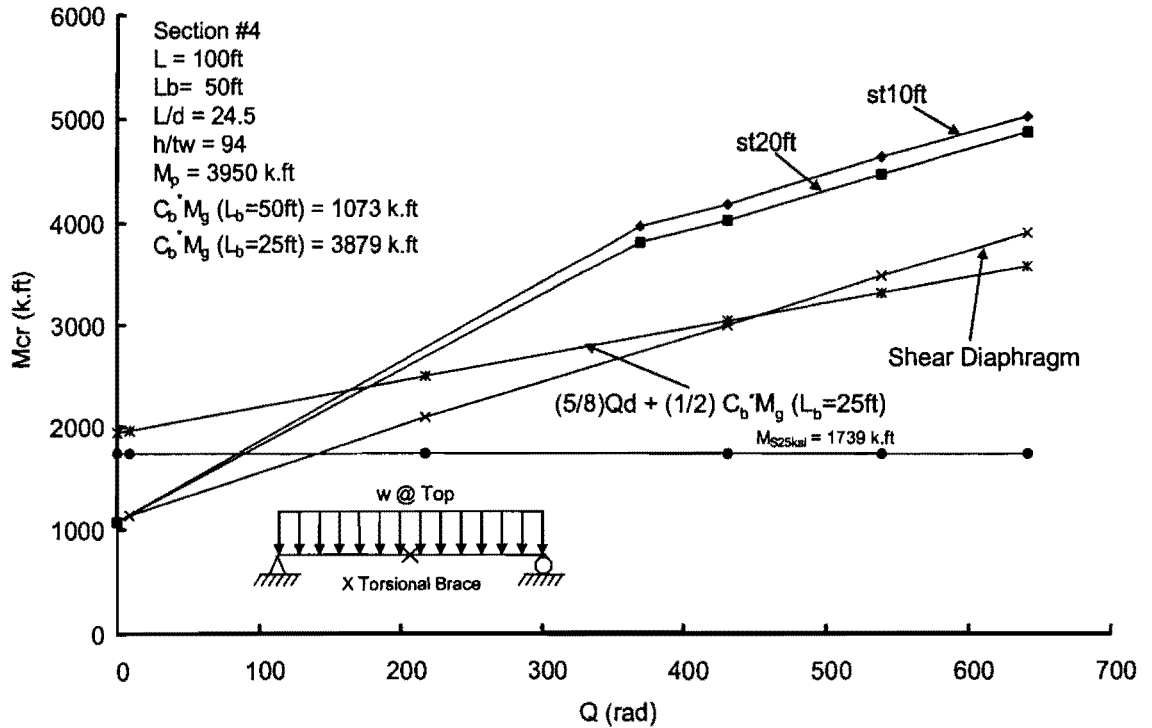


Figure 8.7 Comparison of FEM Results and Deck Component from Eq. (8.2) (Section #4, Midspan Torsional Brace)

Figure 8.8 and Figure 8.9 show the comparison of the FEA results and Eq. (8.2) for Section #5 with midspan and third point torsional braces, respectively. Since there is an intermediate cross frame, the value of m was taken as $5/8$, however the graphs show that this is conservative for this case since the slope is less than the FEA solutions for the stiffened systems. However, Eq. (8.2) provides conservative estimates of the stiffness requirements.

The 75 ft spacing between the cross-frames is rather large and the solution was also looked at with two intermediate braces as shown in Figure 8.9. Although the m -factor for systems with $h/t_w > 60$ were recommended to be $5/8$, the value of 0.85 was used for this systems since there are two intermediate braces and the middle region is getting closer to the case of uniform moment. The use of $m = 0.85$ was conservative relative to the FEA solution and very little stiffness is required from the PMDF to support the load corresponding to 25 ksi.

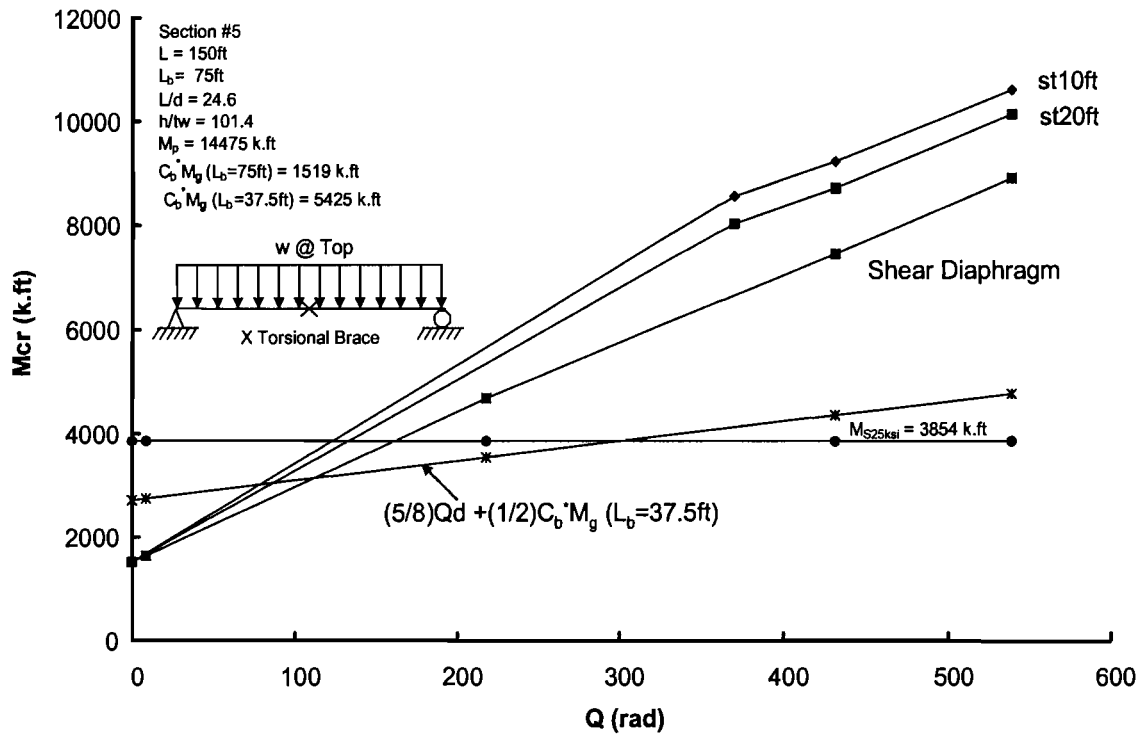


Figure 8.8 Comparison of FEA Results and Deck Component from Eq. (8.2) (Section #5, Midspan Torsional Brace)

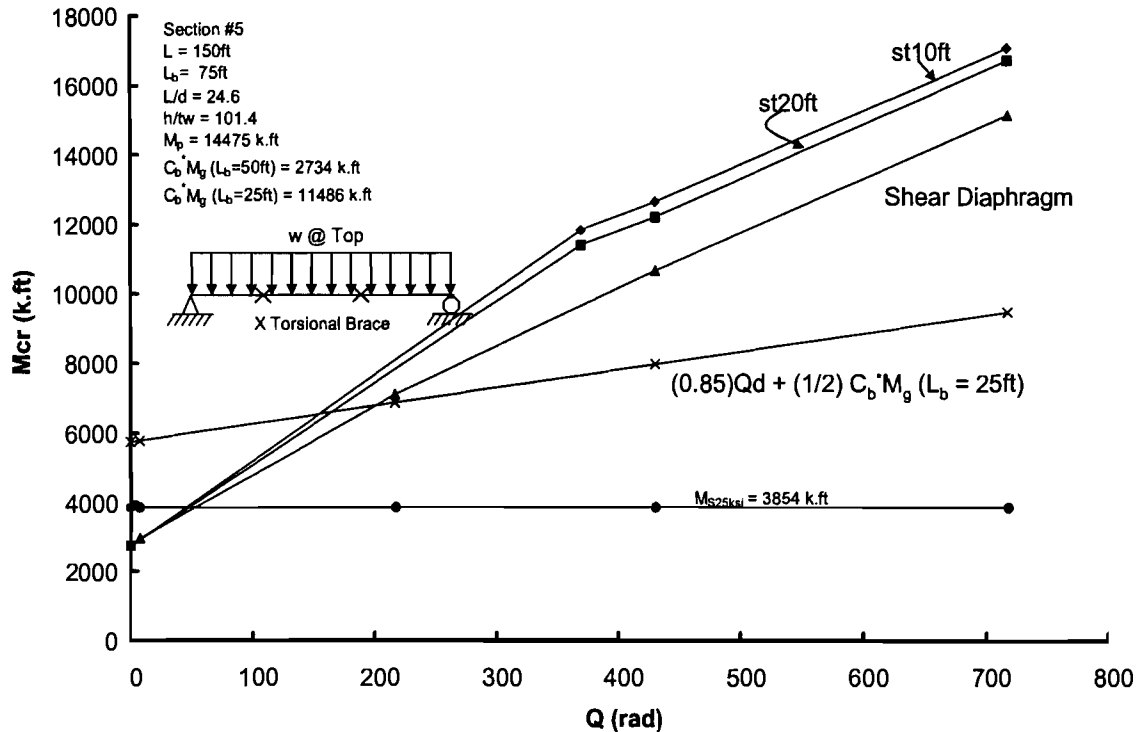


Figure 8.9 Comparison of FEA Results and Deck Component from Eq. (8.2) (Section #5, Third Point Torsional Braces)

8.3 Large Displacement Analyses

As discussed in Chapter 3 the eigenvalue buckling analysis is generally used to determine the ideal stiffness requirements for the bracing. Large displacement analyses are then used to study the effects of imperfections. Generally twice the ideal stiffness is used in large displacement analysis in order to control the displacements. Looking at the eigenvalue analyses presented in the previous section for the W18x119 and also taking into account the buckling capacity of the girders, it can be observed that the moment level corresponding to 25 ksi stress is reached at a deck rigidity Q of 100 k/rad. Therefore the ideal stiffness was accepted to be 100 k/rad. Large displacement analyses were performed with a Q value of 400 k/rad, which is four times the ideal stiffness. The properties of the stiffening angles corresponding to the shear rigidity (Q) of 400 k/rad in Table 6.18 were modified accordingly due to the increase in spacing of the stiffening angles. The initial imperfections used in the FEA models were discussed in Chapter 3.

Figure 8.10 shows the moment vs. twist behavior of the W18x119 section braced with 10 ft and 20 ft stiffened PMDF. The behavior was almost identical for both of the systems. At a moment level of 571 k-ft, corresponding to 30 ksi stress, the total twist was limited to 1.6 times the initial twist.

Figure 8.11 shows a graph of the normalized warping moment (per inch length), M_{br}' , along the girder length from the large displacement analysis at 571 k-ft moment

level corresponding to a maximum stress of 30 ksi. Since the brace moments were symmetrical, only half of the graph is shown. The maximum brace moments occurred at about 1/5th of the span from the supports. The maximum brace moments were calculated to be 1.18 k-in/in and 1.23 k-in/in for 10 ft and 20 ft stiffened decks, respectively. These values are less than 3.4 k-in/in and 4.5 k-in/in, which were the respective failure moments calculated for the 20 ga. unstiffened deck and the stiffened deck from the shear tests.

Figure 8.12 shows the moment vs. twist behavior of the W18x71 section braced with 10 ft and 20 ft stiffened PMDF. Similar to the W18x119 section the behavior was nearly identical for both of the systems. The ratio of the total twist to the initial twist was close to 1.8 at the moment level of 371 k-ft corresponding to 30 ksi maximum stress.

Figure 8.13 shows a graph of the normalized warping moment (per inch length), M_{br}' , along the girder length from the large displacement analysis at a moment level of 317 k-ft corresponding to a maximum stress of 30 ksi for the W18x71 section. Similar to the W18x119 section the maximum brace moments occurred at about 1/5th of the span from the supports. The maximum brace moments were calculated to be 0.98 k-in/in and 0.97 k-in/in for 10 ft and 20 ft stiffened decks, respectively.

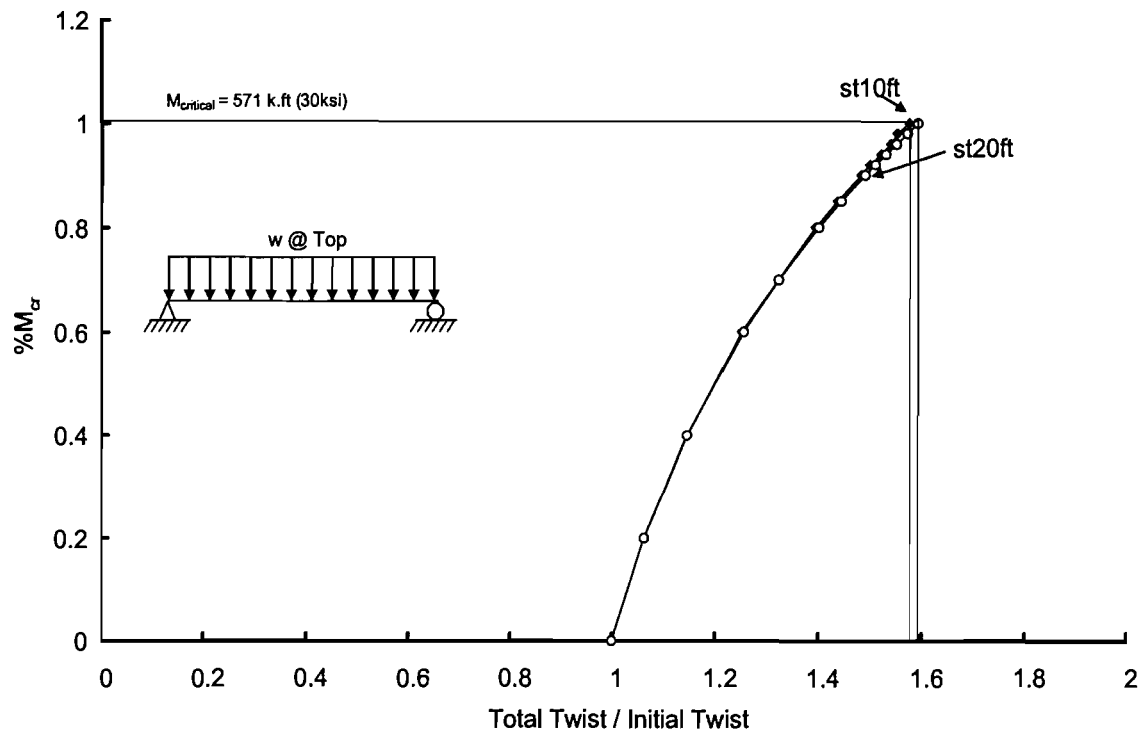


Figure 8.10 Moment vs. Twist Behavior for W18x119

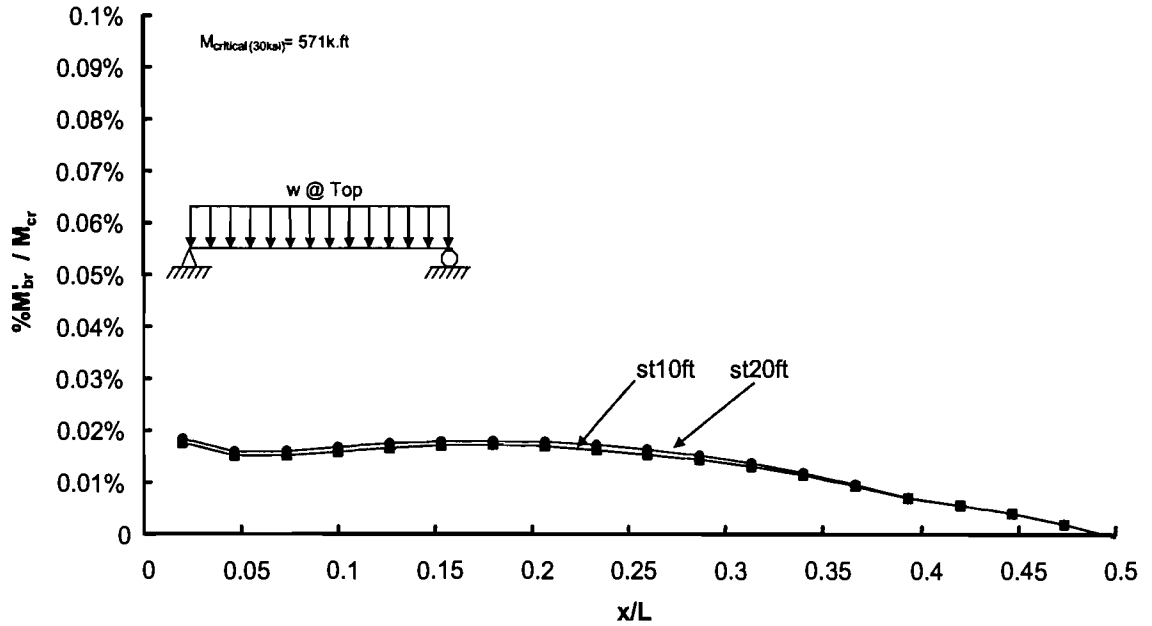


Figure 8.11 Distribution of Brace Moments along Girder Length (W18x119)

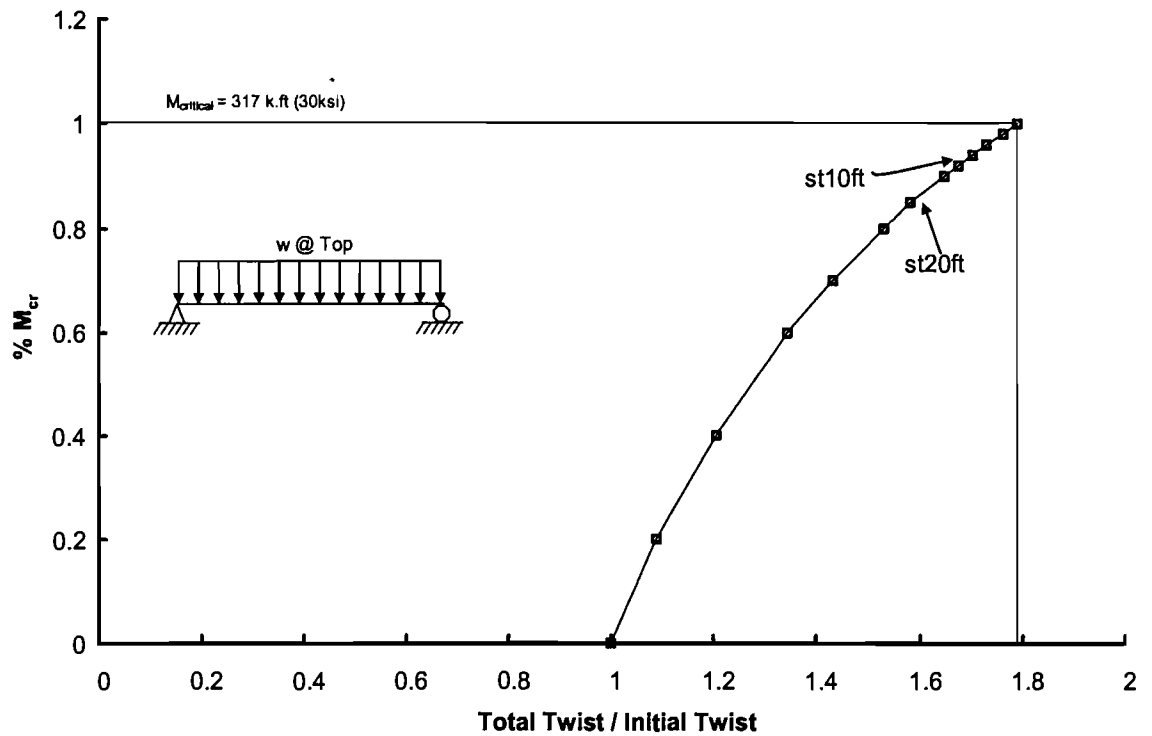


Figure 8.12 Moment vs. Twist Behavior for W18x71

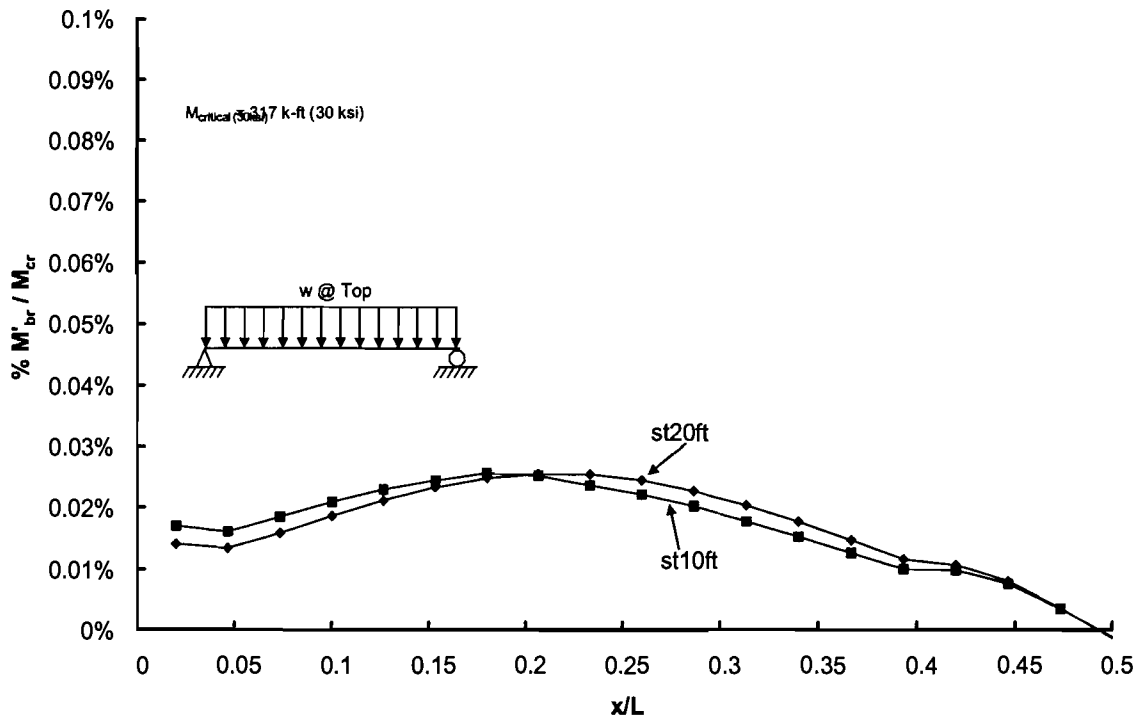


Figure 8.13 Distribution of Brace Moments along Girder Length (W18x71)

Large displacement analyses performed on section #3 with third point loading was previously presented in Chapter 7.

8.4 Design Recommendations

8.4.1 Recommendations for Stiffness

From the eigenvalue analysis it was observed that the stiffened deck provided a substantial increase in the buckling capacity of the girders. Equation (8.1), which was repeated from Chapter 2 was modified slightly to account for the affect of the stiffening angles. The modification consisted of simply using 50% of the buckling moment corresponding to $L_b/2$, where L_b is the spacing between cross-frames. The solution was presented in Eq. (8.2) and compared to the FEA solutions for different values of the stiffening angle spacing. This solution was conservative relative to the FEA eigenvalue buckling equations. Table 8.1 presents the recommended m values for stiffened-deck braced girders.

Table 8.1 Design m Values for Eq. (8.1)

Web Slenderness	Top Flange Loading w/o Midspan Cross-Frame	Top Flange Loading with Midspan Cross-Frames
$h/t_w < 60$	0.5	0.85
$h/t_w > 60$	0.375	0.625

With more than one intermediate cross-frame, the m-values from Table 8.1 provide conservative estimates of the buckling capacity.

Eq. (8.2) can be rewritten in order to calculate the ideal deck stiffness for a given moment level as previously presented in Chapter 2.

$$G'_{ideal} = \frac{(M_u - (1/2)C_b^* M_{g-Lb/2})}{s_d m d} \quad (8.3)$$

where G'_{ideal} = ideal deck stiffness; M_u maximum design moment; s_d = tributary width of deck bracing a single girder (Eq. 2.2); $M_{g-Lb/2}$ is the buckling capacity of the girder using half the spacing between cross-frames, C_b^* , m and d have been defined previously.

To control the deflections the required deck shear stiffness ($G'_{req'd}$) should be taken as 4 times the ideal stiffness given in Eq. (8.3).

8.4.2 Recommendations for Strength

As previously stated large displacement analyses were performed only for sections with a web slenderness ratio smaller than 60. Hence the recommendations presented in this section are only for sections with an h/t_w ratio less than 60. As previously outlined in Chapter 2, Helwig and Yura (2003, "Strength requirements for diaphragm bracing of beams," Draft manuscript to be submitted) suggested the following equation for estimating the required bracing moment per unit length of a girder for a diaphragm with a stiffness given by Eq. (2.12).

$$M'_{req'd} = k \frac{(M_u L)}{d^2} \quad (8.4)$$

where: L = total beam span and d = beam depth, and k is 0.0011. The brace moment given in Eq. (8.4) represents the warping restraint provided to the top flange of the girder per unit length of the span. Eq. (8.4) has the units of (kN-mm)/mm or (kip-in)/in. The expression in Eq. (8.4) can be used to determine the forces in the fasteners used to

connect the metal deck form. Equation (8.4) was developed for shear diaphragm bracing that was only supported along two sides. Therefore this would be the case for the unstiffened PMDF connections.

For systems with stiffening angles, Eq. (8.4) was very conservative. Based upon the large displacement solutions, the values of k for the stiffened-deck braced girders are given in Table 8.2.

Table 8.2 Design k Values for Eq. (8.4)

<i>Web Slenderness</i>	<i>Top Flange Loading w/o Midspan Torsional Brace</i>
<i>$h / t_w < 60$</i>	<i>0.00015</i>
<i>$h / t_w > 60$</i>	<i>-</i>

This page replaces an intentionally blank page in the original.

-- CTR Library Digitization Team

Chapter 9

Bracing Design Example

9.1 Introduction

The bracing requirements for girders were discussed in Chapter 8. The analyses that were presented in the previous chapter mainly focused on twin-girder systems. This chapter will investigate the bracing requirements for two bridge systems with four girders. The bridges that are to be considered both had normal supports and spans of 100 ft and 50 ft.

9.2 Design Examples

9.2.1 Steel Bridge with 100 ft span

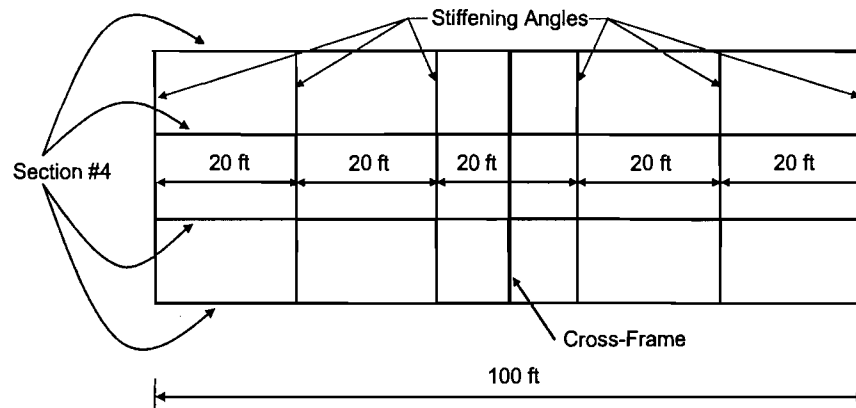


Figure 9.1 Plan view of bridge for Design Example A

DESIGN EXAMPLE A

GIRDER PROPERTIES (Section #4 presented in Chapter 3)

Number of Girders = 4 @ 7'

Gr. 50 Steel

8 in concrete Slab

Span Length = 100 ft

Unbraced Length = 50 ft (Midspan Cross-Frame)

$$I_y = 458 \text{ in}^4$$

$$J = 11.3 \text{ in}^4$$

$$C_w = 263692 \text{ in}^6$$

$$d = 47 \text{ in}$$

$$t_f = 1 \text{ in}$$

$$b_f = 14 \text{ in}$$

$$h/t_w = 94 > 60$$

Use a Load Factor = 1.3 for the construction condition

Steel girder: $A = 51.5 \text{ in}^2$, $wt = 175 \text{ lb/ft}$
 Concrete slab: $7' \times 8/12 \times 150 \text{ lb/ft}^3 = 700 \text{ lb/ft}$
 Construction Live Load: $20 \text{ lb/ft}^2 \times 10' = 200 \text{ lb/ft}$
 $w = 1075 \text{ lb/ft} = 1.075 \text{ k/ft}$

$$M_u = 1.3 \frac{(1.075 \text{ k-ft})(100 \text{ ft})^2}{8} = 1746 \text{ k-ft (Max. Stress = 25 ksi)}$$

Check Lateral Buckling

Check the construction condition. The plan view in Figure 9.1 shows a cross-frame at midspan. This cross-frame was required based upon a check of the erection/construction condition. The girders must have enough stability to support their own self-weight plus a portion of the construction live load ($\sim 5\text{-}10 \text{ lb/ft}^2$). From above the girder self-weight is 175 lb/ft . The total erection design load would therefore be:

$$w_e = 175 \text{ lb/ft} + (10 \text{ lb/ft}^2) \times 7 \text{ ft} = 245 \text{ lb/ft}$$

The required girder erection moment would therefore be:

$$M_e = 1.3 \frac{(0.245 \text{ k-ft})(100 \text{ ft})^2}{8} = 398 \text{ k-ft}$$

Check if the girder can carry this moment with no intermediate braces ($L_b = 100 \text{ ft}$). Use Timoshenko's solution with $L_b = 50 \text{ ft}$ since there is a cross frame at midspan. (Note: Timoshenko's solution is identical to the AASHTO Equation 10-103c in Sect. 10.48.4 from the standard specification). Although part of the construction load may cause top flange loading, most of the moment comes from the girder self-weight. Simply use a $C_b = 1.0$ to check the erection condition.

$$C_b M_{cr} = C_b \frac{\pi}{L_b} \sqrt{EI_y GJ + \frac{\pi^2 E^2 C_w I_y}{L_b^2}}$$

$$C_b M_{cr(L_b=100 \text{ ft})} = 1.0 \frac{\pi}{100 \times 12} \sqrt{29000 \times 458 \times 11200 \times 1.3 + \frac{\pi^2 \times 29000^2 \times 263693 \times 458}{(100 \times 12)^2}}$$

$$= 4036 \text{ k-in} = 336 \text{ k-ft} < 398 \text{ k-ft} = M_e$$

Midspan Cross-frame is required

Therefore put a cross-frame at midspan, which provides an unbraced length L_b of 50 ft . The capacity should be checked to ensure a safe section during girder erection and also to provide an indication of how much bracing is necessary from the PMDF system. Although the beam has top flange load, there is an intermediate brace that substantially reduces the effects of top flange loading. Therefore simply use a $C_b = 1.0$:

$$C_b M_{cr(L_b=50 \text{ ft})} = \frac{\pi}{50 \times 12} \sqrt{29000 \times 458 \times 11200 \times 1.3 + \frac{\pi^2 \times 29000^2 \times 263693 \times 458}{(50 \times 12)^2}}$$

$$= 11055 \text{ k-in} = 921 \text{ k-ft} < 1746 \text{ k-ft}$$

A cross-frame at midspan will help with the girder erection and the early construction stages, however the PMDF will be designed for the remainder of the bracing.

Determine the Number of Stiffening Angles

Use Galvanized 3x2x10 gage stiffening angles

Maximum spacing proposed = 20 ft

Use 6 stiffening angles spaced at 20 ft as shown in Figure 9.1

Ideal Deck Shear Stiffness (G')

To account for the affect of the stiffening angle, compute the buckling capacity of the girders using half the spacing between the cross-frames ($L_b/2 = 25 \text{ ft.}$) Use 50% of this capacity for the girder contribution in Eq. 8.3.

$$(0.5)C_b^* M_{cr(L_b=25ft)} = 0.5 \times 1.0 \frac{\pi}{25 \times 12} \sqrt{29000 \times 458 \times 1200 \times 11.3 + \frac{\pi^2 \times 29000^2 \times 263693 \times 458}{(25 \times 12)^2}}$$

$$= 18728 \text{ k-in} = 1560 \text{ k-ft}$$

Find the tributary width of deck bracing a single girder, s_d : The tributary width will be equal to clear span of the PMDF per girder and can be found by the following expression:

$$s_d = \frac{(s_g - t_f)(n_g - 1)}{n_g} = \frac{(7 \times 12 - 14)(4 - 1)}{4} = 52.5 \text{ in}$$

$$G'_{ideal} = \frac{(M_u - (1/2)C_b^* M_{g-L_b/2})}{s_d m d} = \frac{(1746 \times 12 - 1560 \times 12)}{52.5 \times 47 \times (5/8)} = 1.44 \text{ k/in}$$

Required Deck Shear Stiffness (G'): To control girder deformations provide 4 times the ideal stiffness:

$$G'_{req'd} = 4G'_{ideal} = 5.8 \text{ k/in}$$

Use 20 gage metal deck form $G' = 7 \text{ k/in}$ (Minimum Test results were 6.8 k/in)

$$G'_{provided} = 6.8 \text{ k/in} > 5.8 \text{ k/in O.K.}$$

Brace Strength Requirement

The maximum permissible brace moment per unit length is 3.4 k-in/in from Table 5.3 for eccentric 20-gage shear test.

Use Eq. 8.4 with a coefficient of 0.00015 as proposed in Section 8.4. Even though the h/t_w is greater than 60 we will use this for the strength requirements – this should be reasonable. The web slenderness gets to be a problem for cases when the web may be near stresses for shear buckling or web bend buckling. With a web slenderness of 100 and a relatively long span this section should be okay.

$$M'_{br} = 0.00015 \frac{1746 \times 12 \times 100 \times 12}{47^2} = 1.7 \text{ k-in/in} < 3.4 \text{ k-in/in} \text{ O.K}$$

Final Sizes:

Use 20 gage metal deck forms with 6 (Galvanized 3x2x10 gage) stiffening angles spaced at 20 ft.

9.2.2 Steel Bridge with 50 ft span

The bridge presented in this example is similar to a project in Houston. Due to clearance problems, relatively shallow sections are used for the 50 ft span. The sections to be used are W18x119 sections. So as to make this problem interesting a large construction live load has been assumed (40 lb/ft²):

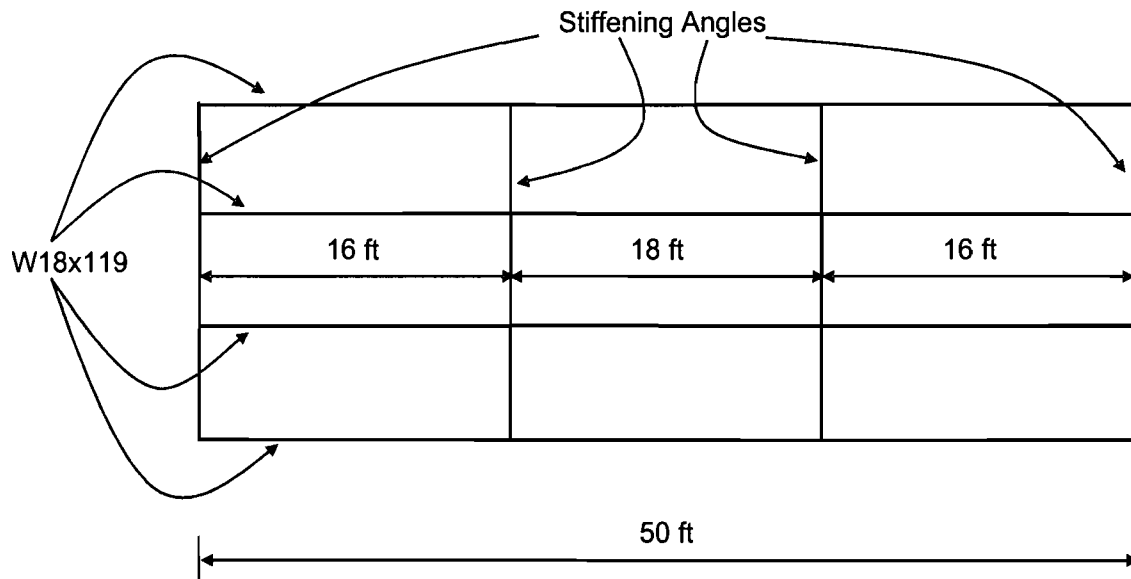


Figure 9.2 Plan view of bridge for Design Example B

DESIGN EXAMPLE B GIRDER PROPERTIES (W18x119)

Number of Girders = 4

Gr 50 Steel

8 in concrete Slab

Spacing of Girders = 5.5 ft

Span Length = 50 ft

$I_y = 255 \text{ in}^4$

$C_w = 20542 \text{ in}^6$

$J = 10 \text{ in}^4$

$d = 19 \text{ in}$

$t_f = 1.06 \text{ in}$

$b_f = 11.3 \text{ in}$

$h/t_w = 25.8 < 60$

Use a Load Factor = 1.3 for the construction condition

Steel girder: $A = 35 \text{ in}^2$, $wt = 119 \text{ lb/ft}$
 Concrete slab: $5.5' \times 8/12 \times 150 \text{ lb/ft}^3 = 550 \text{ lb/ft}$
 Construction Live Load: $40 \text{ lb/ft}^2 \times 5.5' = 220 \text{ lb/ft}$
 $w = 889 \text{ lb/ft} = 0.889 \text{ k/ft}$

$$M_u = 1.3 \frac{(0.889 \text{ k-ft}) (50 \text{ ft})^2}{8} = 361 \text{ k-ft} \text{ (Max. Stress} = 18.8 \text{ ksi)}$$

Check Lateral Buckling

Since the beam has top flange loading and no intermediate bracing, use the provision discussed in Chapter 2 for load height effects. For the case of a uniformly distributed load at midheight of the cross-section, $C_b = 1.12$.

$$C_b^* = \frac{C_b}{1.4} = \frac{1.12}{1.4} = 0.8$$

The spacing between cross-frames is the full length of the beam. Check that the girders can support their self-weight with $L_b = 50 \text{ ft}$ unbraced length (Timoshenko's Solution):

$$C_b^* M_{cr} = C_b^* \frac{\pi}{L_b} \sqrt{EI_y GJ + \frac{\pi^2 E^2 C_w I_y}{L_b^2}}$$

$$C_b^* M_{cr} = 0.8 \frac{\pi}{50 \times 12} \sqrt{29000 \times 255 \times 11200 \times 10 + \frac{\pi^2 \times 29000^2 \times 20542 \times 255}{(50 \times 12)^2}}$$

$$= 4091 \text{ k-ft} = 340 \text{ k-ft} < 361 \text{ k-ft}$$

Number of Stiffening Angles

Use four stiffening angles with the spacing shown in Figure 9.2. Use Galvanized 3x2x10 gage stiffening angles

Ideal Deck Shear Stiffness (G')

To account for the affect of the stiffening angle, compute the buckling capacity of the girders using half the spacing between the cross-frames ($L_b/2 = 25 \text{ ft}$.) Use 50% of this capacity for the girder contribution in Eq. 8.3.

$$(0.5) C_b^* M_{cr(L_b=25ft)} = 0.5 \times 1.0 \frac{\pi}{25 \times 12} \sqrt{29000 \times 255 \times 11200 \times 10 + \frac{\pi^2 \times 29000^2 \times 20542 \times 255}{(25 \times 12)^2}}$$

$$= 5996 \text{ k-in} = 500 \text{ k-ft}$$

500 k-ft > 361 k-ft Therefore no further stiffness calculations are necessary. Decking with a relatively low stiffness will be able to brace these girders with the stiffening angles.

Brace Strength Requirement

The maximum permissible brace moment per unit length is 3.4 k-in/in from Table 5.3 for eccentric 20-gage shear test.

Use Eq. 8.4 with a coefficient of 0.00015 as proposed in Section 8.4.

$$M'_{br} = 0.00015 \frac{361 \times 12 \times 50 \times 12}{19^2} = 1.1 \text{ k-in/in} < 3.4 \text{ k-in/in} \text{ O.K}$$

Final Sizes:

Use 20 gage metal deck forms with 4 (Galvanized 3x2x10 gage) stiffening angles spaced at approximately 16 ft.

This page replaces an intentionally blank page in the original.

-- CTR Library Digitization Team

Chapter 10

Conclusions and Future Work

10.1 Conclusions

The objective of the research outlined in this report was to improve the understanding of the bracing behavior of permanent metal deck forms in steel bridges. General bracing requirements were developed and a new stiffened connection detail was proposed. PMDF are commonly used to support the wet concrete during construction in the bridge industry. The AASHTO Specifications do not currently permit PMDF to be considered for bracing elements. One of the primary reasons that bridge deck forms have not been relied on for bridge girder bracing is because the flexibility in the eccentric connections reduces the overall system stiffness. The eccentricity in the connection is due to the support angle that allows the contractor to adjust the form elevation to account for variations in the flange thickness along the length or differential camber between adjacent girders. One of the major goals of this research was to develop a modification to the connection detail that would reduce the flexibility while still permitting the adjustment of the form elevation. The detail that is proposed consists of intermittent stiffening angles that span between the top flanges of adjacent girders. The stiffening angles are positioned at a sidelap location, which is the point where two adjacent sheets are fastened together. The deck is screwed directly to the stiffening angle, which therefore connects the panel on all four sides. In addition to improving the stiffness and strength of PMDF systems, the proposed connection detail modification also provides structural redundancy.

The research investigation included both experimental and computational studies. The experimental study consisted of 3 phases: shear, lateral displacement and buckling tests. The experimental test results were then used to develop finite element models that were used to conduct parametrical studies on the deck system. A number of conclusions can be made from the different phases of this study. These conclusions are presented in the following subsections of this chapter.

10.1.1 Shear Tests

A test frame was constructed for the purpose of determining the properties of shear stiffness and strength of various PMDF systems with and without the stiffened connection details. Results were presented for several tests with a wide range of variables that were considered. The parameters considered for shear tests were: the metal gage, the deck span, the panel width, and the spacing between the stiffening angles. The decks were tested with and without superimposed load that simulated concrete loading. The stiffness of the deck with the superimposed dead load was slightly higher than for decks without superimposed dead load. The higher stiffness comes from the increased friction that develops between the connection surfaces such as the sheeting to sheeting

contact of adjacent sheets and the sheeting to support angle contact at the ends of the forms. Tests were conducted using both conventional deck connection details as well as proposed stiffened connection details. The conventional connection details consisted of support angles with zero eccentricity as well as support angle with approximately 2 ¾ inch eccentricity. The connection eccentricity substantially reduced the system stiffness for the PMDF system.

The new connection detail with the stiffening angles still permits the contractor to adjust the form elevation. The angle spacing that was tested generally consisted of 8 ft and 16 ft, however isolated cases were also conducted with a spacing of 12 ft. The shear tests showed that the stiffened connection details substantially improve the stiffness and strength for PMDF systems. The stiffness of the PMDF systems with the stiffening angle and the maximum eccentricity (~2.75 in) were similar to the stiffness of conventional details with zero eccentricity. The corresponding strength of the stiffened connections with maximum eccentricity was generally slightly higher than the conventional details with zero eccentricity. The 16 and 18 gage deck systems were generally stiffer and stronger than the 20 gage systems, however there generally was not a large difference between the performances of the different forms. As a result the recommendations for the strength and effective shear stiffness have been based upon the 20 gage deck, which had the lowest strength and stiffness.

10.1.2 Twin Girder, Lateral Displacement Tests

The shear tests that were conducted in the laboratory subjected the PMDF systems to a pure/uniform shear deformation. In practical situations, the shear deformation of bridge deck forms varies along the length of the buckled girder profile. In such cases, the shear deformation is greater at locations where the girder twist is prevented and essentially zero where the top flange lateral displacement is maximum. The lateral stiffness of the buckled girders in regions of small shear deformation is dominated by the in-plane flexural stiffness. To measure the in-plane flexural stiffness of conventional PMDF systems and also to investigate the flexural contribution provided by the new stiffened connection to PMDF lateral stiffness, a twin girder test set-up was constructed so a variety of top flange deflection profiles could be studied. The parameters considered were the metal gage and connection system (Stiffened and conventional systems). For stiffened system 8 ft, 16 ft and 24 ft stiffening angle spacing were investigated. The conventional connection system results from these laboratory tests were compared to FEA results in which shear diaphragms were used to model the deck forms. These comparisons showed that the actual PMDF systems have a greater in-plane capacity than predicted by shear diaphragms. It was also observed that the stiffened connections had a substantial contribution to the lateral stiffness of the overall system. The stiffened test results were used to develop finite element models that reflected the effects of stiffening angles.

10.1.3 Twin Girder, Buckling Tests

The twin girder test set-up constructed to perform lateral displacement tests was also used to perform buckling tests in order to observe the actual buckling behavior of girder systems braced by both stiffened and unstiffened PMDF. These tests enabled the verification of the accuracy of the FEM developed in the second phase of the study.

Stiffened decks with 8 ft, 16 ft and 24 ft spaced stiffening angles were tested in addition to unstiffened deck system. The stiffened deck systems did a much better job in controlling the deformations compared to the unstiffened deck system. The stiffnesses of the three stiffened systems were very close to each other. The system with stiffening angles spaced at 8 ft was the stiffest among them. Although the 24 ft system had one less stiffening angle as compared to the 16 ft spaced system, it was stiffer than the 16 ft spaced system up to load levels where every structural member remained elastic. The reason for that was probably the existence of a stiffener right at midspan where the maximum twist took place.

Large displacement analyses performed on the 16 ft stiffened deck system which was loaded up to failure revealed that the brace moments developed along the length of the girder were significantly less than the brace moments predicted from a shear diaphragm braced beam.

Parametric studies were used to improve the understanding of the bracing behavior of the PMDF systems with and without the stiffening angles. The approach that was taken in developing the FEA models for the bracing systems was generally conservative. The properties of the deck that were used in the FEA studies were usually the lowest values that were measured in the laboratory investigations. As will be covered in the next section, conservative approaches were also taken in developing design approach to utilizing the forms for bracing.

10.1.4 Design Recommendations for Stiffened Deck Braced Girders

The investigations on bracing behavior of metal formwork bracing systems have enhanced the understanding of the behavior of girders braced with PMDF. The FEA investigations were used to help develop a simple design approach for using PMDF for stability bracing. However, since the forms not been utilized for bracing in the bridge industry in the past, a conservative approach has been taken towards developing a simple design procedure.

Utilizing the forms for bracing should reduce the number of intermediate cross-frames or diaphragms that are used on the bridge, however there will always have to be a minimum number of these traditional braces. Cross-frames must always be present at the ends of the bridge. In addition, the capacity of the girders under their own self-weight should also be evaluated along with a minimal construction live load of 5-10 lb/ft² to ensure that the girders have enough stability to be erected and get the forms on. Therefore, the buckling capacity of the girders should always be checked for the erection/early construction condition and cross-frames should be provided to support this

load. Although the construction load will typically be applied at the top flange, the girder self-weight is applied at its centroid. Therefore a C_b of 1.0 is usually safe for checking the construction condition.

The expressions for the shear diaphragm bracing in Chapter 2 were modified to account for bracing provided by PMDF with the stiffening angles. The modification consisted of simply using 50% of the buckling moment corresponding to $L_b/2$, where L_b is the spacing between cross-frames. The diaphragm component for the deck has not changed and equations have been presented in Chapter 8 for determining the ideal effective shear stiffness. To determine the required effective shear stiffness, a value of 4 times the ideal stiffness was recommended for design so as to control deformations. Once the required effective shear stiffness is determined, it can be compared with the capacity of the PMDF. The design capacity of the PMDF is taken as $G' = 7$ k/in, which is close to the minimum value that was recorded in the laboratory tests.

The stiffening angles resulted in a substantial reduction in the strength requirements for the PMDF system. Therefore the coefficient on the PMDF strength requirement was reduced. The strength equation results in a brace moment per unit length in the PMDF, which should be less than the capacity taken from the laboratory tests, which was 3.4 k-in/in.

10.2 Future Research

The approaches that were taken in the FEA studies as well as the design methodology are relatively conservative. The current design equations are relatively conservative, however they still result in a substantial amount of bracing that can significantly reduce the number of cross-frames or diaphragms. However, additional studies should be done to improve the accuracy of these solutions. In addition, only one girder section was tested in the laboratory. A wider variety of cross-sectional shapes should be tested. Some additional tests are planned in the coming months at UH on doubly-symmetric rolled sections. In addition, additional large displacement analyses will be conducted on the girders with spans of 100 ft and 150 ft in order to investigate the bracing behavior of systems with both PMDF and cross-frames and diaphragms. The resulting effects on the cross-frame and diaphragm forces will also be determined.

APPENDIX I. REFERENCES

- [1] AASHTO, (1992), *Standard Specifications for Highway Bridges (LFD)*, American Association of State Highway and Transportation Officials, Fifteenth Edition, Washington, D.C.
- [2] AASHTO, (1994), *LRFD Bridge Design Specifications*, American Association of State Highway and Transportation Officials, First Edition, Washington, D.C.
- [3] AISC, (2001), *Manual of Steel Construction (LRFD)*, 3rd Ed.
- [4] Currah, R. M., "Shear Strength and Shear Stiffness of Permanent Steel Bridge Deck Forms," M. S. Thesis, The University of Texas at Austin, August 1993
- [5] Egilmez, O. O., Jetann C. A. and Helwig T. A. (2003) "Bracing Behavior of Permanent Metal Deck Forms", *Proceedings 2003, Structural Stability Research Council*, pp. 133.
- [6] Errera, S., and Apparao, T. (1976). "Design Of I-shaped beams with diaphragm bracing," *J. Struct. Div., ASCE*, 102(4), 769-781.
- [7] Helwig, T. A., (1994), "Lateral bracing of Bridge Girders by Metal Deck Forms", PhD. Dissertation, University of Texas at Austin
- [8] Helwig, Todd A.; Frank, Karl H.; and Yura, Joseph A., "Lateral-Torsional Buckling of Singly-Symmetric I-Beams," *ASCE Journal of Structural Engineering*, V. 123, No. 9, Sept. 1997, pp. 1172-1179.
- [9] Helwig, T. A. and Frank, K. H. (1999), "Stiffness Requirements for diaphragm bracing of beams," *J. of Structural Engineering, ASCE*, Vol. 125, No. 11, pp. 1249-1256.
- [10] Helwig, T. A., and Yura, J. A. (2003), "Strength requirements for diaphragm bracing of beams," Draft manuscript to be submitted.
- [11] Luttrell, L. D., *Steel Deck Institute Diaphragm Design Manual*, 2nd Ed., Canton, Ohio, 1995.
- [12] Lawson, R., and Nethercot, P. (1985). "Lateral Stability of I-beams Restrained by Profiled Sheeting", *The Struct. Engr.*, London, 63B(1), 3-13
- [13] Nethercot, D., and Trahair, N. (1975). "Design of diaphragm-braced I-beams," *Struct. Div., ASCE*, 101(10), 2045-2061.

- [14] Soderberg, E. (1994). "Strength and Stiffness of Stay-in-Place Metal Deck Form Systems," MS thesis, Univ. of Texas at Austin.
- [15] Stephen P. Timoshenko and James M. Gere., *Theory of Elastic Stability*, 2nd Ed. New York: McGraw-Hill Book Company, Inc., 1961 (pp. 329-328, 351-356)
- [16] Winter, G., (1960), "Lateral Bracing of Columns and Beams," ASCE Transactions, Vol. 125, pp. 809-825.
- [17] Yura, J. A. (2001):"Fundamentals of Beam Bracing", AISC Engineering Journal, 1st Quarter, pp. 11-26.